# **Azobenzene-Containing Polymers for Photoswitching Applications:** Design, Synthesis and Characterization

**Dissertation**
zur Erlangung des Grades
**Doktor der Naturwissenschaften**
im Promotionsfach Chemie

am Fachbereich Chemie, Pharmazie und Geowissenschaften

der Johannes Gutenberg-Universität Mainz

**Philipp Weis**
geboren in Idar-Oberstein

Mainz, 2018

Die vorliegende Arbeit wurde in der Zeit von Juni 2015 bis November 2018 am Max Planck Institut für Polymerforschung angefertigt.

Mainz, November 2018

1. Berichterstatter:
2. Berichterstatter:

Tag der mündlichen Prüfung 18.12.2018

*Dissertation an der Universität Mainz (D77)*

# Zusammenfassung

In dieser Arbeit werden zwei Eigenschaften von Azopolymeren untersucht. Im ersten Teil werden Azopolymere mit Absorption im sichtbaren Bereich des Lichtspektrums hergestellt, charakterisiert und mögliche Anwendungen dieser Polymere werden veranschaulicht. Im zweiten Teil wird der isotherme, photoinduzierte fest-zu-flüssig-Übergang von Azopolymeren untersucht und mit Unterschieden zwischen der *trans*- und der *cis*-Form der Azopolymere verknüpft.

Zur Darstellung von einem Azopolymer mit Absorption im sichtbaren Bereich des Lichts, wird ein Azobenzolmolekül, welches sichtbares Licht absorbiert, in ein Polymethacrylatrückgrat eingebaut. Hierfür wird zuerst ein Monomer synthetisiert, welches auf einem Methacrylat basiert und eben genanntes Azobenzolmolekül enthält. Das Azobenzolmolekül wird mit dem Methacrylat über sechs Methylengruppen verbunden. Im Folgenden werden Strukturverhalten und Lichtschaltbarkeit in Polymerfilmen untersucht und durch Vergleich mit einem konventionellen Azopolymer werden die Vorteile des neuen Polymers aufgezeigt. Basierend auf diesen Eigenschaften werden Informationsspeicherung sowie Sonnenenergiespeicherung als mögliche Anwendungen aufgezeigt.

Die thermischen Eigenschaften, im speziellen die Glasübergangstemperatur, von Azopolymeren werden im zweiten Teil genauer betrachtet. Für bestimmte Azopolymerstrukturen wird je nach Konformation (*trans* oder *cis*) ein Übergang von fest zu flüssig beobachtet, der mit der Glasübergangstemperatur assoziiert wird. Um dieses Phänomen besser zu verstehen werden die thermischen Eigenschaften mehrerer, unterschiedlicher Azopolymere mit verschiedenen Methoden bestimmt. Die Azopolymere unterscheiden sich dabei in Polymerrückgrat, Länge der Seitenkette oder Azobenzolsubstituenten. Außerdem werden mögliche Anwedungen basierend auf photoinduzierten fest-zu-flüssig-Übergängen demonstriert.

# Abstract

In this thesis two properties of azopolymers are investigated. In the first part azopolymers with absorption in the visible range of the light spectrum are synthesized, characterized and possible applications of these polymers are illustrated. In the second part, the isothermal, photoinduced solid-to-liquid transition of azopolymers is investigated and associated to differences between the *trans* and *cis* forms of the azopolymers.

For the preparation of an azopolymer with absorption in the visible light region, an azobenzene molecule, which absorbs visible light, is incorporated into a polymethacrylate backbone. For this purpose, a monomer based on a methacrylate and containing the just mentioned azobenzene molecule is synthesized first. The azobenzene molecule is linked to the methacrylate via six methylene groups. In the following, solid state properties and light switching in polymer films are investigated and the advantages of the new polymer will be demonstrated by comparison with a conventional azopolymer. Based on these properties, information storage and solar energy storage are shown as possible applications.

The thermal properties, in particular the glass transition temperature, of azopolymers are examined in more detail in the second part. For certain azopolymer structures, a solid-to-liquid transition is observed depending on their conformation (*trans* or *cis*), which is associated with the glass transition temperature. In order to better understand this phenomenon, the thermal properties of several different azopolymers are determined by different methods. The azopolymers differ in their polymer backbone, length of the side chain or azobenzene substituents. Furthermore, possible applications based on photoinduced solid-liquid transitions are demonstrated.

# Contents

# 1 Introduction and Theory

Stimuli-responsive materials, also called smart materials, are materials that change according to their environment.[1] Typically, a slight change in their environment is sufficient to cause major changes in the properties of the material. These materials are expected to play an important role in the future as they enable the introduction of new functions in conventional materials and thus increase the value of the material.[2] Stimuli-responsive materials can be responsive to a variety of stimuli such as temperature,[3] pH,[4] light[5] or others.[6–9] Materials that have combined responsiveness to multiple stimuli have also been realized.[10] The stimuli are typically divided into three groups: biological, chemical and physical stimuli (Figure 1.1). Among these stimuli, light is of particular interest. Light can be directed into a specific area, it can be switched on and off fast and it is a clean stimulus. Stimuli-responsive materials which are responsive to light are called light-responsive or photoresponsive materials. In this thesis the focus is on photoresponsive materials.

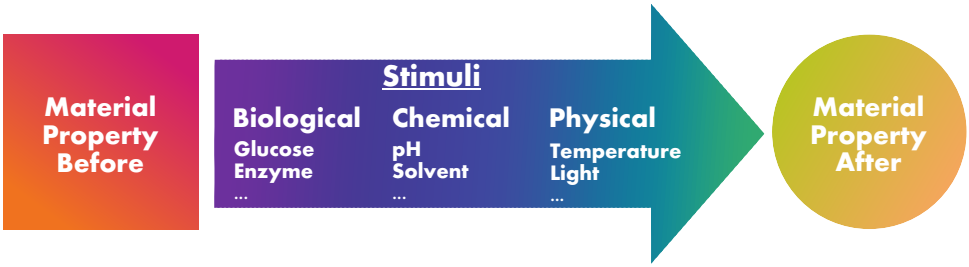


**Figure 1.1:** Principle of stimuli-responsive materials. A material's property is changed by an external stimulus.

## 1.1 Photoresponsive Materials

In general, a photoresponsive material is a material that changes by light irradiation. This can be either irreversible or reversible. A reversible system typically exhibits two forms which can be interconverted into each other by light irradiation with distinct wavelengths (Figure 1.2). Since light irradiation can be used to switch between two states of a material, these materials are also referred to as light switches. This effect is also known under the term photochromism.[11] Organic photochromic materials also include photoswitchable polymers. The development of photoswitchable polymers by introducing photoswitchable units into

polymers or biomacromolecules is the subject of intensive research.[12] The most prominent photoswitchable polymers exhibit *trans-cis* isomerization,[13] zwitterion formation[14] or ring opening/forming.[15] In response to light irradiation the chemical and physical properties of the polymers such as solubility,[16] phase behavior[17] or viscosity[18] are switched. Polymers have several advantages in contrast to other materials. Their properties can generally be easily adjusted by organic synthesis or post-synthesis modification. In addition, they are lightweight, easily processable and have good film-forming, thermal, and mechanical properties. These advantages are important for industrial purposes, but also allow studying the relationship between structure and properties. Photoresponsive polymers contain at least one photoresponsive unit. One of the most prominent examples of photoresponsive units is azobenzene. Due to its photochromic properties, azobenzene is found in many functional materials. Understanding the underlying physical concepts is crucial both for understanding the observed phenomena and for designing new azobenzene-based applications.

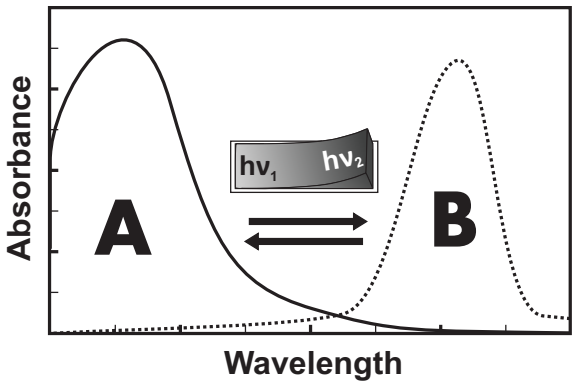


**Figure 1.2:** Typical absorption spectra of the forms A and B of a photochromic material. After the material is irradiated with light in the absorption range of A, it can be transformed to B. B has a different absorption band, that is used to switch it back to A. Thus, it can be switched between the two states with light, which is also called a light switch.

## Azobenzene

Azobenzene is an aromatic molecule with two phenyl rings linked together by an N=N (azo) bond. The $\pi$ conjugation leads to a strong absorption in the ultraviolet (UV) wavelength range (Figure 1.3). Azobenzene has an efficient and reversible photoisomerization. By absorbing light of a suitable wavelength, the thermodynamically stable, planar *trans* azobenzene isomer can transition into the bent *cis* isomer. Physical and spectroscopic changes go along with isomerization to the bent *cis* isomer. For example, the *cis* isomer has a different size and light

absorption. These changes in physical properties are exploited to use azobenzene as a photoresponsive molecule in smart materials.

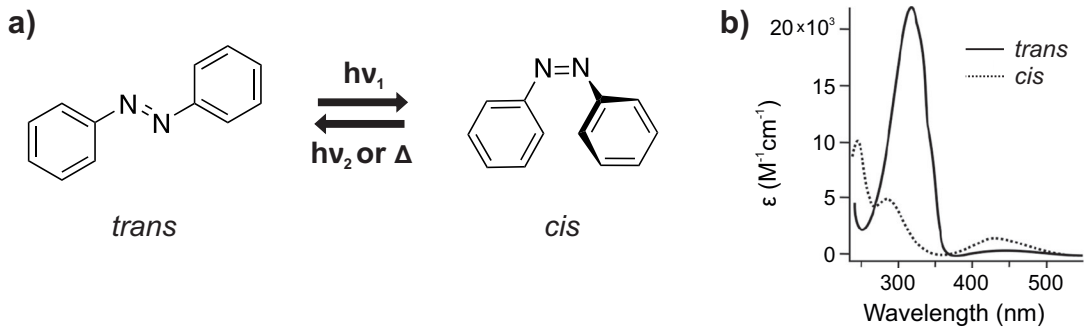


**Figure 1.3:** *Trans* and *cis* azobenzene. a) Chemical structures of *trans* and *cis* azobenzene. b) Asorption spectra of *trans* and *cis* azobenzene. Republished with permission of Royal Society of Chemistry, from Azobenzene photoswitches for biomolecules, Beharry, A. A.; Woolley, G. A. *Chemical Society Reviews* **2011**, *40*, 4422–4437; permission conveyed through Copyright Clearance Center, Inc.

By chemical modification, the azobenzene can be modified whereby substituents can be added to the azobenzene molecule and thus derivatives of azobenzene can be produced. If azobenzene needs to be covalently incorporated into a polymer, at least one substituent must always be introduced. However, chemical modification of azobenzene is always associated with changes in the spectral and photophysical properties of the resulting azobenzene.[19] That is why the molecular structure of the azobenzene and the bond to the polymer must be designed carefully.
If the *trans* isomer of azobenzene is irradiated with UV light, it can be transformed into the *cis* isomer. This photoisomerization changes the absorption spectrum of azobenzene (Figure 1.3). The strong $\pi$-$\pi^*$ band in the UV range becomes significantly weaker, while the weak n-$\pi^*$ band in the visible range becomes stronger. The back reaction from the *cis* into the *trans* isomer can be induced either by light of a suitable wavelength, typically visible light, or thermally.[20] Since the bands are broad and partly overlap, both isomerizations are often excited during irradiation (*trans*-to-*cis* and *cis*-to-*trans*). In the photostationary state (PSS), an equilibrium between *trans* and *cis* isomers is established. The PSS may be different for each wavelength used for irradiation. This depends on the one hand on the quantum yield of the photoisomerization reaction and on the other hand on the thermal half-life ($t_{1/2}$) of the metastable *cis* state (the time required for the amount of the metastable state to reduce to half its initial value and convert to the thermodynamically stable state).[19] Both in turn depend on the local environment as well as on the substitution of azobenzene. There are azobenzenes that can be switched almost completely from a *trans* to a *cis* state with light of one wavelength and from a *cis* to a *trans* state with light of another wavelength and there are

azobenzenes, which change constantly between the *trans* and *cis* state with light of one wavelength (see section 1.2). Both can be desired and used for certain different applications.

The quantum yield of a light-induced reaction describes how often a certain event happens per photon that is absorbed by the material. The photoisomerization quantum yield defines the efficiency of the photoisomerization. In the literature a lot of individual data can be found but two trends can be noticed: Firstly, the quantum yield of the *cis*-to-*trans* photoisomerization is higher than that of the *trans*-to-*cis* photoisomerization and secondly, the quantum yields, especially for the *trans*-to-*cis* photoisomerization, are higher if the n-$\pi^*$ star band is excited instead of the $\pi$-$\pi^*$ star band.[21]

In the dark at equilibrium, the *trans* isomer is the dominant species because it is energetically more stable than the *cis* isomer.[22] After absorbing a photon of appropriate energy, the *trans* form is converted from the ground state to the excited state. The molecule can then relax either to the *trans* isomer or to the metastable *cis* isomer, with higher energy than the *trans* isomer (Figure 1.4). Since the *trans* isomer absorbs more in the UV range than the *cis* isomer, the *cis* isomer is the resulting isomer after prolonged UV irradiation.

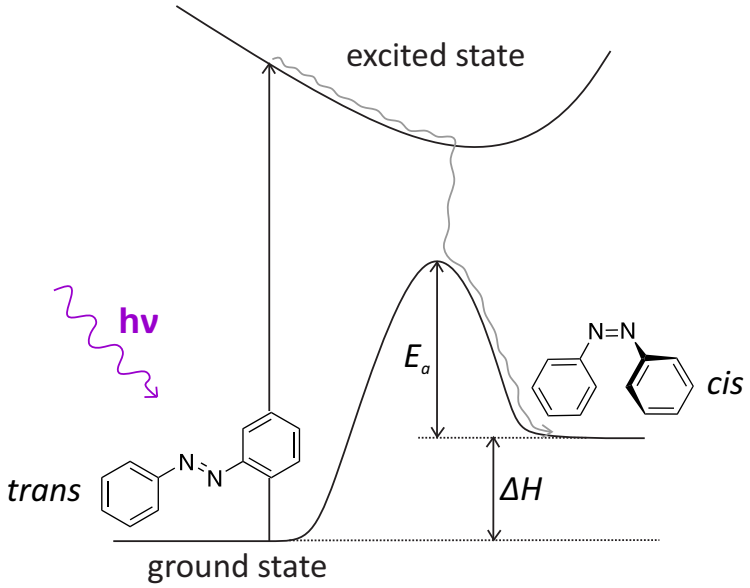


**Figure 1.4:** After absorbing a photon, the thermodynamically more stable *trans* form is excited and relaxes to the metastable *cis* form, with energy difference $\Delta H$ and activation energy $E_a$ between the *trans* and *cis* ground state. Redrawn with permission from Kolpak, A. M.; Grossman, J. C. *Nano Letters* **2011**, *11*, 3156–3162. Copyright 2011 American Chemical Society.

The energy difference of the *trans* and *cis* states of azobenzene derivates was exploited to store solar energy.[23] The thermodynamically more stable *trans* state absorbs light and is then transformed to the metastable *cis* state, which stores the

energy $\Delta H$. The activation energy $E_a$ is a thermal barrier, that hinders the *cis* state from switching back to *trans* under storage conditions. After the *cis* state is externally triggerd to switch back to the *trans* state, energy is released as heat. Next to small molecules[23,24], carbon nanotubes[25–27] and reduced graphene oxide[28–30], azobenzene containing polymers (azopolymers) were used as solar thermal fuels.[31] The utilization of azopolymers offers the possibility to easily modify the molecular structure to change properties like the stored energy density, optical chargeability and the PSS, and to collect photons over a large part of the solar irradiation spectrum. It was found that stacking of the planar azo groups leads to an increase of the energy-storage capacity of azo based solar thermal fuels.[25] Stacking of azobenzene molecules is because of strong intermolecular interactions with neighboring chromophores, due to the extended pi-system. In general, intermolecular interactions between chromophores lead to variations in their electronic transition energies. The details of the interactions and stacking of the chromophores depend on the molecular structure and the resulting physical properties of the chromophores.[32] For example, a spectral shift induced by aggregation was described by a molecular exciton model.[33] The excitonic coupling and therefore the spectral shift depends on the molecular structure and the angle between the chromophores. Strong aggregation between the planar chromophores prevents efficient photoisomerization. This has been demonstrated for example in densely packed monolayers[34] or solid films.[35] That is why photoisomerization is typically studied in diluted solutions. However, there are also studies demonstrating photoisomerization of small molecules in solid state, when the structure of the chromophores is well designed.[36] Azobenzenes incorporated in polymers show efficient photoisomerization also in solid state. In this case, the polymer matrix is like a solvent, which prevents chromophores from aggregating and gives them enough free volume to isomerize.[13] In a solid polymeric state the chromophores can have different environment because of the non-uniformity of the polymer chains which may effect the isomerization properties of the azobenzene chromophore. For example, the *cis* content in the PSS is typically lower in solid state than in solution, because the chromophores have enough free space to isomerize efficiently in solution but in the polymer steric hindrance in some parts may inhibit isomerization.[37] Chromophore–chromophore or chromophore-solvent and especially chromophore-polymer interactions are often neglected even though they can influence the isomerization behavior, which makes interpretation of results complicated. For example, interactions between the rod-shaped *trans* azobenzenes leads to liquid crystalline (LC) phases in many cases. The LC phases in azopolymers are stabilized by the rigid rod like *trans* azo group (Figure 1.5). The bent *cis* form of the azo group destabilizes the LC phase.

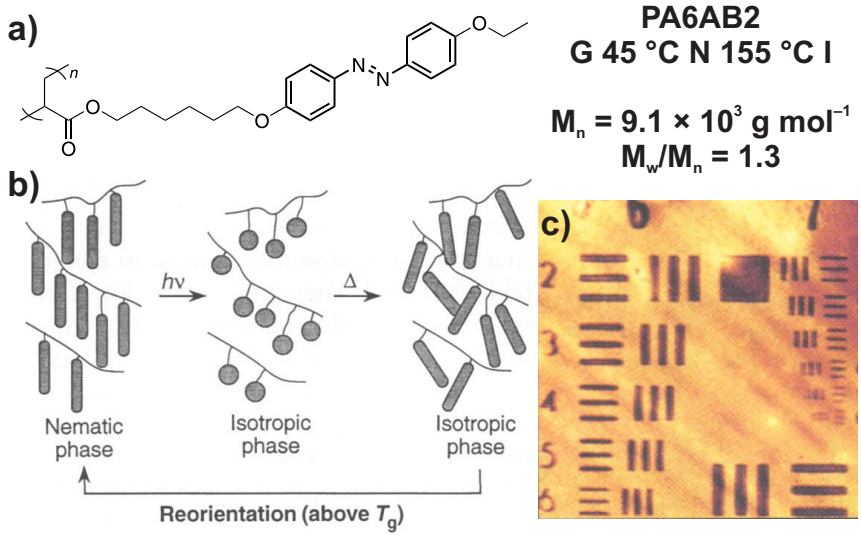


**Figure 1.5:** Photoinduced phase transition of an azopolymer. a) Structure and properties of the liquid crystalline side-chain azopolymer. b) Phase transition of the azopolymer. The *trans* azopolymer exhibits a nematic phase and can be transformed to an isotropic *cis* state by light irradiation. After the *cis* state transforms back to the *trans* state, it is still isotropic. Reorientation to the nematic phase happens after heating above the glass transition temperature ($T_g$). c) Inscribed pattern on the azopolymer film, which was stable up to eight months. From Ikeda, T.; Tsutsumi, O. *Science* **1995**, *268*, 1873–1875. Reprinted with permission from AAAS.

The Ikeda group exploited this phenomenon to demonstrate photoinduced LC to isotropic phase transitions of azopolymers.[38] An azopolymer with molecular weight of $9 \times 10^3$ g $mol^{-1}$ and polydispersity of 1.3 was used. The azopolymer had a glass transition temperature ($T_g$) at 45 °C, an LC phase between 45 °C and 155 °C and an isotropic phase above 155 °C. While the *trans* azopolymer had anisotropic LC phases, the *cis* azopolymer was isotropic. UV irradiation could switch the *trans* to the *cis* form and thereby the anisotropic state to the isotropic state. When a *trans* azopolymer film was irradiated with UV light through a mask, the area covered by the mask stayed in the *trans* LC phase and in the unconvered area the azopolymer switched to the *cis* form and lost its LC order to become isotropic. In this way, images were inscribed into the polymer film. These fabricated images were stable up to eight months. Many LC azopolymers exhibit photoinduced phase transitions that are used for photopatterning or data storage.

Another azopolymer application based on anisotropic phases is photoactuation (Figure 1.6). Photoactuators are made from photoresponsive elastomers. Liquid crystalline elastomers (LCEs) are crosslinked polymer networks which exhibit LC phases. If an azobenzene group is introduced inside the network, the film becomes photoresponsive. Due to *trans*-to-*cis* isomerization and subsequent distortion of the LC phase, the macroscopic shape of the polymer film changes. Light

irradiation induces bending,[39] twisting[40] or contraction[41] of photoactuators, depending on the LC orientation relative to the macroscopic shape of the film. Photoactuators are promising for energy conversion of sunlight and for future mechanical devices such as robotic grippers[42] or photoresponsive muscles.[43]

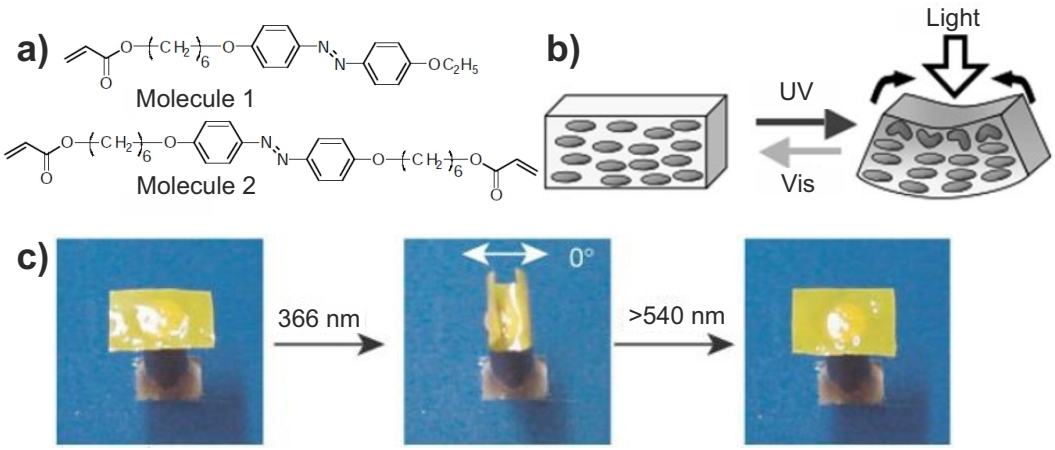


**Figure 1.6:** Photoresponsive LCE actuators made from azopolymers. a) Chemical structures of the LC monomer (molecule 1) and crosslinker (molecule 2) used to prepare the crosslinked azopolymer. b) Scheme of the photoinduced bending mechanism in the LC crosslinked azopolymer film. After UV light irradiation, the chromophores near the surface switch from *trans* to *cis* and therefore from anisotropic to isotropic order. The isotropic *cis* occupies less space and therefore the film bends. c) Photographs of the azopolymer film bending after light irradiation with 366 nm, and being flattened after visible light irradiation with wavelengths longer than 540 nm. The azopolymer film with dimensions of 4.5 mm × 3 mm × 7 $\mu$m is fixed on a 85 °C copper plate to control the temperature of the film. a) and c) adapted by permission from Springer Nature, Photomechanics: Directed bending of a polymer film by light, Yu, Y.; Nakano, M.; Ikeda, T. *Nature* **2003**, *425*, 145–145, Copyright 2006. b) Adapted with permission from Kondo, M.; Yu, Y.; Ikeda, T. *Angewandte Chemie International Edition* **2006**, *45*, 1378–1382. Copyright 2006 John Wiley and Sons.

The most prominent architecture of azopolymers is the side chain polymer structure (homopolymer,[44] copolymers[45] or crosslinked polymers[46]) but a variety of azopolymers with architectures like main-chain polymers,[47] telechelic polymers,[48] supramolecular polymers,[49] hyperbranched polymers[50] or dendrimers[51] have been realized. Thus, light-responsive micellar aggregates,[45] photoshrinkable rigid polymer rods,[47] cloud point shifts,[48] photoinduced birefringence[49] and surface relief gratings (SRGs) formation[51] have been achieved.

## 1.2 Red-Shifted Absorption of Azobenzene-Containing Polymers

*Trans*-to-*cis* photoisomerization of photoswitchable macromolecules, such as azopolymers and azo functionalized biomacromolecules is typically induced by UV light. However, UV light has some drawbacks for biomedical and solar energy applications, such as low penetrability to human tissue, high energy and therefore damage, and it only covers a small portion of sunlight. There are some strategies to red-shift the absorption spectrum of azopolymers, but some challenges prevent applications of red-shifted azopolymers.[52]

### Azobenzene Substitution

Red-shifted azopolymers can be realized by introducing substituents to the azo groups incorporated in the polymer. How the substitution influences the absorption will be described in the following. Based on the relative energetic order of the $\pi$-$\pi^*$ and n-$\pi^*$ states, Rau divided azobenzenes into three types: azobenzene type, aminoazobenzene type, and pseudo stilbene type (Figure 1.7).[53]

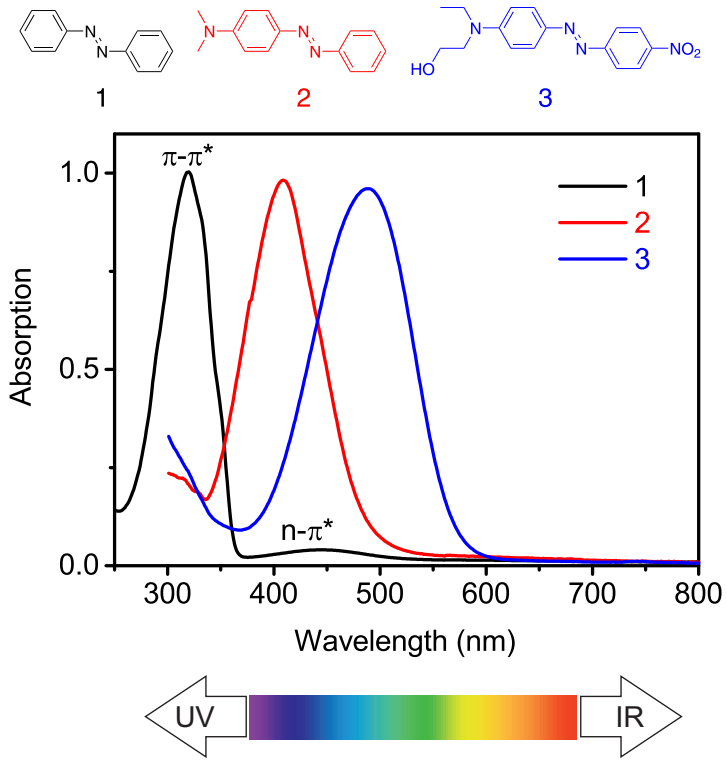


**Figure 1.7:** Structures and spectra of typical examples for azobenzene type (**1**), aminoazobenzene type (**2**) and pseudo stilbene type (**3**) molecules. Adapted with permission from Weis, P.; Tian, W.; Wu, S. *Chemistry – A European Journal* **2018**, *24*, 6494–6505. Copyright 2018 John Wiley and Sons.

Azobenzene type molecules have two well separated absorption bands: a high intensity $\pi$-$\pi^*$ band in the UV-region and a low intensity n-$\pi^*$ in the visible region. The non-substituted azobenzene is the model compound of the azobenzene type group and typically, alkyl, aryl, halide, carbonyl, amide, nitrile, ester and carboxylic acid substituted azobenzenes also belong to this type.[19,53] *Trans*-to-*cis* photoisomerization of azobenzene type molecules is induced by UV light. *Cis*-to-*trans* isomerization is either induced by visible light, because the *cis* isomer has a stronger n-$\pi^*$ band in the visible range, or by heat, because with minor exceptions the *trans* isomer is thermodynamically more stable than the *cis* isomer. One exception is a bridged azobenzene, where due to the ring strain the *cis* isomer is the thermodynamically more stable isomer at room temperature.[54] The n-$\pi^*$ absorption bands are located in the visible light region and are well separated, which enables photoswitching in both directions (*trans*-to-*cis* and *cis*-to-*trans*) with high yields. Incorporated into a peptide, a bridged azobenzene was used to switch the conformation of the biopolymer by visible light irradiation: The *cis* azo peptide forms a coil while the *trans* azo peptide forms a helix (Figure 1.8).[55] The *cis* and *trans* isomers can be distinguished because the chiroptical properties of chiral photochromic compounds, like circular dichroism (CD) spectra, change reversibly.[56] Bridged azobenzenes with hetero atoms have even more red-shifted absorption bands (Figure 1.13).[57] Additionally, these so called heterodiazocines provide high switching efficiencies and quantum yields.

Aminoazobenzene type molecules like Methyl Yellow (**2** in Figure 1.7) have a red-shifted $\pi$-$\pi^*$ band which partly overlaps with the n-$\pi^*$ band. The overlapping bands make it complicated to separately control *trans*-to-*cis* or *cis*-to-*trans* photoisomerization but the spectral overlap is well suited to induce *trans-cis-trans* cycling with a wavelength in the overlap region. Azobenzenes that have at least one amino or hydroxyl group in *ortho* (*o*) or *para* (*p*) position relative to the azo bridge are aminoazobenzene type molecules.[19]

Aminoazobenzene type polymers are visible light-responsive polymers and have been used to induce orientation of azo groups in a polymer film by using polarized blue light[58] and to elongate spherical aggregates of blockcopolymers containing aminoazobenzene sidechains by linearly polarized blue light (Figure 1.9).[59]

Pseudo stilbene type azobenzenes like Disperse Red 1 (**3** in Figure 1.7) have long wavelength $\pi$-$\pi^*$ bands. Both the $\pi$-$\pi^*$ band and the n-$\pi^*$ band are in the visible light region and have similar energy. Pseudo stilbene type molecules are protonated azobenzenes or have a push-pull substitution. Push-pull molecules have both electron donating and withdrawing substituents.[19]

Even though this type of substitution can red-shift the absorption, there is a reason why this kind of azobenzene cannot be used as a stable, red-shifted light

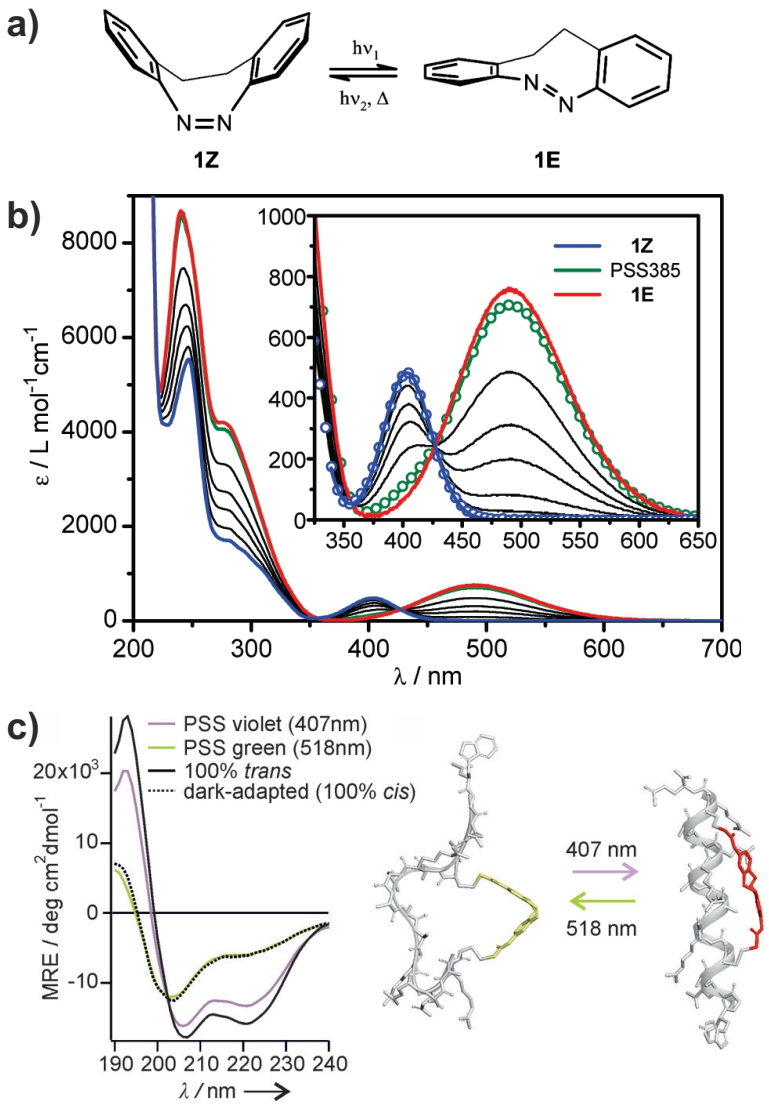


**Figure 1.8:** a) Chemical structure and b) absorption spectra of the *cis* (Z) and *trans* (E) isomers of a bridged azobenzene. c) CD spectra of the bridged azo crosslinked peptide dark adapted, at 100 % *trans* state and at PSS after irradiation with 407 nm or 518 nm light. a) and b) reprinted with permission from Siewertsen, R.; Neumann, H.; Buchheim-Stehn, B.; Herges, R.; Näther, C.; Renth, F.; Temps, F. *Journal of the American Chemical Society* **2009**, *131*, 15594–15595. Copyright 2009 American Chemical Society. c) Adapted with permission from Samanta, S.; Qin, C.; Lough, A. J.; Woolley, G. A. *Angewandte Chemie International Edition* **2012**, *51*, 6452–6455. Copyright 2012 John Wiley and Sons.

switch: The *cis* isomers have short half-lifes and visible light irradiation at the overlapping absorption band of the *trans* and *cis* isomers induces a simultaneous *trans*-to-*cis* and *cis*-to-*trans* isomerization. The rate of the thermal *cis*-to-*trans* isomerization strongly depends on the substituents of azobenzene and the typical half-lifes decrease to minutes, seconds or shorter while the absorption shifts to longer wavelenghts.[53] This makes it impossible to obtain high percentages of the *cis* isomer for long periods of time and makes these molecules useless for visible

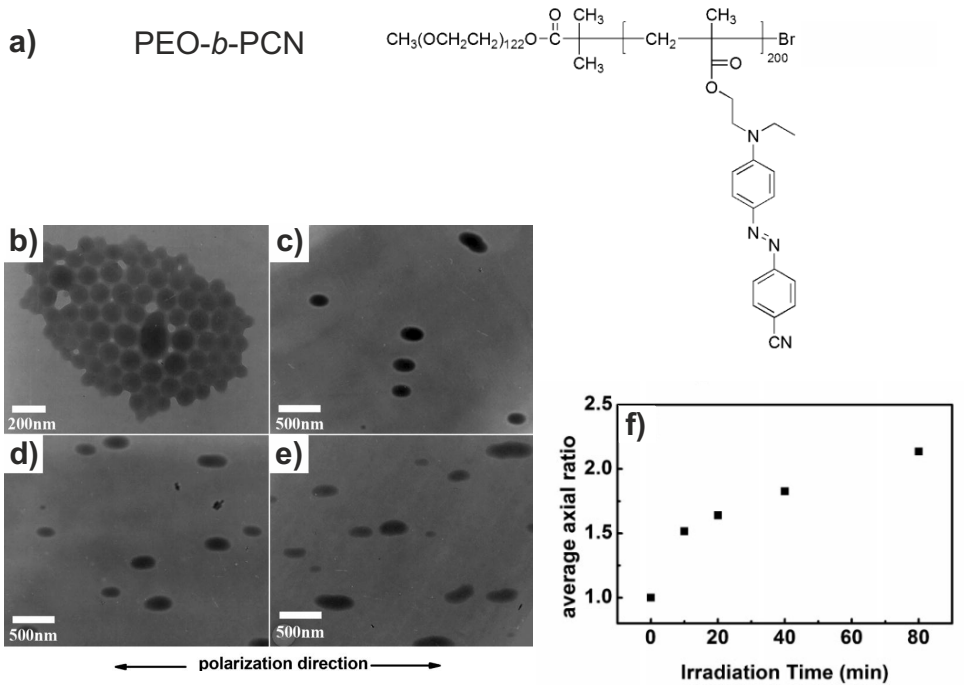


**Figure 1.9:** a) Structure of the aminoazobenzene containing amphiphilic diblock copolymer PEO-*b*-PCN and TEM images of the aggregates b) before and after c) 10, d) 40, and e) 80 min of blue light irradiation. f) Average axial ratio (length/diameter) of the aggregates plotted against the irradiation time. Adapted with permission from Wang, D.; Ye, G.; Wang, X. *Macromolecular Rapid Communications* **2007**, *28*, 2237–2243. Copyright 2007 John Wiley and Sons.

light-responsive applications, which require stable, high percentage *cis* isomer amounts.

These azobenzenes have nevertheless their place of existence: Thousands of azo compounds exist and are used as dyes, which historically is the most common use of azobenzenes. Some of them absorb red and even near-infrared (NIR) light.[60] In a dye, color fastness is desired, that is why long-lived *cis*-isomers and photochromism were undesired and tried to omit in the past. For this reason there is less research about the photochromism of many dyes, but since they are push-pull type molecules, it is likely that they have short-lived *cis* isomers and photoisomerization may be difficult to observe.[61] However, pseudo stilbene type azobenzenes are exploited for photoinduced orientation and photoinduced surface relief gratings below $T_g$ of the polymers.[62–64] For example, a 514 nm laser was used to inscribe SRGs in a poly(4[2-(acryloyloxy)thel]ethyl-amino-4-nitroazobenzene) (pDR1A) film (Figure 1.10). The surface relief gratings were investigated by atomic force microscopy (AFM). For these applications it is necessary to generate many *trans-cis-trans* cycles with one wavelength in a short time, which is possible for many azobenzene, aminoazobenzene and pseudo stilbene type molecules because the absorption bands of the *trans* and *cis* isomer overlap

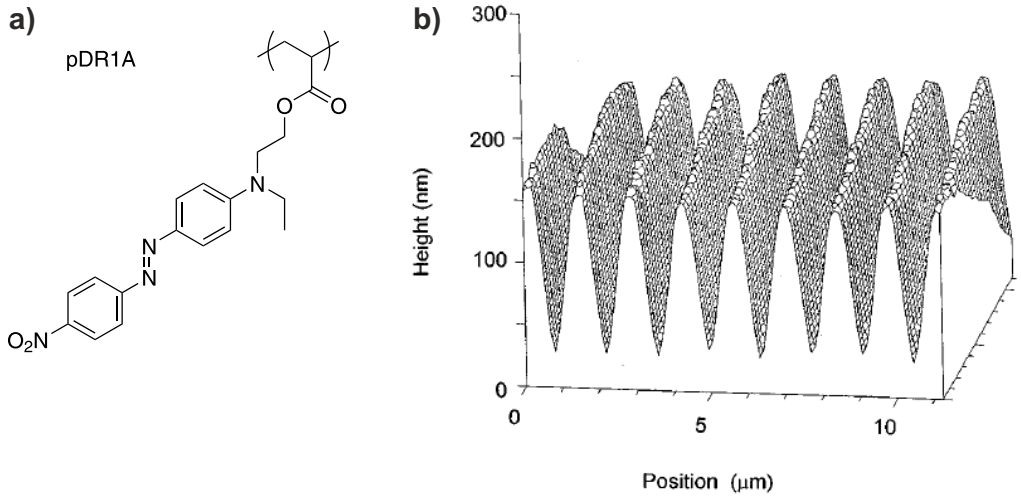


**Figure 1.10:** a) Structure of the pseudo stilbene containing polymer pDR1A and b) AFM surface profile of an SRG demonstrating sinusoidal variation of the height. Reprinted from Rochon, P.; Batalla, E.; Natansohn, A. *Applied Physics Letters* **1995**, *66*, 136–138, with the permission of AIP Publishing.

to a certain amount. However, for applications where high switching ratios and red-shifted absorption of azopolymers is needed another route is chosen. The key to visible light switching ratio performance is separating the absorption bands of both *trans* and *cis* isomers. Only then high ratios of either of the two isomers can be achieved and the two isomers can be reliably switched back and forth.

Recently, the Woolley group demonstrated that azobenzenes substituted with halogens or methoxy groups at all four *o* positions with respect to the azo bridge leads to red-shifted absorption and at the same time separation of the n-$\pi^*$ absorption bands of the *trans* and *cis* isomers.[65] The distortion of the *o*-substituted azobenzene and the repulsive interactions of the n-orbitals with the oxygen atoms' relatively high-energy lone pair orbitals increase the energy level of all orbitals, which leads to the separation. By exciting the n-$\pi^*$ band with green or red light irradiation *trans*-to-*cis* isomerization is induced. The reverse *cis*-to-*trans* isomerization can be triggered by irradiation of the n-$\pi^*$ band of the *cis* isomer with blue light. Later, the same group crosslinked peptides with tetra-*o*-substituted azobenzenes to photocontrol the molecular structure and function with red light.[66] The red light switching between the *trans* and *cis* isomers with different end-to-end distances induced a decrease in helix content (Figure 1.11). This enables photoswitching without the use of UV light, which is necessary for biological applications. Indeed fluorescence switching by red light irradiation was demonstrated *in vivo*. Additionally, a random copolymer of poly acrylic acid and an acrylic ester sidechain with tetra-*o*-substituted azobenzene (PTAPA) self-assembled into nanoparticles in water due to its amphiphilic structure. The micellar nanoparti-

cles could be filled with a fluorescent dye. After green light irradiation, a change in fluorescence occurred along with *trans*-to-*cis* isomerization verified by a change in absoprtion. The dye's fluorescence is known to be strongly influenced by the polarity of its environment. Although green light irradiation did not lead to dissociation or disassembly of nanoparticles and no release of the dye occurred, fluorescence was controlled after irradiation and could be restored after blue irradiation.[67] Tetra-*o*-methoxy-substituted azobenzene was also used to prepare a red light-responsive supramolecular hydrogel, where the azo chromophores in the side chain of a poly acrylic acid copolymer (PAA-mAzo) act as the guest and the $\beta$-cyclodextrin ($\beta$-CD) functionalized poly acrylic acid copolymer (PAA-$\beta$-CD) acts as the host.[68] Since tetra-*o*-methoxy-substituted azobenzene is a larger molecule than azobenzene, ($\beta$-CD) was used as the host, as the mAzo-$\beta$-CD-complex has a higher association constant than the mAzo-$\alpha$-CD-complex. In contrast, the association constant of the azobenzene-$\alpha$-CD is larger than the association constant of azobenzene-$\beta$-CD. The supramolecular hydrogel showed reversible sol–gel transitions under red and blue light respectively and was used for controlled protein release. The hydrogel was loaded with a protein which was released when the protein-loaded supramolecular hydrogel was irradiated with red light (Figure 1.11). This concept can be further expanded and even more space-consuming groups need a larger host molecule. Recently, a tetra-*o*-isopropoxy-substituted azobenzene (ipAzo) was synthesized.[69] ipAzo has similar absorption to other tetra-*o*-substituted azobenzene, namely a n-$\pi^*$ absorption band that has absorption up to the red light region. The bulky isopropyl groups make ipAzo a large molecule, that can form complexes with $\gamma$-CD, which has an even larger cavity than $\beta$-CD.[70] ipAzo has not yet been introduced to polymers, but the concept can be easily transfered.

While the tetra-*o*-substituted azobenzene structures mentioned above are distorted around the azo bond due to the bulky substituents, tetra-*o*-fluoro-substituted azobenzenes have no strongly distorted structure, because of the small radius of the fluoro substituents.[71] For many applications it may be advantageous to have a planar structure, similar to the original azobenzene structure, for example when chromophore stacking is necessary as in LC polymers. The n-$\pi^*$ absorption bands are well separated, enabling selective excitation of both isomers in the visible light region. Additionally, the *cis* isomer of *o*-fluoro-substituted azobenzenes have half-lifes up to two years at room temperature. The long half-life times of *o*-fluoro-substituted azobenzenes were exploited to prepare shape persistent LC polymer networks.[72] In order to preserve the photo-activated bending of the polymer film on a macroscopic scale, thermal stability as well as cross linking density are important parameters.[71] Tetra-*o*-fluoro-substituted azopoly-

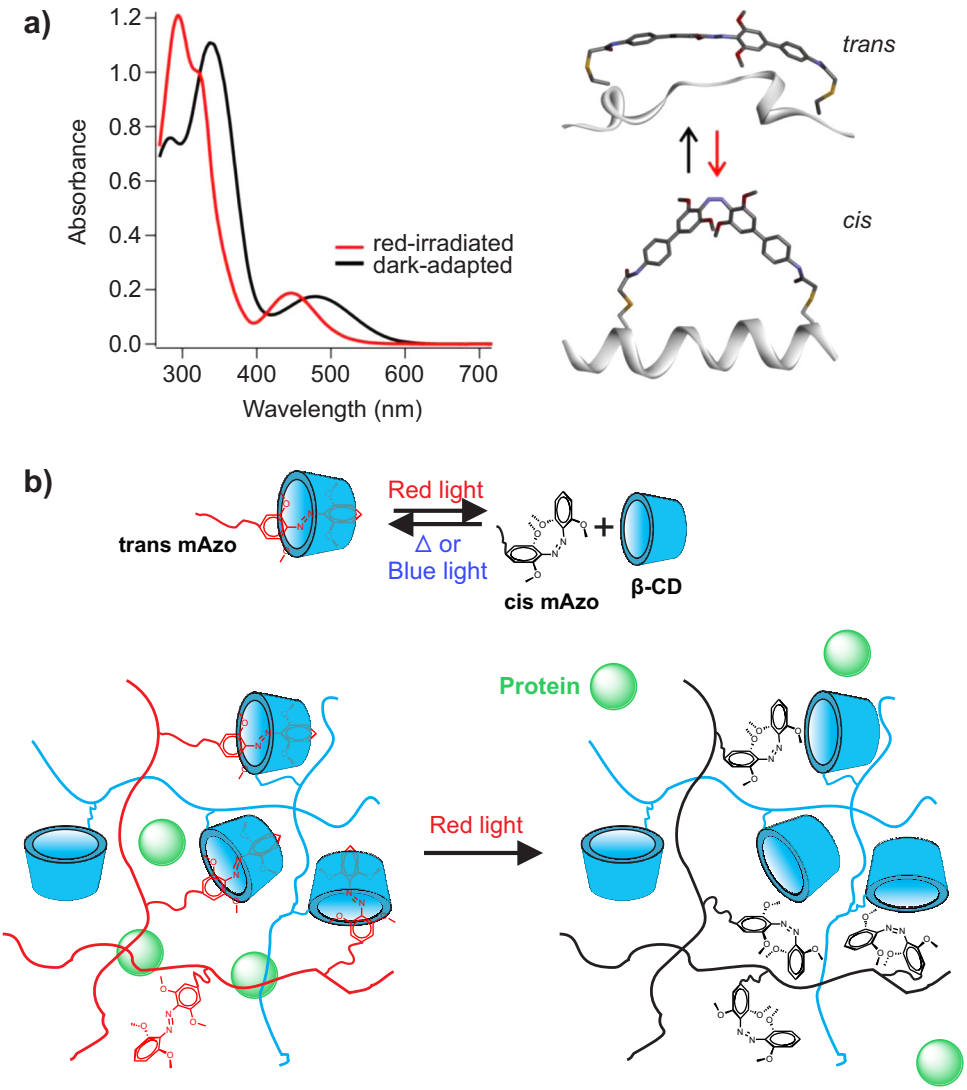


**Figure 1.11:** Polymers with tetra-*o*-substituted azobenzenes. a) Red light photoswitching a crosslinked peptide *in vivo*. Spectra of red-irradiated and dark-adapted crosslinked peptides as well as switching concept between a helical and coiled form. b) Red light-controlled protein release from a tetra-*o*-methoxy-substituted azopolymer-$\beta$-CD supramolecular hydrogel. a) Adapted with permission from Samanta, S.; Beharry, A. A.; Sadovski, O.; McCormick, T. M.; Babalhavaeji, A.; Tropepe, V.; Woolley, G. A. *Journal of the American Chemical Society* **2013**, *135*, 9777–9784. Copyright 2013 American Chemical Society. b) Adapted with permission from Wang, D.; Wagner, M.; Butt, H.-J.; Wu, S. *Soft Matter* **2015**, *11*, 7656–7662. Published by The Royal Society of Chemistry.

mers were also used to reversibly control the mechanical properties of hydrogels by green and blue light (Figure 1.12).[73] The reversibly phototunable elasticity of the hydrogel was attributed to the disruption of physical crosslinks between chromophores upon isomerization. In addition, a sun light-driven polymer film was prepared using an *o*-fluoro-substituted azo crosslinker.[74] The polymer film with LC structure showed chaotic oscillatory motion when exposed to ambient

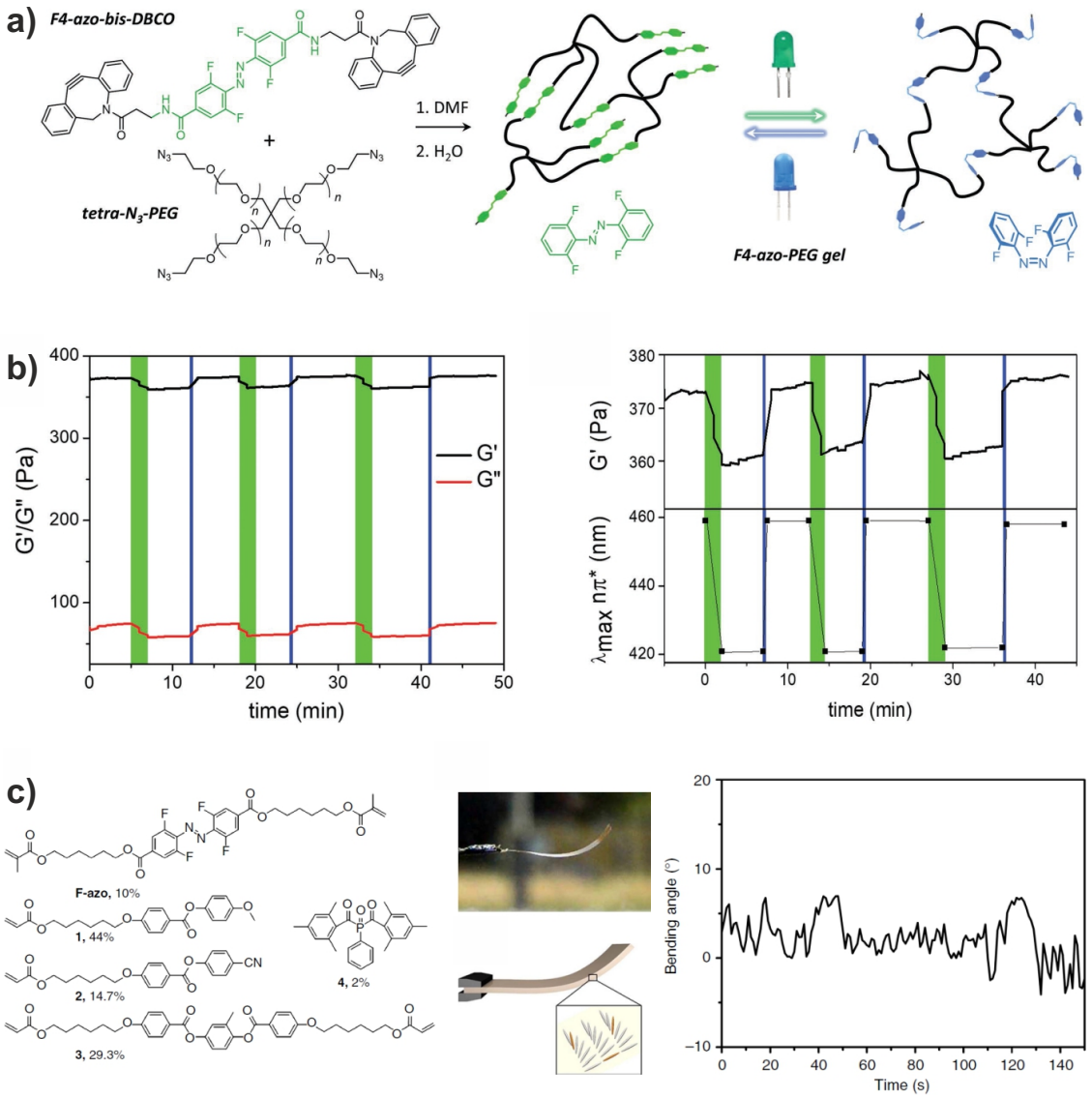


**Figure 1.12:** a) Design and photoresponsive change of a tetra-*o*-fluoro-substituted azobenzene modified hydrogel (F4-azo-PEG gel). b) Cyclic changes of G′ and G″ of F4-azo-PEG gel under alternating green and blue LED irradiation (left). Zoomed-in G′ data and corresponding maximum absorption wavelength at the same time period under alternating green and blue LED irradiation, demonstrating the synchronicity of G′ and photoisomerization (right). c) Components of the oscillating LC azopolymer film containing *o*-fluoro-substituted azobenzenes (left). Photograph and schematic of the film after removal from the LC cell (middle). Plot of deflection angle as a function of time under solar simulator light exposure (right). a) and b) adapted with permission from Zhao, F.; Bonasera, A.; Nöchel, U.; Behl, M.; Bléger, D. *Macromolecular Rapid Communications* **2018**, *39*, 1700527. Copyright 2017 John Wiley and Sons. c) Adapted with permission from Kumar, K.; Knie, C.; Bléger, D.; Peletier, M. A.; Friedrich, H.; Hecht, S.; Broer, D. J.; Debije, M. G.; Schenning, A. P. H. J. *Nature Communications* **2016**, *7*, 11975. Copyright 2016 Nature Publishing Group.

sunlight and therefore can harvest and convert solar energy (Figure 1.12). When irradiated with only blue or green light, a bending rather than oscillation is ob-

served, which means the observation of a chaotic oscillatory motion should not be due to the *cis–trans* ratio alone and therefore not only be a thermodynamic effect. Only under irradiation of both wavelengths (e.g. sunlight or simultaneous green and blue light LED irradiation) oscillation is observed. The chaotic oscillation is not yet completely understood, but a combination of many effects could lead to this behavior, making it difficult to reveal the single effects.[74]

The implementation of new, low molecular weight azobenzene compounds in polymers is an easy way to create new visible or NIR light sensitive azopolymers. However, it should be kept in mind that molecular structures that are different to the original azobenzene molecule might have different properties apart from the absorption. Especially solid state properties like chromophore stacking might be different. In addition to the already mentioned structures, there are several visible or NIR light sensitive azobenzenes that have been reported as low molecular weight compounds but have not yet been implemented into polymers (Figure 1.13). For example, other existing *o*-substituted azobenzenes with red-shifted absorption spectra such as ipAzo,[69] protonated tetra-*o*-methoxy[75], tetra-*o*-thioether[76] or *ortho-meta* arrangement of methoxy groups[77,78] have not yet been used for visible light-responsive azopolymers. Similar to mAzo, the concept can be easily transfered and they can be inserted into polymer structures. In this way the resistance to biological environment or absorption spectra can be tuned. Likewise, $BF_2$ complexed azo compounds are visible or NIR light-responsive azobenzenes.[79,80] They have well separated *trans* and *cis* absorption bands and their *cis* isomers have relatively long half-lifes (up to half a day[79]). Their high quantum yields and stability against reduction by glutathione making them interesting candidates for biological applications. Another structure, with a half-life of 27 h in acetonitrile at 54°C, is an azopyridine functionalized Ni-porphyrin.[81] The molecule shows a reversible light-induced magnetic switching, which is based on a large geometry change that controls the coordination of the metal ion. A different azobenzene that is connected to a metal complex is the green light-responsive ferrocenylazobenzene (FcAB).[82] What distinguishes this molecule from others is that a single light source can be used to switch between the *trans* and *cis* states, depending on the oxidation state of the iron center. Fe(II) FcAB is switched from *trans* to *cis* by the same green light as Fe(III) FcAB is switched from *cis* to *trans*, because the Fe(III) state is lacking an electronic state which is existent in the Fe(II) form and enables the switching. Finally, there are several other light switches which do not contain azobenzene but absorb in the visible or NIR light range. This would go beyond the scope of this thesis and is therefore not discussed here.

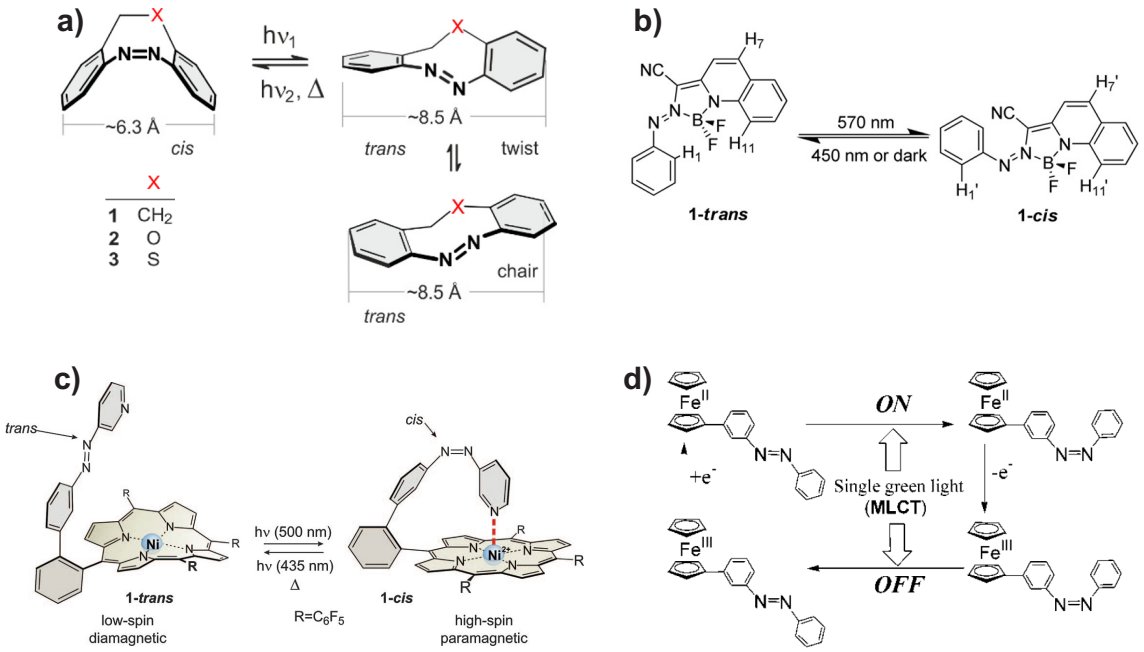


**Figure 1.13:** Visible or NIR light-responsive azobenzene small molecules that have not yet been implemented into polymers. a) Heterodiazocines with different heteroatoms show photoinduced *trans-cis* isomerization. b) $BF_2$ complexed azo compounds with visible light-responsive isomerization. c) Azopyridine functionalized Ni-porphyrin with large geometry change after photoisomerization. d) Single wavelength light-responsive ferrocenylazobenzene. a) Adapted with permission from Hammerich, M.; Schütt, C.; Stähler, C.; Lentes, P.; Röhricht, F.; Höppner, R.; Herges, R. *Journal of the American Chemical Society* **2016**, *138*, 13111–13114. Copyright 2016 American Chemical Society. b) Adapted with permission from Yang, Y.; Hughes, R. P.; Aprahamian, I. *Journal of the American Chemical Society* **2012**, *134*, 15221–15224. Copyright 2012 American Chemical Society. c) From Venkataramani, S.; Jana, U.; Dommaschk, M.; Sönnichsen, F. D.; Tuczek, F.; Herges, R. *Science* **2011**, *331*, 445–448. Reprinted with permission from AAAS. d) Reprinted with permission from Kurihara, M.; Hirooka, A.; Kume, S.; Sugimoto, M.; Nishihara, H. *Journal of the American Chemical Society* **2002**, *124*, 8800–8801. Copyright 2002 American Chemical Society.

## Nonlinear Optical Processes

While direct methods like chemically modifying azobenzene to red-shift the absorption wavelength of azobenzene was explained in the previous section, the following section will introduce indirect methods that do not alter the chemical structure but modify the utilized light, like upconversion processes or two-photon absorption. The sequential absorption of two or more photons with subsequent emission of light with a wavelength shorter than the excitation wavelength is called photon upconversion. Inorganic nanoparticles (NPs) which convert long wavelength light to shorter wavelength light through photon upconversion are called upconverting nanoparticles (UCNPs). Lanthanide-doped UCNPs have

been developed to convert NIR light to visible or UV light, which can then be utilized to induce photoisomerization of photoresponsive molecules.[83] UCNPs, that convert NIR light to blue light, were incorporated into LCEs containing azotolane groups.[84] The azotolane that was used absorbs blue light. NIR light irradiation of UCNP containing LCE films induced bending of the film. The film returned to its original state, after the light was switched off (Figure 1.14).

Red light was also used to actuate an LCE film.[85] A blue light-responsive LCE azopolymer film was assembled with a triplet-triplet annihilation upconversion (TTA-UC) system which converted red light to blue light. After red light irradiation, the LCE film bent because the upconverted blue light induced photoisomerization of the azo groups (Figure 1.14). TTA-UC is a different type of upconversion. A photosensitizer and an annihilator are included in a typical TTA-UC system. After absorption of a photon, the photosensitizer is excited to a singlet state from which it relaxes to a triplet state. From the triplet state the energy is transfered to the annihilator to excite the annihilator to a triplet state. Two annihilator molecules in triplet states are then converted into a ground state and a singlet state molecule. The singlet state annihilator relaxes to the ground state while emitting an upconverted photon.[86] Platinum(II) tetraphenyltetrabenzoporphyrin was used as the photosensitizer and 9,10-bis(diphenylphosphoryl)anthracene was the annihilator in the TTA-UC system. The better tissue penetrability of red light compared to UV light was demonstrated by passing the light through a piece of tissue to induce bending of the LCE film.

Two-photon absorption is the absorption of two photons to excite a molecule from a lower energy state to a higher energy state and is another process that has been used to isomerize azopolymers using long wavelength light.[87] The sum of the energy of the two absorbed photons is equal to the energy difference between the two states. Thus, two long wavelength light photons can induce photoisomerization of UV light-responsive azopolymers. For example, a pulsed laser with 800 nm wavelength was used to write diffraction gratings on an azopolymer film which has an absorption band around 500 nm.[87] The advantage of two-photon absorption lies in its high spatial resolution, since photoisomerization only occurs at the laser focus. This technique was used to write patterns below 250 nm into the polymer film, which is below the half-wavelength diffraction limit of the laser beam (Figure 1.14).[87] However, two-photon absorption requires high intensities and is typically less efficient than one photon absorption.[88,89] It is a local process that is not intended for macroscopic samples.

Additionally, the high intensity light that is needed in nonlinear optical processes may damage materials or human skin. This may limit possible applications of red-shifted photoswitching of azopolymers based on nonlinear processes. Only

when upconversion and energy transfer efficiencies are enhanced, this path may be suitable for future applications.[52]

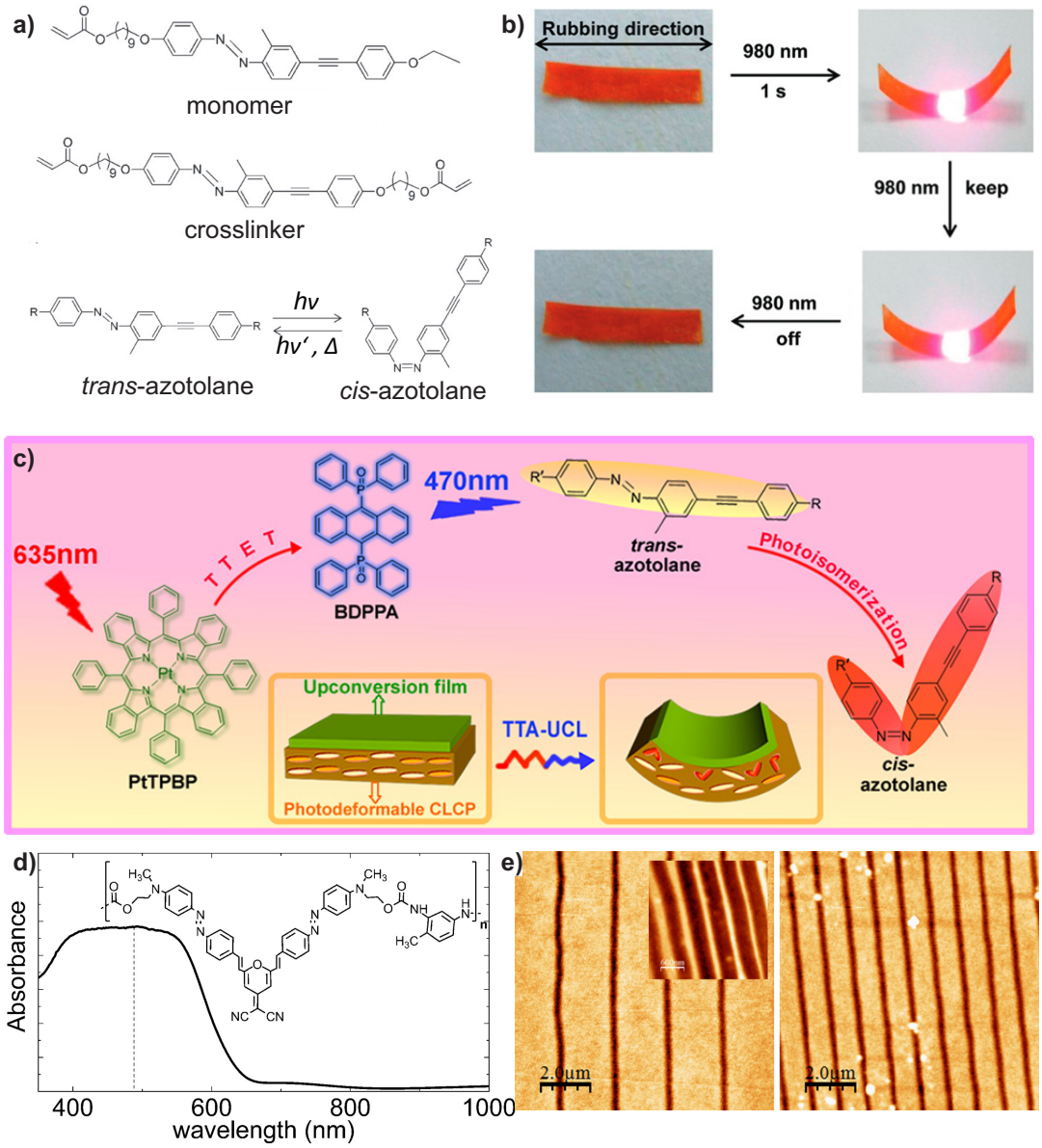


**Figure 1.14:** Nonlinear optical processes used to induce photoisomerization by long wavelength light irradiation. a) NIR light-induced photoisomerization and bending of an azopolymer free standing film assisted by UCNPs. Molecular structure of the monomer and the crosslinker to prepare the polymer film. b) NIR light-induced bending of the azobenzene and UCNP containing polymer film. c) Red light-induced photoisomerization and bending of an azopolymer free standing film assisted by TTA UC. Molecular structure of the photosensitizer, annihilator and azotolane to construct the polymer film. Red light is upconverted to blue light which induces isomerization and bending of the polymer film. d) Two-photon absorption used for NIR photoswitching of an azopolymer film. Absorption spectrum and molecular structure of the used polymer. e) AFM images of gratings induced by two-photon absorption. The inset shows 500 nm gratings on the polymer film. a) and b) Reprinted with permission from Jiang, Z.; Xu, M.; Li, F.; Yu, Y. *Journal of the American Chemical Society* **2013**, *135*, 16446–16453. Copyright 2011 American Chemical Society. c) Reprinted with permission from Jiang, Z.; Xu, M.; Li, F.; Yu, Y. *Journal of the American Chemical Society* **2013**, *135*. Copyright 2013 American Chemical Society. d) and e) reprinted from Li, Y.; He, Y.; Tong, X.; Wang, X. *Journal of the American Chemical Society* **2005**, *127*, 2402–2403, with the permission of AIP Publishing.

## 1.3 Photoinduced Liquefaction of Azobenzene-Containing Materials

Light can transform solid azobenzene materials to liquids based on photoisomerization. Different types of photoinduced liquid-to-solid transition of azobenzene materials have previously been described in literature: The first is the switching between two states (*trans* and *cis*) of a compound having different melting points ($T_m$'s), which causes a reversible transition from solid to liquid. The second ist the flowing of solid azobenzene materials along the light polarization direction, known as directional photofluidization.[90] It is well known that a material is solid if the temperature is below its $T_m$, and liquid if the temperature is above its $T_m$. The $T_m$ of a substance depends strongly on its chemical structure. For example, oleic acid and elaidic acid have almost the same structure. They are both carboxylic acids with an 18 carbon chain. Both have a double bond between the nineth and tenth carbon. The only difference is the *cis* or *trans* double bond configuration in the long carbon chain. This small difference leads to a $T_m$ difference of more than 30 °C.[91] Because oleic acids $T_m$ is below, and elaidic acids $T_m$ is above room temperature, oleic acid is a liquid and elaidic acid is a solid at room temperature (Figure 1.15). Oleic acid and elaidic acid cannot be easily transfered into each other.

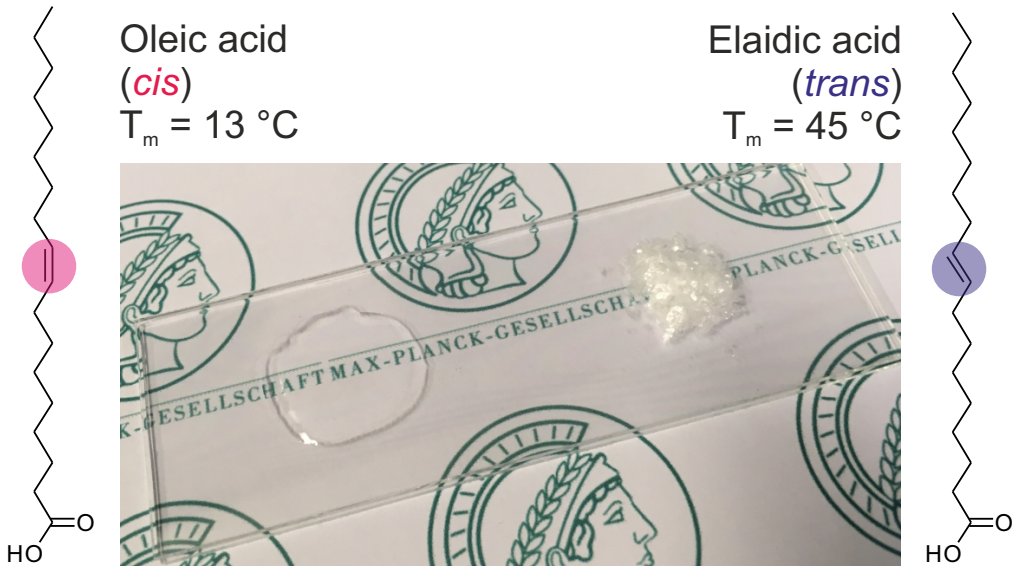


**Figure 1.15:** Molecular structures and $T_m$'s of oleic acid (left) and elaidic acid (right). The molecular structures of oleic and elaidic acid only differ in the *cis* and *trans* configuration of the double bond. The $T_m$'s of oleic acid and elaidic acid have a difference of 30 °C. Oleic acids $T_m$ is below and elaidic acids $T_m$ is above room temperature, which explains why oleic acid is liquid and elaidic acid is solid at room temperature.

## Reversible Solid-to-Liquid Transition of Azobenzene Derivatives

In 1937, when Hartley discovered the photoisomerization of azobenzene,[92] he recognized that the *trans* and *cis* forms of azobenzene have different $T_m$'s. A few years later, the $T_m$'s of *trans* and *cis* chloro azobenzene were found to have a difference of ~60 °C.[93] If one of the *trans* and *cis* azobenzene $T_m$'s is above the surrounding temperature and the other $T_m$ is below the surrounding temperature (and photoisomerization is possible), light irradiation can induce a reversible, isothermic solid-to-liquid transition which is based on photoisomerization.
In 2012 two groups synthesized independently from each other azobenzene small molecules and demonstrated they can use light irradiation to switch between a solid *trans* state and a liquid *cis* state (Figure 1.16).[94,95] In both works substituents were used to modify the azobenzene molecule which results in two effects: Firstly, the packing of molecules is decreased because of long chains, which leads to more space between the chromophores to isomerize in the solid state and thus making photoisomerization in the solid state possible. Secondly, the phase transition temperatures are decreased. In this way a solid-to-liquid transition at room temperature is made possible, because one $T_m$ is above and one is below room temperature.
In Akiyama's work, multi azo substituted sugar derivatives were liquefied isothermally.[95] By UV light irradiation the solid transformed into a liquid at room temperature. The liquid could then be transformed into a solid by visible light irradiation. The solid-to-liquid transition was reversible and could be repeated in a cycle. Three characteristics, that azobenzene compounds need to exhibit for a photoinduced solid-to-liquid transition at room temperature, were mentioned:

1. a molecular weight in the range of a few thousand Daltons
2. the azo chromophores are hemmed in a molecular center
3. a homogeneous, monodisperse structure

All points speak against azopolymers to exhibit a photoinduced solid-to-liquid transition at room temperature, because polymers are chains that have polydisperse high molecular weights.
In Okui's work, a crystalline *trans* azo compound with a $T_m$ of 50 °C turns into a liquid under UV light irradiation at room temperature.[94] The underlying principle of the photoinduced solid-to-liquid transition was not investigated in this study. The photoinduced solid-to-liquid transition of a similar azo compound was investigated by X-ray diffraction analysis of crystalline structures.[96] The transition of the azo compound was shown to be a photoinduced transition from

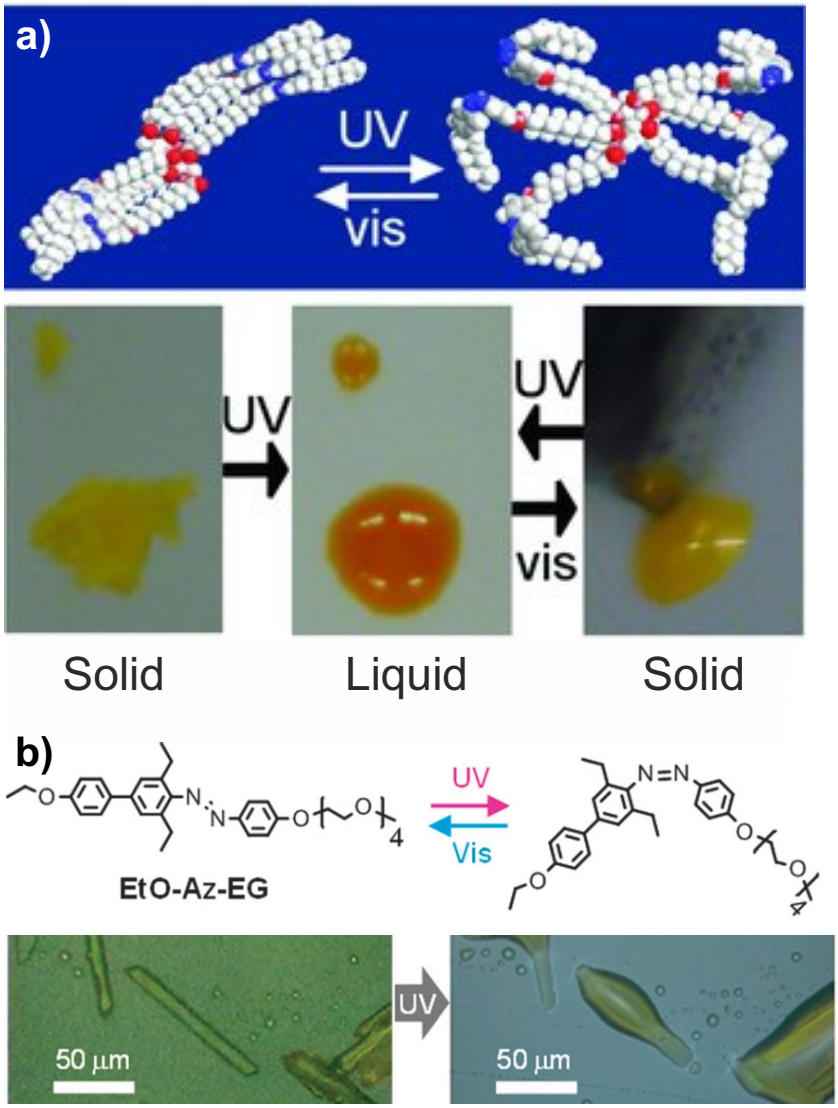


**Figure 1.16:** Photoinduced solid-to-liquid transition of small molecule azo materials. a) A sugar alcohol scaffold with multi azo arms is transformed from a solid to a liquid and back to a solid by light irradiation at room temperature b) Molecular structure and photoisomerization of EtO-Az-EG and microscopy images of UV-induced liquefaction at ambient temperature . a) Adapted with permission from Akiyama, H.; Yoshida, M. *Advanced Materials* **2012**, *24*, 2353–2356. Copyright 2012 John Wiley and Sons. b) Republished with permission of Royal Society of Chemistry, from Rational design of light-directed dynamic spheres, Okui, Y.; Han, M. *Chemical Communications* **2012**, *48*, 11763–11765; permission conveyed through Copyright Clearance Center, Inc.

a crystalline to a melt state. Additionally, a photoinduced solid-to-liquid transition based on an ionic crystal (IC) to ionic liquid (IL) phase transition was demonstrated by X-ray diffraction.[24] This was the first example of photoinduced reversible liquefaction of ICs. The design based on a solid-to-liquid transition increased the energy storage capacity of the system and the ion conductivity was increased parallel to liquefaction (Figure 1.17).

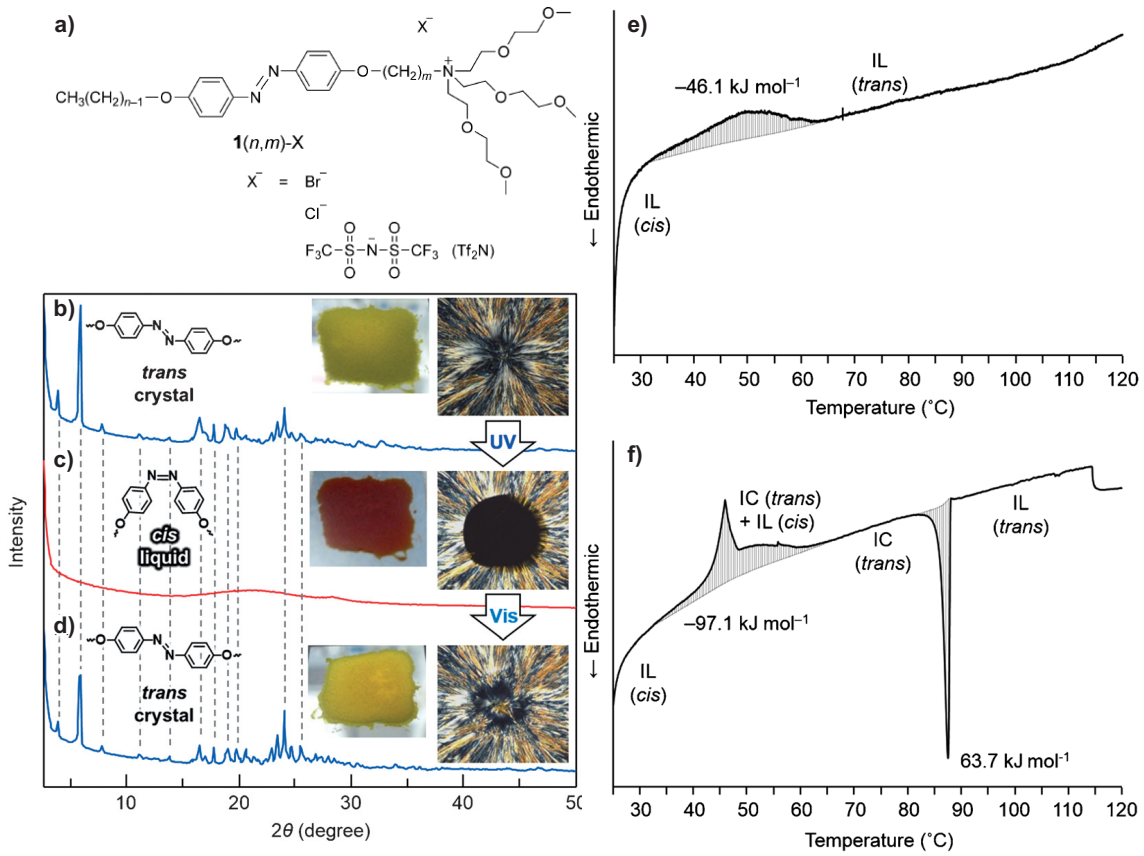


**Figure 1.17:** Photoinduced crystal-to-liquid transition of an IC. a) Molecular structure of the IC. X-ray diffraction patterns, images and polarized optical microscopy images of b) an as prepared film, c) after UV irradiation, and d) after visible light irradiation, demonstrating photoisomerization induced liquefaction. Differential scanning calorimetry (DSC) curves of the *cis* forms of e) **1**(6,4)-$Tf_2N$ and f) **1**(6,4)-Br, demonstrating their energy storage properties. Adapted with permission from Ishiba, K.; Morikawa, M.-a.; Chikara, C.; Yamada, T.; Iwase, K.; Kawakita, M.; Kimizuka, N. *Angewandte Chemie International Edition* **2015**, *54*, 1532–1536. Copyright 2014 John Wiley and Sons.

The molecular design of the azobenzene plays a key role in designing materials with photoinduced solid-to-liquid transitions. While symmetrical azobenzenes showed no photoinduced solid-to-liquid transition, which was attributed to their solid state packing, asymmetrically substituted azobenzenes showed a transition.[97] As revealed by optical observations, spectroscopy and viscosity techniques, an azobenzene with a methyl group at the 3-position to the azo bridge exhibited a photoinduced solid-to-liquid transition and was used as a photoresist. Selective etching of copper was achieved by combining photoinduced solid-to-liquid transition and material removal by organic solvents (Figure 1.18). The advantage of this system is that the material can be reused and no acids or bases have to be used.

The photoinduced reversible solid-to-liquid transitions and adhesive properties

of azobenzenes with a methyl group in the 3-position and alkoxy groups of increasing chain lengths in the 4- and 4'-position were studied.[98] Azobenzenes with alkyl chain lengths between six and ten methylene groups had faster photoinduced solid-to-liquid transitions than azobenzenes with chains less than six or more than ten methylene groups. UV and visible light switched the adhesive strength of the materials between low and high values, respectively. The study gives an insight into molecular design criteria that are useful for the development of new photoresponsive materials.

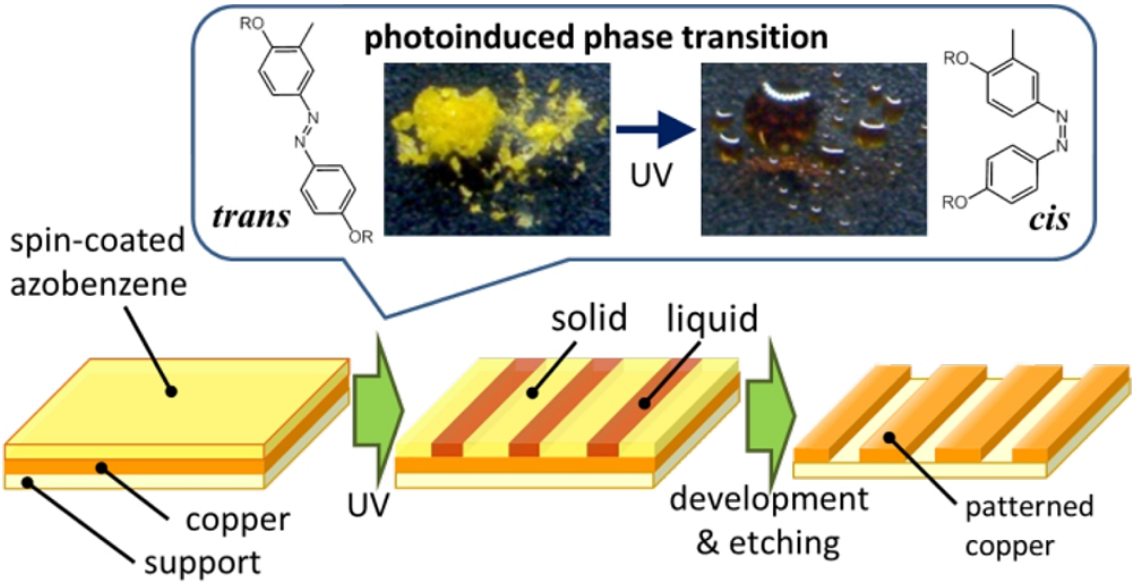


**Figure 1.18:** Molecular structure and photographs of *trans* and *cis* azobenzene derivatives. Scheme demonstrating the photolithographic process for selectively etching copper substrates supported by a photoinduced phase transition. Reprinted with permission from Norikane, Y.; Uchida, E.; Tanaka, S.; Fujiwara, K.; Koyama, E.; Azumi, R.; Akiyama, H.; Kihara, H.; Yoshida, M. *Organic Letters* **2014**, *16*, 5012–5015. Copyright 2014 American Chemical Society.

The reversible solid-to-liquid transition of the aforementioned azo containing small molecules is based on the transition from a crystal to a melt.[96] However, crystalline materials are typically hard and brittle and have poor film-forming properties, for example. Polymers have several advantages over other materials and are therefore the preferred choice for many applications (see section 1.1). Unlike small molecules, polymers have a chain entanglement which leads to a $T_g$. Lots of polymers used everyday are solids at room temperature and processing of these polymers requires melting the polymers. Thermoplastic amorphous polymers melt when heated above $T_g$ and solidify when cooled below $T_g$. The $T_g$ of a polymer strongly depends on the molecular structure and therefore on the configuration of the polymer. For different double chain configurations in a polymer the free volume and the chain stiffness are different. For example, the

$T_g$'s of *trans* and *cis* poly(1-butenylene) are 215 and 171 K, respectively.[99] If an azopolymer is switched from a *trans* to a *cis* state using light irradiation, it may also have different $T_g$ values in the *trans* and *cis* state.

## Photofluidization of Azopolymers

Some solid azopolymers show photoinduced flow under light irradiation. The effect is explained by alternating *trans-cis-trans* cycling photoisomerization and subsequent motion of the polymers and is different from the above mentioned reversible solid-to-liquid transition. In the solid state, azobenzene has a photochemical property which is called photoinduced orientation under polarized light irradiation. Azobenzene is tranformed from *trans* to *cis* by absorbing light that is preferably polarized parallel to its transition dipole axis. Light that is polarized perpendicular to the transition dipole axis of azobenzene is not absorbed. Between parallel and perpendicular polarization, light has a certain probability to be absorbed varying with $\cos^2\phi$, where $\phi$ is the angle between the azobenzene transition dipole axis and the light polarization. The *cis* form isomerizes with a random direction back to the *trans* form, which can then photoisomerize again. The *trans* azobenzene molecules isomerize until all of them are perpendicular to the light polarization. Afterwards they can not absorb light anymore. The effect can be measured using transmission spectroscopy, because the birefringence changes during that process.[100,101] Photoinduced orientation was exploited to directionally photofluidize azopolymers,[102]form SRGs,[63,64] deform azopolymer colloids[103] or reshape azopolymer pillars by light irradiation.[104] Photosoftening and photoplasticization of azopolymers were reported as well.[105,106] Various theories have been proposed to explain photofluidization of azopolymers but the mechanism is still under investigation.[107] It is widely agreed that photoisomerization of azobenzene is necessary to allow the azopolymers to flow far below $T_g$ and repeated *trans-cis-trans* cycles soften the polymer by increasing the mobility of the polymer chains. However, mass transport can also be induced without high amounts of photoresponsive units, for example in supramolecular azobenzene polymers with only 1 mol% azobenzene ratio[108] or when a non responsive poly(methyl methacrylate) (PMMA) is mixed with an azopolymer.[109] Vapaavuori *et al.* suggested that the change of the local environment of azo groups during photoisomerization results in an increase of an effective temperature.[110] Similar to heating, light irradiation leads to heterogenous changes in the submolecular environment of azopolymers, which leads to azo side groups with a higher temperature than the polymer backbone. Their findings are based on the relation of IR band shifts and temperature. Another possible mechanism explaining photoin-

duced liquefaction might be that the $T_g$ of the azopolymers is decreased by *trans-cis-trans* cycling which causes mass transport of the azopolymers.[111] Yet there has been no experimental proof of this hypothesis. Some technical issues such as thermal instability of the *cis*-isomer, low light transmittance in azopolymers and a lack of specialized equipment make the in situ measurement of azopolymer $T_g$ under light irradiation difficult.

Photofluidization based on *trans-cis-trans* cycles is observed only under polarized light irradiation and differs from the above-mentioned photoinduced solid-to-liquid transitions based on *trans*-to-*cis* isomerization. The liquid-like state is light polarization dependent in photofluidization and it is only present if the azopolymer is under permanent illumination, making pseudo stilbene type molecules very suitable for this kind of fluidization. Thus *trans*-to-*cis* as well as *cis*-to-*trans* photoisomerization can be induced simultaneously with light of one wavelength because the absorption bands of the *trans* and *cis* isomers of pseudo stilbene type molecules overlap. For photoinduced reversible solid-to-liquid transition explained above azobenzene derivatives with high *cis* contents and long *cis* half-lifes are better suited, because the *cis* state remains as an isotropic liquid even when the light is switched off. As long as the *cis* state is present, the material is a liquid. In this thesis only unpolarized light from LEDs is used, hence photofluidization based on *trans-cis-trans* cycles should not play a role.

# Bibliography


[1] Roy, D.; Cambre, J. N.; Sumerlin, B. S. *Progress in Polymer Science* **2010**, *35*, 278–301.

[2] Stuart, M. A. C.; Huck, W. T. S.; Genzer, J.; Muller, M.; Ober, C.; Stamm, M.; Sukhorukov, G. B.; Szleifer, I.; Tsukruk, V. V.; Urban, M.; Winnik, F.; Zauscher, S.; Luzinov, I.; Minko, S. *Nature Materials* **2010**, *9*, 101–113.

[3] Roy, D.; Brooks, W. L. A.; Sumerlin, B. S. *Chemical Society Reviews* **2013**, *42*, 7214–7243.

[4] Kocak, G.; Tuncer, C.; Butun, V. *Polymer Chemistry* **2017**, *8*, 144–176.

[5] Bertrand, O.; Gohy, J.-F. *Polymer Chemistry* **2017**, *8*, 52–73.

[6] Manouras, T.; Vamvakaki, M. *Polymer Chemistry* **2017**, *8*, 74–96.

[7] Liu, H.; Lin, S.; Feng, Y.; Theato, P. *Polymer Chemistry* **2017**, *8*, 12–23.

[8] de la Rica, R.; Aili, D.; Stevens, M. M. *Advanced Drug Delivery Reviews* **2012**, *64*, 967–978.

[9] Priya, B.; Viness, P.; Yahya, E. C.; Lisa, C. d. T. *Biomedical Materials* **2009**, *4*, 022001.

[10] Sudhina, G.; Prasad, B. B.; Victor, M.; Kenichi, N.; Yusuke, Y. *Chemistry – A European Journal* **2015**, *21*, 13164–13174.

[11] Junji, Z.; Qi, Z.; He, T. *Advanced Materials* **2013**, *25*, 378–399.

[12] Ercole, F.; Davis, T. P.; Evans, R. A. *Polymer Chemistry* **2010**, *1*, 37–54.

[13] Kumar, G. S.; Neckers, D. C. *Chemical Reviews* **1989**, *89*, 1915–1925.

[14] Klajn, R. *Chemical Society Reviews* **2014**, *43*, 148–184.

[15] Luo, Q.; Cheng, H.; Tian, H. *Polymer Chemistry* **2011**, *2*, 2435–2443.

[16] Irie, M.; Tanaka, H. *Macromolecules* **1983**, *16*, 210–214.

[17] J., E. J.; T., K. J. C. *Angewandte Chemie International Edition in English* **1995**, *34*, 88–90.

[18] Irie, M.; Hirano, Y.; Hashimoto, S.; Hayashi, K. *Macromolecules* **1981**, *14*, 262–267.

[19] Bandara, H. M. D.; Burdette, S. C. *Chemical Society Reviews* **2012**, *41*, 1809–1825.

[20] Beharry, A. A.; Woolley, G. A. *Chemical Society Reviews* **2011**, *40*, 4422–4437.

[21] Granucci, G.; Persico, M. J. T. C. A. *Theoretical Chemistry Accounts* **2007**, *117*, 1131–1143.

[22] Dias, A. R.; Minas Da Piedade, M. E.; Martinho Simões, J. A.; Simoni, J. A.; Teixeira, C.; Diogo, H. P.; Meng-Yan, Y.; Pilcher, G. *The Journal of Chemical Thermodynamics* **1992**, *24*, 439–447.

[23] Masutani, K.; Morikawa, M.-a.; Kimizuka, N. *Chemical Communications* **2014**, *50*, 15803–15806.

[24] Ishiba, K.; Morikawa, M.-a.; Chikara, C.; Yamada, T.; Iwase, K.; Kawakita, M.; Kimizuka, N. *Angewandte Chemie International Edition* **2015**, *54*, 1532–1536.

[25] Kucharski, T. J.; Ferralis, N.; Kolpak, A. M.; Zheng, J. O.; Nocera, D. G.; Grossman, J. C. *Nature Chemistry* **2014**, *6*, 441–447.

[26] Kolpak, A. M.; Grossman, J. C. *Nano Letters* **2011**, *11*, 3156–3162.

[27] Kolpak, A. M.; Grossman, J. C. *The Journal of Chemical Physics* **2013**, *138*, 034303.

[28] Feng, W.; Li, S.; Li, M.; Qin, C.; Feng, Y. *Journal of Materials Chemistry A* **2016**, *4*, 8020–8028.

[29] Luo, W.; Feng, Y.; Cao, C.; Li, M.; Liu, E.; Li, S.; Qin, C.; Hu, W.; Feng, W. *Journal of Materials Chemistry A* **2015**, *3*, 11787–11795.

[30] Luo, W.; Feng, Y.; Qin, C.; Li, M.; Li, S.; Cao, C.; Long, P.; Liu, E.; Hu, W.; Yoshino, K.; Feng, W. *Nanoscale* **2015**, *7*, 16214–16221.

[31] Zhitomirsky, D.; Cho, E.; Grossman, J. C. *Advanced Energy Materials* **2016**, *6*, 1502006.

[32] Tang, Z.; Johal, M. S.; Scudder, P.; Caculitan, N.; Magyar, R. J.; Tretiak, S.; Wang, H.-L. *Thin Solid Films* **2007**, *516*, 58–66.

[33] Kasha, M.; Rawls, H. R.; El-Bayoumi, M. A. *Pure and Applied Chemistry* **1965**, *11*, 371–392.

[34] Titov, E.; Granucci, G.; Götze, J. P.; Persico, M.; Saalfrank, P. *The Journal of Physical Chemistry Letters* **2016**, *7*, 3591–3596.

[35] Dos Santos, D. S.; Mendonça, C. R.; Balogh, D. T.; Dhanabalan, A.; Cavalli, A.; Misoguti, L.; Giacometti, J. A.; Zilio, S. C.; Oliveira, O. N. *Chemical Physics Letters* **2000**, *317*, 1–5.

[36] Baroncini, M.; d'Agostino, S.; Bergamini, G.; Ceroni, P.; Comotti, A.; Sozzani, P.; Bassanetti, I.; Grepioni, F.; Hernandez, T. M.; Silvi, S.; Venturi, M.; Credi, A. *Nature Chemistry* **2015**, *7*, 634–640.

[37] Paik, C. S.; Morawetz, H. *Macromolecules* **1972**, *5*, 171–177.

[38] Ikeda, T.; Tsutsumi, O. *Science* **1995**, *268*, 1873–1875.

[39] Yu, Y.; Nakano, M.; Ikeda, T. *Nature* **2003**, *425*, 145.

[40] Iamsaard, S.; Aßhoff, S. J.; Matt, B.; Kudernac, T.; CornelissenJeroen, J. L. M.; Fletcher, S. P.; Katsonis, N. *Nature Chemistry* **2014**, *6*, 229–235.

[41] Finkelmann, H.; Nishikawa, E.; Pereira, G. G.; Warner, M. *Physical Review Letters* **2001**, *87*, 015501.

[42] Kizilkan, E.; Strueben, J.; Staubitz, A.; Gorb, S. N. *Science Robotics* **2017**, *2*.

[43] Iwaso, K.; Takashima, Y.; Harada, A. *Nature Chemistry* **2016**, *8*, 625.

[44] Ichimura, K. *Chemical Reviews* **2000**, *100*, 1847–1874.

[45] Wang, G.; Tong, X.; Zhao, Y. *Macromolecules* **2004**, *37*, 8911–8917.

[46] Zhou, J.; Shen, J.; Yang, J.; Ke, Y.; Wang, K.; Zhang, Q. *Optics Letters* **2006**, *31*, 1370–1372.

[47] Bléger, D.; Liebig, T.; Thiermann, R.; Maskos, M.; Rabe, J. P.; Hecht, S. *Angewandte Chemie International Edition* **2011**, *50*, 12559–12563.

[48] Shi, Y.; Yang, J.; Zhao, J.; Akiyama, H.; Yoshida, M. *Polymer* **2016**, *97*, 309–313.

[49] Priimagi, A.; Vapaavuori, J.; Rodriguez, F. J.; Faul, C. F. J.; Heino, M. T.; Ikkala, O.; Kauranen, M.; Kaivola, M. *Chemistry of Materials* **2008**, *20*, 6358–6363.

[50] Che, P.; He, Y.; Wang, X. *Macromolecules* **2005**, *38*, 8657–8663.

[51] Archut, A.; Vögtle, F.; De Cola, L.; Azzellini, G. C.; Balzani, V.; Ramanujam, P. S.; Berg, R. H. *Chemistry – A European Journal* **1998**, *4*, 699–706.

[52] Weis, P.; Wu, S. *Macromolecular Rapid Communications* **2018**, *39*, 1700220.

[53] Rau, H. In *Photochemistry and Photophysics*; Rabek, J., Scott, G., Eds.; Taylor & Francis: Boca Raton, FL, 1989; Vol. 2; pp 119–141.

[54] Siewertsen, R.; Neumann, H.; Buchheim-Stehn, B.; Herges, R.; Näther, C.; Renth, F.; Temps, F. *Journal of the American Chemical Society* **2009**, *131*, 15594–15595.

[55] Samanta, S.; Qin, C.; Lough, A. J.; Woolley, G. A. *Angewandte Chemie International Edition* **2012**, *51*, 6452–6455.

[56] Feringa, B. L.; Jager, W. F.; De Lange, B.; Meijer, E. W. *Journal of the American Chemical Society* **1991**, *113*, 5468–5470.

[57] Hammerich, M.; Schütt, C.; Stähler, C.; Lentes, P.; Röhricht, F.; Höppner, R.; Herges, R. *Journal of the American Chemical Society* **2016**, *138*, 13111–13114.

[58] Wu, S.; Yu, X.; Huang, J.; Shen, J.; Yan, Q.; Wang, X.; Wu, W.; Luo, Y.; Wang, K.; Zhang, Q. *Journal of Materials Chemistry* **2008**, *18*, 3223–3229.

[59] Wang, D.; Ye, G.; Wang, X. *Macromolecular Rapid Communications* **2007**, *28*, 2237–2243.

[60] Salvador, M. A.; Almeida, P.; Reis, L.; Santos, P. *Dyes and Pigments* **2009**, *82*, 118 – 123.

[61] Dong, M.; Babalhavaeji, A.; Samanta, S.; Beharry, A. A.; Woolley, G. A. *Accounts of Chemical Research* **2015**, *48*, 2662–2670.

[62] Rochon, P.; Gosselin, J.; Natansohn, A.; Xie, S. *Applied Physics Letters* **1992**, *60*, 4–5.

[63] Rochon, P.; Batalla, E.; Natansohn, A. *Applied Physics Letters* **1995**, *66*, 136–138.

[64] Kim, D. Y.; Tripathy, S. K.; Li, L.; Kumar, J. *Applied Physics Letters* **1995**, *66*, 1166–1168.

[65] Beharry, A. A.; Sadovski, O.; Woolley, G. A. *Journal of the American Chemical Society* **2011**, *133*, 19684–19687.

[66] Samanta, S.; Beharry, A. A.; Sadovski, O.; McCormick, T. M.; Babalhavaeji, A.; Tropepe, V.; Woolley, G. A. *Journal of the American Chemical Society* **2013**, *135*, 9777–9784.

[67] Wang, G.; Yuan, D.; Yuan, T.; Dong, J.; Feng, N.; Han, G. *Journal of Polymer Science Part A: Polymer Chemistry* **2015**, *53*, 2768–2775.

[68] Wang, D.; Wagner, M.; Butt, H.-J.; Wu, S. *Soft Matter* **2015**, *11*, 7656–7662.

[69] Wang, D.; Wagner, M.; Saydjari, A. K.; Mueller, J.; Winzen, S.; Butt, H.-J.; Wu, S. *Chemistry – A European Journal* **2017**, *23*, 2628–2634.

[70] Wang, D.; Zhao, W.; Wei, Q.; Zhao, C.; Zheng, Y. *ChemPhotoChem* **2018**, *2*, 403–415.

[71] Bléger, D.; Schwarz, J.; Brouwer, A. M.; Hecht, S. *Journal of the American Chemical Society* **2012**, *134*, 20597–20600.

[72] Iamsaard, S.; Anger, E.; Aßhoff, S. J.; Depauw, A.; Fletcher, S. P.; Katsonis, N. *Angewandte Chemie International Edition* **2016**, *55*, 9908–9912.

[73] Zhao, F.; Bonasera, A.; Nöchel, U.; Behl, M.; Bléger, D. *Macromolecular Rapid Communications* **2018**, *39*, 1700527.

[74] Kumar, K.; Knie, C.; Bléger, D.; Peletier, M. A.; Friedrich, H.; Hecht, S.; Broer, D. J.; Debije, M. G.; Schenning, A. P. H. J. *Nature Communications* **2016**, *7*, 11975.

[75] Samanta, S.; Babalhavaeji, A.; Dong, M.-x.; Woolley, G. A. *Angewandte Chemie International Edition* **2013**, *52*, 14127–14130.

[76] Samanta, S.; McCormick, T. M.; Schmidt, S. K.; Seferos, D. S.; Woolley, G. A. *Chemical Communications* **2013**, *49*, 10314–10316.

[77] Dong, M.; Babalhavaeji, A.; Hansen, M. J.; Kalman, L.; Woolley, G. A. *Chemical Communications* **2015**, *51*, 12981–12984.

[78] Dong, M.; Babalhavaeji, A.; Collins, C. V.; Jarrah, K.; Sadovski, O.; Dai, Q.; Woolley, G. A. *Journal of the American Chemical Society* **2017**, *139*, 13483–13486.

[79] Yang, Y.; Hughes, R. P.; Aprahamian, I. *Journal of the American Chemical Society* **2012**, *134*, 15221–15224.

[80] Yang, Y.; Hughes, R. P.; Aprahamian, I. *Journal of the American Chemical Society* **2014**, *136*, 13190–13193.

[81] Venkataramani, S.; Jana, U.; Dommaschk, M.; Sönnichsen, F. D.; Tuczek, F.; Herges, R. *Science* **2011**, *331*, 445–448.

[82] Kurihara, M.; Hirooka, A.; Kume, S.; Sugimoto, M.; Nishihara, H. *Journal of the American Chemical Society* **2002**, *124*, 8800–8801.

[83] Carling, C.-J.; Boyer, J.-C.; Branda, N. R. *Journal of the American Chemical Society* **2009**, *131*, 10838–10839.

[84] Wu, W.; Yao, L.; Yang, T.; Yin, R.; Li, F.; Yu, Y. *Journal of the American Chemical Society* **2011**, *133*, 15810–15813.

[85] Jiang, Z.; Xu, M.; Li, F.; Yu, Y. *Journal of the American Chemical Society* **2013**, *135*, 16446–16453.

[86] Zhou, J.; Liu, Q.; Feng, W.; Sun, Y.; Li, F. *Chemical Reviews* **2015**, *115*, 395–465.

[87] Ambrosio, A.; Orabona, E.; Maddalena, P.; Camposeo, A.; Polo, M.; Neves, A. A. R.; Pisignano, D.; Carella, A.; Borbone, F.; Roviello, A. *Applied Physics Letters* **2009**, *94*, 011115.

[88] Wang, F.; Liu, X. *Chemical Society Reviews* **2009**, *38*, 976–989.

[89] Auzel, F. *Chemical Reviews* **2004**, *104*, 139–174.

[90] Weis, P.; Tian, W.; Wu, S. *Chemistry – A European Journal* **2018**, *24*, 6494–6505.

[91] Menaa, F.; Menaa, B.; Kahn, B. A.; Menaa, A. In *Handbook of Lipids in Human Function*; Watson, R. R., De Meester, F., Eds.; AOCS Press, 2016; pp 21–38.

[92] Hartley, G. S. *Nature* **1937**, *140*, 281.

[93] Le Fèvre, R. J. W.; Northcott, J. *Journal of the Chemical Society* **1953**, 867–870.

[94] Okui, Y.; Han, M. *Chemical Communications* **2012**, *48*, 11763–11765.

[95] Akiyama, H.; Yoshida, M. *Advanced Materials* **2012**, *24*, 2353–2356.

[96] Hoshino, M.; Uchida, E.; Norikane, Y.; Azumi, R.; Nozawa, S.; Tomita, A.; Sato, T.; Adachi, S.-i.; Koshihara, S.-y. *Journal of the American Chemical Society* **2014**, *136*, 9158–9164.

[97] Norikane, Y.; Uchida, E.; Tanaka, S.; Fujiwara, K.; Koyama, E.; Azumi, R.; Akiyama, H.; Kihara, H.; Yoshida, M. *Organic Letters* **2014**, *16*, 5012–5015.

[98] Norikane, Y.; Uchida, E.; Tanaka, S.; Fujiwara, K.; Nagai, H.; Akiyama, H. *Journal of Photopolymer Science and Technology* **2016**, *29*, 149–157.

[99] Brandrup, J.; Andrews, R. J.; Grulke, E. A. *Polymer Handbook*, 4th ed.; Wiley, 1999; Vol. VI; pp VI/193–VI/278.

[100] Todorov, T.; Nikolova, L.; Tomova, N. *Applied Optics* **1984**, *23*, 4309–4312.

[101] Natansohn, A.; Rochon, P. *Chemical Reviews* **2002**, *102*, 4139–4176.

[102] Karageorgiev, P.; Neher, D.; Schulz, B.; Stiller, B.; Pietsch, U.; Giersig, M.; Brehmer, L. *Nature Materials* **2005**, *4*, 699–703.

[103] Li, Y.; He, Y.; Tong, X.; Wang, X. *Journal of the American Chemical Society* **2005**, *127*, 2402–2403.

[104] Lee, S.; Kang, H. S.; Park, J.-K. *Advanced Functional Materials* **2011**, *21*, 1770–1778.

[105] Ikawa, T.; Hoshino, F.; Matsuyama, T.; Takahashi, H.; Watanabe, O. *Langmuir* **2006**, *22*, 2747–2753.

[106] Ikawa, T.; Hoshino, F.; Watanabe, O.; Li, Y.; Pincus, P.; Safinya, C. R. *Physical Review Letters* **2007**, *98*, 018101.

[107] Lee, S.; Kang, H. S.; Park, J.-K. *Advanced Materials* **2012**, *24*, 2069–2103.

[108] Koskela, J. E.; Vapaavuori, J.; Ras, R. H. A.; Priimagi, A. *ACS Macro Letters* **2014**, *3*, 1196–1200.

[109] Pirani, F.; Angelini, A.; Frascella, F.; Rizzo, R.; Ricciardi, S.; Descrovi, E. *Scientific Reports* **2016**, *6*, 31702.

[110] Vapaavuori, J.; Laventure, A.; Bazuin, C. G.; Lebel, O.; Pellerin, C. *Journal of the American Chemical Society* **2015**, *137*, 13510–13517.

[111] Yager, K. G.; Barrett, C. J. In *Polymeric Nanostructures and Their Applications*; Nalwa, H. S., Ed.; American Scientific, 2006; Chapter 8, pp 1–38.

# 2 Results and Discussion

The following results have been published/prepared as scientific articles in/for peer-reviewed journals and are reprinted in the following with the permission of the publishers.

This chapter is divided into two parts. In the first part the synthesis and applications of a visible light responsive azopolymer is shown. The second part will describe the solid-to-liquid transition of azopolymers and the influence of polymer structure.

The synthesis, characterization and an application of PmAzo are described in section 2.1 "Visible-Light-Responsive Azopolymers with Inhibited $\pi$-$\pi$ Stacking Enable Fully Reversible Photopatterning". While the synthesis and characterization of the polymer and intermediates as well as the photopatterning and photobleaching has already been demonstrated in part in the diploma thesis of Philipp Weis, the solid state properties were investigated and the photopatterning performance of PmAzo films was elaborated during the time of this dissertation. The untypical inhibited $\pi$-$\pi$ stacking of the polymer is described and compared to a conventional azopolymer. Using visible light for photoswitching demonstrates less photobleaching compared to UV light.

In section 2.2 "Spanning the Solar Spectrum: Azopolymer Solar Thermal Fuels for Simultaneous UV and Visible Light Storage" a second application of PmAzo, solar energy storage, is established in a four layer system. The long wavelength absorption of PmAzo enables sun light energy storage by *trans*-to-*cis* isomerization. Potential *cis*-to-*trans* back-isomerization is blocked by a dye layer. Combined with a UV-pass filter and a PAzo layer a four layer device was built and its performance investigated.

2.3 "Photoswitching of Glass Transition Temperatures of Azobenzene-Containing Polymers Induces Reversible Solid-to-Liquid Transitions" presents azopolymers with photoswitchable $T_g$. The thermodynamically more stable *trans* form can be transformed to the *cis* form by UV light irradiation. While the *trans* polymer is a solid with a high $T_g$, the *cis* polymer is a liquid with low $T_g$. The change in $T_g$ is investigated with different techniques and three applications are demonstrated.

The influence of spacer length on photoswitchable $T_g$ in azopolymers is investigated in 2.4 "Photo-Healing Azopolymers Based on Photoinduced Reversible Solid-to-Liquid Transitions". Azopolymers with increasing spacer length, from no methylene group up to 20 methylene groups between the polyacrylate backbone and the azobenzene are investigated. Healing scratches on an azopolymer surface by light irradiation is demonstrated.

The individual contributions are expressed in more detail at the beginning of the respective article.

## 2.1 Visible-Light-Responsive Azopolymers with Inhibited $\pi$-$\pi$ Stacking Enable Fully Reversible Photopatterning

Philipp Weis, Dongsheng Wang, and Si Wu
*Macromolecules* **2016**, *49*, 6368-6373

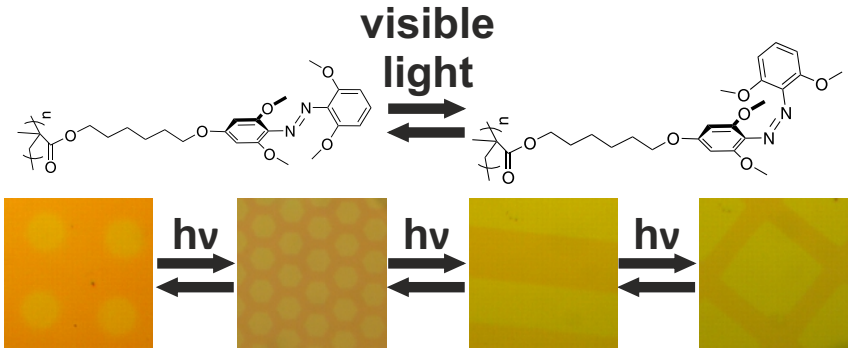


A visible light responsive azobenzene containing polymer is presented, being able to reversibly store and delete information in a polymer film. The non-stackable polymer shows reversible *trans-cis* isomerization in solid state and stores information for more than half a year. Moreover, using visible light decreases photodamage compared to UV responsive polymers.

**Author Contributions**

Si Wu conceived the idea and led the project. The synthesis and characterization of PmAzo and intermediates as well as photoisomerization and photopatterning of PmAzo films were in part performed by Philipp Weis during his diploma thesis. Improvement of the photopatterning performance of PmAzo films was elaborated during the time of this dissertation. Additonally solid state properties and photostability of PmAzo was investigated and compared to PAzo. Dongsheng Wang took some of the NMR spectra. The manuscript was written through contributions of all authors. All authors have given approval to the final version of the manuscript.

**Supporting Information** can be found on page 85 or at `http://pubs.acs.org/doi/suppl/10.1021/acs.macromol.6b01367`

Macromolecules

Article

pubs.acs.org/Macromolecules

# Visible-Light-Responsive Azopolymers with Inhibited $\pi-\pi$ Stacking Enable Fully Reversible Photopatterning

Philipp Weis, Dongsheng Wang, and Si Wu*

Max Planck Institute for Polymer Research, Ackermannweg 10, 55128 Mainz, Germany

Supporting Information

**ABSTRACT:** Photoswitchable polymers are promising candidates for information storage. However, two general problems for photoswitchable polymers used in rewritable optical storage are photobleaching and inefficient switching processes in solid state. To overcome both of these obstacles, we demonstrate the synthesis of a new visible-light-switchable azobenzene-containing polymer (azopolymer) with nonstackable azo chromophores for reversible and stable information storage. The new azopolymer (PmAzo) contains ortho-methoxy-substituted azobenzene (mAzo) groups on the polymer side chains and shows reversible trans-to-cis or cis-to-trans isomerization by using distinct wavelengths of visible light. PmAzo is better suited for reversible optical storage than conventional UV-responsive azopolymers because visible light avoids the photodamage caused by UV light. Additionally, mAzo groups do not $\pi-\pi$ stack in solid state, making photopatterning of PmAzo fully reversible. Moreover, photoinduced patterns on PmAzo can be stored for more than half a year. These properties distinguish PmAzo as a promising candidate for rewritable and stable information storage.

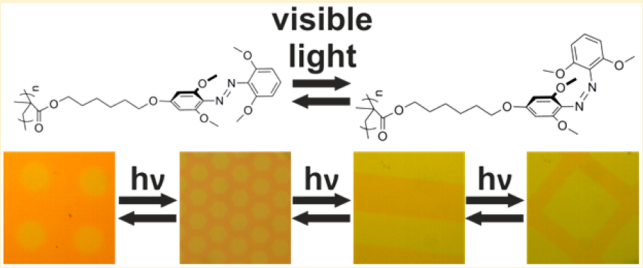


## INTRODUCTION

In the 21st century, the information age, a tremendous amount of data is created each day. Optical recording, which uses light to record information on storage media such as DVDs, represents one approach for large amounts of data storage. Recently, conventional photoswitchable compounds, including azobenzenes, spiropyrans, and diarylethenes, were proposed for use in optical recording.[1] These photoswitchable compounds can be switched between two states, representing "0" and "1" in the binary system, for reversible information storage.

A major problem with using photoswitchable compounds for information storage media is the general lack of efficient switching processes in solid state. While conventional photoswitchable compounds usually show reversible photoisomerization in solution, their photoisomerization in solid state is usually hindered by $\pi-\pi$ stacking of the chromophores.[2] In some cases, photoswitchable compounds can be dispersed in polymer matrices to improve their photoresponsiveness. However, simply mixing photoswitchable compounds with polymers can lead to undesirable phase separation and aggregation which even further inhibits photoresponse.[3] This problem can be partially solved by grafting photoswitchable compounds on polymers either covalently or using supramolecular interaction.[1d,3] However, even covalently bonded photoresponsive compounds on polymers may exhibit strong stacking interactions,[2e,4] which have been demonstrated to hinder the photoisomerization of azobenzenes in azobenzene-containing polymers (azopolymers).[4c,d] Thus, it is necessary to reduce $\pi-\pi$ stacking of photoswitchable compounds to enhance their photoresponse in solid state.

Another problem with using conventional photoswitchable compounds for optical storage is that UV light used in photoswitching can cause damage due to photooxidation and other photoinduced side reactions.[5] This photodamage thus makes multiple cycles of writing and deleting information on the photoswitchable material impractical. Some have attempted to overcome this problem by synthesizing photoswitchable compounds which are more resistant to UV light.[1c,6] However, an alternative, using long-wavelength-switchable compounds for optical storage, has rarely been studied. Compared to UV light, long-wavelength light is less likely to cause photodamage.

To overcome the problems of photobleaching and inefficient switching processes in solid state, we synthesized a novel polymer with tetra-ortho-methoxy-substituted azobenzene (mAzo) groups on the polymer side chains in this work (Scheme 1a). The mAzo group is nonplanar and responsive to visible light.[7−10] Compared to the conventional UV-responsive azopolymer (Scheme 1b), the mAzo-containing polymer maintains the advantageous visible-light sensitivity and realizes decreased $\pi-\pi$ stacking in solid state. Thus, the introduction of mAzo into polymer matrices can avoid both the photodegradation problem and inefficient photoswitching in solid state. Because of these features, this new mAzo-containing polymer is a promising candidate for reversible photopatterning and rewritable information storage.

Received: June 27, 2016
Revised: August 15, 2016
Published: August 26, 2016





DOI: 10.1021/acs.macromol.6b01367
Macromolecules 2016, 49, 6368−6373

**Scheme 1. Chemical Structures of (a) Visible-Light-Responsive Azopolymer PmAzo and (b) a Conventional UV-Light-Responsive Azopolymer PAzo[a]**

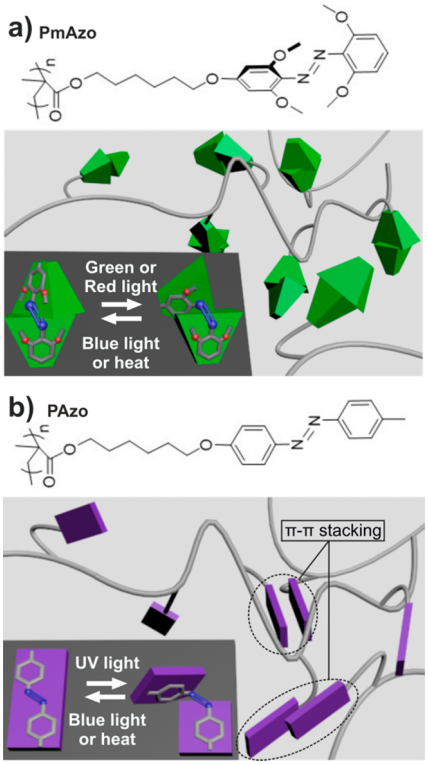


[a]Insets show cis−trans isomerization of azobenzene groups. PmAzo can be switched from trans to cis by visible light, while PAzo must be switched by UV light. In PmAzo, $\pi-\pi$ stacking of azo chromophores was prevented by the nonplanar molecular structure, while azo chromophores in PAzo exhibit strong $\pi-\pi$ stacking.

## EXPERIMENTAL SECTION

**Materials.** 2,6-Dimethoxyaniline (97%) was purchased from Alfa Aesar. 3,5-Dimethoxyphenol (99%), 6-chlorohexan-1-ol (96%), methacryloyl chloride (97%), 2-cyanopropan-2-yl benzodithioate (>97%), other reactants and all solvents were purchased from Sigma-Aldrich and used without further purification. 2,2′-Azobis-(isobutyronitrile) (98%) was purchased from Sigma-Aldrich and was recrystallized from ethanol before use. Milli-Q water was provided by a Sartorius Arium 611 VF purification system.

**Methods.** Proton nuclear magnetic resonance ($^1$H NMR) spectra were recorded on a Bruker Avance spectrometer (250, 300 or 400 MHz). Mass spectra (MS) were obtained using a VG instrument ZAB 2-SE-FPD. The molecular weights and molecular weight distributions of azopolymers were determined using an Agilent Technologies 1260 Infinity PSS SecCurity GPC (pump: 1260 IsoPump) equipped with UV and RI detectors running in tetrahydrofuran (THF) at 30 °C and a PLgel MIXED-B column (dimensions: 0.8 × 30 cm; particle size: 10 $\mu$m). UV−vis absorption spectra were measured on a PerkinElmer Lambda 900 spectrometer and on a Varian Cary 4000 spectrometer. Differential scanning calorimetry (DSC) data were collected using a Mettler Toledo DSC-822 under a nitrogen atmosphere. The polymers were measured at a temperature range between −50 and 140 °C with a heating or cooling rate of 10 °C min$^{-1}$. A Zeiss microscope III equipped with a yellow filter and a PixeLINK PL-A662 camera was used to capture patterns on polymer films. The same microscope, equipped with crossed polarizers (90°) and a heating stage plus Linkam TMS 94 controller, was used to observe textures of the polymers at different temperatures. Photoisomerization was induced by LEDs with wavelengths of 365, 470, 530, and 625 nm (Mightex Systems, device types LCS-0365-07-22, LCS-0470-03-22, LCS-0530-15-22, and LCS-0625-03-22, respectively). The output intensities were controlled by an LED controller (Mightex Systems, device type SLC-MA04-MU), calibrated by an optical powermeter (Spectra-Physics Corporation, Model 407A).

**Synthesis.** The synthesis route of the mAzo-containing polymer (PmAzo) is shown in Scheme 2. The details are provided below. The synthesis of the UV light-responsive azopolymer (PAzo) is shown in the Supporting Information (Scheme S1).

*Synthesis of* ***3****.* 2,6-Dimethoxyaniline **1** (300 mg, 1.96 mmol) was mixed with hydrochloric acid (0.8 mL 10%) and cooled to 0 °C. Sodium nitrite (138 mg, 1.96 mmol), dissolved in water (2 mL), was added quickly to the solution of **1**. After 10 min, 3,5-dimethoxyphenol **2** (302 mg, 1.96 mmol) dissolved together with sodium hydroxide (150 mg, 3.75 mmol) in water (20 mL) was added dropwise at 0 °C. The mixture was stirred for 3 days, then acidified to pH 6, and stirred for an additional 3 h. The precipitate was cooled with ice, filtered, and washed with ice cold water (100 mL). The orange powder was dried overnight in a vacuum oven. Yield: 97%. $^1$H NMR (250 MHz, $CD_3OD$, $\delta$): 7.36 (t, $J$ = 8.4 Hz, 1H, Ar−$H$), 6.86 (d, $J$ = 8.5 Hz, 2H,

**Scheme 2. Synthesis of the Visible-Light-Responsive Azopolymer PmAzo**

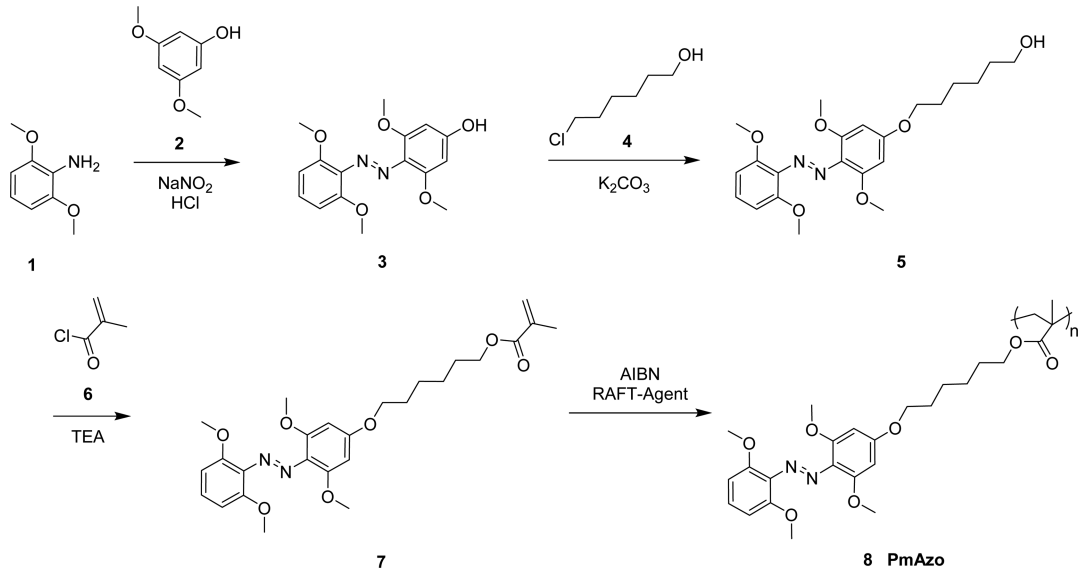




DOI: 10.1021/acs.macromol.6b01367
Macromolecules 2016, 49, 6368−6373

Ar−*H*), 6.13 (s, 2H, Ar−*H*), 4.04 (s, 6H, O−$CH_3$), 3.96 (s, 6H, O−$CH_3$). $^{13}$C NMR (176 MHz, $CD_3OD$, deprotonated by NaOH to prevent tautomerism, $\delta$): 174.86 (Ar−*C*−OH), 156.95 (Ar−*C*−O), 152.00 (Ar−*C*−O), 133.42 (Ar−*C*−N), 127.66 (Ar−*C*), 122.82 (Ar−*C*−N), 104.87 (Ar−*C*), 95.38 (Ar−*C*), 55.38 (O−$CH_3$), 54.70 (O−$CH_3$). MS (FD$^+$): $[M]^+$ 318.1; found 318.4.

*Synthesis of* ***5***. 4-(2,6-Dimethoxyphenyl)diazenyl)-3,5-dimethoxyphenol **3** (575 mg, 1.81 mmol) was dissolved in dry DMF (20 mL). Potassium carbonate (283 mg, 2.05 mmol) was added, and the solution was heated to 110 °C under an argon atmosphere. 6-Chlorohexan-1-ol **4** (267 μL, 2.00 mmol) was added, and the mixture was stirred at 110 °C under an argon atmosphere for 12 h. The solvent was evaporated under reduced pressure, and the residue was dried in the vacuum oven. The residue was purified by column chromatography (silica gel, dichloromethane/acetone (10/1), $R_f$ = 0.2) to receive the product as a red powder. Yield: 65%. $^1$H NMR (250 MHz, $CDCl_3$, $\delta$): 7.18 (t, $J$ = 8.4 Hz, 1H, Ar−*H*), 6.64 (d, $J$ = 8.4 Hz, 2H, Ar−*H*), 6.22 (s, 2H, Ar−*H*), 4.03 (t, $J$ = 6.5 Hz, 2H, Ar−O−$CH_2$), 3.88 (s, 6H, O−$CH_3$), 3.84 (s, 6H, O−$CH_3$), 3.67 (t, $J$ = 6.3 Hz, 2H, HO−$CH_2$), 1.48−1.82 (m, 8H, $CH_2$−$CH_2$−$CH_2$−$CH_2$−$CH_2$−$CH_2$). $^{13}$C NMR (67 MHz, DMSO-$d_6$, $\delta$): 161.04 (Ar−*C*−O), 154.09 (Ar−*C*−O), 151.00 (Ar−*C*−O), 134.34 (Ar−*C*−N), 128.09 (Ar−*C*), 127.09 (Ar−*C*−N), 105.26 (Ar−*C*), 91.84 (Ar−*C*), 67.79 (O−*C*−$CH_2$), 60.62 (*C*−OH), 56.02 (O−$CH_3$), 55.99 (−$CH_2$−), 32.45 (−$CH_2$−), 28.68 (−$CH_2$−), 25.40 (−$CH_2$−), 25.28 (−$CH_2$−). MS (FD$^+$): $[M + H]^+$ 419.2; found 419.3.

*Synthesis of* ***7***. 6-(4-((2,6-Dimethoxyphenyl)diazenyl)-3,5-dimethoxyphenoxy)hexan-1-ol **5** (487 mg, 1.17 mmol) and triethylamine (178 μL, 1.28 mmol) were dissolved in dichloromethane (10 mL) and cooled to 0 °C under argon. Methacryloyl chloride **6** (125 μL, 1.28 mmol) was added dropwise, and the mixture was stirred for 12 h. Ethanol (1 mL) was added, and the solvent was removed under reduced pressure. The residue was purified by column chromatography (silica gel, dichloromethane/acetone (10/1), $R_f$ = 0.2) to receive the product as a red powder. Yield: 73%. $^1$H NMR (250 MHz, $CDCl_3$, $\delta$): 7.18 (t, $J$ = 8.4 Hz, 1H, Ar−*H*), 6.64 (d, $J$ = 8.4 Hz 2H, Ar−*H*), 6.22 (s, 2H, Ar−*H*), 6.10 (m, 1H, C=$CH_2$), 5.55 (m, 1H, C=$CH_2$), 4.17 (t, $J$ = 6.6 Hz, 2H, O−$CH_2$), 4.02 (t, $J$ = 6.4 Hz, 2H, Ar−O−$CH_2$), 3.88 (s, 6H, O−$CH_3$), 3.84 (s, 6H, O−$CH_3$), 1.94 (m, 3H, $CH_3$), 1.48−1.82 (m, 8H, −$CH_2$−$CH_2$−$CH_2$−$CH_2$−). $^{13}$C NMR (63 MHz, DMSO-$d_6$, $\delta$): 166.64 (C=O), 161.08 (Ar−*C*), 154.15 (Ar−*C*), 151.08 (Ar−*C*), 136.02 (−C=$CH_2$), 134.40 (Ar−*C*), 128.27 (−C=$CH_2$), 127.18 (Ar−*C*), 126.61 (Ar−*C*), 105.35 (Ar−*C*), 91.94 (Ar−*C*), 67.79 (−$H_2$C−O−Ar), 64.29 (−$H_2$C−O−C=O), 56.08 ($H_3$C−O−Ar), 28.54 (Ar−O−$H_2$C−$CH_2$−$CH_2$−), 28.06 (−$H_2$C−$CH_2$−$CH_2$−O−C=O), 25.24 (−$H_2$C−$CH_2$−$CH_2$−$CH_2$), 25.20 (−$H_2$C−$CH_2$−$CH_2$−$CH_2$), 18.05 (C−$CH_3$). MS (FD$^+$): $[M]^+$ 486.2; found 486.3.

*Synthesis of* ***8*** *(PmAzo)*. 6-(4-((2,6-Dimethoxyphenyl)diazenyl)-3,5-dimethoxyphenoxy)hexyl methacrylate **7** (400 mg, 0.82 mmol), 2,2′-azobis(isobutyronitrile) (2 mg, 0.01 mmol), and 2-cyanopropan-2-yl benzodithioate (6 mg, 0.03 mmol) were dissolved in anisole (0.8 mL). The mixture was degassed via four freeze−pump−thaw cycles and stirred at 70 °C for 22 h. The product was precipitated in methanol. After three times washing with methanol, the polymer was dried in a vacuum oven at 60 °C for 24 h to receive the product as a red powder. Yield: 61%. $^1$H NMR (250 MHz, $CDCl_3$, $\delta$): 7.17 (1H, Ar−*H*), 6.64 (2H, Ar−*H*), 6.21 (2H, Ar−*H*), 3.98 (4H, O−$CH_2$ and Ar−O−$CH_2$), 3.81 (12H, O−$CH_3$), 2.0−0.8 (13H, C−$CH_2$, C−$CH_3$, and $CH_2$−$CH_2$−$CH_2$−$CH_2$−$CH_2$−$CH_2$). The number-averaged molecular weight of the polymer determined by GPC was 6.7 × $10^3$ g mol$^{-1}$, and the PDI was 1.13.

**Drop Casting.** The 5 wt % solutions of the polymer in cyclopentanone were filtered, dropped onto clean quartz substrates, and dried overnight. After annealing in a vacuum oven at 40 °C for 8 h, the films were kept in a sealed container until they were used.

**Spin Coating.** The 1 wt % solutions of the polymer in cyclopentanone were filtered and spin-coated with a PM 101D spin-coater (Headway Research Inc.) in a laminar flow box. After annealing in a vacuum oven at 40 °C for 8 h, the films were kept in a sealed container until they were used.

## RESULTS AND DISCUSSION

**Photoisomerization and Photostability of PmAzo.** First, we studied the photoisomerization of PmAzo in THF (Figure 1). PmAzo exhibited a $\pi$−$\pi$* absorption band in the UV range and a broad n−$\pi$* absorption band in the visible light range which even extended to red wavelengths (Figure S1). Irradiation of the trans n−$\pi$* absorption band with either red or green light decreased the $\pi$−$\pi$* band and increased the n−$\pi$* band, indicative of trans-to-cis isomerization of PmAzo as is well documented in azo chromophores (Figure 1 and Figure S2).[7−9] The reverse cis-to-trans isomerization can be induced by blue light irradiation of the cis n−$\pi$* absorption band (Figure 1). In contrast, UV light can excite the $\pi$−$\pi$* band, which also induced trans-to-cis isomerization (Figure S3) due to the larger $\pi$−$\pi$* transition dipole moment of trans as compared to cis azo chromophores. Complete recovery of the initial spectrum using red followed by blue light irradiation implied that the visible-light-induced isomerization was fully reversible. The energy of cis PmAzo was 12.2 kJ mol$^{-1}$ higher than that of trans PmAzo (Figure S4). The half-life of cis PmAzo in solution was about 16 h (Figure S5).

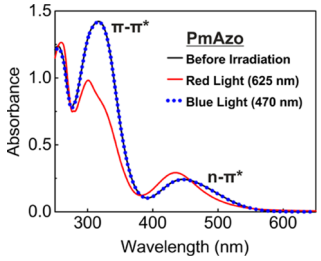


**Figure 1.** Absorption spectra of PmAzo in THF before irradiation (black line), after red light (625 nm, 1 mW cm$^{-2}$, 1 h) irradiation (red line), and after subsequent blue light (470 nm, 1 mW cm$^{-2}$, 10 min) irradiation (blue dots).

With low irradiation intensity at short times, UV light does not cause serious photodamage to azopolymers. However, photodegradation becomes increasing likely at large irradiation doses.[5] Thus, to test if visible light switching of PmAzo can solve the problem of photodamage caused by UV light, we studied the photostability of solutions of PmAzo to red and UV light with high doses of irradiation (32 mW cm$^{-2}$, 3 h) (Figure 2). The solution irradiated with red light could be switched back to the original state after subsequent blue light irradiation (Figure 2a). Thus, red light did not damage PmAzo. In contrast, the solution irradiated with UV light could not be switched back to the original state, indicating that PmAzo was damaged by UV light. Thus, utilizing visible light switching of PmAzo was demonstrated to prevent undesirable photodamage at these dosages. Similar results were found when a PmAzo film was irradiated with high doses of irradiation (32 mW cm$^{-2}$, 5 h) (Figure S6). The red light irradiated film showed less damage than the UV-light-irradiated film.

**Packing of Azo Chromophores in Solid State.** While the conventional azobenzene is a planar molecule that can easily $\pi$−$\pi$ stack, the nonplanar mAzo group has a much larger free volume and distorted $\pi$-electron system, both of which may prevent stacking of the mAzo chromophore. Experimental evidence for the inhibition of $\pi$−$\pi$ stacking came from a comparison of UV−vis absorption spectra for the azo chromophores in PmAzo and those in a conventional



DOI: 10.1021/acs.macromol.6b01367
Macromolecules 2016, 49, 6368−6373

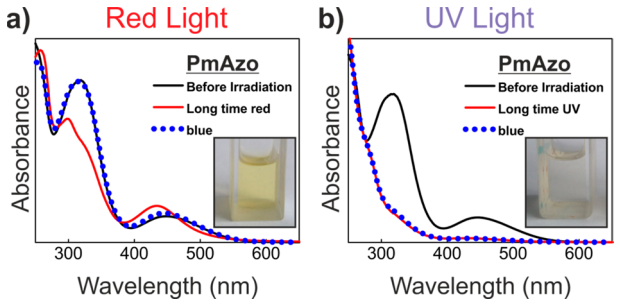


**Figure 2.** UV−vis absorption spectra of PmAzo in THF, before irradiation (black line), after high-intensity (a) red or (b) UV (32 mW $cm^{-2}$) irradiation for 3 h (red line) and after subsequent blue light irradiation (1 mW $cm^{-2}$) for 10 min (blue dotted line). Insets show the color of solutions after irradiation: (a) yellow after red light irradiation and (b) colorless after UV light irradiation, which indicated photobleaching.

azopolymer PAzo (Figure 3). The $\pi-\pi^*$ band of PAzo in a spin-cast film was blue-shifted by 15 nm and broadened with

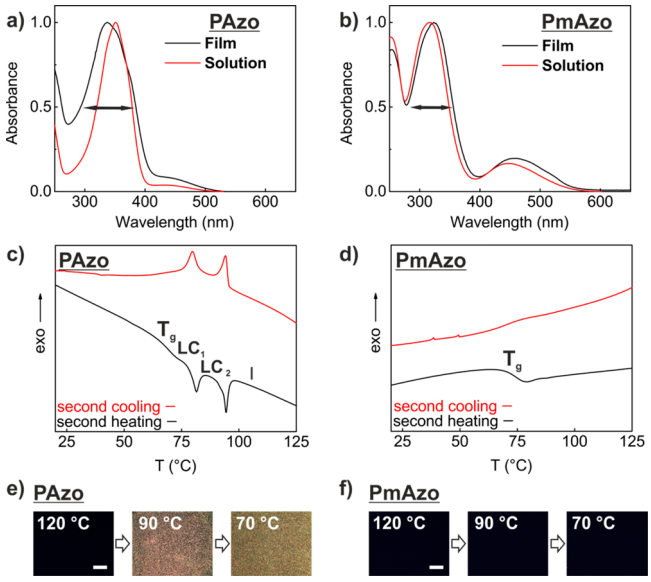


**Figure 3.** Normalized UV−vis absorption spectra of (a) PAzo and (b) PmAzo in solution and film. The arrows indicate the full width at half-maxima of the absorption bands (91 and 68 nm for PAzo film and solution, respectively, and 77 and 72 nm for PmAzo film and solution, respectively). DSC curves of second cooling and second heating of (c) PAzo and (d) PmAzo. POM images during cooling at different temperatures of (e) PAzo and (f) PmAzo. Scale bars are 250 $\mu$m. Abbreviations: $T_g$, glass transition temperature; $LC_1$, liquid crystalline phase 1; $LC_2$, liquid crystalline phase 2; I, isotropic phase.

respect to the band of PAzo in solution (Figure 3a) which are indicative of collective dipole alignment associated with aggregation.[2b,d,e,3a,4a,c,d] In contrast, the $\pi-\pi^*$ bands of PmAzo in a spin-cast film and in solution were almost identical (Figure 3b), suggesting minimal $\pi-\pi$ stacking of mAzo in the film.

Thermogravimetric analysis (TGA) showed that both PmAzo and PAzo were thermally stable up to 200 °C (Figure S7). Further studies by differential scanning calorimetry (DSC) and polarized optical microscopy (POM) also supported strong $\pi-\pi$ stacking of azo chromophores in PAzo and minimal stacking of mAzo chromophores in PmAzo (Figure 3c−f). DSC data showed that the conventional azopolymer PAzo had a glass transition temperature, $T_g$, at 70 °C and two different phase transitions at 80 and 94 °C (Figure 3c). Further, POM images showed that while PAzo was isotropic at 120 °C, anisotropy was present at 90 and 70 °C (Figure 3e), indicating that PAzo is a liquid crystalline polymer. In contrast, PmAzo had a $T_g$ at 72 °C and did not show any phase transitions between 20 and 125 °C (Figure 3d). PmAzo was isotropic at 120, 90, and 70 °C (Figure 3f), which indicates PmAzo is an amorphous polymer. Thus, the decreased intermolecular interactions due to the loss of $\pi-\pi$ stacking manifest as a change from a liquid crystalline to an amorphous polymer. The nonstackable feature of mAzo groups in PmAzo is good for fully reversible photopatterning (see the results below).

**Rewritable Optical Recording.** To demonstrate potential application to information storage, reversible photoisomerization of PmAzo in a film between the "0" and "1" states was repeated by alternating red and blue light irradiation (Figure 4a). This photoisomerization was performed five times without detectable photodegradation (Figure 4b).

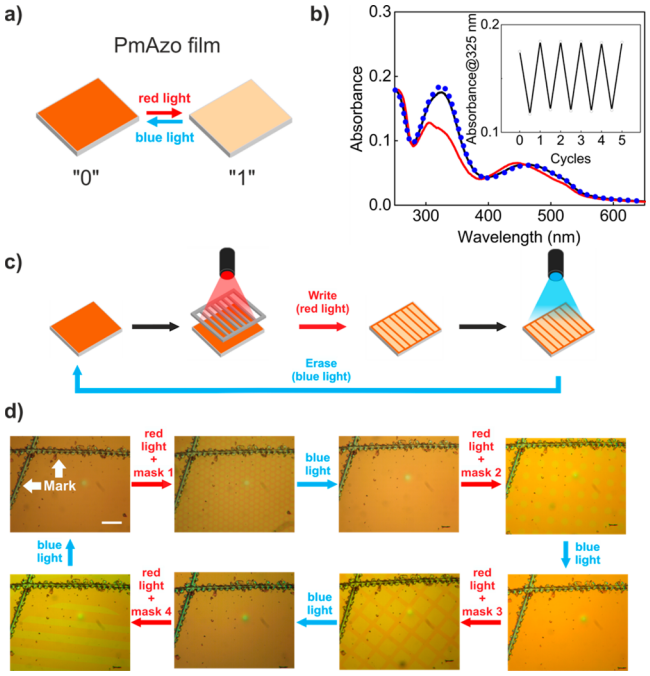


**Figure 4.** (a) Scheme demonstrating the switching of a PmAzo film between the two states representing "0" and "1". (b) UV−vis absorption spectra of a PmAzo film before irradiation (black solid line), after red light irradiation (625 nm, 1 mW $cm^{-2}$, 20 min, red solid line), and after blue light irradiation (470 nm, 1 mW $cm^{-2}$, 1 min, blue dotted line). Inset shows absorbance at 325 nm for five irradiation cycles. (c) Schematic illustration of reversible photopatterning of PmAzo. (d) Photopatterning PmAzo imaged by optical microscopy. Patterns were fabricated by red light irradiation (625 nm, 1 mW $cm^{-2}$, 30 min) through a mask; patterns were erased by blue light irradiation (470 nm, 1 mW $cm^{-2}$, 2 min). Scale bar is 250 $\mu$m.

Visible-light-induced reversible isomerization of PmAzo was subsequently applied to photopatterning (Figure 4c). Optical patterns were fabricated on a drop-cast film of PmAzo by irradiating the film with red light through a photomask. The stored "information" was then reversibly deleted by irradiating the film with blue light (Figure 4c). The storage and erasure of patterns on the same area of a PmAzo film was demonstrated to



DOI: 10.1021/acs.macromol.6b01367
Macromolecules 2016, 49, 6368−6373

be reversible up to at least four times (Figure 4d). Therefore, photopatterning of PmAzo is fully reversible.

To test the stability of patterns on PmAzo, a patterned film was stored in the dark at room temperature and monitored for "information loss" over time. The pattern remained visible after 32 weeks, demonstrating the excellent stability of the stored "information" (Figure 5). When cis PmAzo film was stored in the dark for 5 days, the $\pi-\pi^*$ band gradually increased, which indicates thermally cis-to-trans isomerization occurred within a few days (Figure S8). However, the $n-\pi^*$ band of cis PmAzo after stored in the dark for 5 days did not overlap with that of the trans PmAzo before irradiation. The different spectra of these two trans PmAzo resulted in long-term optical contrast in the pattern.


**Figure 5.** Optical microscopy images of a pattern on a PmAzo film after storage in the dark at room temperature for 1 day, 19 weeks, and 32 weeks. Scale bar is 250 $\mu$m.

We also studied photopatterning of the conventional PAzo film for comparison (Figure 6). POM images showed anisotropy implying that azobenzene groups in PAzo were ordered in a "frozen" liquid crystalline state (Figure 6a,e). Patterned UV irradiation on PAzo film induced trans-to-cis isomerization and anisotropic-to-isotropic transition on the exposed areas (Figure 6b,f). This phenomenon was called a photochemical phase transition.[1b,11] Blue light irradiation on cis PAzo can induce cis-to-trans transition, but the pattern on PAzo could not be erased by blue light (Figure 6c,g). Below the $T_g$, blue light cannot induce an isotropic-to-anisotropic transition because the polymer chains are not mobile enough to reorder.[1b,11] Thus, the regenerated trans PAzo by blue light was isotropic, which still showed a contrast with the unirradiated trans PAzo. When the patterned PAzo film was irradiated using UV light through the second mark, the patterns from the first mask and the second mask overlapped (Figure 6d,h). Therefore, the pattern could not be erased optically. Trans PAzo with a liquid crystalline ordering could only be regenerated by annealing above $T_g$,[4b] an impractical temperature for information storage devices. Thus, the design of PmAzo demonstrated a large improvement over conventional azopolymers in the ability to store information as optical patterns on films.

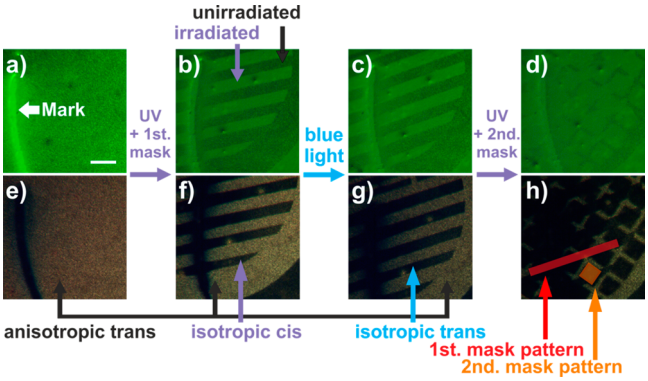


**Figure 6.** Optical microscope images (upper part) and POM images (lower part) of conventional PAzo film after patterned UV irradiation and blue light irradiation. Blue light could not erase the patterns on the PAzo film. The scale bar is 250 $\mu$m.

## CONCLUSIONS

In conclusion, a new visible light switchable azopolymer with nonstackable azo chromophores, PmAzo, was synthesized. The visible-light-induced isomerization of PmAzo avoids degradation due to photodamage from UV light. In addition, the nonplanar molecular structure of trans mAzo group prevents $\pi-\pi$ stacking and attendant aggregation. This design thus enabled reversible patterning on PmAzo films which could be written and erased by visible light. Further, the patterns on PmAzo were exceptionally stable, storing for more than half a year. These features make PmAzo an excellent alternative for conventional azopolymers in optical storage and photoswitchable devices. Beyond information storage, azopolymer photoisomerization can convert solar energy to mechanical[12] and thermal[13] energy. In fact, visible light switchable azopolymers should also be better suited for solar energy harvesting due to improved spectral overlap with the output of the sun. In the near future, other recently reported small molecules[14] suitable for constructing visible light switchable polymers will likely lead to similar reports and may further tailor material properties to specific applications. Thus, the present work provides the foundation for the design of visible light switchable polymers, which have broad applications spanning information and energy storage as well as the biomedical industry.

## ASSOCIATED CONTENT

### Supporting Information

The Supporting Information is available free of charge on the ACS Publications website at DOI: 10.1021/acs.macromol.6b01367.

Synthesis of PAzo, UV−vis absorption spectra, DSC curve, TGA data, and NMR spectra (PDF)

## AUTHOR INFORMATION

### Corresponding Author

*E-mail: wusi@mpip-mainz.mpg.de (S.W.).

### Author Contributions

S.W. led the project. P.W. and D.W. conducted the experiments. The manuscript was written through contributions of all authors. All authors have given approval to the final version of the manuscript.

### Funding

This work was supported by the Deutsche Forschungsgemeinschaft (DFG, WU 787/2-1) and Fonds der Chemischen Industrie (FCI, Nr. 661548).

### Notes

The authors declare no competing financial interest.

## ACKNOWLEDGMENTS

D.W. was supported by the CSC program. We acknowledge technical support from G. Kircher, J. Thiel, A. Best, and A. Hanewald and helpful discussions with Dr. M. Wagner and Prof. H.-J. Butt. This work was supported by the Deutsche Forschungsgemeinschaft (DFG, WU 787/2-1) and Fonds der Chemischen Industrie (FCI, Nr. 661548).



DOI: 10.1021/acs.macromol.6b01367
Macromolecules 2016, 49, 6368−6373

## REFERENCES


(1) (a) Kawata, S.; Kawata, Y. Three-Dimensional Optical Data Storage Using Photochromic Materials. *Chem. Rev.* **2000**, *100* (5), 1777−1788. (b) Yu, Y. L.; Ikeda, T. Alignment Modulation of Azobenzene-containing Liquid Crystal Systems by Photochemical Reactions. *J. Photochem. Photobiol., C* **2004**, *5* (3), 247−265. (c) Chan, J. C.; Lam, W. H.; Yam, V. W. A Highly Efficient Silole-Containing Dithienylethene with Excellent Thermal Stability and Fatigue Resistance: A Promising Candidate for Optical Memory Storage Materials. *J. Am. Chem. Soc.* **2014**, *136* (49), 16994−7. (d) Wu, S.; Duan, S. Y.; Lei, Z. Y.; Su, W.; Zhang, Z. S.; Wang, K. Y.; Zhang, Q. J. Supramolecular Bisazopolymers Exhibiting Enhanced Photoinduced Birefringence and Enhanced Stability of Birefringence for Four-Dimensional Optical Recording. *J. Mater. Chem.* **2010**, *20* (25), 5202−5209.

(2) (a) Anzai, J. I.; Osa, T. Photosensitive Artificial Membranes Based on Azobenzene and Spirobenzopyran Derivatives. *Tetrahedron* **1994**, *50* (14), 4039−4070. (b) Stumpe, J.; Fischer, T.; Menzel, H. Langmuir-Blodgett Films of Photochromic Polyglutamates. 9. Relation between Photochemical Modification and Thermotropic Properties. *Macromolecules* **1996**, *29* (8), 2831−2842. (c) Kuiper, J. M.; Engberts, J. B. F. N. H-Aggregation of Azobenzene-Substituted Amphiphiles in Vesicular Membranes. *Langmuir* **2004**, *20* (4), 1152−1160. (d) Ma, N.; Wang, Y. P.; Wang, B. Y.; Wang, Z. Q.; Zhang, X.; Wang, G.; Zhao, Y. Interaction between Block Copolymer Micelles and Azobenzene-Containing Surfactants: From Coassembly in Water to Layer-by-Layer Assembly at the Interface. *Langmuir* **2007**, *23* (5), 2874−2878. (e) Wu, S.; Wang, L.; Kroeger, A.; Wu, Y. P.; Zhang, Q. J.; Bubeck, C. Block Copolymers of PS-b-PEO Co-Assembled with Azobenzene-Containing Homopolymers and their Photoresponsive Properties. *Soft Matter* **2011**, *7* (24), 11535−11545.

(3) (a) Priimagi, A.; Kaivola, M.; Rodriguez, F. J.; Kauranen, M. Enhanced Photoinduced Birefringence in Polymer-Dye Complexes: Hydrogen Bonding Makes a Difference. *Appl. Phys. Lett.* **2007**, *90*, 121103. (b) Priimagi, A.; Vapaavuori, J.; Rodriguez, F. J.; Faul, C. F. J.; Heino, M. T.; Ikkala, O.; Kauranen, M.; Kaivola, M. Hydrogen-Bonded Polymer-Azobenzene Complexes: Enhanced Photoinduced Birefringence with High Temporal Stability through Interplay of Intermolecular Interactions. *Chem. Mater.* **2008**, *20* (20), 6358−6363. (c) Brown, D.; Natansohn, A.; Rochon, P. Azo Polymers for Reversible Optical Storage. 5. Orientation and Dipolar Interactions of Azobenzene Side-Groups in Copolymers and Blends Containing Methyl-Methacrylate Structural Units. *Macromolecules* **1995**, *28* (18), 6116−6123.

(4) (a) Wu, S.; Bubeck, C. Macro- and Microphase Separation in Block Copolymer Supramolecular Assemblies Induced by Solvent Annealing. *Macromolecules* **2013**, *46* (9), 3512−3518. (b) Tong, X.; Cui, L.; Zhao, Y. Confinement Effects on Photoalignment, Photochemical Phase Transition, and Thermochromic Behavior of Liquid Crystalline Azobenzene-Containing Diblock Copolymers. *Macromolecules* **2004**, *37* (9), 3101−3112. (c) Wu, S.; Zhang, Q. J.; Bubeck, C. Solvent Effects on Structure, Morphology, and Photophysical Properties of an Azo Chromophore-Functionalized Polydiacetylene. *Macromolecules* **2010**, *43* (14), 6142−6151. (d) Deng, Y. H.; Li, Y. B.; Wang, X. G. Colloidal Sphere Formation, H-Aggregation, and Photoresponsive Properties of an Amphiphilic Random Copolymer Bearing Branched Azo Side Chains. *Macromolecules* **2006**, *39* (19), 6590−6598.

(5) Malatesta, V.; Milosa, M.; Millini, R.; Lanzini, L.; Bortolus, P.; Monti, S. Oxidative-Degradation of Organic Photochromes. *Mol. Cryst. Liq. Cryst. Sci. Technol., Sect. A* **1994**, *246*, 303−310.

(6) Herder, M.; Schmidt, B. M.; Grubert, L.; Patzel, M.; Schwarz, J.; Hecht, S. Improving the Fatigue Resistance of Diarylethene Switches. *J. Am. Chem. Soc.* **2015**, *137* (7), 2738−47.

(7) Beharry, A. A.; Sadovski, O.; Woolley, G. A. Azobenzene Photoswitching without Ultraviolet Light. *J. Am. Chem. Soc.* **2011**, *133* (49), 19684−19687.

(8) Samanta, S.; Beharry, A. A.; Sadovski, O.; McCormick, T. M.; Babalhavaeji, A.; Tropepe, V.; Woolley, G. A. Photoswitching Azo Compounds in Vivo with Red Light. *J. Am. Chem. Soc.* **2013**, *135* (26), 9777−9784.

(9) (a) Wang, D. S.; Wagner, M.; Butt, H. J.; Wu, S. Supramolecular Hydrogels Constructed by Red-Light-Responsive Host-Guest Interactions for Photo-Controlled Protein Release in Deep Tissue. *Soft Matter* **2015**, *11* (38), 7656−7662. (b) Wang, D. S.; Wu, S. Red-Light-Responsive Supramolecular Valves for Photocontrolled Drug Release from Mesoporous Nanoparticles. *Langmuir* **2016**, *32* (2), 632−636.

(10) Samanta, S.; Beharry, A. A.; Sadovski, O.; McCormick, T. M.; Babalhavaeji, A.; Tropepe, V.; Woolley, G. A. Photoswitching Azo Compounds in Vivo with Red Light. *J. Am. Chem. Soc.* **2013**, *135* (26), 9777−84.

(11) Ikeda, T.; Tsutsumi, O. Optical Switching and Image Storage by Means of Azobenzene Liquid-Crystal Films. *Science* **1995**, *268* (5219), 1873−1875.

(12) (a) Zhang, L. D.; Liang, H. R.; Jacob, J.; Naumov, P. Photogated Humidity-Driven Motility. *Nat. Commun.* **2015**, *6*, 7429. (b) Jiang, Z.; Xu, M.; Li, F.; Yu, Y. Red-Light-Controllable Liquid-Crystal Soft Actuators via Low-Power Excited Upconversion Based on Triplet-Triplet Annihilation. *J. Am. Chem. Soc.* **2013**, *135* (44), 16446−53.

(13) Kucharski, T. J.; Ferralis, N.; Kolpak, A. M.; Zheng, J. O.; Nocera, D. G.; Grossman, J. C. Templated Assembly of Photoswitches Significantly Increases the Energy-Storage Capacity of Solar Thermal Fuels. *Nat. Chem.* **2014**, *6* (5), 441−447.

(14) (a) Bléger, D.; Schwarz, J.; Brouwer, A. M.; Hecht, S. o-Fluoroazobenzenes as Readily Synthesized Photoswitches Offering Nearly Quantitative Two-Way Isomerization with Visible Light. *J. Am. Chem. Soc.* **2012**, *134* (51), 20597−20600. (b) Shi, Z.; Peng, P.; Strohecker, D.; Liao, Y. Long-Lived Photoacid Based upon a Photochromic Reaction. *J. Am. Chem. Soc.* **2011**, *133* (37), 14699−14703. (c) Abeyrathna, N.; Liao, Y. A Reversible Photoacid Functioning in PBS Buffer under Visible Light. *J. Am. Chem. Soc.* **2015**, *137* (35), 11282−11284.




DOI: 10.1021/acs.macromol.6b01367
*Macromolecules* 2016, 49, 6368−6373

## 2.2 Spanning the Solar Spectrum: Azopolymer Solar Thermal Fuels for Simultaneous UV and Visible Light Storage

Andrew K. Saydjari[†], Philipp Weis[†], and Si Wu
*Advanced Energy Materials* **2017**, *7*, 1601622

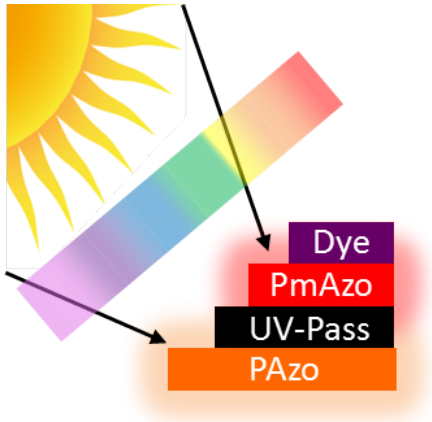


Implementation of azobenzene-based solar thermal fuels remains challenging because UV light, a small fraction of the solar spectrum, is required for charging. In article number 1601622, Si Wu and co-workers report a four-layer solar thermal cell that stores both UV and visible light from the sun. This cell achieves a record solar efficiency (0.4%) amongst azobenzene-based solar thermal fuels.

**Author Contributions**

Si Wu and Philipp Weis conceived the idea and Si Wu led the project. Andrew K. Saydjari and Philipp Weis contributed equally to this work. Photoinduced cycling of polymer solutions and films, parts of the DFT calculations, fluorescence spectra, NMR spectra, thermal reversion rates and solar efficiency were obtained by Andrew K. Saydjari. Polarized optical microscopy images, photoinduced cycling of PmAzo films, parts of the DFT calculations, DSC measurements and enthalpy determination from DSC measurements were obtained by Philipp Weis. The manuscript was written through contributions of all authors. All authors have given approval to the final version of the manuscript. The cover idea came from Philipp Weis.

**Supporting Information** can be found on page 102 or at https://onlinelibrary.wiley.com/action/downloadSupplement?doi=10.1002%2Faenm.201601622&file=aenm201601622-sup-0001-S1.pdf

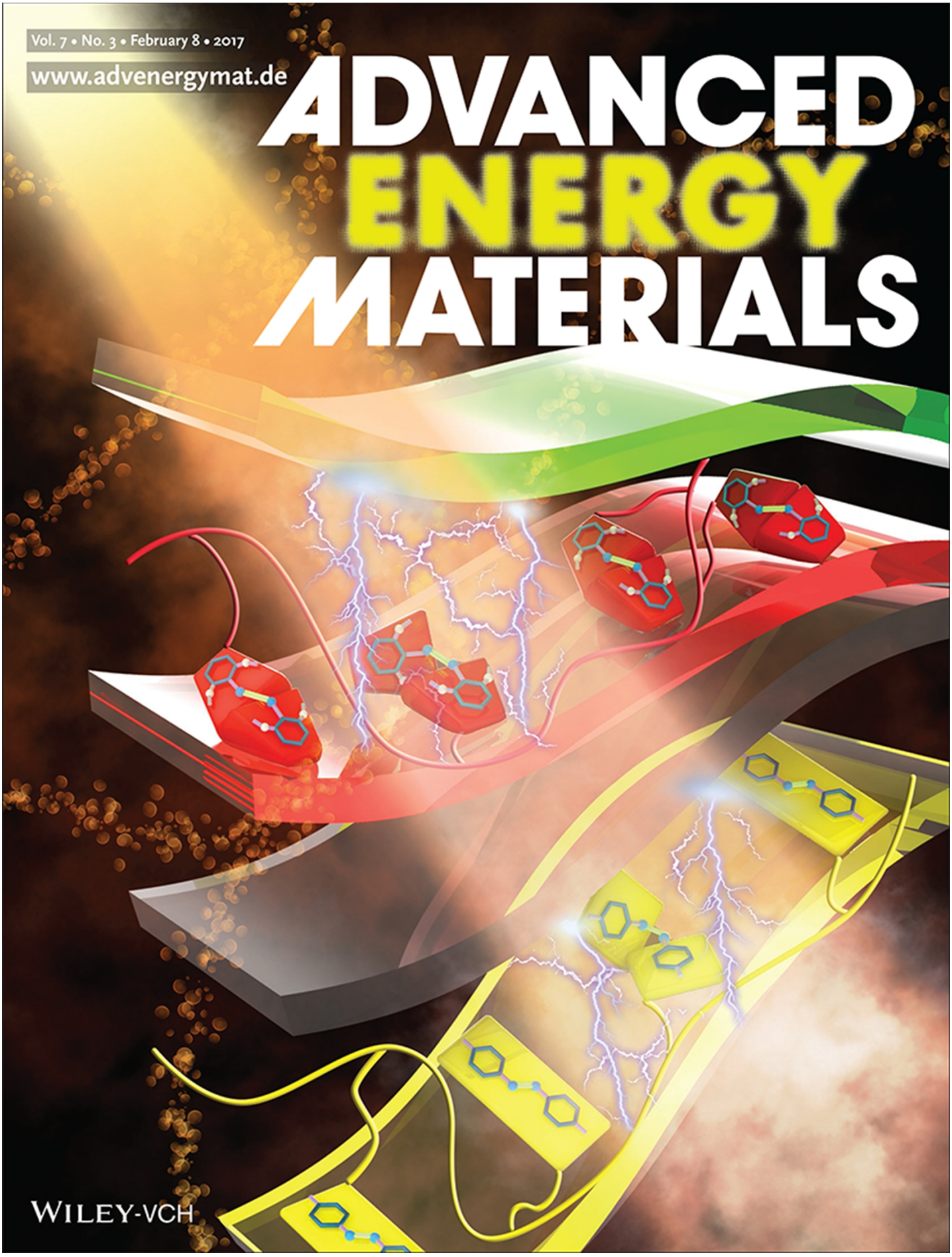
Vol. 7 • No. 3 • February 8 • 2017
www.advenergymat.de
ADVANCED ENERGY MATERIALS
WILEY-VCH

Materials Views
www.MaterialsViews.com

ADVANCED ENERGY MATERIALS
www.advenergymat.de

COMMUNICATION

# Spanning the Solar Spectrum: Azopolymer Solar Thermal Fuels for Simultaneous UV and Visible Light Storage

*Andrew K. Saydjari, Philipp Weis, and Si Wu**

As the energy consumption continues its precipitous rise, the need for alternative energy sources has become more pressing. The sun represents one such promising source since current energy consumption levels correspond to only ≈0.1% of the yearly solar output incident on the earth's surface.[1] Solar thermal cells (STCs) chemically store solar energy when photon absorption from sun light converts low-energy isomers to high-energy isomers. Heating or catalysis can release the stored solar energy as heat, generating only the low-energy isomer which is ready for additional charging.[2] Fuel cells derived from this technology enable portable electricity which is notably independent of an electric grid. Currently, the three main photoisomerizations of interest for STCs are electrocyclic reactions, organometallic ligand reorientation, and double-bond isomerization. While electrocyclic isomerizations such as [norbornadiene ↔ quadricyclane] can store large enthalpies (57 kJ $mol^{-1}$), difficult syntheses or the occurrence of intermolecular reactions at high concentrations hinder application.[3] Organometallic (fulvalene) tetracarbonyl-diruthenium systems display high gravimetric energy densities (30.6 W h $kg^{-1}$) but have limited application due to high cost.[4] In contrast, reversible cis-trans photoisomerization in azobenzene derivatives shows promise for solar energy storage due to stability, straightforward synthesis, and highly tunable absorption bands (**Figure 1**A).[6]

A major problem for azo-STCs is that trans-to-cis isomerization usually requires UV light.[7] However, UV comprises only a small fraction (4.5%) of the total solar irradiance, which severely inhibits azo-STC efficiency. Additionally, visible light in the solar spectrum hinders the storage of UV energy using conventional azo-STCs because visible light converts the charged cis isomers back to uncharged trans isomers (Azo, Figure 1B). Due to visible light-induced back isomerization, broad-spectrum sunlight irradiation of azobenzene can only generate a low content of cis isomers (≈25%), resulting in low storage capacity.[8] Thus, reported azo-STCs only store monochromatic UV light as proof of concept. Recently, several new azobenzene derivatives which show visible-light-induced trans-to-cis isomerization were synthesized.[9] These chromophores provide the opportunity to store visible light; however, blue light still induces cis-to-trans back isomerization, making the storage of sun light problematic (mAzo, Figure 1B). Therefore, fabrication of an azo-STC that can operate efficiently under full-spectrum solar irradiation remains a challenge.

Herein, we demonstrated an integrated azo-STC device that could efficiently store both UV and visible light under full-spectrum solar irradiation. From top to bottom, the device consisted of Coumarin 314, PmAzo, a UV-pass filter, and PAzo (Figure 1C,D). The four-layer device featured two active cells to store solar energy and two filtering layers to modify the effective incident spectrum. The two active layers were different azopolymers, PAzo and PmAzo which store energy by isomerization of the chromophores on the polymer side chains from the low energy trans isomers to the higher energy cis isomers.

The top layer of the device was comprised of 3 drop cast films of Coumarin 314 (≈1–2 μm) in a poly(4-vinyl)phenol (PvPh) matrix which absorbs strongly around 460 nm (blue) while transmitting UV and green wavelengths (Figure 1E,F). Moreover, Coumarin 314 is also a fluorescent dye and thus actively down-converts absorbed blue wavelengths. Broad fluorescence emission from Coumarin 314 centered at 560 nm can then be stored by the layer of PmAzo immediately following (Figure 1G; Figure S1, Supporting Information). Thus, the dye which serves as a filter, also actively down converts light that would have caused cis-to-trans isomerization to wavelengths which instead drive trans-to-cis energy storage. The second layer contained PmAzo which efficiently stores visible light. Specifically, irradiation of PmAzo at wavelengths corresponding to the trans $\pi^*\leftarrow\pi$ ($\lambda_{max}$ = 323 nm) and $\pi^*\leftarrow n$ ($\lambda_{max}$ = 460 nm) bands induces trans-to-cis isomerization, storing energy.[10] The cis $\pi^*\leftarrow n$ transition occurs at shorter wavelengths ($\lambda_{max}$ = 447 nm) and thus the back-isomerization of PmAzo can be prevented by blocking only 400–510 nm (blue) light using the Coumarin 314 layer. Thus, the separation of the trans and cis $\pi^*\leftarrow n$ transitions enables energy storage from longer (green/orange) wavelengths of visible light. In case PmAzo does not completely absorb all long-wavelengths of light which can induce cis-to-trans back-isomerization in PAzo, a UV-pass filter was inserted before the final PAzo layer (Figure 1H). The PAzo layer was used to efficiently store UV light (Figure 1I). Other than occurring at longer wavelengths (lower energy) with respect to PmAzo, the $\pi^*\leftarrow\pi$ transition ($\lambda_{max}$ = 351 nm) of PAzo behaves similarly. However, the previous UV-pass filter was necessary to prevent irradiation of the cis $\pi^*\leftarrow n$ ($\lambda_{max}$ = 441 nm) transition which causes predominantly cis-to-trans back-isomerization due to the relatively larger absorption coefficient relative to the trans transition which occurs at similar wavelengths.

First, to study charging of solution-phase solar thermal cells, solutions of PmAzo and PAzo in tetrahydrofuran (THF) were used as solution-phase solar thermal cells in the integrated device (**Figure 2**A–C). UV–vis spectra showed that solar

A. K. Saydjari, P. Weis, Dr. S. Wu
Max Planck Institute for Polymer Research
Ackermannweg 10, 55128 Mainz, Germany
E-mail: wusi@mpip-mainz.mpg.de
A. K. Saydjari
Department of Chemistry
Yale University
New Haven, CT 06520, USA

DOI: 10.1002/aenm.201601622

  

ADVANCED ENERGY MATERIALS
www.advenergymat.de
www.MaterialsViews.com

COMMUNICATION

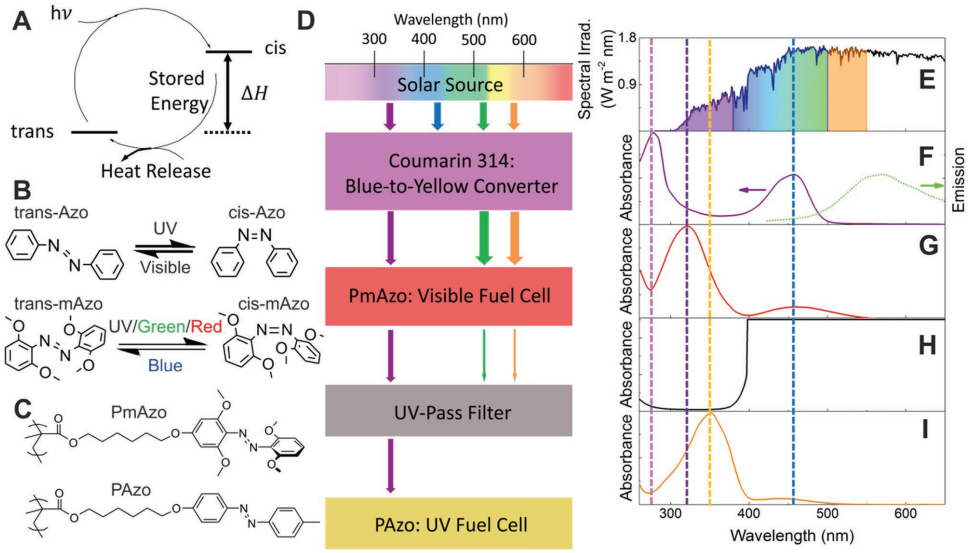


**Figure 1.** A) Cyclic process of energy storage by photoinduced trans-to-cis isomerization of azobenzene followed by subsequent release of $\Delta H_{\text{cis-trans}}$ in excess of heat used to cause thermal back-isomerization regenerating the uncharged solar thermal fuel without byproducts. B) Schematic representation of photoswitching of Azo and mAzo chromophores. C) Structures of polymers used in this study containing UV (PAzo) and visible (PmAzo) responsive chromophores. D) Schematic of 4-layer UV–vis solar thermal cell depicting transmission or absorbance of representative wavelengths. E) Solar spectrum (AM 1.5),[5] UV–vis spectra of F) Coumarin 314 film (reduced conc.) along with emission following 470 nm excitation, G) PmAzo in THF ($2 \times 10^{-4}$ M), H) UV-pass (UG-11) filter, and I) PAzo in THF ($6 \times 10^{-5}$ M).

irradiation converted PmAzo and PAzo 100% trans solutions to cis-rich photostationary states (Figure 2B,C). Quantitation using $^1$H-NMR showed the cis conversions achieved using the entire solar spectrum were 72% for PmAzo and 65% for PAzo (Figure 2A; Figures S2 and S3, Supporting Information), which are competitive with current literature values (60%–70%) using monochromatic UV light.[11] Further, the time-dependence of energy storage (cis conversion) indicated that while PmAzo achieved its photostationary state within 15 min, PAzo charged with a single-exponential time constant of 2.6(5) h (Figure 2A). This result indicates that photoisomerization of PAzo was likely intensity-limited while photoisomerization of PmAzo was spectrally-limited (further discussion in Supporting Information; Figure S4). Hence, while device design to reduce reflection losses could reduce the charging time for PAzo, only thickening or further spectral tuning of the top dye layer will

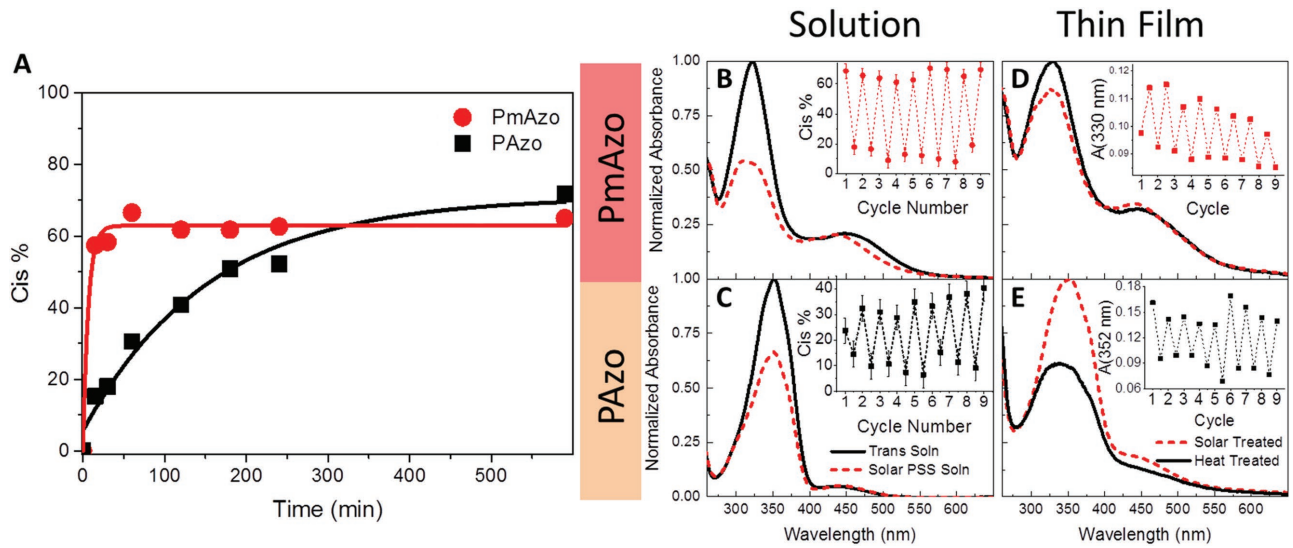


**Figure 2.** A) Time-dependent charging of solution-phase solar thermal cells, where cis% was determined by $^1$H-NMR. Normalized UV–vis spectra of B) PmAzo $2 \times 10^{-4}$ M in THF and C) PAzo $6 \times 10^{-5}$ M in THF before (100% trans) and after 10 h solar irradiation. Insets show cis content determined by $^1$H-NMR of (B, inset) 1% w/w PmAzo in d6-DMSO and (C, inset) PAzo in d7-DMF following cycles of 1 h solar irradiation (integers) and 2.5 h heating (half-integers) in oil bath at 110 °C. Representative UV–vis spectra of D) PmAzo and E) PAzo films during cycles of 1 h solar irradiation and 2.5 h heating in vacuum oven at 90 °C. Insets track absorbance of the $\pi^*\leftarrow\pi$ band during cycling for PmAzo (D, inset) and PAzo (E, inset).

www.MaterialsViews.com

ADVANCED ENERGY MATERIALS
www.advenergymat.de



improve PmAzo conversion. This device represents a significant improvement over the cis conversions of PmAzo or PAzo alone which were 38.1% and 32.9%, respectively (Supporting Information; Figures S2 and S3). Furthermore, in a series of control experiments, each layer was shown to be essential to device performance (Supporting Information; Figure S4).

To fabricate a device with all solid layers, spin-coated films of PmAzo (≈20 nm) and PAzo (≈35 nm) were integrated in the device. UV–vis spectra of the films in the devices before and after solar irradiation are presented in Figure 2D,E. The expected decrease in the $\pi^*\leftarrow\pi$ transition and increase in the $\pi^*\leftarrow n$ transition accompanying trans-to-cis isomerization was observed for PmAzo, an amorphous polymer. Surprisingly, the $\pi^*\leftarrow\pi$ transition intensity increased in PAzo upon irradiation despite the fact that solar irradiation induced trans-to-cis isomerization as demonstrated by solution $^1$H-NMR (Supporting Information; Figure S5) and suggested by the increase in the $\pi^*\leftarrow n$ absorption band. This phenomenon was explained by a photochemical phase transition characteristic of liquid crystalline azopolymers, such as PAzo.[12] Trans azo groups in liquid crystalline azopolymers prefer orientations perpendicular to the substrate.[13] UV irradiation then changes the azopolymer from a "frozen" liquid crystalline state to an amorphous state (Supporting Information; Figure S6). On one hand, some of the trans isomers convert to cis isomers, which decreases the $\pi^*\leftarrow\pi$ transition band. On the other hand, the azo chromophores shift away from a perpendicular orientation toward a more random orientation, increasing the $\pi^*\leftarrow\pi$ transition band. In order to separate the orientation effect from trans-to-cis isomerization, solid-state switching was estimated by charging in solid-state and then dissolving the films in THF. Using the method of Victor and Torkelson,[14] cis conversion was estimated to be 72.7% for PmAzo and 23.9% for PAzo, demonstrating substantial solid-state switching (Supporting Information; Equation (S1) and Figure S5).[14] To demonstrate applicability as a solar thermal cell, both the solution- and solid-state systems were repeatedly charged (1 h solar) and discharged (2.5 h at 110 °C, solution; 2.5 h at 90 °C under vacuum, solid). Stable cycling of both the solution and film-based systems up to nine cycles was demonstrated with no apparent degradation in PAzo (Figure 2D). While a gradual decrease in the magnitude of change in absorbance was observed for PmAzo, this does not necessarily indicate degradation and could instead correspond to progressive photoinduced orientation (Figure 2C).[15] Additionally, no attenuation of the absorbance of a PmAzo film was observed when trans-cis cycling of the PmAzo film was induced by alternating red and blue light irradiation (Figure S7, Supporting Information). Further, while a slight broadening of the absorption bands of the Coumarin 314 layer was observed, the filter still served to attenuate blue more than UV or green light after irradiation. Therefore, increasing the stability of the dye (e.g., Coumarin 314) layer may be a goal for further improvement of the system.

Differential scanning calorimetry (DSC) was used to measure the stored energy in cis PmAzo and cis PAzo. The cis-trans enthalpy difference was found to be 54.8 kJ mol$^{-1}$ for PAzo and 12.2 kJ mol$^{-1}$ for PmAzo (**Figure 3**). These enthalpies are slightly less than the calculated (DFT/6-311G(d,p)/B3LYP) enthalpy differences of 69.9 and 29.5 kJ mol$^{-1}$ (Supporting Information; Figure S8). An often cited metric for solar thermal fuels converts this enthalpy difference to gravimetric energy density: PmAzo 4.4 W h kg$^{-1}$, PAzo 34.8 W h kg$^{-1}$. In addition to the larger mass of PmAzo relative to PAzo, the small gravimetric energy density of PmAzo partly derives from the increased steric interactions present in the trans form. This steric effect decreases the enthalpy difference upon isomerization as reflected in the theoretical calculations. While PmAzo cannot store as much energy/mass due in part to its sensitivity to longer wavelengths of light, PAzo exhibits the highest gravimetric energy density reported for azopolymer-STCs. Further, combining the gravimetric energy density with the spectral overlap of the azo chromophores and the solar spectrum, the solar efficiency was calculated by the method of Scharf et al.[16] (Supporting Information; Equation (S8)).[16] Overall, the device has an efficiency of 0.4%, the highest to date for azo-STCs, and is competitive with photosynthesis (0.1%–0.3%).[16] In calculating solar efficiency, care must be taken to account for back isomerization induced by the $\pi^*\leftarrow n$ transition. Thus, much of the spectrum of standard azo chromophores is rendered unusable, inflating previous solar efficiency estimates. Recalculated efficiencies excluding these regions would still be subject to the condition that deleterious wavelengths could be practically blocked.

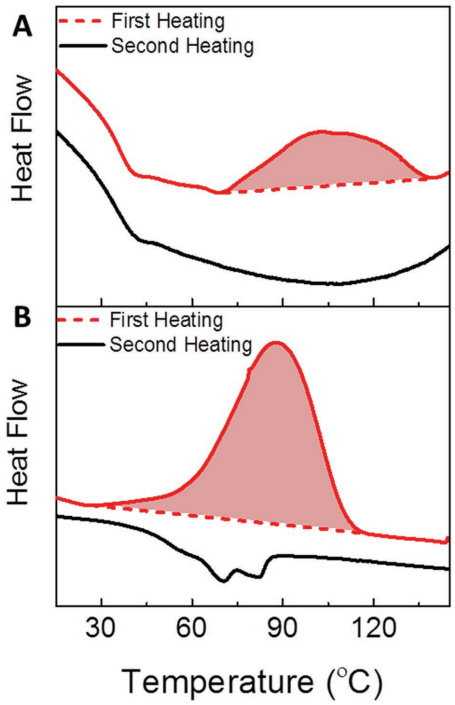


**Figure 3.** DSC curves for A) PmAzo (530 nm, 4 mW cm$^{-2}$, 40 min) and B) PAzo (365 nm, 2 mW cm$^{-2}$, 20 min) charged in solution demonstrated heat release from cis-to-trans isomerization present in the first heating, but absent in the second (offset). Shaded areas were integrated to find the bulk energy density by Equation (S9) (Supporting Information). The two peaks in the second heating curve of PAzo indicate phase transitions, ≈70 °C (anisotropic to anisotropic) and ≈80 °C (anisotropic to isotropic).

Thermal relaxation from cis-to-trans isomerization was approximated by a single exponential yielding half-lives of PmAzo (16(2) h solution) and PAzo (12.45(8) h solution) (**Table 1**; Figures S9 and S10, Supporting Information). Both

  

ADVANCED ENERGY MATERIALS
www.advenergymat.de

www.MaterialsViews.com

COMMUNICATION

**Table 1.** Measured energy-storage metrics for PmAzo and PAzo.

| Azopolymer | $\Delta H_{cis\text{-}trans}$ [a] [kJ mol$^{-1}$] | Gravimetric energy density[a] [W h kg$^{-1}$] | Theoretical gravimetric energy density[b] [W h kg$^{-1}$] | Cis solution half-life[c] [h] |
|---|---|---|---|---|
| PmAzo | 12.2 | 4.4 | (16.9) | 16(2) |
| PAzo | 54.8 | 34.8 | (51.0) | 12.45(8) |

[a]Determined from DSC; [b]Calculated using Gaussian09 (Opt DFT/6-311G(d,p)/B3LYP); [c]Determined by fitting a monoexponential decay to UV–vis absorbance at the peak $\pi^*\leftarrow\pi$ wavelength after attaining PSS 365 nm (45 min, 2 mW cm$^{-2}$).

PmAzo and PAzo achieve storage on the order of a half-day. Thus, the overall device can mitigate the daily periodicity of solar irradiance by charging during the day and discharging at night.

In summary, we demonstrated an azo-STC that can utilize both UV and visible wavelengths from a solar simulator for higher-efficiency light harvesting. By selectively blocking wavelengths that induce cis-to-trans back isomerization, cis conversion competitive with monochromatic irradiation (60%–70%) was achieved. Rational device design along with improved spectral overlap permitted a remarkable enhancement of the solar efficiency to 0.4%, the highest for azo-STCs to date. PAzo also demonstrated that chemical structure of the chromophore can serve as a handle for increasing the gravimetric energy density (40.9 W h kg$^{-1}$). Estimations of solid-state switching up to 72.7% represent progress toward the ideal of solid-state STCs. However, solid-state effects, such as aggregation and polymer crystallinity, were shown to play an important role, thus emphasizing the need for specification of the exact nature of the "solid-state."

## Supporting Information

Supporting Information is available from the Wiley Online Library or from the author.

## Acknowledgements

A.K.S. and P.W. contributed equally to this work. This work was graciously supported by the Deutsche Forschungsgemeinschaft (DFG, WU 787/2-1) and the Fonds der Chemischen Industrie (FCI, No. 661548). A.K.S. acknowledges the DAAD RISE program, Alan S. Tetelman 1958 Fellowship for International Research in the Sciences (Yale), and Timothy Dwight Bergin Fellowship (Yale) for generous financial support.

Received: July 25, 2016
Revised: September 5, 2016
Published online:

[1] C. J. Chen, *Physics of Solar Energy*, Wiley, Hoboken, NJ **2011**, p. 2.
[2] T. J. Kucharski, Y. Tian, S. Akbulatov, R. Boulatov, *Energy Environ. Sci.* **2011**, *4*, 4449.
[3] a) V. Gray, A. Lennartson, P. Ratanalert, K. Börjesson, K. Moth-Poulsen, *Chem. Commun.* **2014**, *50*, 5330; b) M. Cacciarini, A. B. Skov, J. Martyn, A. S. Hansen, J. Elm, H. G. Kjaergaard, K. V. Mikkelsen, M. B. Nielsen, *Chem. Eur. J.* **2015**, *21*, 7454.
[4] a) K. Moth-Poulsen, D. Ćoso, K. Börjesson, N. Vinokurov, S. K. Meier, A. Majumdar, K. P. C. Vollhardt, R. A. Segalman, *Energy Environ. Sci.* **2012**, *5*, 8534; b) Y. Kanai, V. Srinivasan, S. K. Meier, K. P. C. Vollhardt, J. C. Grossman, *Angew. Chem. Int. Ed.* **2010**, *49*, 8926.
[5] ASTM G173-03(2012), *Standard Tables for Reference Solar Spectral Irradiances: Direct Normal and Hemispherical on 37° Tilted Surface*, ASTM International, West Conshohocken, PA, **2012**, www.astm.org (accessed: June, 2016).
[6] a) J. Olmsted, J. Lawrence, G. G. Yee, *Solar Energy* **1983**, *30*, 271; b) H. Rau, in *Photochemistry and Photophysics*, Vol. *2* (Ed. J. Rabeck), CRC Press, Boca Raton, FL **1990**, pp. 119–141; c) H. M. D. Bandara, S. C. Burdette, *Chem. Soc. Rev.* **2012**, *41*, 1809; d) K. Ishiba, M.-A. Morikawa, C. Chikara, T. Yamada, K. Iwase, M. Kawakita, N. Kimizuka, *Angew. Chem. Int. Ed.* **2015**, *54*, 1532; e) A. M. Kolpak, J. C. Grossman, *J. Chem. Phys.* **2013**, *138*, 034303; f) W. Luo, Y. Y. Feng, C. Q. Qin, M. Li, S. P. Li, C. Cao, P. Long, E. Z. Liu, W. P. Hu, K. Yoshino, W. Feng, *Nanoscale* **2015**, *7*, 16214; g) A. M. Kolpak, J. C. Grossman, *Nano Lett.* **2011**, *11*, 3156; h) D. Zhitomirsky, E. Cho, J. C. Grossman, *Adv. Energy Mater.* **2016**, *6*, 1502006.
[7] a) L. D. Zhang, H. R. Liang, J. Jacob, P. Naumov, *Nat. Commun.* **2015**, *6*, 7429; b) A. Priimagi, A. Shevchenko, *J. Polym. Sci. Part B Polym. Phys.* **2014**, *52*, 163.
[8] H. Taoda, K. Hayakawa, K. Kawase, H. Yamakita, *J. Chem. Eng. Jpn.* **1987**, *20*, 265.
[9] a) R. Siewertsen, H. Neumann, B. Buchheim-Stehn, R. Herges, C. Näther, F. Renth, F. Temps, *J. Am. Chem. Soc.* **2009**, *131*, 15594; b) Y. Yang, R. P. Hughes, A. Aprahamian, *J. Am. Chem. Soc.* **2012**, *134*, 15221; c) D. Bléger, J. Schwarz, A. Brouwer, S. Hecht, *J. Am. Chem. Soc.* **2012**, *124*, 20597; d) S. Samanta, A. A. Beharry, O. Sadovski, T. M. McCormick, A. Balbalhavaeji, V. Tropepe, G. A. Woolley, *J. Am. Chem. Soc.* **2013**, *135*, 9777; e) S. Samanta, A. Balbalhavaeji, M. Dong, G. A. Woolley, *Angew. Chem. Int. Ed* **2013**, *52*, 14127; f) S. Samanta, T. M. McCormick, S. K. Schmidt, D. S. Seferos, G. A. Woolley, *Chem. Commun.* **2013**, *49*, 10314; g) A. A. Beharry, O. Sadovski, G. A. Woolley, *J. Am. Chem. Soc.* **2011**, *133*, 19684; h) O. Sadovski, A. A. Beharry, F. Shang, G. A. Woolley, *Angew. Chem. Int. Ed.* **2009**, *48*, 1484; i) F. Cheng, Y. Zhang, R. Yin, Y. Yu, *J. Mater. Chem.* **2010**, *20*, 4888.
[10] While the cis $\pi^*\leftarrow\pi$ transition occurs at the same wavelengths, the relatively smaller absorption coefficient makes photoinduced back-isomerization minor.
[11] a) K. Masutani, M.-A. Morikawa, N. Kimizuka, *Chem. Commun.* **2014**, *50*, 15803; b) W. Feng, S. Li, M. Li, C. Qin, Y. Feng, *J. Mater. Chem. A* **2016**, *4*, 8020; c) T. J. Kucharski, N. Ferralis, A. M. Kolpak, J. O. Zheng, D. G. Nocera, J. C. Grossman, *Nat. Chem.* **2014**, *6*, 441.
[12] a) T. Ikeda, O. Tsutsumi, *Science* **1995**, *268*, 1873; b) Y. L. Yu, T. Ikeda, *J. Photoch. Photobio. C* **2004**, *5*, 247.
[13] K. Nishizawa, S. Nagano, T. Seki, *Chem. Mater.* **2009**, *21*, 2624.
[14] J. G. Victor, J. M. Torkelson, *Macromolecules.* **1987**, *20*, 2241.
[15] M. Schönhoff, M. Mertesdorf, M. Lösche, *J. Phys. Chem.* **1996**, *100*, 7558.
[16] H.-D. Scharf, J. Fleischauer, H. Leismann, I. Ressler, W. Schleker, R. Weitz, *Angew. Chem. Int. Ed. Engl.* **1979**, *18*, 652.

## 2.3 Photoswitching of Glass Transition Temperatures of Azobenzene-Containing Polymers Induces Reversible Solid-to-Liquid Transitions

Hongwei Zhou†, Changguo Xue†, Philipp Weis†, Yasuhito Suzuki, Shilin Huang, Kaloian Koynov, Günter K. Auernhammer, Rüdiger Berger, Hans-Jürgen Butt and Si Wu

*Nature Chemistry* **2017**, *9*, 145-151

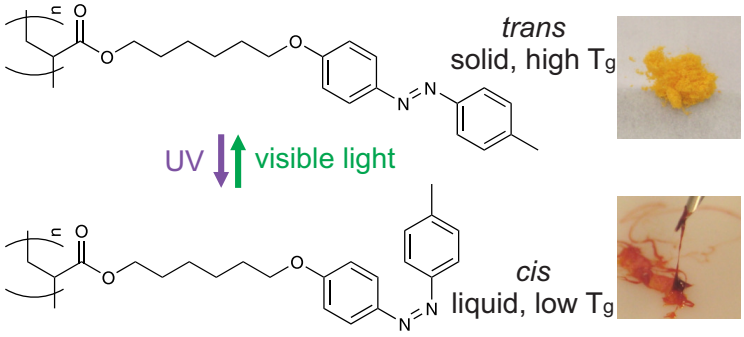


Reversibly inducing solid-to-liquid transitions of polymers at room temperature represents a challenge for enhanced processability and applications of polymers. Now, three azopolymers have been shown to exhibit photoswitchable glass transition temperatures, resulting in reversible solid-to-liquid transitions. Light exposure can heal cracks in hard azopolymers, reduce surface roughness of azopolymer films and control azopolymer adhesion.

**Author Contributions**

Si Wu conceived the idea and led the project. Parts of DSC measurements, parts of NMR measurements and transfer printing was done by Si Wu. Si Wu, Kaloian Koynov, Günter K. Auernhammer, Rüdiger Berger and Hans-Jürgen Butt designed the experiments. Hongwei Zhou, Changguo Xue and Philipp Weis contributed equally to this work. Synthesis of P1 and P2, parts of the optical microscopy images, confocal microscopy images, scratch healing experiments, smoothening of surfaces were obtained by Hongwei Zhou. Optical microscopy and AFM images were taken by Changguo Xue. UV-vis absorption spectra, parts of NMR spectra, parts of polarized optical microscopy images as well as parts of DSC and TGA measurements, preparation of polymers for photographs, synthesis of polymer P4 and intermediates, characterization of polymers P3, P4 and P5 and intermediates were obtained by Philipp Weis. Yasuhito Suzuki assissted in doing the DSC measurements. Shilin Huang did the piezo-rheology measurements. The manuscript was written through contributions of all authors. All

authors have given approval to the final version of the manuscript.

**Supporting Information** can be found on page 126 or at `https://www.nature.com/article-assets/npg/nchem/journal/v9/n2/extref/nchem.2625-s1.pdf`

nature chemistry

ARTICLES

PUBLISHED ONLINE: 10 OCTOBER 2016 | DOI: 10.1038/NCHEM.2625

# Photoswitching of glass transition temperatures of azobenzene-containing polymers induces reversible solid-to-liquid transitions

Hongwei Zhou†, Changguo Xue†, Philipp Weis†, Yasuhito Suzuki, Shilin Huang, Kaloian Koynov, Günter K. Auernhammer, Rüdiger Berger, Hans-Jürgen Butt and Si Wu*

**The development of polymers with switchable glass transition temperatures ($T_g$) can address scientific challenges such as the healing of cracks in high-$T_g$ polymers and the processing of hard polymers at room temperature without using plasticizing solvents. Here, we demonstrate that light can switch the $T_g$ of azobenzene-containing polymers (azopolymers) and induce reversible solid-to-liquid transitions of the polymers. The azobenzene groups in the polymers exhibit reversible *cis–trans* photoisomerization abilities. *Trans* azopolymers are solids with $T_g$ above room temperature, whereas *cis* azopolymers are liquids with $T_g$ below room temperature. Because of the photoinduced solid-to-liquid transitions of these polymers, light can reduce the surface roughness of azopolymer films by almost 600%, repeatedly heal cracks in azopolymers, and control the adhesion of azopolymers for transfer printing. The photoswitching of $T_g$ provides a new strategy for designing healable polymers with high $T_g$ and allows for control over the mechanical properties of polymers with high spatiotemporal resolution.**

Polymers are widely used in our daily lives. The glass transition temperature ($T_g$) of a polymer is the temperature region where a polymer transitions from a hard, glassy state into a soft, rubbery state. Polymers with $T_g$ below room temperature are usually processable and healable at room temperature. However, these polymers are too soft to be used as hard coatings or as structural elements at ambient or higher temperatures[1,2]. Polymers with high $T_g$ are better suited for these applications. To process or heal high-$T_g$ polymers, the conventional approach involves heating the polymers above $T_g$ or exposing them to plasticizing solvents, which may pollute the environment[3]. The development of high-$T_g$ polymers that are processable and healable at room temperature, without the use of plasticizing solvents, is challenging, because their polymer chains do not have sufficient mobility for processing or healing[1,2]. A promising approach to address this scientific challenge involves the development of polymers that can be reversibly softened and hardened at room temperature. Currently, almost no attention has been paid to the development of such polymers that can be reversibly switched between low- and high-$T_g$ states.

Azobenzene is a switchable compound with reversible *cis–trans* photoisomerization abilities. Photoresponsive azobenzene-containing materials have been used for applications in information storage[4], lithography[5], solar energy storage[6], photoswitchable porous materials[7], actuators[8,9] and photopharmacology[10]. Photoisomerization of some azobenzene-containing small molecules can reversibly convert the compounds from solids to isotropic liquids[7,11–15]. For example, by using X-ray crystal structure analysis, Hoshino *et al.* showed that the transition of their azobenzene-containing small molecule was a photoinduced crystal-to-melt transition[13]. In contrast to these azobenzene-containing small molecules, azopolymers exhibit $T_g$ values that determine whether the polymers are solid-like or liquid-like. It is well documented that photoinduced *trans–cis–trans* cycling can induce polarization-dependent mass transport of azopolymers[16–20] (also called directional photofluidization[20]). Directional photofluidization has many applications, including inscription of surface relief gratings, light-powered healing of a wearable electrical conductor and smoothing of surface roughness[16,17,21,22]. The precise mechanism of directional photofluidization of azopolymers is still subject to debate[19,20], but one possibility is that the change in local environment of the azo moiety upon photoisomerization corresponds to an increase in effective temperature[23]. Another possibility is that photoisomerization in azopolymers changes their $T_g$ values[19]. However, photoswitching of the $T_g$ values of azopolymers has never been experimentally demonstrated. Moreover, the photoswitching of azopolymers from solids to isotropic liquids has not been reported.

Here, we demonstrate a new phenomenon where azopolymers can be reversibly converted from solids to isotropic liquids as a result of photoswitchable $T_g$. Photoswitchable $T_g$ provide a strategy for designing healable and processable hard polymers that exhibit high $T_g$.

## Results and discussion

**Synthesis and characterization of azopolymers.** We synthesized two azopolymers (**P1** and **P2**) with different molecular weights by reversible addition-fragmentation chain-transfer (RAFT) polymerization (Fig. 1a and Supplementary Figs 1 and 2). **P1** and **P2** are polyacrylates with a flexible spacer and an azobenzene group on the polymer side chain. Their molecular weights, polydispersity indices, $T_g$, phase transition temperatures, shear storage moduli and shear loss moduli were measured (Supplementary Figs 2–5) and are listed in Table 1. The number-average molecular weights ($M_n$) of **P1** and **P2** are $9.9 \times 10^3$ g mol$^{-1}$ and $2.7 \times 10^4$ g mol$^{-1}$, respectively. **P1** and **P2** are solids at room temperature and exhibit $T_g$ at 48 and 68 °C, respectively. Both polymers have two liquid-crystalline phases above their $T_g$ values.

Max Planck Institute for Polymer Research, Ackermannweg 10, 55128 Mainz, Germany. †These authors contributed equally to this work.
*e-mail: wusi@mpip-mainz.mpg.de

ARTICLES NATURE CHEMISTRY DOI: 10.1038/NCHEM.2625

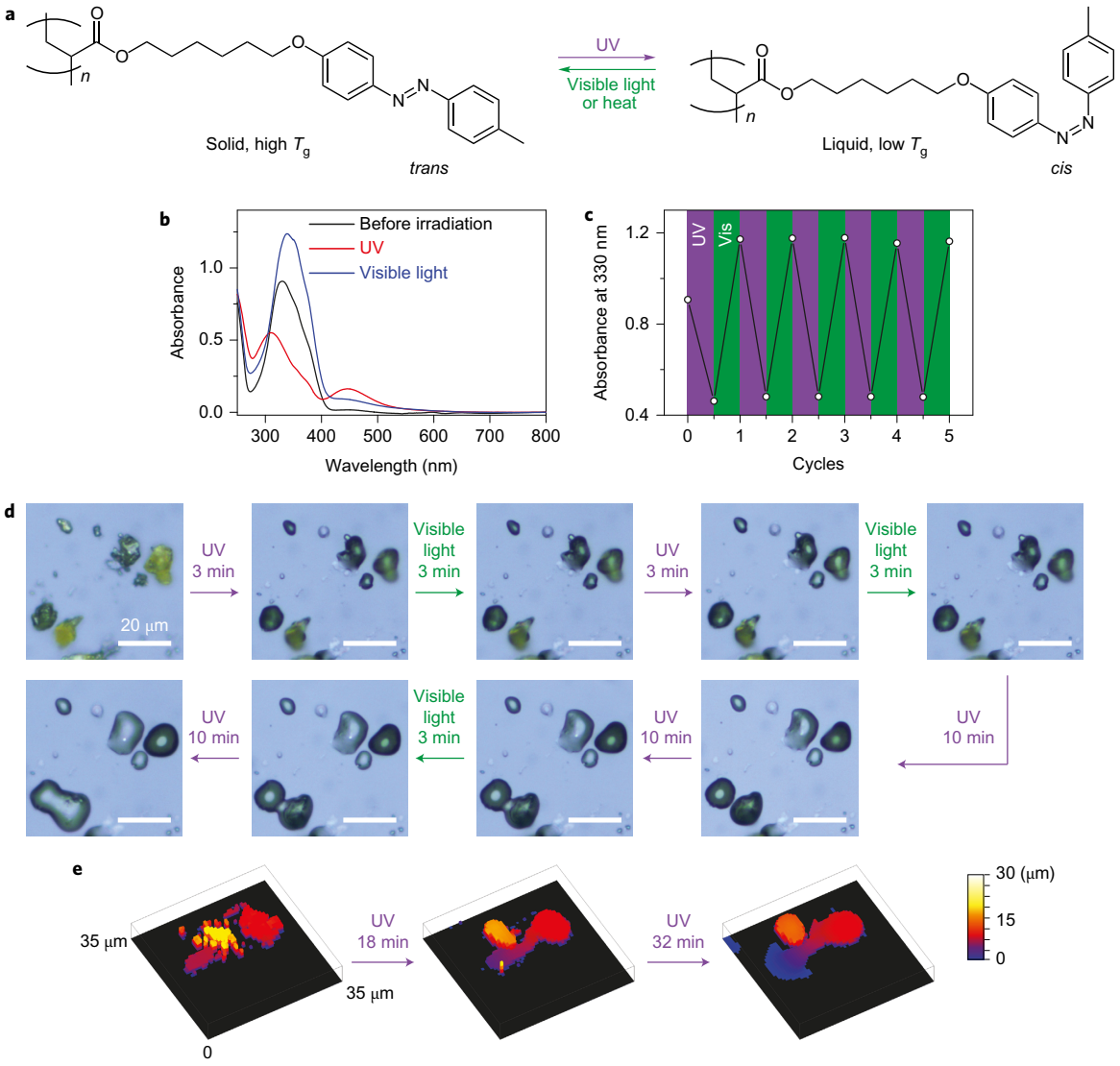


**Figure 1 | Chemical structure, photoisomerization and photoinduced solid-to-liquid transition of azopolymer P1. a**, Reversible photoisomerization of **P1**. **P1** is a solid with a high $T_g$ in the *trans* state and is a liquid with a low $T_g$ in the *cis* state. **b**, UV–vis absorption spectra of a spin-coated film of **P1** before irradiation, after ultraviolet irradiation (365 nm, 67 mW cm$^{-2}$, 1 min) and subsequent visible light irradiation (530 nm, 0.2 mW cm$^{-2}$, 1 min). **c**, Absorption changes under alternating ultraviolet and visible light irradiation. Scale bars, 20 μm. **d**, Optical microscopy images of **P1** powders under alternating ultraviolet (365 nm, 67 mW cm$^{-2}$) and visible light (530 nm, 5 mW cm$^{-2}$) irradiation. **e**, Confocal microscope images of **P1** powders before and after ultraviolet irradiation (365 nm, 67 mW cm$^{-2}$). Ultraviolet irradiation induced the flow of **P1** powders. UV, ultraviolet; Vis, visible light.

**Table 1 | Some properties of azopolymers P1 and P2.**

| Azopolymer | $M_n$ (g mol$^{-1}$) (GPC) | PDI (GPC) | $T_g$ (°C) (DSC) | $T_g$ (°C) (DMA) | $G'$ (Pa) (DMA) | $G''$ (Pa) (DMA) | Phase transition (°C) (DSC, second cooling) |
|---|---|---|---|---|---|---|---|
| P1 | $9.9 \times 10^3$ | 1.32 | 48 | 47 | $2.6 \times 10^8$ | $1.7 \times 10^7$ | G 48 $LC_1$ 93 $LC_2$ 110 I |
| P2 | $2.7 \times 10^4$ | 1.07 | 68 | 63 | $2.2 \times 10^8$ | $1.8 \times 10^7$ | G 68 $LC_1$ 95 $LC_2$ 103 I |

$M_n$, number-average molecular weight; PDI, polydispersity index; $T_g$, glass transition temperature; $G'$, storage modulus at 35 °C under a frequency of 1 rad s$^{-1}$; $G''$, loss modulus at 35 °C under a frequency of 1 rad s$^{-1}$; GPC, gel permeation chromatography; DSC, differential scanning calorimetry; DMA, dynamic mechanical analysis; G, glass; $LC_1$, liquid crystalline phase 1; $LC_2$, liquid crystalline phase 2; I, isotropic phase. $T_g$ values determined by DSC used the middle temperature of the transition in the second heating curve (Supplementary Fig. 3). $T_g$ values determined by DMA used the declining of the storage moduli (Supplementary Fig. 4).

**Photoisomerization and photoinduced solid-to-liquid transition.** UV–vis absorption spectroscopy showed that thin films of **P1** exhibit reversible *cis–trans* photoisomerization (Fig. 1b). The azobenzene groups in the as-prepared spin-coated film are in the stable *trans* state and exhibit a strong $\pi$–$\pi^*$ band at 330 nm. Following ultraviolet irradiation, the $\pi$–$\pi^*$ band of the *trans* isomer decreased and the $n$–$\pi^*$ band of the *cis* isomer at 450 nm increased. Subsequent visible light irradiation on *cis* **P1** switched it back to the *trans* state. The reversible photoisomerization of **P1** could be recycled at least five times (Fig. 1c). The absorbance of **P1** before irradiation was lower than that of **P1** after visible light irradiation because the stacking and orientation of the azobenzene

NATURE CHEMISTRY DOI: 10.1038/NCHEM.2625 ARTICLES

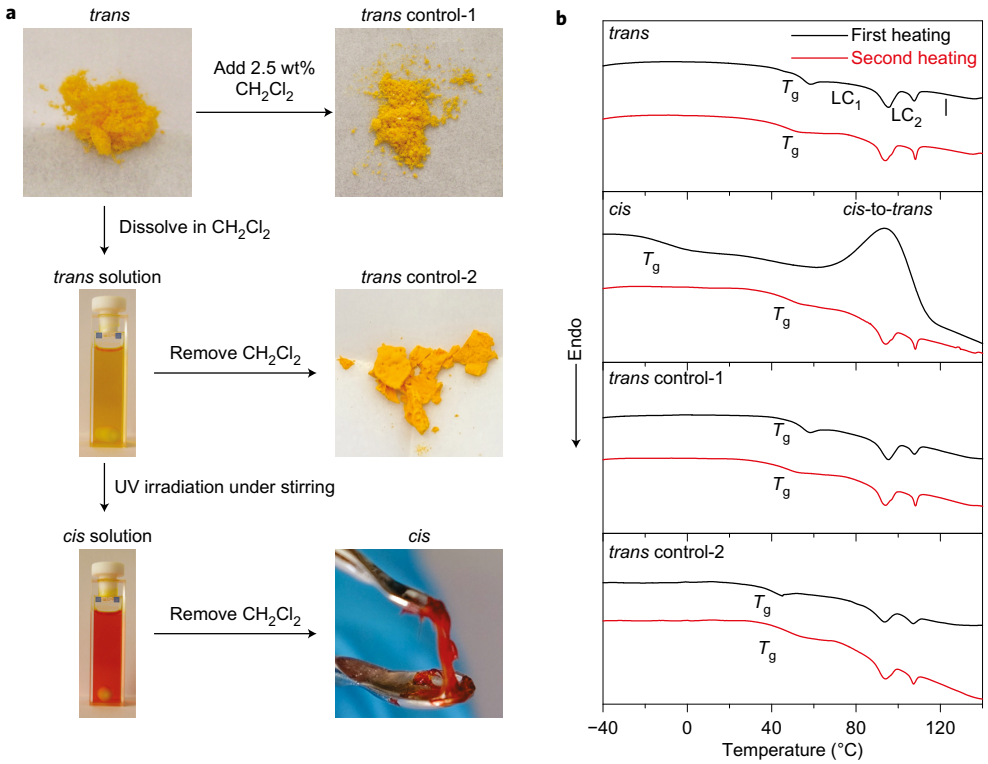


**Figure 2 | Photographs of P1 in the sample preparation processes and photoswitchable $T_g$ values of P1 studied by DSC. a**, Preparation of *cis* **P1** and two control samples from *trans* **P1**. The *trans* **P1** and two control samples are solid, but *cis* **P1** is liquid. **b**, DSC curves of *trans* **P1**, *cis* **P1** and the two control samples. The $T_g$ value of *cis* **P1** is much lower than that of *trans* **P1**. The *cis* content in *cis* **P1** determined by $^1$H NMR is more than 90%. Endothermic processes in the DSC data in **b** are indicated by the arrow. $LC_1$, liquid crystalline phase 1; $LC_2$, liquid crystalline phase 2; I, isotropic phase.

groups changed (Supplementary Fig. 6). The half-life of *cis* **P1** in the dark at room temperature is ~6 h (Supplementary Fig. 7).

The azopolymers showed an interesting photoinduced solid-to-liquid transition. **P1** powders were illuminated by alternating 365 nm ultraviolet light and 530 nm visible light (Fig. 1d). Ultraviolet illumination changed the irregularly shaped **P1** powders into drops. Adjacent drops fused into single drops. Both observations indicate that ultraviolet illumination induced flow of the polymer. In contrast, visible light irradiation did not change the morphology of **P1**. Three-dimensional confocal microscopy images showed that ultraviolet illumination decreased the heights of the powders and enlarged their areas of contact with the substrate (Fig. 1e). Ultraviolet illumination of **P2** powders also induced similar morphology changes (Supplementary Fig. 8), suggesting that ultraviolet light could also liquefy an azopolymer with a higher molecular weight ($M_n = 2.7 \times 10^4$ g mol$^{-1}$).

Three additional experiments were performed to study the photoinduced solid-to-liquid transitions. First, the surface temperature of **P1** under ultraviolet irradiation (67 mW cm$^{-2}$), measured by an infrared thermometer, was 35 °C (Supplementary Fig. 9), which was lower than the $T_g$ (48 °C) of **P1**. Therefore, the photothermal effect was insufficient to liquefy **P1**. Second, annealing **P1** at 38 °C for 1 h did not liquefy it (Supplementary Fig. 10). Third, ultraviolet light with a lower intensity (30 mW cm$^{-2}$), which only increased the surface temperature of **P1** to 28.5 °C, could still liquefy **P1** (Supplementary Fig. 11). These control experiments showed that the photoinduced solid-to-liquid transition was not a photothermal process but was due to photoisomerization.

The *trans* azobenzene groups in the **P1** film exhibit liquid-crystalline order. Ultraviolet irradiation changed **P1** from the anisotropic state to the isotropic *cis* state (Supplementary Figs 12 and 13), in what is known as a photochemical phase transition[24]. However, the photoinduced solid-to-liquid transition of **P1** was not due to the loss of the liquid-crystalline order. Amorphous **P1**, which was prepared by quenching **P1** above its isotropic temperature, also showed the photoinduced solid-to-liquid transition (Supplementary Fig. 14). The photoinduced solid-to-liquid transition takes place because *trans*-to-*cis* isomerization decreases the $T_g$ of **P1** (see the results below).

**Photoswitchable $T_g$.** Differential scanning calorimetry (DSC) is the standard method for directly measuring $T_g$. However, ultraviolet irradiation of *trans* **P1** powders could not generate enough *cis* **P1** for DSC measurements because the strong absorption of *trans* **P1** at 365 nm allowed only the top layer of the powders to be converted to *cis* **P1** (Supplementary Fig. 15). We therefore used the route shown in Fig. 2a to prepare enough *cis* **P1** for DSC measurements. First, *trans* **P1** was dissolved in $CH_2Cl_2$. The polymer solution was then illuminated with ultraviolet light under stirring, and $CH_2Cl_2$ was removed under vacuum (25 mbar, 25 min). $^1$H NMR analysis of the photoisomerization in $CD_2Cl_2$ under the same irradiation conditions showed that 95% of the *trans* isomers were converted to *cis* isomers (Supplementary Fig. 16). The boiling temperature of $CH_2Cl_2$ is as low as 40 °C. Thermogravimetric analysis (TGA) showed that $CH_2Cl_2$ was completely removed during the sample preparation process (Supplementary Fig. 17). The *cis* **P1** was a liquid (Fig. 2a). Two control samples were prepared to further prove that the liquefaction was not due to possible residual solvents in the polymer (Fig. 2a). Control-1 was prepared by adding 2.5 wt% $CH_2Cl_2$ to *trans* **P1**, and Control-2 was prepared by removing $CH_2Cl_2$ from the *trans* **P1** solution at 25 mbar for 25 min. Control-1 and Control-2 were both solids.

Subsequently, *trans* **P1**, *cis* **P1** and the two control samples were studied using DSC (Fig. 2b). *Trans* **P1** showed a $T_g$ of 48 °C and two

ARTICLES NATURE CHEMISTRY DOI: 10.1038/NCHEM.2625

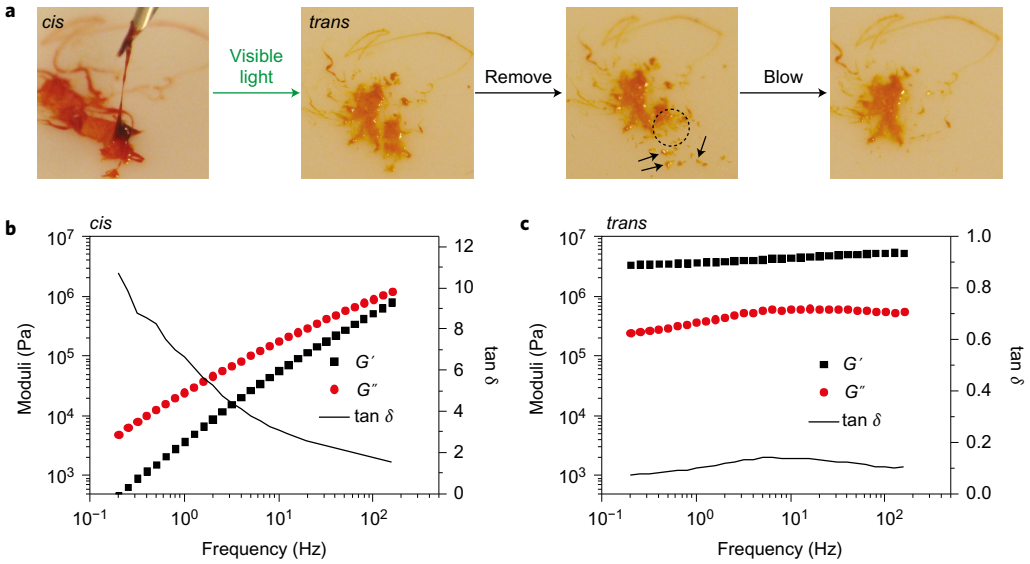


**Figure 3 | Photoinduced liquid-to-solid transition of *cis* P1 demonstrated by photographs and rheology tests. a**, Photographs of *cis* **P1** before irradiation and after visible light irradiation (530 nm, 5 mW cm$^{-2}$, 20 min), scraped by a needle and blown by a stream of $N_2$. The dashed circle and arrows in the third photograph show that *trans* **P1** was removed from the substrate and formed powders. **b**,**c**, Measured storage modulus ($G'$), loss modulus ($G''$) and loss tangent (tan $\delta$) of *cis* **P1** before (**b**) and after (**c**) visible light irradiation (530 nm, 6.3 mW cm$^{-2}$, 15 min). *Cis* **P1** is liquid and *trans* **P1** is solid. Note that $G'$ and $G''$ in **c** are relative values because part of the sample lost contact with the sample holder during its photoinduced liquid-to-solid transition. The use of the relative values did not influence tan $\delta$.

phase transitions at 94 and 108 °C in both the first and second heating curves. In contrast to *trans* **P1**, *cis* **P1** had a $T_g$ at −10 °C and a broad exothermic band at ~94 °C due to the thermal *cis*-to-*trans* isomerization in the first heating curve. The low $T_g$ of *cis* **P1** was verified by DMA measurements, which revealed that $T_g$ of *cis* **P1** was −6 °C (Supplementary Fig. 18). The low $T_g$ of *cis* **P1** was in accordance with the observation that *cis* **P1** was a liquid at room temperature. The second heating DSC curve of this sample was the same as that of *trans* **P1**, showing that *cis* **P1** was thermally converted to *trans* **P1** in the first heating process. The DSC curves of the two control samples were similar to those of *trans* **P1**. These data confirmed that the photoinduced solid-to-liquid transition of **P1** was due to its photoswitchable $T_g$.

To study the effects of *cis* content on $T_g$, **P1** samples with different *cis* contents were prepared by keeping *cis* **P1** in the dark for different times (Supplementary Fig. 19). DSC measurements showed that the $T_g$ of **P1** decreased as the *cis* content in **P1** increased, suggesting that the *cis* isomer acted as a plasticizer.

**Photoinduced liquid-to-solid transition.** To demonstrate that the liquid *cis* **P1** could switch back to a solid, we studied *cis*-to-*trans* photoisomerization of **P1** (Fig. 3a). *Cis* **P1** prepared via the route shown in Fig. 2a was dropped onto a Teflon substrate. When *cis* **P1** was put in contact with a needle, it stuck to the needle, showing that the *cis* **P1** is a viscous liquid. Subsequently, *cis* **P1** was converted to *trans* **P1** by illumination with 530 nm visible light. After irradiation, the sample was a solid that could be detached from the Teflon substrate by a needle and blown away by a stream of nitrogen.

The photoinduced liquid-to-solid transition was also quantified by piezo-rheology (Fig. 3b,c). *Cis* **P1** was sandwiched between two quartz glass plates (gap of 100 μm) in a piezo-rheometer to measure its shear modulus. *Cis* **P1** showed the classical behaviour of a polymer melt in the measured frequency range (Fig. 3b and Supplementary Fig. 20). Its elastic modulus ($G'$) was lower than its loss modulus ($G''$). $G''$ was proportional to the frequency at low frequency (Fig. 3b). The corresponding loss tangent (tan $\delta = G''/G'$) was greater than 1. These data further confirmed that *cis* **P1** is a

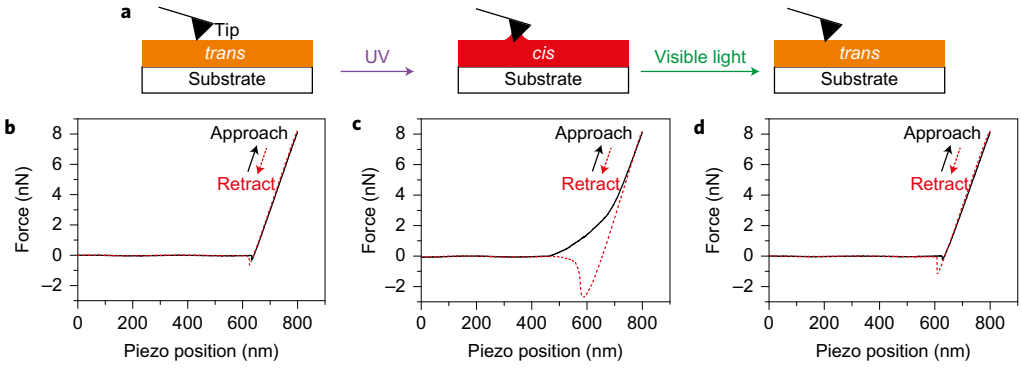


**Figure 4 | Reversible photoinduced solid-to-liquid transition of P1 in a spin-coated film studied by scanning force microscopy. a**, Schematic illustration of measuring force–piezo position curves. They were measured by approaching the tip to the **P1** film and then retracting the tip. **b**–**d**, Force–piezo position curves of the **P1** film before irradiation (**b**), after 365 nm ultraviolet irradiation (56 mW cm$^{-2}$, 6 min) (**c**) and after 530 nm visible light irradiation (7 mW cm$^{-2}$, 6 min) (**d**). The adhesion of **P1** film is photoswitchable.

NATURE CHEMISTRY DOI: 10.1038/NCHEM.2625 ARTICLES

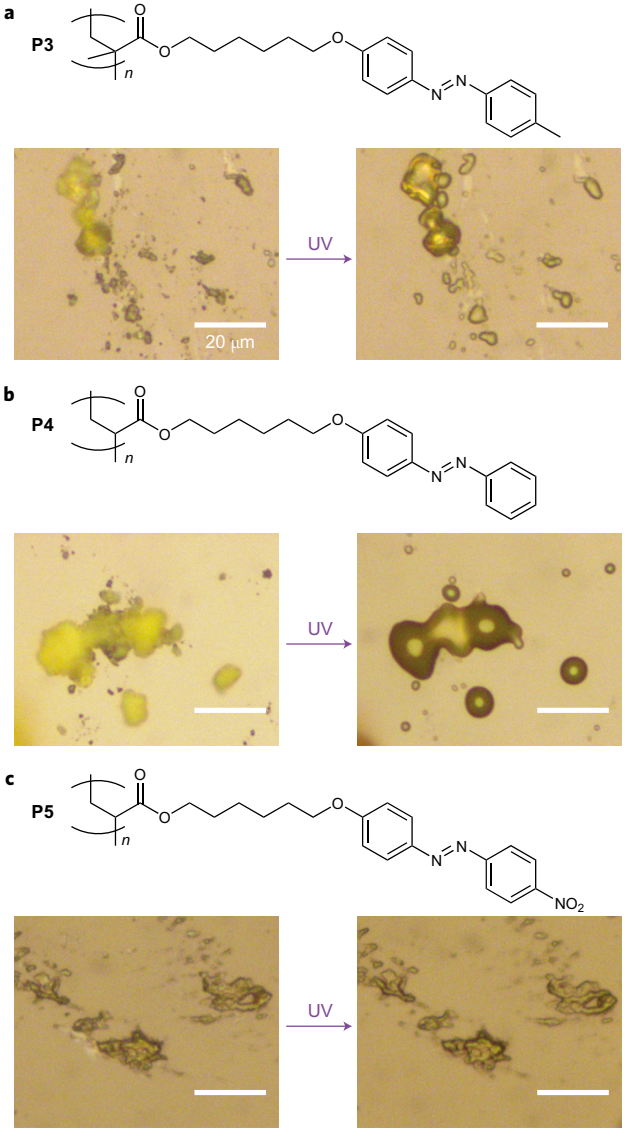


**Figure 5 | Chemical structures of three azopolymers and photoinduced solid-to-liquid transitions of these azopolymers studied by optical microscopy. a–c**, Optical microscopy images of powders of **P3** (**a**), **P4** (**b**) and **P5** (**c**) before and after 365 nm light irradiation (30 mW $cm^{-2}$, 20 min). Although UV irradiation induced the flow of **P3** and **P4** powders, it did not induce the flow of **P5** powders. Scale bars, 20 μm.

liquid. In addition, the viscosity of *cis* **P1** was constant (~$4 \times 10^3$ Pa s) at low frequencies (0.25–2 Hz) and decreased at high frequencies (2–160 Hz) (Supplementary Fig. 20), which showed that *cis* **P1** behaves as a typical polymer melt. *Cis* **P1** was converted to *trans* **P1** in the rheometer by illumination with 530 nm light (6.3 mW $cm^{-2}$, 15 min). The value of $G'$ for *trans* **P1** was larger than its $G''$ and its tan $\delta$ was less than 0.15 (Fig. 3c). The absolute values of $G'$ and $G''$ may have been influenced by shrinkage of the sample during the solidification process and subsequent partial detachment of the sample from the plates. The low value of tan $\delta$, however, showed that visible light converted liquid *cis* **P1** to solid *trans* **P1**.

**Photoinduced reversible solid-to-liquid transition.** The DSC and rheology measurements required bulk samples that could not be penetrated deeply by ultraviolet light. To demonstrate that **P1** showed reversible photoinduced solid-to-liquid transitions, we performed scanning force microscopy (SFM) measurements on thin films of **P1** (Fig. 4a). The force–piezo position curves obtained with a spin-coated film of *trans* **P1** showed all the signs of a hard surface (Fig. 4b)[25]. After contact with the tip, the force increased linearly as the piezo position increased. The adhesion force of *trans* **P1** was 0.67 nN.

Subsequently, the *trans* **P1** film was converted to *cis* **P1** film by ultraviolet illumination, and the force–piezo position curves of *cis* **P1** film were measured (Fig. 4c). The adhesion force increased to 2.7 nN, indicating that *cis* **P1** is more adhesive than *trans* **P1**. Additionally, the force–piezo position curves of *cis* **P1** were different from those of *trans* **P1**. In the approach process, the SFM tip contacted *cis* **P1** at 470 nm and the slope of the curve gradually increased as the piezo position increased. At a piezo extension of 750 nm, a linear behaviour was observed. In the retract process, the force exhibited a minimum at 586 nm. Further withdrawal of the tip gradually decreased the force to 0 nN. These results revealed that *cis* **P1** was a viscous material that formed a meniscus with the tip, while in the *trans* form, the adhesion was dominated by van der Waals forces. The meniscus led to a capillary force larger than the van der Waals forces.

The *cis* **P1** was switched back to *trans* **P1** by illumination with visible light. The force–piezo position curves of the regenerated *trans* **P1** film (Fig. 4d) were similar to those of the as-prepared *trans* **P1** film (Fig. 4b), indicating that visible light had solidified the sample. This experiment showed that **P1** exhibits a photoinduced reversible solid-to-liquid transition where the mechanical properties of the film can be controlled with light.

**Photoinduced solid-to-liquid transitions of other azopolymers.** To study the necessary chemical constituents for the photoinduced solid-to-liquid transitions, we synthesized three additional azopolymers (Fig. 5 and Supplementary Fig. 1). **P3** is a polymethacrylate with the same side chain as **P1**. **P4** and **P5** are polyacrylates. Compared to **P1**, **P4** does not have a methyl group on the 4-position of the azo moiety and **P5** has a nitro group on the 4-position of the azo moiety.

Both **P3** and **P4** showed photoinduced solid-to-liquid transitions (Fig. 5a,b). The shear moduli of **P3** and **P4** measured using a piezo-rheometer showed that *cis* **P3** and *cis* **P4** are liquid, while *trans* **P3** and *trans* **P4** are solid (Supplementary Figs 20 and 21). In addition, the $T_g$ values of *trans* **P3** and *trans* **P4** were above room temperature, while $T_g$ for *cis* **P3** and *cis* **P4** were below room temperature (Supplementary Figs 21 and 22). The studies on **P1**, **P2**, **P3** and **P4** revealed that the photoinduced solid-to-liquid transition is a general phenomenon for these azopolymers.

However, ultraviolet irradiation on **P5** powders did not induce the flow of the powders (Fig. 5c). In contrast to the azobenzene groups in the other azopolymers, both *trans* and *cis* azobenzene groups in **P5** have large dipole moments (Supplementary Fig. 23). The azobenzene group in **P5** is a push–pull-type azobenzene[26], with a short lifetime in the *cis* state (half-life of ~16 min, Supplementary Fig. 24). The $T_g$ and shear moduli of *cis* **P5** could not be measured by DSC and rheometry due to this short lifetime. Comparison of **P5** with the other azopolymers indicates that push–pull azobenzene groups are not suitable for the construction of azopolymers that show photoinduced solid-to-liquid transitions.

**Comparison of azopolymers in this study with some related polymers.** It is well known that the $T_g$ of a polymer can be greatly influenced by *cis* and *trans* configurations in the polymer because the volume, chain stiffness and interchain cohesion of polymer chains with *cis* and *trans* configurations are different[27]. For example, $T_g$ for *cis* and *trans* poly(1-butenylene) are 171 and 215 K, respectively[27]. Similar to *cis* and *trans* poly(1-butenylene), *cis* and *trans* azopolymers may have different $T_g$ values.

The photoinduced solid-to-liquid transition reported here is different from the conventional directional photofluidization

ARTICLES NATURE CHEMISTRY DOI: 10.1038/NCHEM.2625

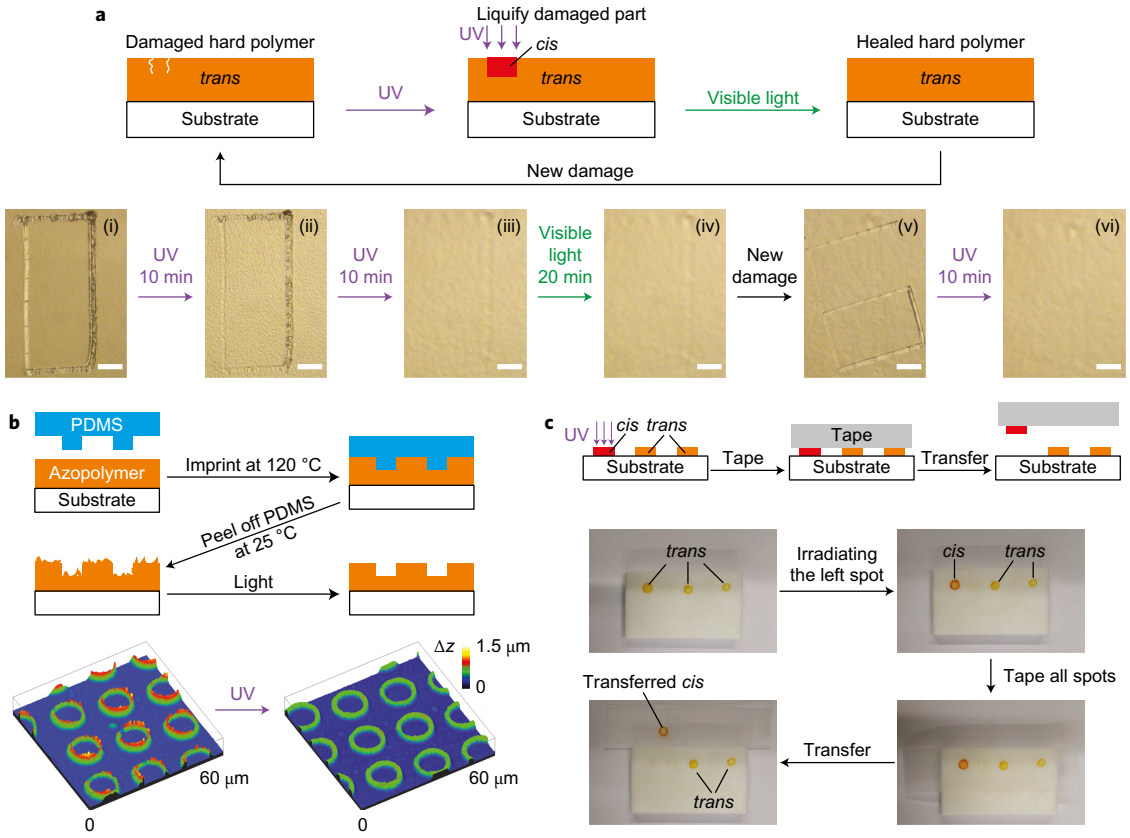


**Figure 6 | Healing, reduction of surface roughness and transfer printing based on photoinduced solid-to-liquid transitions. a**, Healing of scratches on a hard azopolymer coating with light. Top: Schematic illustration of the healing process. Bottom: Optical microscopy images showing repeated healing of **P2** by light. Scale bars, 20 μm. The ultraviolet and visible light used for irradiation were 365 nm at 67 mW $cm^{-2}$ and 530 nm at 5 mW $cm^{-2}$, respectively. **b**, Photoinduced reduction of surface roughness. Top: Schematic illustration of the patterning of **P1** using imprint lithography. **P1** formed a rough surface when the PDMS master was peeled off. The surface roughness could be reduced by light irradiation. Bottom: Patterned **P1** before and after irradiation with 365 nm ultraviolet light (20 mW $cm^{-2}$, 30 min). **c**, Schematic illustration (top) and photographs (bottom) of transfer printing based on the photoinduced solid-to-liquid transition. The spot on the left side was irradiated by 365 nm light (67 mW $cm^{-2}$, 20 min).

(inscription of surface relief gratings) of azopolymers. Directional photofluidization is based on photoinduced *trans*–*cis*–*trans* cycling; that is, light induces repeated *trans*-to-*cis* and *cis*-to-*trans* isomerizations[19,20]. Polymers with push–pull azobenzene groups such as Disperse Red 1 are better suited for directional photofluidization because the absorption bands of *trans* and *cis* isomers overlap and both *trans*-to-*cis* and *cis*-to-*trans* isomerizations can be induced by visible light at the same wavelength. This kind of fluid-like state only exists when the polymer is under continuous light irradiation. Additionally, the direction of mass transport of azopolymers via directional photofluidization is polarization-dependent[19,20].

Different from the conventional directional photofluidization, the solid-to-liquid transition reported here is based on the different $T_g$ of *trans* and *cis* azopolymers; that is, the *trans* polymer is solid and the *cis* polymer is liquid. Once a *trans* azopolymer is converted to the *cis* azopolymer, the *cis* azopolymer is in the liquid state even when the ultraviolet light is switched off. Additionally, the liquid *cis* azopolymers are isotropic and the photoinduced flow is non-directional. *Cis* azopolymers with a long lifetime and high *cis* content (for example, **P1**) are better suited for photoinduced solid-to-liquid transitions. Azopolymers with push–pull azobenzene groups (for example, **P5**) are not suited for photoinduced solid-to-liquid transitions.

**Applications based on photoinduced solid-to-liquid transitions.** One application of azopolymers is the fabrication of healable hard coatings (Fig. 6a). To demonstrate photoinduced healing, a scratch on a *trans* **P2** ($T_g$ = 68 °C) film (Fig. 6a(i)) was locally irradiated with ultraviolet light. As a result, the damaged part was converted to the liquid state and the scratch was healed due to capillary flow of the polymer (Fig. 6a(ii), a(iii)). Visible light switched the healed **P2** back to the solid state (Fig. 6a(iv)). A new scratch was then made in the same place on the film (Fig. 6a(v)). The new scratch was then healed with light (Fig. 6a(vi)). The azopolymer could thus be repeatedly healed with light. We also used confocal microscopy to quantify the depth and width of a healable scratch. A scratch with a depth of 300 nm and a width of 12 μm was healed with light (Supplementary Fig. 25).

Another application of a photoinduced solid-to-liquid transition is the fabrication of smooth surfaces. To demonstrate a photoinduced decrease in surface roughness, **P1** was patterned via imprint lithography (Fig. 6b). Peeling off the polydimethylsiloxane (PDMS) master from the polymer film created patterns with rough surfaces. The photoinduced solid-to-liquid transition reduced the surface roughness of patterned **P1** by a factor of almost 600% (defined as the ratio of the initial roughness to the final roughness) under a moderate dose of irradiation (20 mW $cm^{-2}$, 30 min) (Fig. 6b). The irregular edges on the pattern became smooth after irradiation (Fig. 6b and Supplementary Fig. 26). Hence, a photoinduced reversible solid-to-liquid transition enabled the fabrication of smooth microstructures.

The photoswitchable adhesion (Fig. 4) of **P1** also has potential applications in transfer printing. To demonstrate transfer printing,

NATURE CHEMISTRY DOI: 10.1038/NCHEM.2625 ARTICLES

three spots of **P1** were prepared on a Teflon substrate (Fig. 6c). The spot on the left side was liquefied by ultraviolet irradiation (Supplementary Fig. 27). A tape was then pressed on all three spots. Only the liquefied spot was transferred to the tape.

## Conclusions

In conclusion, we have demonstrated that azopolymers show a reversible solid-to-liquid transition due to photoswitchable $T_g$. The photoswitching of $T_g$ was applied to repeatedly heal damage on an azopolymer with a $T_g$ of 68 °C, to reduce the surface roughness of a patterned azopolymer, and for transfer printing. The photoswitching of $T_g$ is a new strategy for designing healable polymers with high $T_g$ and hard polymer coatings that can be processed at room temperature without the use of plasticizing solvents. One advantage of this new approach is that light provides high spatiotemporal resolution to precisely and locally heal and process polymers. We anticipate that, like azopolymers, other stimuli-responsive polymers may exhibit switchable $T_g$. Our study opens up an avenue for manipulating the $T_g$ of polymers, which is important for both the fundamental understanding of $T_g$ and applications of such polymeric materials.

## Methods

Detailed procedures for the synthesis and characterization of the azopolymers are provided in the Supplementary Information.

**Preparation of polymer films.** The polymer films were prepared with a spin-coating or drop-casting method. In brief, the azopolymers were dissolved in cyclopentanone and the solutions (2–5 wt%) were stirred overnight at room temperature before use. To prepare thin films (<500 nm), the polymer solutions were spin-coated onto clean glass, silicon wafer or quartz substrates. Film thickness was controlled by adjusting the spin speed and the concentration of the polymer solutions. To prepare thick polymer films (6–8 μm), the polymer solutions were dropcast on substrates. To remove residual solvents, the films were first dried in a fume hood, before being transferred to an oven and dried under vacuum at 120 °C overnight.

**Patterning of P1 films.** A PDMS mould was pressed onto a **P1** film at 120 °C for 8 h. The sample was then cooled to room temperature, and the PDMS mould was peeled off to obtain patterned **P1**.

**Preparation of *trans* P1 for DSC measurements.** After **P1** was synthesized, it was dried in a vacuum oven at 40 °C for 24 h. The **P1** was then further dried in a vacuum oven at 120 °C for 6 h and at 40 °C for two days. The dried **P1** was transferred to a DSC sample pan to measure its DSC curves.

**Preparation of *cis* P1 for DSC measurements.** *Trans* **P1** (30 mg) was dissolved in $CH_2Cl_2$ (3 ml). The polymer solution was irradiated with 365 nm light (4.5 mW $cm^{-2}$) for 10 min under stirring to induce *trans*-to-*cis* isomerization. $CH_2Cl_2$ was then removed by a rotary evaporator at 10–25 mbar for 25 min. The dried *cis* **P1** was quickly transferred to a DSC sample pan. The DSC measurements were taken immediately.

Received 25 November 2015; accepted 24 August 2016; published online 10 October 2016

## References


1. Colquhoun, H. M. Self-repairing polymers: materials that heal themselves. *Nat. Chem.* **4,** 435–436 (2012).
2. Yang, Y. & Urban, M. W. Self-healing polymeric materials. *Chem. Soc. Rev.* **42,** 7446–7467 (2013).
3. Fiore, G. L., Rowan, S. J. & Weder, C. Optically healable polymers. *Chem. Soc. Rev.* **42,** 7278–7288 (2013).
4. Wu, S. *et al.* Supramolecular bisazopolymers exhibiting enhanced photoinduced birefringence and enhanced stability of birefringence for four-dimensional optical recording. *J. Mater. Chem.* **20,** 5202–5209 (2010).
5. Kravchenko, A., Shevchenko, A., Ovchinnikov, V., Priimagi, A. & Kaivola, M. Optical interference lithography using azobenzene-functionalized polymers for micro- and nanopatterning of silicon. *Adv. Mater.* **23,** 4174–4177 (2011).
6. Kucharski, T. J. *et al.* Templated assembly of photoswitches significantly increases the energy-storage capacity of solar thermal fuels. *Nat. Chem.* **6,** 441–447 (2014).
7. Baroncini, M. *et al.* Photoinduced reversible switching of porosity in molecular crystals based on star-shaped azobenzene tetramers. *Nat. Chem.* **7,** 634–640 (2015).
8. Yu, Y. L., Nakano, M. & Ikeda, T. Directed bending of a polymer film by light—miniaturizing a simple photomechanical system could expand its range of applications. *Nature* **425,** 145 (2003).
9. Zhang, L., Liang, H., Jacob, J. & Naumov, P. Photogated humidity-driven motility. *Nat. Commun.* **6,** 7429 (2015).
10. Velema, W. A. *et al.* Optical control of antibacterial activity. *Nat. Chem.* **5,** 924–928 (2013).
11. Akiyama, H. & Yoshida, M. Photochemically reversible liquefaction and solidification of single compounds based on a sugar alcohol scaffold with multi azo-arms. *Adv. Mater.* **24,** 2353–2356 (2012).
12. Okui, Y. & Han, M. Rational design of light-directed dynamic spheres. *Chem. Commun.* **48,** 11763–11765 (2012).
13. Hoshino, M. *et al.* Crystal melting by light: X-ray crystal structure analysis of an azo crystal showing photoinduced crystal–melt transition. *J. Am. Chem. Soc.* **136,** 9158–9164 (2014).
14. Ishiba, K. *et al.* Photoliquefiable ionic crystals: a phase crossover approach for photon energy storage materials with functional multiplicity. *Angew. Chem. Int. Ed.* **54,** 1532–1536 (2015).
15. Uchida, E., Azumi, R. & Norikane, Y. Light-induced crawling of crystals on a glass surface. *Nat. Commun.* **6,** 7310 (2015).
16. Kim, D. Y., Tripathy, S. K., Li, L. & Kumar, J. Laser-induced holographic surface-relief gratings on nonlinear-optical polymer-films. *Appl. Phys. Lett.* **66,** 1166–1168 (1995).
17. Rochon, P., Batalla, E. & Natansohn, A. Optically induced surface gratings on azoaromatic polymer-films. *Appl. Phys. Lett.* **66,** 136–138 (1995).
18. Karageorgiev, P. *et al.* From anisotropic photo-fluidity towards nanomanipulation in the optical near-field. *Nat. Mater.* **4,** 699–703 (2005).
19. Yager, K. G. & Barrett, C. J. in *Polymeric Nanostructures and Their Applications* (ed. Nalwa, H. S.) Ch. 8 (American Scientific, 2006).
20. Lee, S., Kang, H. S. & Park, J. K. Directional photofluidization lithography: micro/nanostructural evolution by photofluidic motions of azobenzene materials. *Adv. Mater.* **24,** 2069–2103 (2012).
21. Kang, H. S., Kim, H. T., Park, J. K. & Lee, S. Light-powered healing of a wearable electrical conductor. *Adv. Funct. Mater.* **24,** 7273–7283 (2014).
22. Lee, S., Kang, H. S. & Park, J. K. High-resolution patterning of various large-area, highly ordered structural motifs by directional photofluidization lithography: sub-30-nm line, ellipsoid, rectangle, and circle arrays. *Adv. Funct. Mater.* **21,** 1770–1778 (2011).
23. Vapaavuori, J., Laventure, A., Bazuin, C. G., Lebel, O. & Pellerin, C. Submolecular plasticization induced by photons in azobenzene materials. *J. Am. Chem. Soc.* **137,** 13510–13517 (2015).
24. Ikeda, T. & Tsutsumi, O. Optical switching and image storage by means of azobenzene liquid-crystal films. *Science* **268,** 1873–1875 (1995).
25. Cappella, B. Mechanical properties and adhesion of a micro structured polymer blend. *Polymers* **3,** 1091–1106 (2011).
26. Bandara, H. M. D. & Burdette, S. C. Photoisomerization in different classes of azobenzene. *Chem. Soc. Rev.* **41,** 1809–1825 (2012).
27. Andrews, R. J. & Grulke, E. A. in *Polymer Handbook* 4th edn (eds Brandrup, J. *et al.*) VI 193–VI 278 (Wiley, 1999).


## Acknowledgements

This work was supported by the Deutsche Forschungsgemeinschaft (DFG, WU 787/2–1). H.Z. was supported by the MPG-CAS Joint Doctoral Promotion Programme (DPP). C.X. was supported by the CSC programme. S.H. and G.K.A. acknowledge support by DFG through SPP 1681, project no. AU321/3-1. The authors thank G. Fytas, G. Floudas and T. Bereau for helpful discussion and G. Kircher, U. Rietzler, J. Thiel and A. Hanewald for technical support.

## Author contributions

S.W. conceived the idea and led the project. S.W., K.K., G.K.A., R.B. and H.-J.B. designed the experiments. H.Z., C.X., P.W., Y.S., S.H., K.K., R.B. and S.W. performed the experiments and analysed the data. All authors wrote the paper. H.Z., C.X. and P.W. contributed equally to this work.

## Additional information

Supplementary information is available in the online version of the paper. Reprints and permissions information is available online at www.nature.com/reprints. Correspondence and requests for materials should be addressed to S.W.

## Competing financial interests

The authors declare no competing financial interests.

## 2.4 Photo-Healing Azopolymers Based on Photoinduced Reversible Solid-to-Liquid Transitions

Philipp Weis, Andreas Hess, Gunnar Kircher, Shilin Huang, Günter K. Auernhammer and Si Wu

*in preparation*

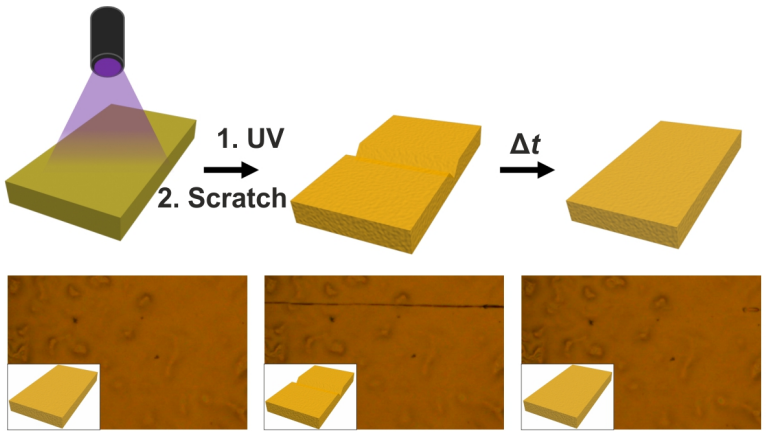


The influence of azopolymer side chain spacer length on solid-to-liquid transitions is investigated. While moderate spacer length exhibit solid-to-liquid transitions, short and long spacers do not. Healing scratches by light irradiation is demonstrated on hard surfaces made from azopolymer coatings with moderate spacer length.

**Author Contributions**

Si Wu conceived the idea and led the project. Si Wu, Günter K. Auernhammer and Philipp Weis designed the experiments. Philipp Weis performed UV vis and NMR spectroscopy, (polarized) optical microscopy, photoisomerization experiments, TGA and DSC measurements, healing experiments and did the synthesis of compound 14 together with Andreas Hess. Andreas Hess synthesized compound 12 and 13. Gunnar Kircher synthesized P-0-Azo, P-2-Azo and P-20-Azo. Shilin Huang did the piezo-rheology measurements. The manuscript was written through contributions of all authors. All authors have given approval to the final version of the manuscript.

**Supporting Information** can be found on page 160.

**Photo-Healing Azopolymers Based on Photoinduced Reversible Solid-to-Liquid Transitions**

*Philipp Weis, Andreas Hess, Gunnar Kircher, Shilin Huang, Günter K. Auernhammer, Kaloian Koynov, Si Wu**

Philipp Weis, Andreas Hess, Gunnar Kircher, Shilin Huang, Günter K. Auernhammer, Kaloian Koynov, Si Wu
Max Planck Institute for Polymer Research, Ackermannweg 10, 55128 Mainz, Germany
E-mail: wusi@mpip-mainz.mpg.de

Keywords: stimuli-responsive, polymer, photoliquefaction, azobenzene, photoisomerization,

Photoswitchable polymers are promising candidates for healable materials. However, a general lack in knowledge about the influence of polymer structure on solid-to-liquid transition due to *trans*-to-*cis* photoisomerization hinders progression and application of photoswitchable polymers. Here, the synthesis and behavior under light irradiation of azobenzene-containing side chain polymers (azopolymers) with different carbon chain spacer lengths between the polymer backbone and photoresponsive azobenzene groups (P-n-Azo) is demonstrated. While no carbon spacer (P-0-Azo) and 20 carbon spacer (P-20-Azo) do not show photoinduced solid-to-liquid transition at room temperature, a twelve carbon spacer (P-12-Azo) is sufficient for photoinduced solid-to-liquid transition at room temperature and is utilized for photohealable scratches of azopolymer film surfaces. Furthermore, this is the first time that flowing of *cis* P-12-Azo was monitored at real time.

## 1. Introduction

The melting point or glass transition temperature ($T_g$) of a chemical compound is highly dependent on the chemical structure of the material.[1, 2] In order to bring a material from a solid to a liquid state, the material is typically heated above its melting point or $T_g$. In some cases, however, it can be advantageous to transfer a material from a solid to a liquid and vice versa isothermally by using a different external stimulus. The chemical structure can be changed using an external stimulus which can be exploited to change the materials properties like solid-to-liquid transition temperature. External stimuli such as light can be used to switch polymer structures.[3] Light is a non-contact stimulus, it is clean and can be switched on and off fast. Photoswitchable polymers typically exhibit two forms with different absorption spectra.[4] In this way they can be transformed into each other by utilizing different wavelengths. Compared to heat induced liquefaction, photoinduced liquefaction has a higher spatiotemporal resolution.

One of the most renowned photoswitchable units is azobenzene. Azobenzene has a thermodynamically stable *trans*-isomer, which is a rod like molecule. The metastable *cis*-isomer is a bent molecule. *Trans*-to-*cis* isomerization is induced by UV light irradiation. The *cis*-to-*trans* back reaction can be induced by either visible light irradiation or heating. Azobenzene-containing small molecules show reversible photoinduced solid-to-liquid transition based on a isothermal crystal-to-melt transition.[5-11] While in small molecule compounds photoisomerization can sometimes be restricted in solid state due to crystallization, polymers have the advantage of free volume for chromophores to undergo *trans*-to-*cis* isomerization.[12-16] This *trans*-to-*cis* isomerization of azobenzene-containing polymers (azopolymers) leads to an isothermal solid-to-liquid transition of some azopolymers.[1] The adhesion of azopolymers with different alkyl substitutions has been

investigated.[17] It was found that the length of the alkyl chain has only minor influence on the adhesion strength. However, the solid-to-liquid transition based on photoswitching $T_g$ and other properties have not been investigated.

While our previous work has focused on demonstrating the proof-of-concept of photoswitching $T_g$ of azopolymers, this work focuses on understanding the influence of the side chain length of the azopolymer, which is an important step towards a deeper understanding of this phenomenon and the possibility for future applications.

## 2. Results and Discussion

### 2.1 Synthesis and Characterization of P-n-Azo

First, the azobenzene-containing polymers P-n-Azo were synthesized by free radical polymerization. P-n-Azo are polyacrylates with different spacer length between the polymer backbone and the azobenzene unit (no spacer, two, six, twelve or 20 $CH_2$ units, Scheme 1). Molecular weights of P-n-Azo are listed in Table 1 and were 7.6, 8.9, 9.9, 8.6 and $10.6 \times 10^3$ g $mol^{-1}$ respectively.

P-n-Azo exhibit a strong π-π* absorption band in the UV range and a weak n-π* band in the visible light range. UV light irradiation of P-n-Azo films decreased the π-π* band and increased the n-π* band, demonstrating *trans*-to-*cis* isomerization of P-n-Azo which is well known for azo chromophores. The *cis*-to-*trans* back isomerization can be induced by visible light irradiation of the *cis* n-π* absorption band, enabling reversible photoisomerization (Figure 1).

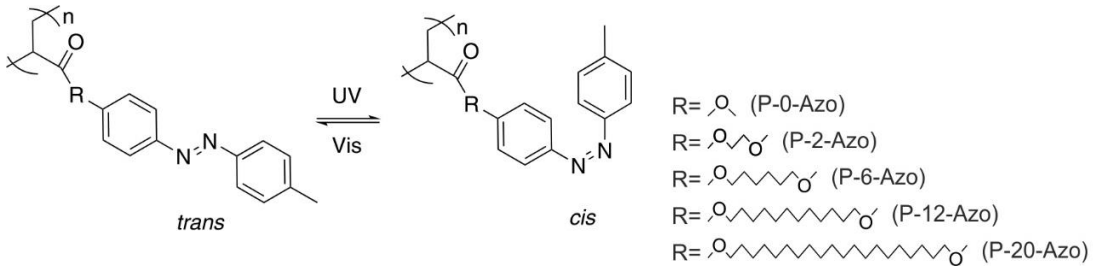


**Scheme 1.** Photoisomerization and chemical structures of P-n-Azo polymers used in this study. Polyacrylates with azobenzene sidechains bearing different spacer lengths ranging from zero to 20.

**Table 1.** Comparison of photoinduced reversible solid-to-liquid transitions of P-n-Azo.

| | **Spacer Length (number of carbon atoms)** | **$M_n$ / $10^3$ g mol$^{-1}$ (GPC)** | **Solid-to-Liquid Transition** |
|---|---|---|---|
| **P-0-Azo** | 0 | 7.6 | No |
| **P-2-Azo** | 2 | 8.9 | Unclear |
| **P-6-Azo** | 6 | 9.9 | Yes |
| **P-12-Azo** | 12 | 8.6 | Yes |
| **P-20-Azo** | 20 | 10.6 | No |

### 2.2 Photoinduced solid-to-liquid transition

UV light triggers *trans*-to-*cis* isomerization of conventional azobenzene. While the *trans* form is a rigid rod, the *cis* form is a bent molecule (Scheme 1). Here, azobenzene is incorporated in the side chain of polyacrylates. All P-n-Azo in this study can be switched from *trans* to *cis* in solid state, demonstrated by UV-vis absorption spectroscopy of P-n-Azo polymer films before and after light irradiation (Figure 1). The absorbance of some polymer films was lower before irradiation than after UV and visible light irradiation because stacking and orientation of the chromophores changed (Figure S1). Recently, UV light induced liquefaction of P-6-Azo at room temperature was demonstrated by our group.[1] Here, light induced liquefaction of the other P-n-Azo is investigated. While light induced liquefaction of P-0-Azo and P-20-Azo is not observed, P-12-Azo shows light induced liquefaction (Figure 1). P-2-Azo shows no distinct change and is therefore not further investigated.

Photoswitching *trans* P-12-Azo to *cis* P-12-Azo liquefies the polymer sample. The liquid *cis* P-12-Azo can be switched back to a solid P-12-Azo using green light irradiation (Figure 2a). While c*is* P-12-Azo is soft and sticks to a needle, *trans* P-12-Azo is hard and can be removed from the surface by scratching with a needle and blowing away the powder. Accordingly, in piezo rheology measurements the moduli of P-12-Azo change from low values for *cis* P-12-Azo to high values for *trans* P-12-Azo. (Figure 2b,c). *Cis* P-12-Azo behaves like a typical polymer melt (Figure 2 and S2)

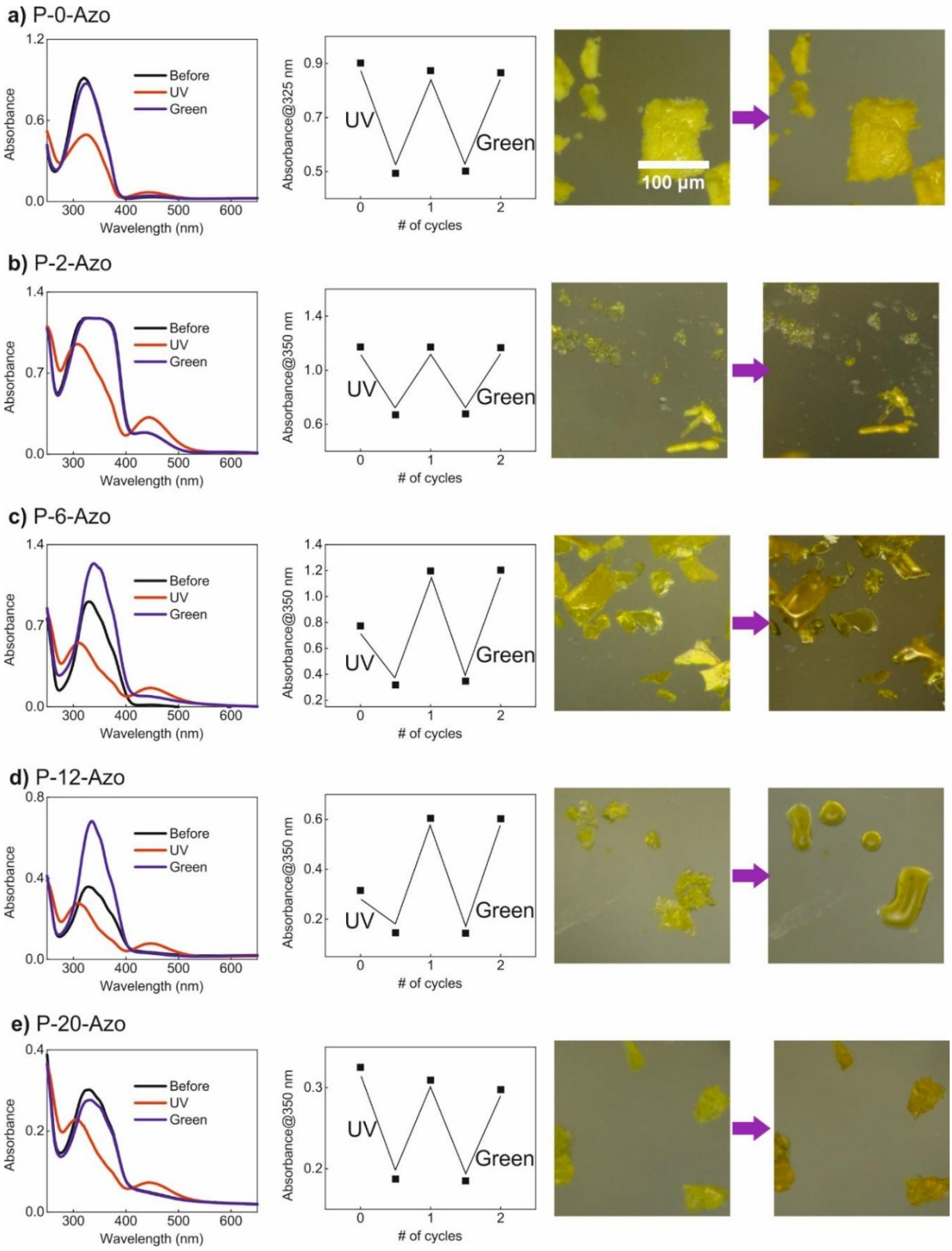


**Figure 1.** Photoisomerization of P-n-Azo. UV-vis absorption spectra of P-n-Azo films before irradiation (black line), after UV irradiation (10 min, 45 mW $cm^{-2}$) (red line) and after subsequent green light irradiation (blue line) (2 min, 50 mW $cm^{-2}$). Value of absorbance maximum after repeated UV and green light irradiation demonstrating switching cycles. Optical microscopy images of P-n-Azo powders before and after UV light irradiation (8 min, 20 mW $cm^{-2}$).

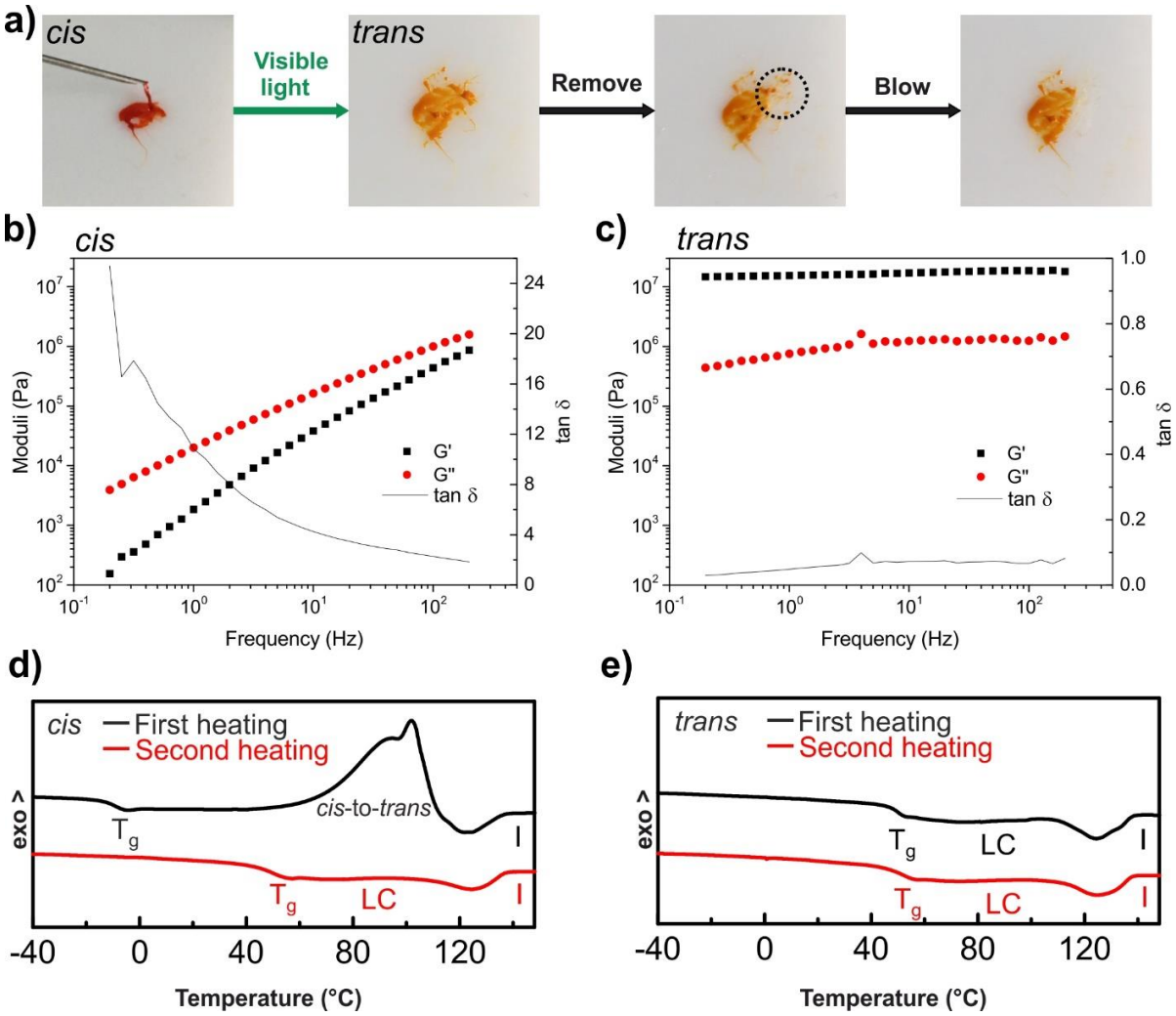


**Figure 2.** Liquid-to-solid transition of P-12-Azo powders. a) Photographs of liquid *cis* P-12-Azo sticking to a needle and solid *trans* P-12-Azo after visible light irradiation, scratching solid *trans* P-12-Azo powders with a needle from the substrate (dashed circle) and remove powders by blowing with a needle. b) Piezo Rheology of *cis* P-12-Azo and c) after it was switched back to *trans* P-12-Azo using green light irradiation. d) DSC first and second heating curves of *cis* P-12-Azo. During first heating the *cis* form switches back to the *trans* form thermally, demonstrated by the exothermic peak around 100 °C. The second heating curve is similar to the *trans* heating curves in e), demonstrating the *cis* form is completely switched back to *trans* by heating. LC: liquid crystalline phase; I: isotropic phase.

To better understand why P-12-Azo can be liquefied at room temperature by UV light irradiation but P-0-Azo and P-20-Azo cannot, Differential Scanning Calorimetry (DSC) data of the polymers were obtained (Figure 2d,e, 3 and 4a). All P-n-Azo are stable at least up to 200 °C (Figure S3). DSC curves of *trans* P-n-Azo were measured and compared to DSC curves of *cis* P-n-Azo. *Trans* P-12-Azo shows a glass transition temperature ($T_g$) at 45 °C (Figure 2 and S4) and a phase transition at 120 °C. P-12-Azo is isotropic above 120 °C and anisotropic below 120 °C (Figure S5). After UV light irradiation, *trans* P-12-Azo is transformed into *cis* P-12-Azo (Figure S6). *Cis* P-12-Azo shows a $T_g$ below room temperature and thus is liquid at room temperature. During the first heating, *cis* P-12-Azo starts to thermally transform back to *trans* P-12-Azo at 50 °C and is completely switched to *trans* P-12-Azo after the first heating. In the second heating the DSC curve is the same as for the solid *trans* P-12-Azo. It can be concluded that the $T_g$ difference of *cis* and *trans* P-12-Azo leads to liquefaction. The $T_g$ difference was confirmed by DMA (Figure S7). In the *trans* state P-12-Azo has an anisotropic order. UV light irradiation changes the anisotropic *trans* state to an isotropic *cis* state (Figure S8 and S9) but the loss of the anisotropic order is not the reason for the solid-to-liquid transition. By quenching P-12-Azo from the isotropic state at high temperature, amorphous P-12-Azo was prepared, which also showed the photoinduced solid-to-liquid transition (Figure S10). P-12-Azo, which has a slightly longer carbon spacer between the backbone and the chromophore than P-6-Azo, shows very similar behavior to P-6-Azo.[1]

Light induced liquefaction of P-0-Azo is not observed (Figure 1). T*rans* P-0-Azo has a $T_g$ around 100 °C (Figure 3 and Figure S4). Anisotropic phases of P-0-Azo could not be observed because the temperature for P-0-Azo to become isotropic is close to the degradation temperature of P-0-Azo. For *cis* P-0-Azo a $T_g$ shift was not observed. $T_g$ of *trans* P-0-Azo is

in the same temperature range as the broad exothermic peak of the thermal *cis*-to-*trans* back reaction. $T_g$ of *cis* P-0-Azo could overlap with the *cis*-to-*trans* peak. Additionally, the step in DSC which is considered as $T_g$ is small. After preparation for DSC measurements, *cis* P-0-Azo is a fine powder (Figure 3), in contrast to *cis* P-12-Azo, which is a melt state (Figure 2a). Typically, a spacer is used between the azo chromophore and the polymer backbone to provide enough space and freedom to move for the azo chromophores.[18-20]

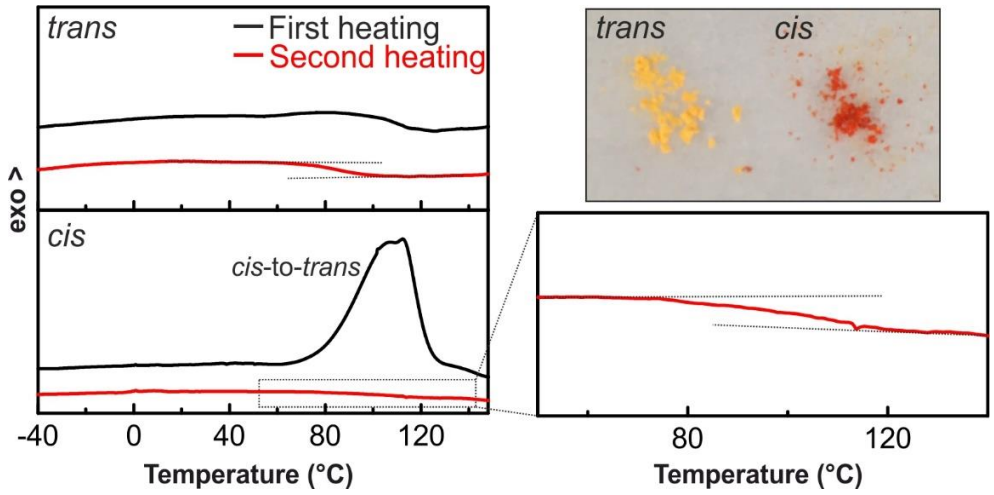


**Figure 3.** First and second heatings of *trans* and *cis* P-0-Azo. Note, that the y-axis of the *trans* and *cis* DSC curves have different dimensions because of the large exothermic *cis*-to-*trans* peak in the first heating of the *cis* DSC curve. The zoomed-in *cis* DSC curve has the same y axis dimensions as the *trans* curve to demonstrate similarity of second heating curves of P-0-Azo. Dotted lines are guides for the eye to see the step which corresponds to $T_g$. Photographs show solid *trans* (yellow) and *cis* (red) P-0-Azo powders.

*Trans* P-20-Azo shows phase transitions around 80 °C and 110 °C (Figure 4 and S5). Above 125 °C P-20-Azo is isotropic, below 125 °C P-20-Azo is anisotropic. After irradiation, *trans* P-20-Azo is transformed to *cis* P-20-Azo and shows a phase transition around 40 °C. Even though *cis* P-20-Azo has a lower phase transition than *trans* P-20-Azo, *cis* P-20-Azo is not a liquid at room temperature because the phase transition is above room temperature. However, if *cis* P-20-Azo is heated to 50 °C it becomes liquid (Figure 4b). Heating *trans* P-20-Azo to 50 °C does not liquefy the polymer. Also, *cis* P-20-Azo is isotropic at 60 °C, while it is anisotropic at 36 °C and can be reversibly switched between the two states (Figure 4c). Azopolymers typically exhibit liquid crystalline phases.[21]

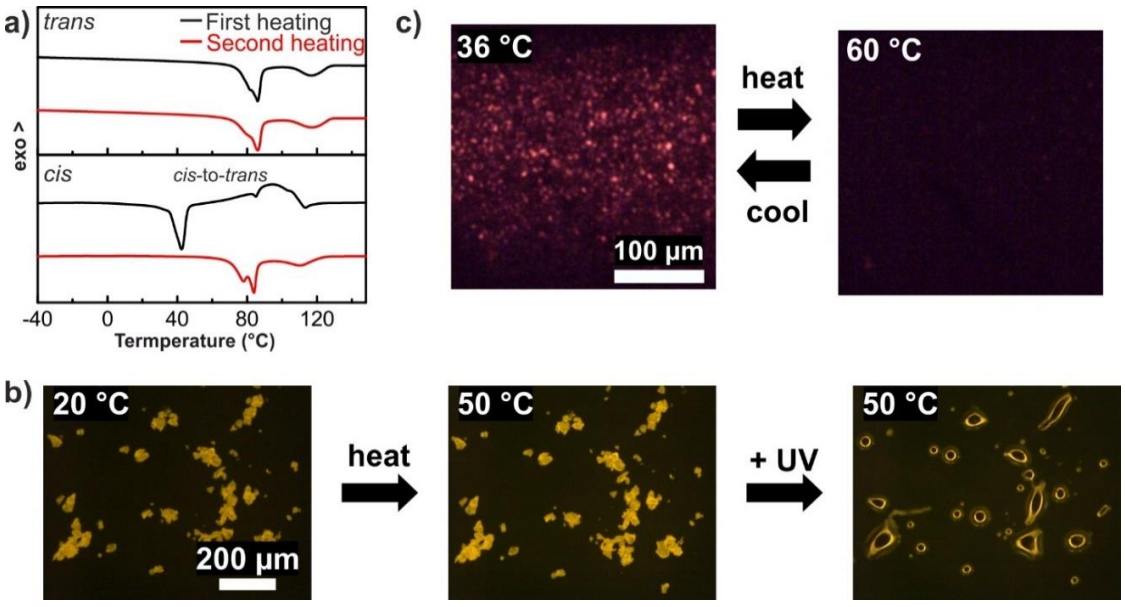


**Figure 4.** a) DSC first and second heating curves of *trans* and *cis* P-20-Azo. b) Optical microscopy of P-20-Azo powder at 20 °C, after heating to 50 °C and after UV light irradiation at 50 °C. c) POM images of a *cis* P-20-Azo film losing anisotropy after heating to 60 °C and recovers it after cooling to 36 °C.

Switching trans azobenzene groups in polymer side chains to cis azobenzene disrupts the anisotropic phase because in contrast to the rigid trans azobenzene, cis azobenzene is a bent molecule.22 Longer carbon side chains increase the interaction of polymer side chains. When the azobenzene at the end of the long side chain is switched from trans to cis there is still interaction between the long alkyl side chains, similar to polyacrylales with side chains in the same length range but without azobenzene.23 That explains why a phase transition rather than Tg is observed.

### 2.3 Flowing of *cis* P-12-Azo

Inspired by the properties of P-12-Azo the polymer was used for photohealing surfaces and the flow of the *cis* polymer was followed by optical microscopy. Spincoated films of P-12-Azo were scratched with an AFM tip attached to a micromanipulator at characteristic spots to demonstrate the same area is used for all measurements. After UV light irradiation and subsequent visible light irradiation, the scratch was healed because *cis* P-12-Azo is a liquid and can flow to fill the gap of the scratch (Figure 5 a,b). Visible light switches back the liquid *cis* to a solid *trans* film.

The flowing of the material on a *cis* P-12-Azo surface was also studied. To demonstrate healing of *cis* P-12-Azo a film was irradiated with UV light (6 min, 65 mW $cm^{-2}$) to obtain a *cis* rich film. After irradiation, P-12-Azo is in a *cis* rich state and the film is soft. Then, the film surface was scratched with an AFM tip attached to a micromanipulator. Immediately the polymer flows to fill the gap of the scratch after 10 s (Figure 5 b and Movie 1).

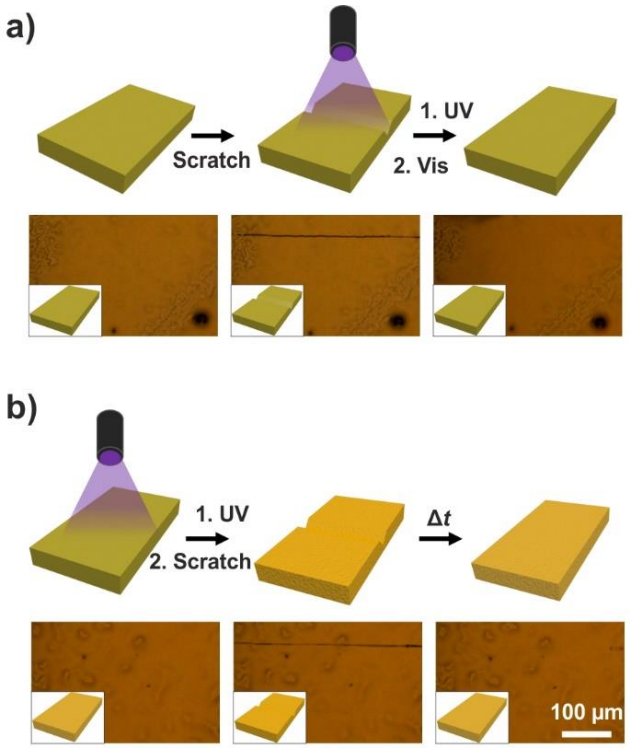


**Figure 5.** a) Scheme and optical microscope images of a *trans* rich film before scratching, after scratching and healed after UV and visible light irradiation. b) Scheme and optical microscope images of a *cis* rich film before scratching, after scratching and healed after 10 s. Characteristic areas of the films were used to find the exact same position on the films after irradiation.

To neglect any heating effect during irradiation several control experiments were made:

1. Between irradiation and scratching were 30 minutes. The film could still be healed.
2. A thermal imager was used to detect the temperature of the polymer film during irradiation. The temperature of the film did not rise above 25 °C (Figure S11) which is below $T_g$.
3. Irradiating the film with blue light for 30 sec to transform the liquid *cis* film back to

the solid *trans* film immediately stopped the film from flowing (Figure S12 a and Movie 2).

4. Heating the film to 35 °C for 10 min did not liquefy the film (Figure S12 b and Movie 3). After that the same film was irradiated with UV light again (6 min, 65 mW $cm^{-2}$) to obtain a *cis* rich film and scratches on it could immediately be healed again (Figure S13 and Movie 4).

**3. Conclusions**

In conclusion, light switchable azopolymers with increasing spacer lengths were synthesized and compared to the original azopolymer which shows photoswitching of $T_g$. The polymers show different behavior depending on their side chain length. There is a spacer length range around six and twelve carbon atoms where photoliquefaction is observed. If the linker between the azo group and the polymer backbone is too short or too long photoliquefaction at room temperature is not observed. P-0-Azo does not show photoliquefaction. A decrease of $T_g$ after irradiation which could lead to photoliquefaction was not observed. P-20-Azo does not show photoliquefaction at room temperautre but it shows a decreased phase transition. Most probably because the side chain is so long that forces between chains enable anisotropy of the polymer. It could also be that entanglement hinders movement of polymer chains. However, the phase transition of the *cis* form is above room temperature and photoliquefaction cannot be seen at room temperature. If *cis* P-20-Azo is heated to 50 °C photoliquefaction can be reached. P-12-Azo shows similar behavior to the original P-6-Azo. Thus, P-12-Azo was used for photohealing and for the first time flowing of *cis* azopolymer was observed at real time. In

the future, this kind of polymers can be used for smart material printing or micro structure preparation or manipulation by light irradiation. By UV light irradiation the polymer can flow or be processed and after the desired structure is formed the polymer can be solidified by visible light irradiation to obtain a tough surface. To obtain a more detailed understanding of the structural behavior of the *trans* and *cis* state, X-Ray studies could be done in the future. However, large sample needs and long preparation times require a thermally more stable *cis* state.

**4. Experimental Section**

**Materials:** Phenol (>99%), p-toluidine (99%), acryloyl chloride (97%), reactants and solvents were purchased from Sigma Aldrich and used without further purification. 12-bromo-1-dodecanol (>98%) was purchased from TCI. Dimethyl Icosanedioate (>95%) was purchased from TCI. 2,2'-azobisisobutyronitrile (AIBN) (98%) was purchased from Sigma Aldrich and was recrystallized from ethanol before use. Milli-Q water was provided by a Sartorius Arium 611 VF Purification System.

**Methods:** Proton and carbon nuclear magnetic resonance (NMR) spectra were recorded on Bruker Avance 250 MHz, 300 MHz or 500 MHz spectrometer. Mass spectra (MS) were obtained using a VG instrument ZAB 2-SE-FPD. The molecular weights and molecular weight distributions of P-n-Azo were determined using an Agilent Technologies 1260 Infinity PSS SECurity GPC (pump: 1260 IsoPump) equipped with UV and RI detectors running in tetrahydrofuran (THF) at 30 °C and a PLgel MIXED-B column (dimension: 0.8 × 30 cm, particle size: 10 µm) with a polystyrene standard. UV-vis absorption spectra were recorded on

a Perkin Elmer Lambda 900 spectrometer. Baselines were corrected and spectra were normalized using OriginPro software. Optical microscopy images were captured on a Zeiss optical microscope equipped with a CCD camera. Thermogravimetric analysis (TGA) was carried out on a Mettler Toledo TGA-851 under nitrogen atmosphere with a heating rate of 10 °C $min^{-1}$. Differential scanning calorimetry (DSC) data were collected using a Mettler Toledo DSC-822 under nitrogen atmosphere. The polymers were measured with a heating or cooling rate of 10 °C $min^{-1}$. The shear moduli were measured using a homemade piezo-rheometer in shear mode at room temperature. *Cis* azopolymers with a thickness of 100 μm was sandwiched between two quartz plates that were used as transparent sample holders. The shear moduli of *cis* azopolymers were measured. Subsequently, *cis* azopolymers between the quartz plates were converted to *trans* azopolymers by 530 nm light. *Trans* azopolymers were measured by the piezo-rheometer under the same conditions. Dynamic mechanical analysis (DMA) was conducted on an Advanced Rheometric Expansion System (ARES, Rheometric Scientific Company). Shear deformation was applied under conditions of controlled deformation amplitude, which was kept in the range of the linear viscoelastic response of the studied samples. Plate-plate geometry was used with plate diameters of 6 mm. The experiments were conducted under dry nitrogen atmosphere at a heating rate of 3 °C/min and a constant deformation frequency between 1 and 10 rad/s. Photoisomerization was induced by LEDs with wavelengths of 365 nm, 470 nm and 530 nm (Mightex Systems, device types LCS-0365-07-22, LCS-0470-03-22 and LCS-0530-15-22, respectively). The output intensities were controlled by an LED controller (Mightex Systems, device type SLC-MA04-MU), calibrated by an optical powermeter (Spectra-Physics Corporation, Model 407A). Preparation of *cis* Polymers for DSC and DMA measurements is described elsewhere.[1] An MMO-203 hydraulic

micromanipulator (Narishige, Tokyo, Japan) equipped with an AFM cantilever was used to scratch polymer films.

**Synthesis:** The synthesis route of the P-n-Azo polymers is shown in Scheme S1. Details are provided in the Supporting Information.

**Supporting Information**

Synthesis details, NMR, TGA, DMA, DSC, POM, Thermal Imaging, UV Vis data and Movies are available free of charge via the Internet.

**Acknowledgements**

We acknowledge technical support from J. Thiel, A. Best, A. Hanewald, Dr. M. Kappl and helpful discussions with Prof. G. Floudas and Prof. H.-J. Butt.

**References**

1. Zhou, H.; Xue, C.; Weis, P.; Suzuki, Y.; Huang, S.; Koynov, K.; Auernhammer, G. K.; Berger, R.; Butt, H.-J.; Wu, S., Photoswitching of glass transition temperatures of azobenzene-containing polymers induces reversible solid-to-liquid transitions. *Nat Chem* **2017,** *9* (2), 145-151.
2. Pipertzis, A.; Hess, A.; Weis, P.; Papamokos, G.; Koynov, K.; Wu, S.; Floudas, G., Multiple Segmental Processes in Polymers with cis and trans Stereoregular Configurations. *ACS Macro Letters* **2018,** *7* (1), 11-15.
3. Kumar, G. S.; Neckers, D. C., Photochemistry of azobenzene-containing polymers. *Chemical Reviews* **1989,** *89* (8), 1915-1925.
4. Ercole, F.; Davis, T. P.; Evans, R. A., Photo-responsive systems and biomaterials: photochromic polymers, light-triggered self-assembly, surface modification, fluorescence modulation and beyond. *Polymer Chemistry* **2010,** *1* (1), 37-54.

5. Norikane, Y.; Uchida, E.; Tanaka, S.; Fujiwara, K.; Nagai, H.; Akiyama, H., Photoinduced Phase Transitions in Rod-shaped Azobenzene with Different Alkyl Chain Length. *Journal of Photopolymer Science and Technology* **2016,** *29* (1), 149-157.
6. Uchida, E.; Azumi, R.; Norikane, Y., Light-induced crawling of crystals on a glass surface. *Nature Communications* **2015,** *6*, 7310.
7. Hoshino, M.; Uchida, E.; Norikane, Y.; Azumi, R.; Nozawa, S.; Tomita, A.; Sato, T.; Adachi, S.-i.; Koshihara, S.-y., Crystal Melting by Light: X-ray Crystal Structure Analysis of an Azo Crystal Showing Photoinduced Crystal-Melt Transition. *Journal of the American Chemical Society* **2014,** *136* (25), 9158-9164.
8. Norikane, Y.; Uchida, E.; Tanaka, S.; Fujiwara, K.; Koyama, E.; Azumi, R.; Akiyama, H.; Kihara, H.; Yoshida, M., Photoinduced Crystal-to-Liquid Phase Transitions of Azobenzene Derivatives and Their Application in Photolithography Processes through a Solid–Liquid Patterning. *Organic Letters* **2014,** *16* (19), 5012-5015.
9. Yamamoto, T.; Norikane, Y.; Akiyama, H., Photochemical liquefaction and softening in molecular materials, polymers, and related compounds. *Polymer Journal* **2018**.
10. Baroncini, M.; d'Agostino, S.; Bergamini, G.; Ceroni, P.; Comotti, A.; Sozzani, P.; Bassanetti, I.; Grepioni, F.; Hernandez, T. M.; Silvi, S.; Venturi, M.; Credi, A., Photoinduced reversible switching of porosity in molecular crystals based on star-shaped azobenzene tetramers. *Nat Chem* **2015,** *7* (8), 634-640.
11. Akiyama, H.; Yoshida, M., Photochemically Reversible Liquefaction and Solidification of Single Compounds Based on a Sugar Alcohol Scaffold with Multi Azo-Arms. *Advanced Materials* **2012,** *24* (17), 2353-2356.
12. Anzai, J.-I.; Osa, T., Photosensitive artificial membranes based on azobenzene and spirobenzopyran derivatives. *Tetrahedron* **1994,** *50* (14), 4039-4070.
13. Stumpe, J.; Fischer, T.; Menzel, H., Langmuir−Blodgett Films of Photochromic Polyglutamates. 9. Relation between Photochemical Modification and Thermotropic Properties. *Macromolecules* **1996,** *29* (8), 2831-2842.
14. Kuiper, J. M.; Engberts, J. B. F. N., H-Aggregation of Azobenzene-Substituted Amphiphiles in Vesicular Membranes. *Langmuir* **2004,** *20* (4), 1152-1160.
15. Wu, S.; Wang, L.; Kroeger, A.; Wu, Y.; Zhang, Q.; Bubeck, C., Block copolymers of PS-b-PEO co-assembled with azobenzene-containing homopolymers and their photoresponsive properties. *Soft Matter* **2011,** *7* (24), 11535-11545.
16. Rochon, P.; Gosselin, J.; Natansohn, A.; Xie, S., Optically induced and erased birefringence and dichroism in azoaromatic polymers. *Applied Physics Letters* **1992,** *60* (1), 4-5.
17. Akiyama, H.; Fukata, T.; Yamashita, A.; Yoshida, M.; Kihara, H., Reworkable adhesives composed of photoresponsive azobenzene polymer for glass substrates. *The Journal of Adhesion* **2017,** *93* (10), 823-830.
18. Manouras, T.; Vamvakaki, M., Field responsive materials: photo-, electro-, magnetic- and ultrasound-sensitive polymers. *Polymer Chemistry* **2017,** *8* (1), 74-96.
19. Han, G. D.; Park, S. S.; Liu, Y.; Zhitomirsky, D.; Cho, E.; Dinca, M.; Grossman, J. C., Photon energy storage materials with high energy densities based on diacetylene-azobenzene derivatives. *Journal of Materials Chemistry A* **2016,** *4* (41), 16157-16165.
20. Menzel, H.; Weichart, B.; Schmidt, A.; Paul, S.; Knoll, W.; Stumpe, J.; Fischer, T., Small-Angle X-ray Scattering and Ultraviolet-Visible Spectroscopy Studies on the Structure and Structural Changes in Langmuir-Blodgett Films of Polyglutamates with

Azobenzene Moieties Tethered by Alkyl Spacers of Different Length. *Langmuir* **1994,** *10* (6), 1926-1933.
21. Ikeda, T.; Sasaki, T.; Kurihara, S., Image Recording in Polymer Liquid Crystals. *Proceedings of the Japan Academy, Series B* **1993,** *69* (1), 7-12.

# 3 Summary and Outlook

In this work, the successful synthesis and characterization as well as applications of novel azopolymers is presented. The key concept in all applications is based on the *trans-cis* isomerization of the photoresponsive azopolymers.

The first part of the results describes the synthesis and applications of a visible light-responsive azopolymer, called PmAzo, with non-stackable azochromophores. The choice of tetra-*o*-methoxy-substituted azobenzene has two advantages: Firstly, the visible light-induced isomerization of PmAzo prevents degradation by UV light damage. Secondly, the non-planar molecular structure of the *trans* mAzo group prevents stacking and associated aggregation. This design enabled reversible patterning of PmAzo films that could be written and erased with visible light. These patterns on a PmAzo film were stored for more than half a year. Both these properties make PmAzo an excellent alternative for conventional azopolymers in optical storage.

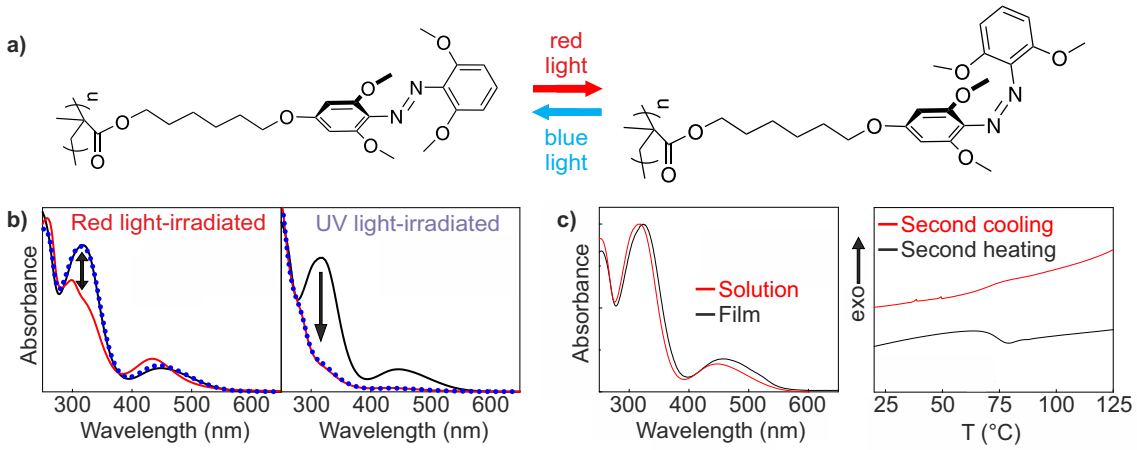


**Figure 3.1:** Concept of a visible light-switchable azopolymer. a) Chemical structures and photoisomerization. b) Degradation is lower under red light compared to UV light, demonstrated by absorption spectroscopy. c) This polymer has less chromophore-chromophore interaction in solid state than conventional azopolymers, confirmed by absorption spectroscopy and DSC. Adapted with permission from Weis, P.; Wang, D; Wu, S. *Macromolecules* **2016**, *49*, 6368-6373. Copyright 2016 American Chemical Society.

Azopolymers that absorb visible light should be better suited for solar energy generation due to the greater spectral overlap with the solar spectrum. By combining PmAzo with a conventional azopolymer, PAzo, a device has been created that can use both UV and visible wavelengths for highly efficient light harvesting.

A sophisticated device design, namely selective blocking of wavelengths that induce *cis*-to-*trans* back isomerization, combined with improved spectral overlap, enabled a high solar efficiency for azo solar thermal cells. The study also showed that solid state properties such as crystallinity and aggregation play an important role, but also the chemical structure of the chromophores can serve to tune the gravimetric energy density. For this reason, the need to specify the exact nature of the solid state is of utmost importance for any modification of the chromophore, especially in the case of solid-state azo solar cells.

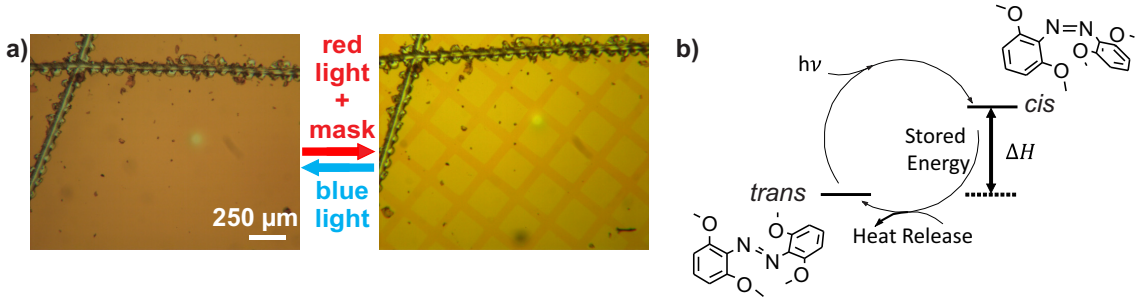


**Figure 3.2:** Applications of a visible light-switchable azopolymer. a) Photopatterns can be writen on a PmAzo film using red light and a mask. Blue light erases the patterns. b) Energy storage cycle based on isomerization of a visible light-responsive azobenzene. a) Adapted with permission from Weis, P.; Wang, D; Wu, S. *Macromolecules* **2016**, *49*, 6368-6373. Copyright 2016 American Chemical Society. b) Adapted with permission from Saydjari, A. K.; Weis, P.; Wu, S. *Advanced Energy Materials* **2017**, *7*, 1601622. Copyright 2016 John Wiley and Sons.

In the near future, other visible light switchable polymers could probably lead to similar reports and further adapt the material properties to specific applications. For further improvements, however, a fundamental problem has to be considered, namely that a red-shift of azobenzene absorption is also accompanied by a lower energy storage due to the relationship $E \propto \frac{1}{\lambda}$. The work thus forms the basis for the further improvement and development of switchable polymers with visible light, which are widely used in information and energy storage as well as in the biomedical industry.

The second half of this thesis deals with the reversible solid-liquid transition of azopolymers. For some azopolymers a reversible solid-liquid transition attributed to a photoswitchable $T_g$ was demonstrated. While *trans* isomers were solids with high $T_g$, the *cis* isomers were liquids with low $T_g$. In order to better understand this phenomenon, the polymer structure was modified with respect to backbone, side chain length and azobenzene substituents, and their influence on the photoinduced solid-liquid phase transition were investigated. The polymers exhibit different behavior depending on the side chain length between the

polymer backbone and the azo chromophore. There is a spacer length range around six to twelve methylene groups in which the photo liquefaction was observed. If the linker between the azo group and the polymer backbone is less than six methylene groups or more than twelve methylene groups, photoinduced liquefaction was not observed at room temperature.

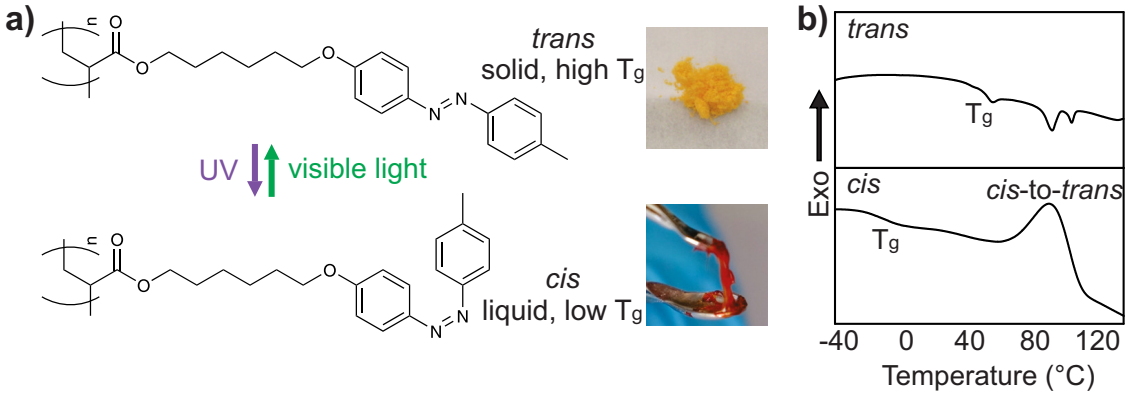


**Figure 3.3:** Concept of photoswitching $T_g$. a) Chemical structures and photoisomerization of an azopolymer which is solid with high $T_g$ *trans* state, and liquid with low $T_g$ in the *cis* state. b) DSC curves support the concept of photoswitchable $T_g$. Adapted with permission from Zhou, H.; Xue, C.; Weis, P.; Suzuki, Y.; Huang, S.; Koynov, K.; Auernhammer, G. K.; Berger, R.; Butt, H.-J.; Wu, S. *Nature Chemistry* **2017**, *9*, 145-151. Copyright 2016 Nature Publishing Group.

Photoswitching $T_g$ is a new strategy for developing photohealable polymers with $T_g$ above room temperature. Hard polymer surfaces were photohealed from scratches at room temperature without using plasticizers, the surface roughness of a patterned azopolymer film was reduced and an azopolymer film was transfer printed, all by photoswitching $T_g$. The concept of photoswitching the $T_g$ of polymers is interesting both for the basic understanding of $T_g$ and for the application of polymers that exhibit a switchable $T_g$.

In the future, such polymers can be used for smart material printing or microstructure-preparation and -manipulation by light irradiation. In order to gain a more precise understanding of the structural behavior of the *trans* and *cis* state, a standard method for investigation of such polymers should be introduced. Otherwise different findings in the literature cannot be compared easily. In future work the influence of azopolymer structure as well as the geometry of azopolymers on $T_g$ will be investigated to better understand the underlying principle of $T_g$ switching. By investigating the azomonomers or other small molecule azobenzenes, a deeper insight and understanding of the behavior of azopolymers could be gained. For example, small molecule *cis*-azobenzenes may be liquid materials. But they may not be obtained by direct light irradiation of the *trans* monomers in the solid state, because strong stacking hinders photoisomerization in solid state. The way to

obtain them might be the irradiation and isomerization in solution by subsequent removal of the solvent.

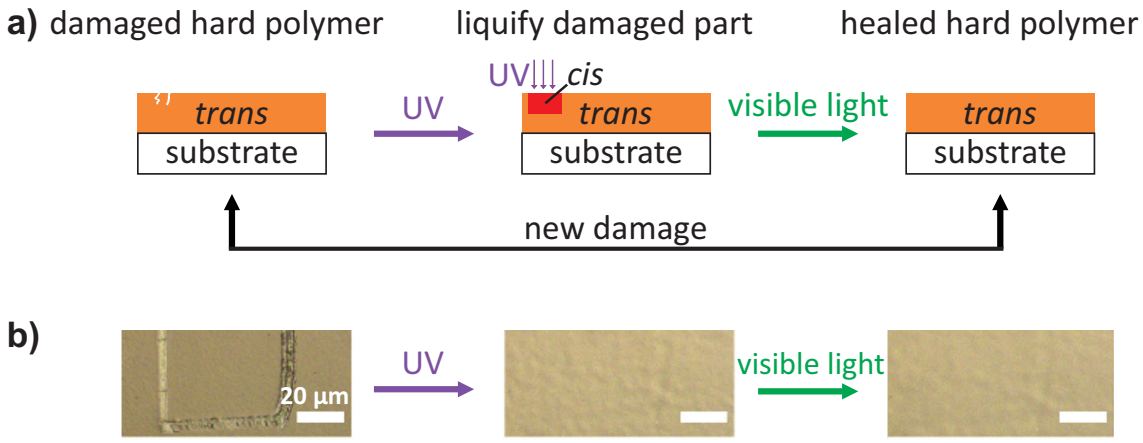


**Figure 3.4:** Healing of scratches on an azopolymer film. a) Schematic illustration and b) optical microscopy images of the healing process. Adapted with permission from Zhou, H.; Xue, C.; Weis, P.; Suzuki, Y.; Huang, S.; Koynov, K.; Auernhammer, G. K.; Berger, R.; Butt, H.-J.; Wu, S. *Nature Chemistry* **2017**, *9*, 145. Copyright 2016 Nature Publishing Group.

Additionally the controlled synthesis of azopolymers using RAFT polymerization and ATRP will be developed. Moreover, new applications for azopolymers, based on photoinduced solid-liquid transitions, can be developed, such as reworkable adhesives.

Finally, other stimuli-responsive polymers might also have switchable $T_g$, which could be discovered soon.

# 4 Appendix

## 4.1 Visible-Light-Responsive Azopolymers with Inhibited $\pi$-$\pi$ Stacking Enable Fully Reversible Phototopatterning

Supporting Information

*Philipp Weis, Dongsheng Wang, Si Wu**

Max Planck Institute for Polymer Research, Ackermannweg 10, 55128 Mainz, Germany

E-mail: wusi@mpip-mainz.mpg.de

**Synthesis**

The synthesis of the UV light-responsive azopolymer (PAzo) is shown in Scheme S1. The details are provided below.

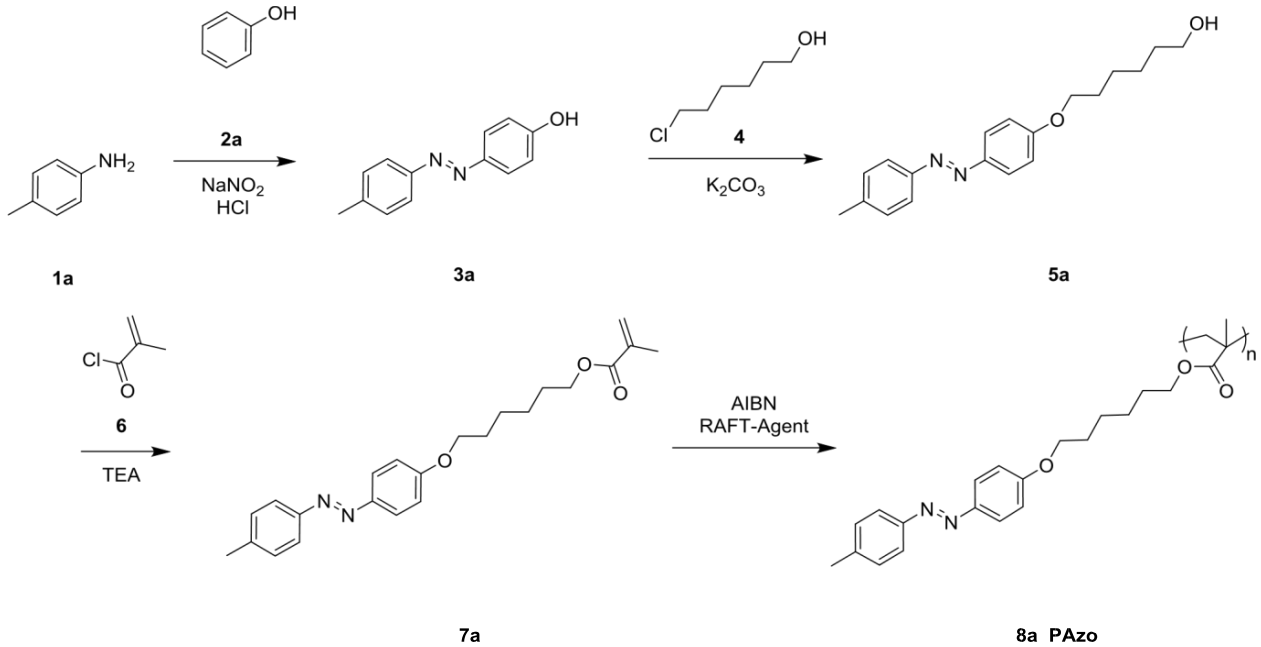


**Scheme S1**. Synthesis of the UV light responsive azobenzene-containing polymer PAzo.

**Synthesis of 3a**: p-Toluidine **1a** (8 g, 0.075 mol) was mixed with hydrochloric acid (16 mL), ice (16 g), and acetone (110 mL). To the above mixture, sodium nitrite (5.020 g, 0.075 mol) dissolved in water (28 mL) with ice (28 g) was added slowly. After 30 min an aqueous solution of phenol (7.0 g, 0.075 mol) in 2 mol $L^{-1}$ sodium hydroxide was added to the mixture. The mixture was stirred for 2 h. After neutralization with HCl, the precipitate was filtered and washed with water. The crude product was dried and purified by recrystallization from ethanol to obtain the compound as a red-brown solid. Yield: 75%. $^{1}$H-NMR (300 MHz, $CD_2Cl_2$, $\delta$): 7.84 (d, 2H, J = 9 Hz, Ar-*H*), 7.74 (d, 2H, J = 8 Hz, Ar-*H*), 7.32 (d, 2H, J = 8 Hz, Ar-*H*), 6.95 (d, 2H, J = 9 Hz, Ar-*H*), 2.43 (s, 3H, Ar-$CH_3$). $^{13}$C-NMR (63 MHz, $CD_2Cl_2$, $\delta$): 158.82 (Ar-*C*), 151.25 (Ar-*C*), 147.64 (Ar-*C*), 141.73 (Ar-*C*), 130.26 (Ar-*C*), 125.25 (Ar-*C*), 122.99 (Ar-*C*), 116.30 (Ar-*C*), 21.72 (Ar-$CH_3$).

**Synthesis of 5a**: 4-(p-tolyldiazenyl)phenol **3**a (7.5 g, 0.036 mol) was dissolved in dry DMF (40 ml), potassium carbonate (4.9 g, 0.036 mol) was added and the solution was stirred for 30 min at 30 °C. Then, KI (0.015 g, 0.090 mmol) and 6-chloro-1-hexanol (5.335 g, 0.039 mol) were added to the solution. The reaction mixture was then stirred vigorously for 24 h at 110 °C. The resulting mixture was cooled to room temperature and poured into crushed ice (900 g), and the resulting red-brown precipitate was filtered off. The crude product was dried and purified by recrystallization from ethanol to obtain the compound as a red-brown solid. Yield: 86%. $^{1}$H NMR (300 MHz, $CD_2Cl_2$, $\delta$): 7.88 (d, 2H, J = 9 Hz, Ar-*H*), 7.77 (d, 2H, J = 8 Hz, Ar-*H*), 7.31 (d, 2H, J = 8 Hz, Ar-*H*), 7.01 (d, 2H, J = 9 Hz, Ar-*H*), 4.05 (t, 2H, J = 7 Hz, Ar-O-$CH_2$), 3.62 (t, 2H, J = 6 Hz, HO-$CH_2$), 2.42 (s, 3H, Ar-$CH_3$), 1.83 (q, 2H, J = 7 Hz, -O-$CH_2$-$CH_2$-$CH_2$), 1.63-1.40 (m, 6H (+$H_2O$), $CH_2$-$CH_2$-$CH_2$-$CH_2$-$CH_2$-OH). $^{13}$C NMR (63 MHz, $CD_2Cl_2$, $\delta$): 162.14 (Ar-*C*), 151.34 (Ar-*C*), 147.35 (Ar-*C*), 141.57 (Ar-*C*), 130.23 (Ar-*C*), 125.01 (Ar-*C*), 122.95 (Ar-*C*), 115.21 (Ar-*C*), 68.87 (-$H_2C$-O-Ar), 63.23 (-$H_2C$-O-C=O),

33.33 (Ar-O-$H_2C$-*C*$H_2$-$CH_2$-), 29.74 (-$H_2C$-*C*$H_2$-$CH_2$-OH), 26.40 (-$H_2C$-*C*$H_2$-$CH_2$-$CH_2$), 26.11 (-$H_2C$-$CH_2$-*C*$H_2$-$CH_2$), 21.71 (Ar-*C*$H_3$).

**Synthesis of 7a**: Under ice-water bath conditions, a solution of methacryloyl chloride (1.986 g, 0.019 mol) in dry $CH_2Cl_2$ (10 mL) was added drop wise into a solution containing 6-(4-(p-tolyldiazenyl)phenoxy)hexan-1-ol **5a** (4.754 g, 0.016 mol), triethylamine (1.624 g, 0.016 mol) and dry $CH_2Cl_2$ (50 mL) and stirred at room temperature for 20 h. The reaction mixture was concentrated with a rotary evaporator, washed with diluted hydrochloric acid, a $NaHCO_3$ solution and a NaCl solution. The organic layer was collected and the solvent was removed with a rotary evaporator. The crude product was purified by elution on a silica gel column with $CH_2Cl_2$. After removing the solvent, the product was recrystallized to obtain the azobenzene-containing monomer as a yellow solid. Yield: 73%. $^1$H NMR (400 MHz, $CDCl_3$, $\delta$): 7.89 (d, 2H, J = 9.0 Hz, Ar-*H*), 7.78 (d, 2H, J = 8.2 Hz, Ar-*H*), 7.29 (d, 2H, J = 8.0 Hz, Ar-*H*), 6.98 (d, 2H, J = 9.0 Hz, Ar-*H*), 6.10 (m, 1H, C=*CH*$_2$), 5.55 (m, 1H, C=*CH*$_2$), 4.17 (t, 2H, J = 6.6, Ar-O-*CH*$_2$), 4.04 (t, 2H, J = 6.4, -O-*CH*$_2$), 2.43 (s, 3H, Ar-*CH*$_3$), 1.95 (s, 3H, C-*CH*$_3$), 1.83 (q, 2H, J = 6.6 Hz, Ar-O-$CH_2$-*CH*$_2$-CH2), 1.73 (q, 2H, J = 7.2 Hz, O=C-O-$CH_2$-*CH*$_2$-CH2), 1.42-1.60 (m, 4H, -$CH_2$-*CH*$_2$-*CH*$_2$-$CH_2$-). $^{13}$C NMR (63 MHz, $CD_2Cl_2$, $\delta$): 167.64 (*C*=O), 161.94 (Ar-*C*), 151.16 (Ar-*C*), 147.19 (Ar-*C*), 141.40 (Ar-*C*), 137.12 (-*C*=$CH_2$), 130.06 (Ar-*C*), 125.11 (-C=*C*$H_2$), 124.84 (Ar-*C*), 122.78 (Ar-*C*), 115.02 (Ar-*C*), 68.63 (-$H_2$*C*-O-Ar), 64.95 (-$H_2$*C*-O-C=O), 29.48 (Ar-O-$H_2C$-*C*$H_2$-$CH_2$-), 28.95 (-$H_2C$-*C*$H_2$-$CH_2$-O-C=O), 26.18 (-$H_2C$-*C*$H_2$-$CH_2$-$CH_2$), 26.08 (-$H_2C$-$CH_2$-*C*$H_2$-$CH_2$), 21.54 (Ar-*C*$H_3$), 18.47 (C-*C*$H_3$).

**Synthesis of 8a**: PAzo was synthesized according to the procedure used for PmAzo. 7a was used as the monomer. $^1$H NMR (400 MHz, $CDCl_3$, $\delta$): 7.83 (2H, Ar-*H*), 7.75 (2H, Ar-*H*), 7.24 (2H, Ar-*H*), 6.91 (2H, Ar-*H*), 3.93 (4H, Ar-O-*CH*$_2$ and -O-*CH*$_2$), 2.38 (3H, Ar-*CH*$_3$), 2-0.8(13H, C-*CH*$_2$, C-C*H*$_3$, and $CH_2$-C*H*$_2$-C*H*$_2$-C*H*$_2$-C*H*$_2$-$CH_2$). The number averaged molecular weight and PDI of the polymer, determined by GPC, were $5.8 \times 10^3$ g mol$^{-1}$ and 1.16, respectively.

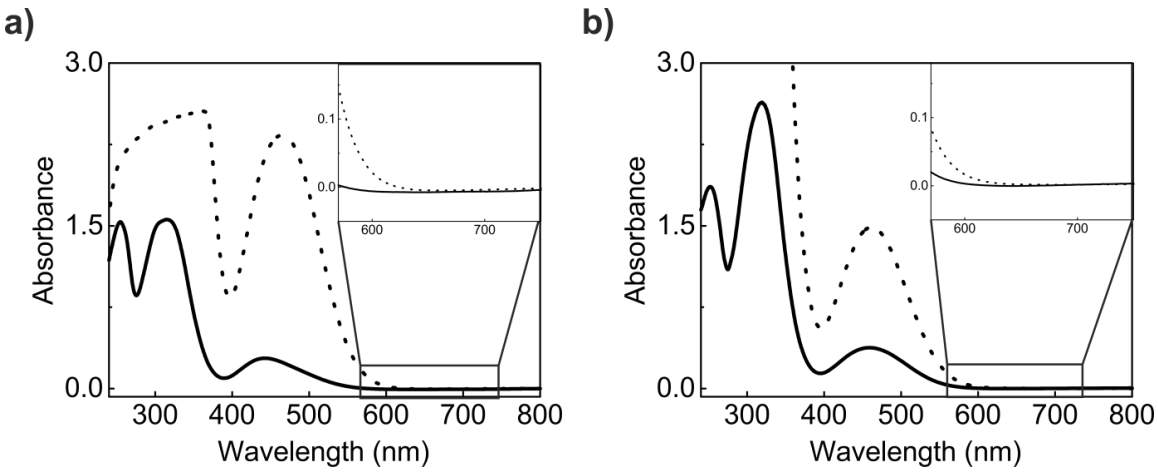


**Figure S1**. a) UV-vis absorption spectra of a high (0.10 wt%, dotted line) and low (0.01 wt%, solid line) concentrated 6-(4-((2,6-dimethoxyphenyl)diazenyl)-3,5-dimethoxyphenoxy)hexyl methacrylate solution in THF. b) UV-vis absorption spectra of a high (0.06 wt%, dotted line) and a low (0.02 wt%, solid line) concentrated PmAzo solution in THF. The mAzo chromophore can absorb red light.

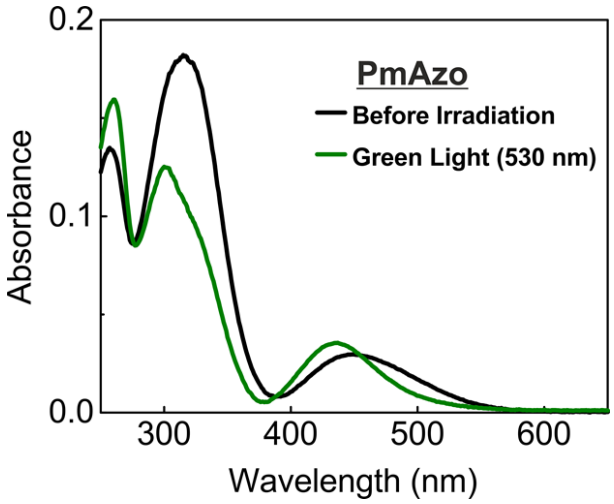


**Figure S2**. Absorption spectra of PmAzo in THF before irradiation (black line) and after green light (530 nm, 1 mW $cm^{-2}$, 1 h) irradiation (green line). Green light induced trans-to-cis isomerization.

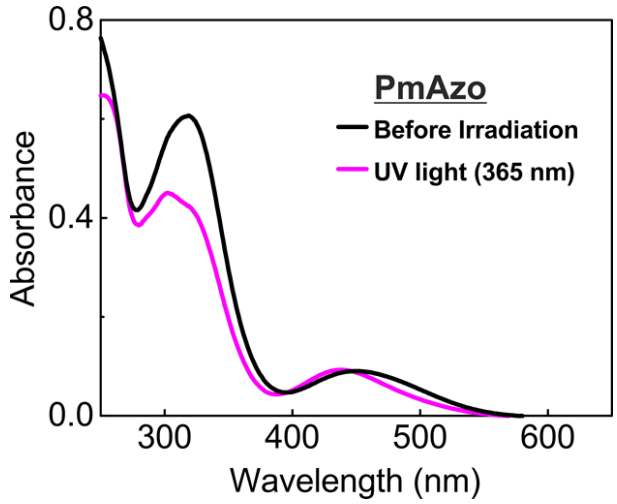


**Figure S3**. Absorption spectra of PmAzo in THF before irradiation (black line) and after UV light (365 nm, 2 mW $cm^{-2}$, 30 min) irradiation (purple line). UV light induced trans-to-cis isomerization.

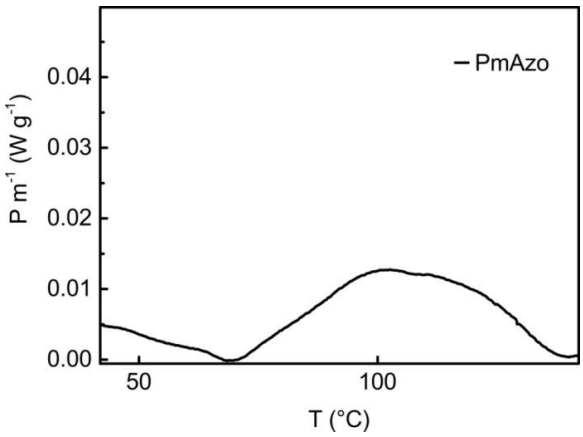


**Figure S4.** DSC first heating curve of cis PmAzo and calculation of the energy difference between trans and cis PmAzo by DSC. The peak around 100 ℃ corresponds to the thermally cis-to-trans isomerization.

For DSC measurements, PmAzo was dissolved into DCM and irradiated with red light. DCM was then removed by a rotary evaporator and subsequently the dry polymer was used to for DSC measurements and $^{1}$H-NMR to determine the cis content. DSC measurements were used to determine the energy difference between cis and trans PmAzo. The bulk energy density was obtained by integrating the thermal back isomerization peak (Equation S1).

$$\frac{q}{m} = \frac{\left[\int_{T_1}^{T_2} P\ dT\right]}{m\ v} \qquad (\mathbf{S1})$$

Here P $m^{-1}$ is the power per mass given by the DSC measurement in the temperature interval dT, $T_1$ and $T_2$ are the limits of the thermal back isomerization process, and v is the heating rate.

By measuring the cis percentage of the sample ($\chi_{cis}$) using $^{1}$H-NMR, the energy difference of cis and trans PmAzo was obtained by Equation S2 where M is the molar mass of the repeating unit of PmAzo.

$$\Delta H_{cis-trans} = \frac{qM}{m\chi_{cis}} \qquad (\mathbf{S2})$$

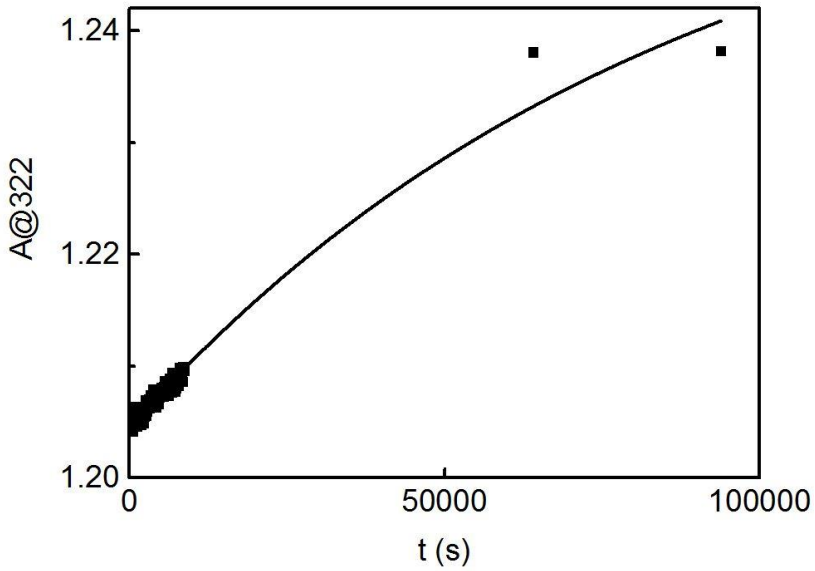


**Figure S5.** Thermally cis-to-trans isomerization of cis PmAzo solution followed by absorbance measurements at 322 nm.

$$y = y0 + Ae^{kx} \qquad (\boldsymbol{S3})$$

With y0 = 1.26; A = -0.06 and k = -1.15 $\cdot 10^{-5}$.

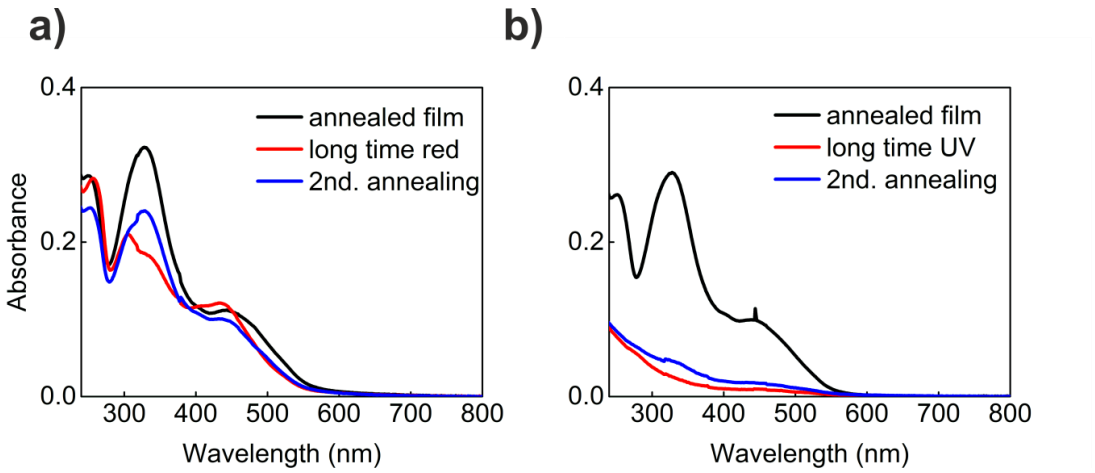


**Figure S6.** UV-vis absorption spectra of annealed PmAzo films, before irradiation (black line), after high-intensity (a) red or (b) UV (32 mW $cm^{-2}$) irradiation for 5 h (red line) and after annealing. The red light irradiated film (a) showed cis-to-trans isomerization after annealing, while the UV light irradiated film (b) showed photobleaching.

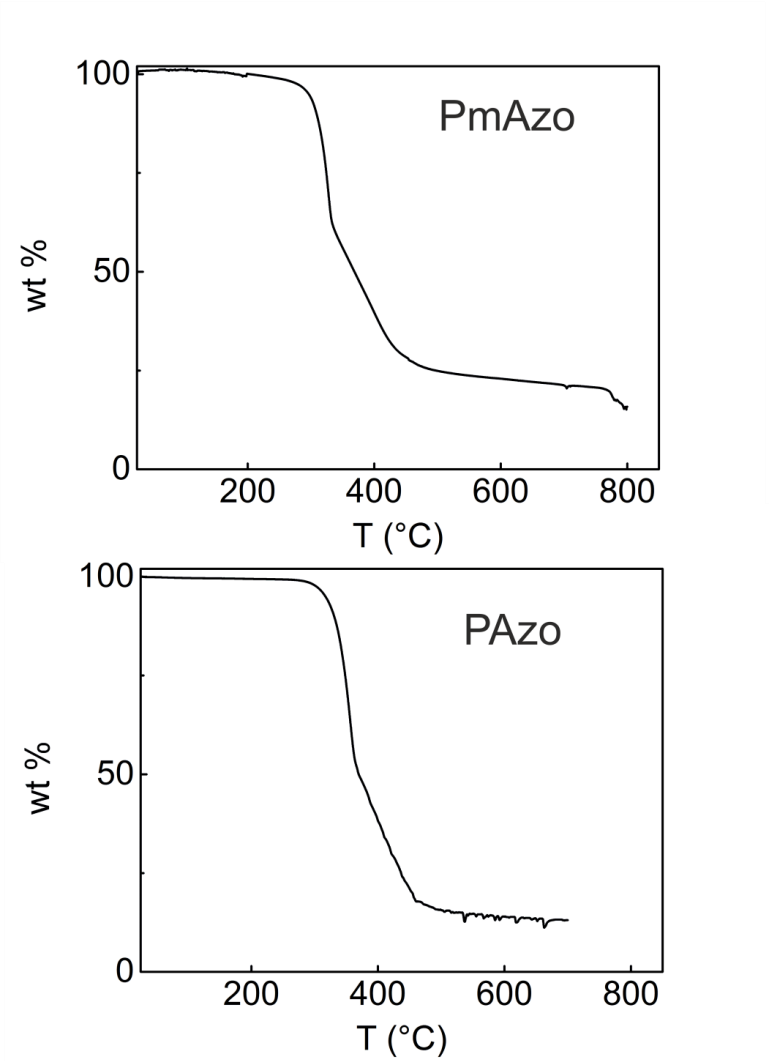


**Figure S7**. TGA of PmAzo and PAzo. PmAzo and PAzo were thermally stable up to 200 ℃.

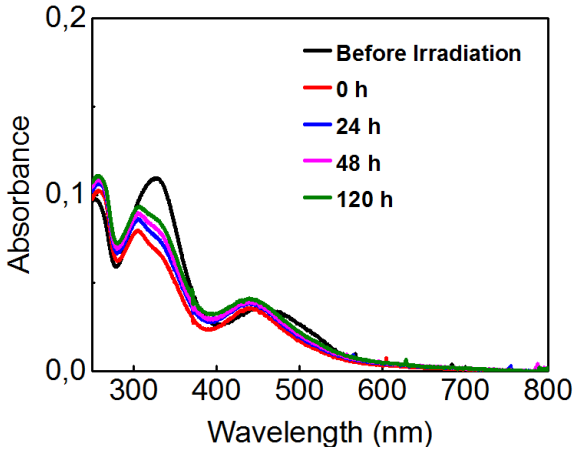


**Figure S8.** UV-vis spectra showing thermally cis-to-trans isomerization of a cis PmAzo film at room temperature. UV-vis spectrum of the film before irradiation was measured (black line). Then, the irradiated film was kept in the dark for 0, 24, 48 and 120 h.

When the irradiated PmAzo film was stored in the dark, the π-π* band in the UV region gradually increased, indicating thermally cis-to-trans isomerization. However, the n-π* band of cis PmAzo after stored in the dark for 120 h did not overlap with that of the trans PmAzo before irradiation.

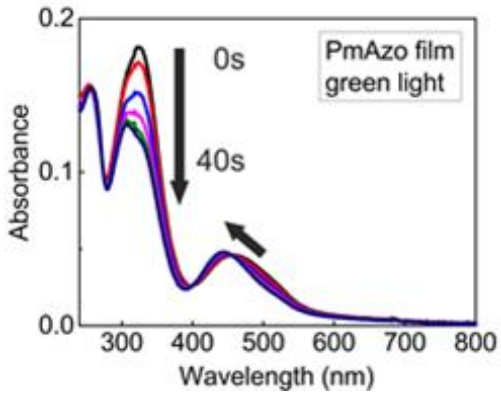


Figure S9. UV-vis absorption spectra of a PmAzo film irradiated with green light (530 nm, 35 mW $cm^{-2}$). The photoisomerization rate fitted with a first-order kinetic equation was 0.11 $s^{-1}$ in the PmAzo film.

**NMR spectra**

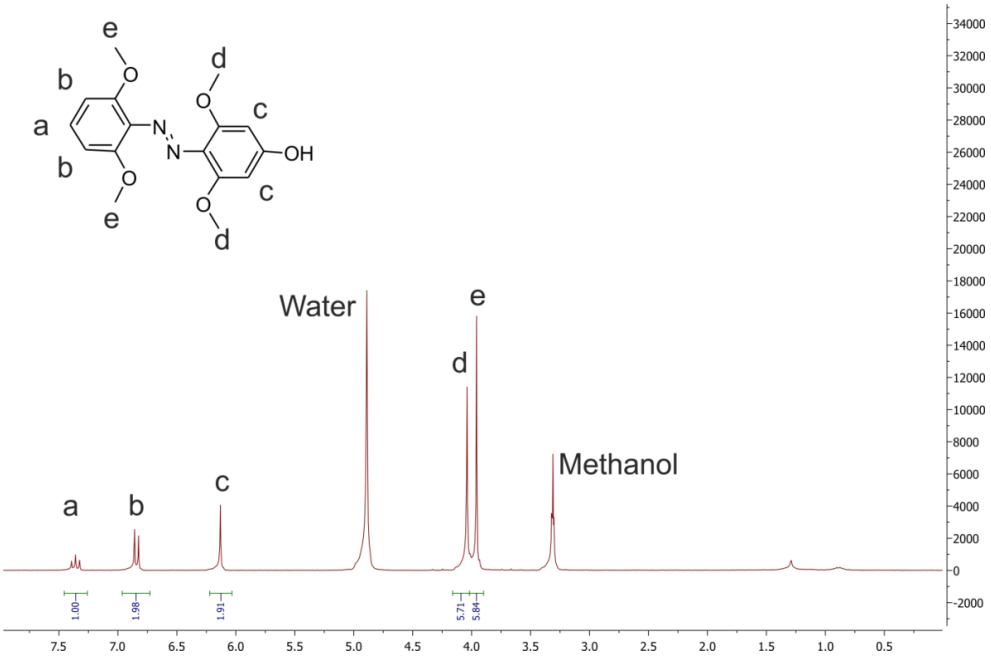


Figure S10. $^{1}$H-NMR spectrum (250 MHz, $CD_3OD$) of Compound 3.

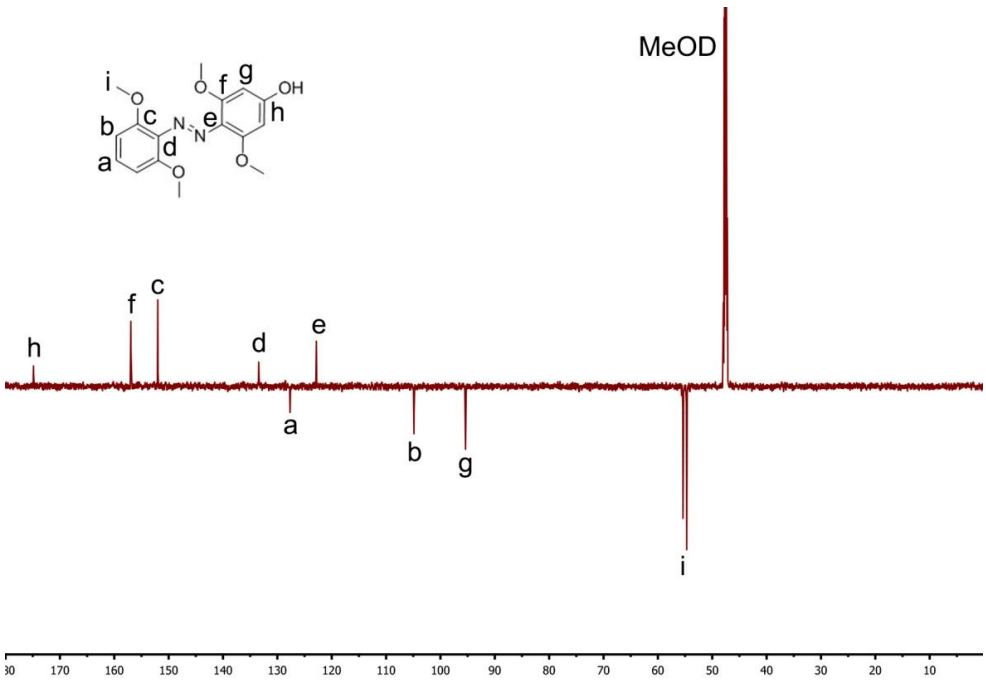


Figure S11. $^{13}$C-NMR spectrum (176 MHz, $CD_3OD$, deprotonated by NaOH to prevent tautomerism) of Compound 3.

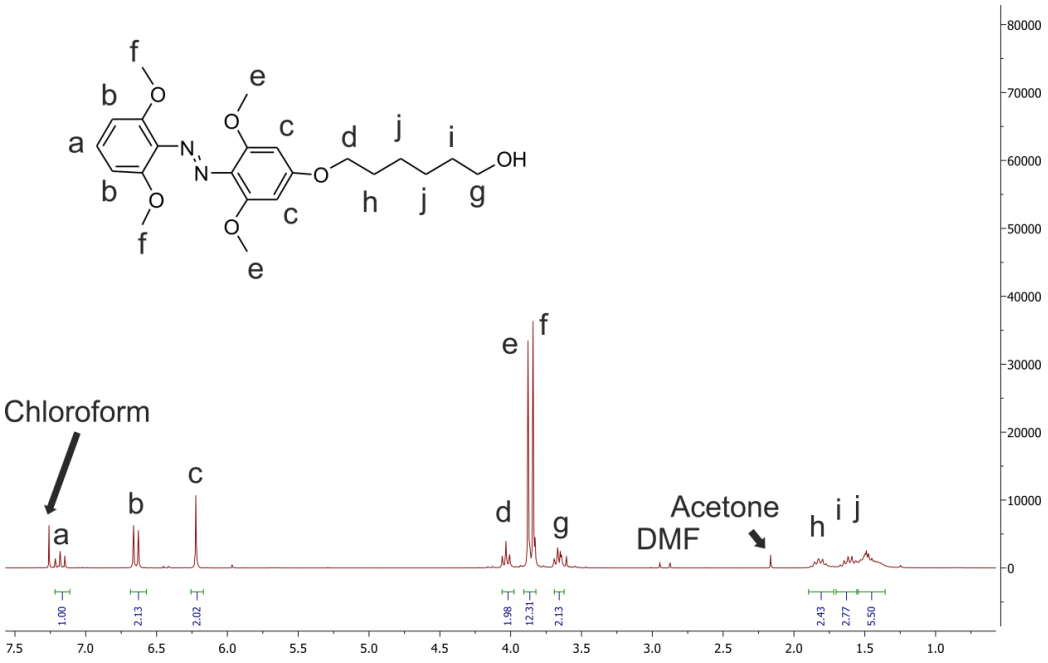


Figure S12. $^{1}$H-NMR spectrum (250 MHz, $CDCl_3$) of Compound 5.

Figure S13. $^{13}$C-NMR spectrum (67 MHz, DMSO-d6) of Compound 5.

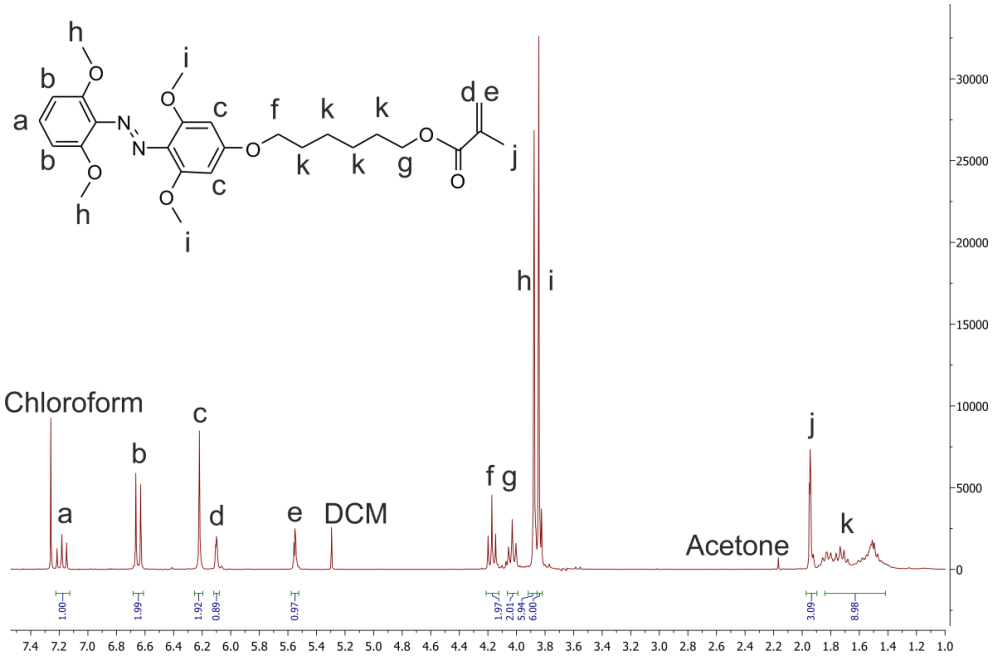


Figure S14. $^{1}$H-NMR spectrum (250 MHz, $CDCl_3$) of Compound 7.

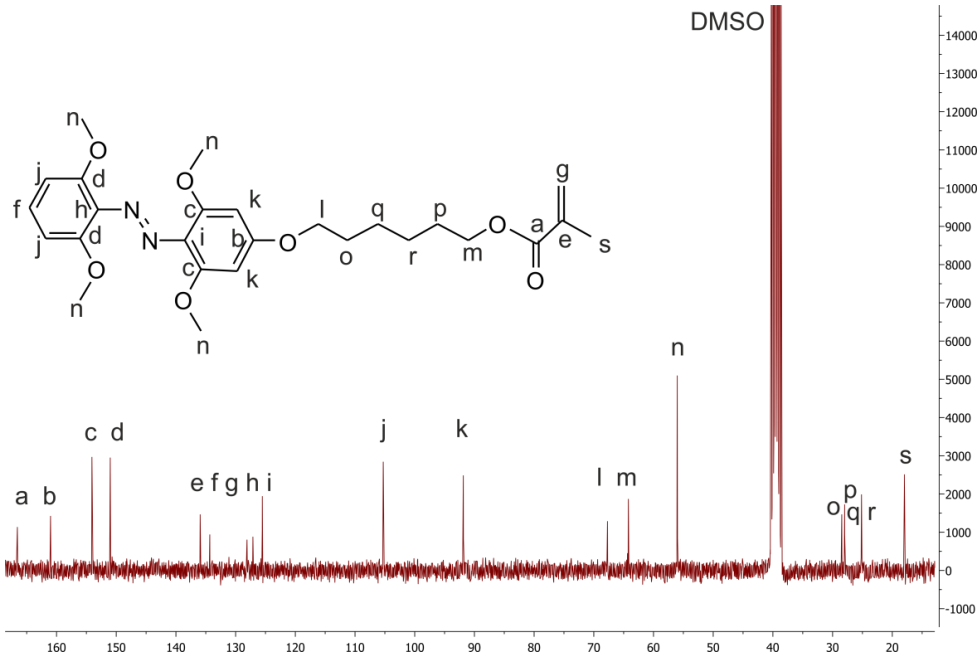


Figure S15. $^{13}$C-NMR spectrum (63 MHz, DMSO-d6) of Compound 7.

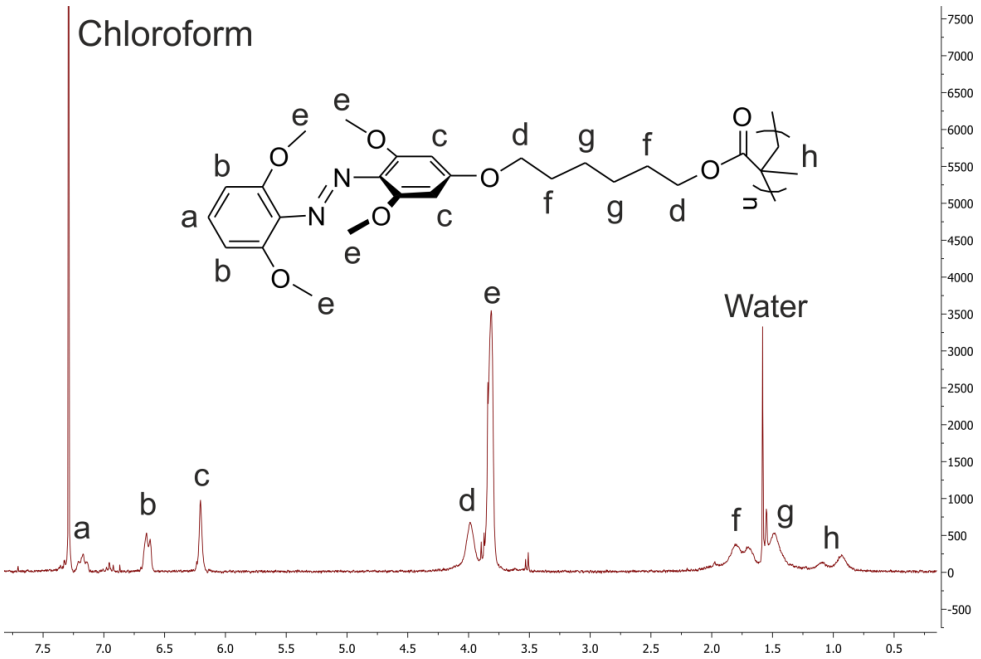


Figure S16. $^{1}$H-NMR spectrum (250 MHz, $CDCl_3$) of PmAzo.

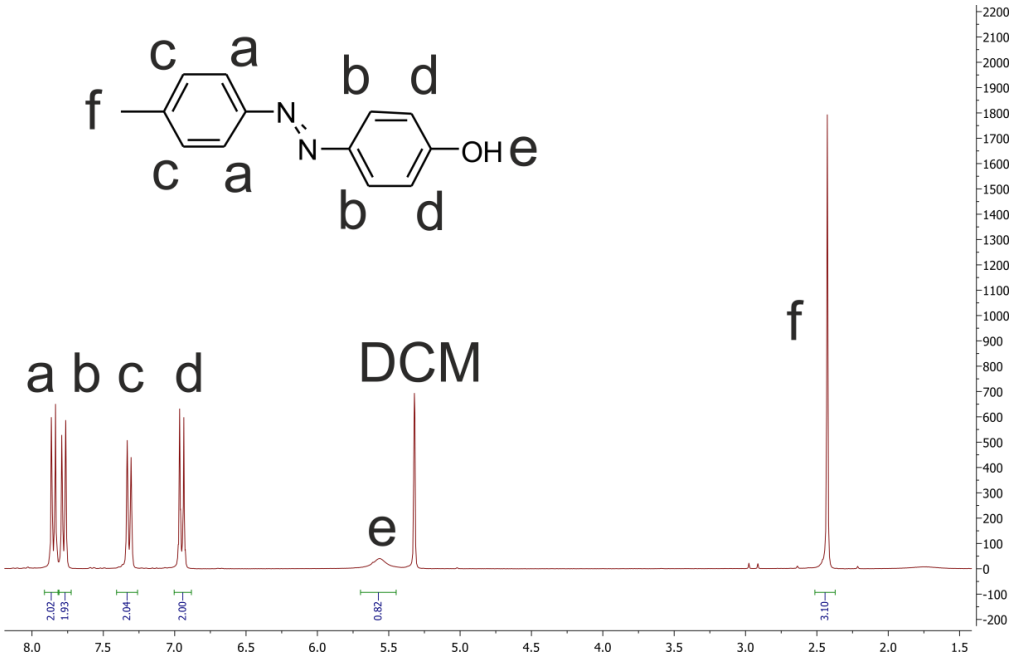


Figure S17. $^{1}$H-NMR spectrum (300 MHz, $CD_2Cl_2$) of Compound 3a.

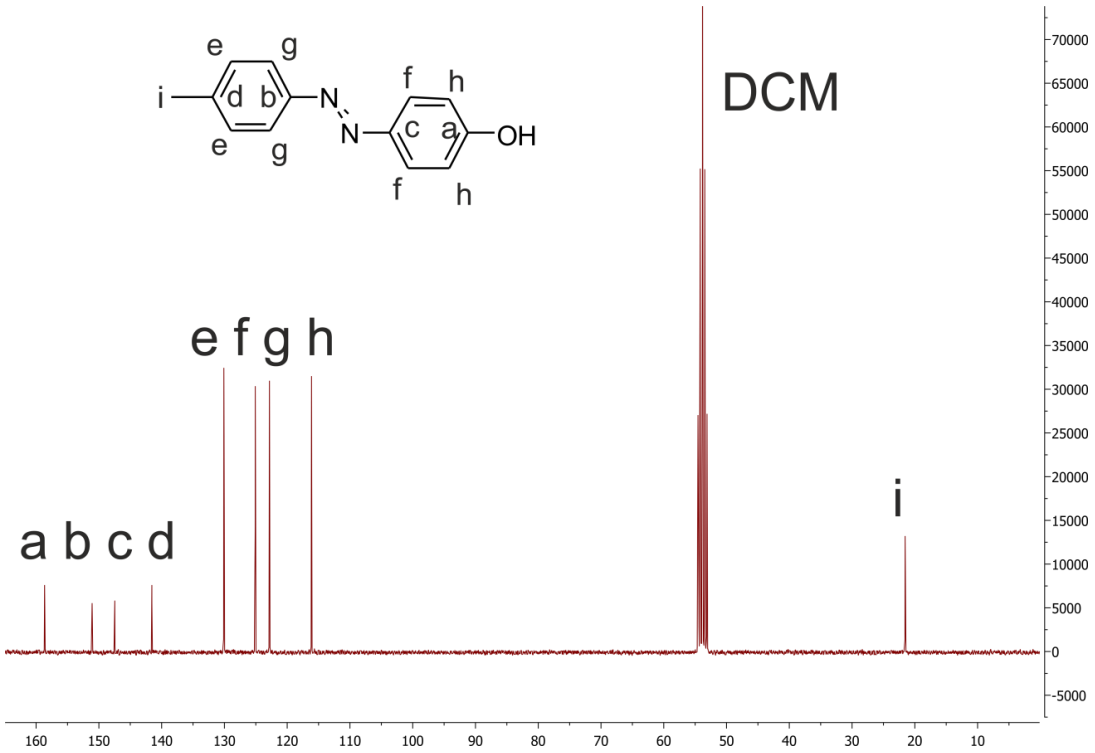


Figure S18. $^{13}$C-NMR spectrum (63 MHz, $CD_2Cl_2$) of Compound 3a.

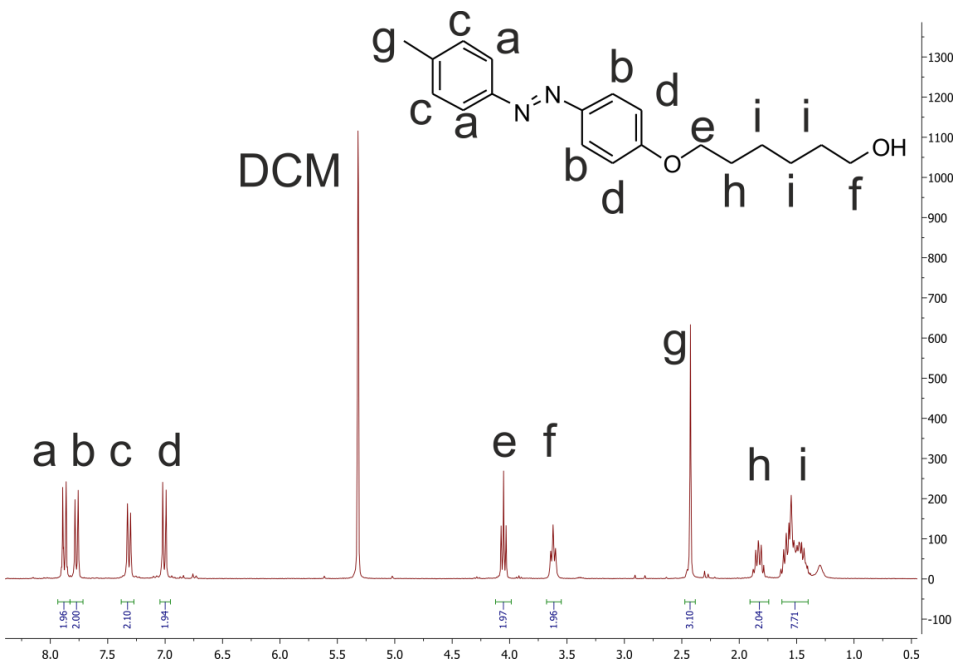


Figure S19. $^{1}$H-NMR spectrum (300 MHz, $CD_2Cl_2$) of Compound 5a.

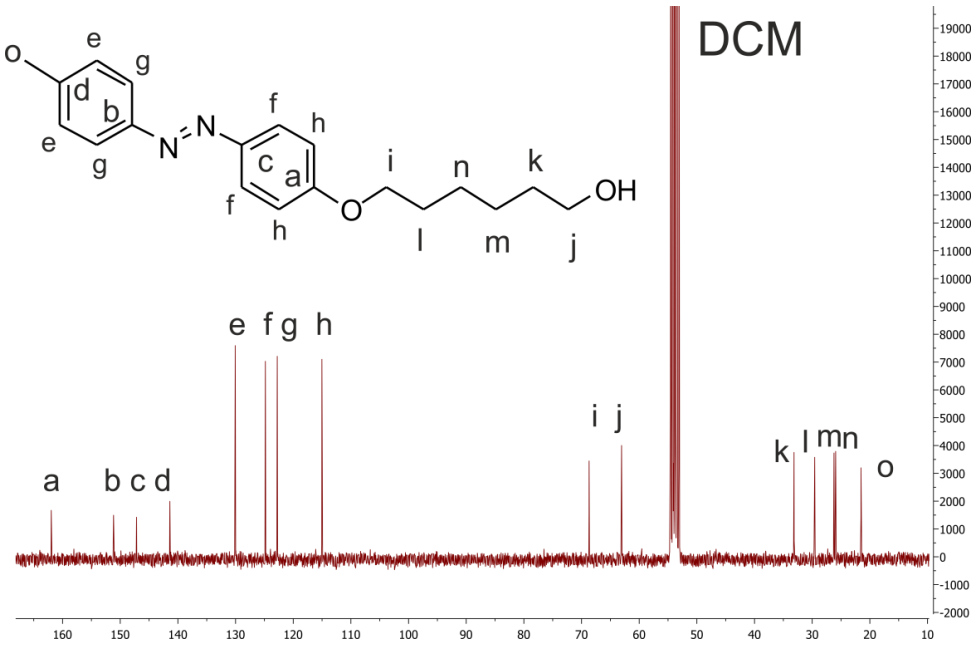


Figure S20. $^{13}$C-NMR spectrum (63 MHz, $CD_2Cl_2$) of Compound 5a.

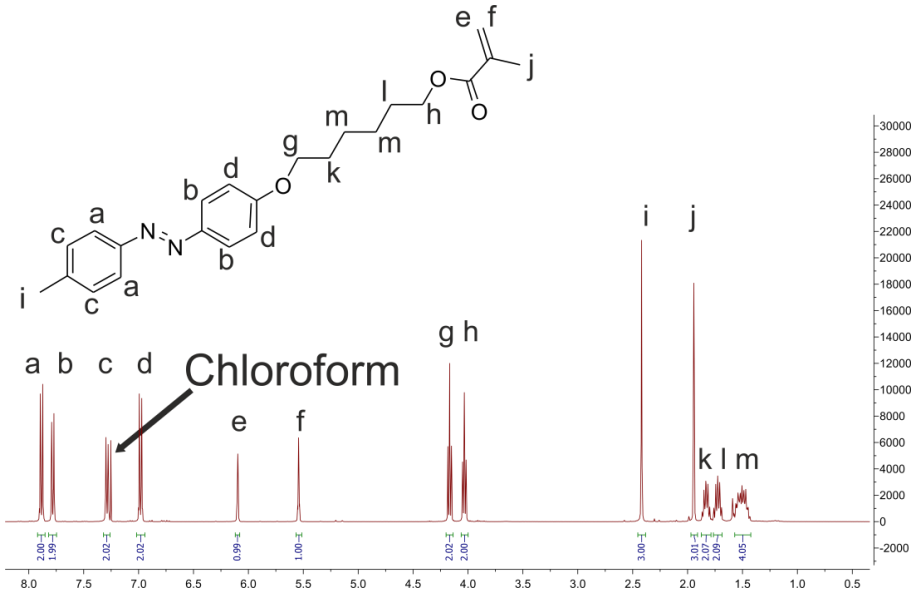


Figure S21. $^{1}$H-NMR spectrum (400 MHz, $CDCl_3$) of Compound 7a.

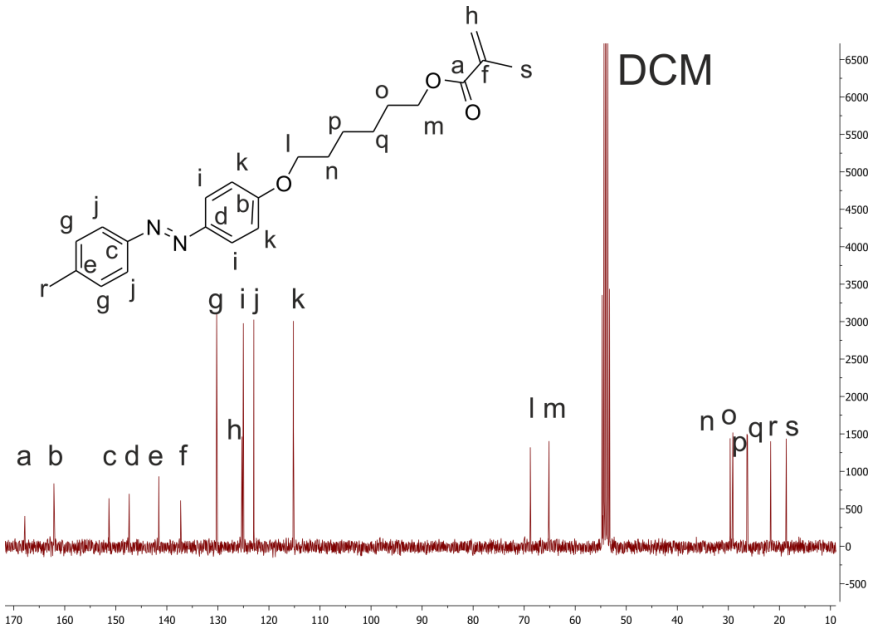


Figure S22. $^{13}$C-NMR spectrum (63 MHz, $CD_2Cl_2$) of Compound 7a.

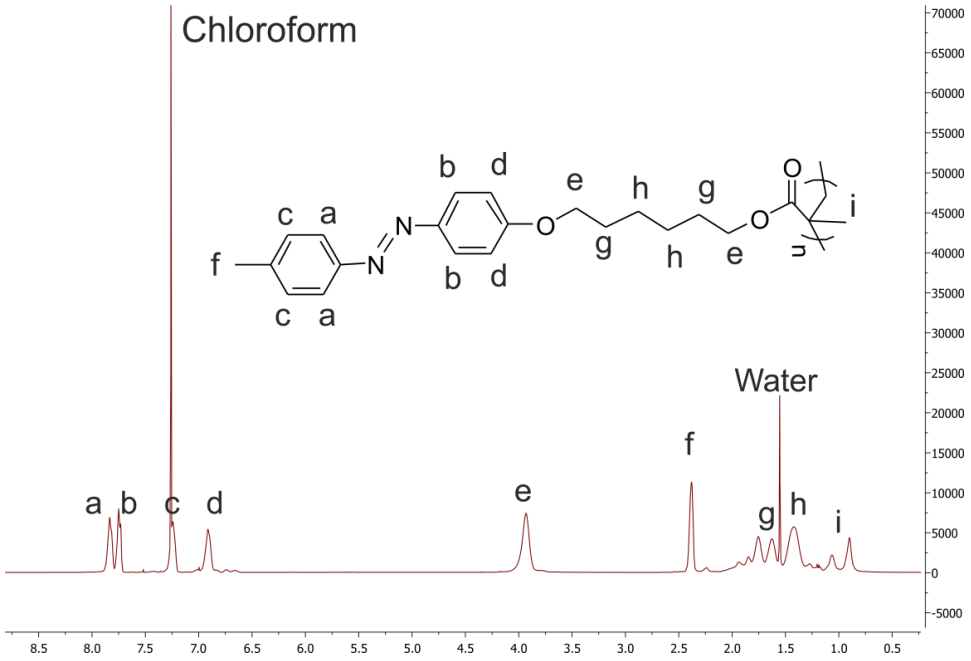


Figure S23. $^{1}$H-NMR spectrum (400 MHz, $CDCl_3$) of PAzo.

## 4.2 Spanning the Solar Spectrum: Azopolymer Solar Thermal Fuels for Simultaneous UV and Visible Light Storage



ADVANCED ENERGY MATERIALS

Supporting Information

for *Adv. Energy Mater.,* DOI: 10.1002/aenm.201601622

Spanning the Solar Spectrum: Azopolymer Solar Thermal Fuels for Simultaneous UV and Visible Light Storage

*Andrew K. Saydjari, Philipp Weis, and Si Wu**

WILEY-VCH



# Supporting Information

Spanning the Solar Spectrum: Azopolymer Solar Thermal Fuels for Simultaneous UV and Visible Light Storage

*Andrew K. Saydjari, Philipp Weis, and Si Wu**

A. K. Saydjari, P. Weis, Dr. S. Wu
Max Planck Institute for Polymer Research
Ackermannweg 10, 55128 Mainz, Germany
E-mail: wusi@mpip-mainz.mpg.de

A. K. Saydjari
Department of Chemistry
Yale University
*New Haven, CT 06520, USA*

WILEY-VCH

**Table of Contents**

**1. Experimental**

PAzo ($M_n$ = 6.7 × $10^3$ g $mol^{-1}$ and PDI = 1.13) and PmAzo ($M_n$ = 5.8 × $10^3$ g $mol^{-1}$ and PDI = 1.16) were synthesized via reversible addition−fragmentation chain-transfer (RAFT) polymerization. The details of syntheses and characterization of PAzo and PmAzo were reported elsewhere.[S1] Tetrahydrofuran (Lot# STBG0146V/STBF7044V, Sigma), d8-tetrahydrofuran (Lot# A0257504/A0230598, ACROS), d6-dimethyl sulfoxide (Lot# 150099/130080/140056, VWR), d7-dimethyl formamide (Lot# MKBV2188V, Aldrich), cyclopentanone (Lot# D7924, Aldrich), Coumarin 314 (Lot# E1712, Santa Cruz Biotech), and poly(4-vinyl)phenol (Lot# 92235, Polysciences) were used as received. Quartz substrates (20 x 10 x 1 mm) for films were obtained from Yixin Puxi Optical Element. UV-pass filter was 2 mm thick UG-11, Schott.

Substrates were washed with liquid soap, rinsed with 18.2 MΩ·cm Millipore (Milli-Q Plus 185) water (10x), sonicated in Hellmanex II (Lot# 146322, Sigma) detergent (2% v/v, 15 min), rinsed with water (10x), sonicated in water (15 min), sonicated in ethanol (15 min), and were stored in ethanol until use.

Filtered solutions of PmAzo, PAzo, or Coumarin in cyclopentanone were used to spin cast (1% w/w PmAzo or PAzo) and drop cast (1% w/w Coumarin in 1% w/w PvPh) films. Drop cast films (80 $\mu L$) were allowed to dry under $N_2$ laminar flow (Bleymehyl ASW-UD) before thermal annealing under vacuum (40 ℃, 8 h, Model VD 23 WTB Binder). Spin coating was performed using a PM 101D spin-coater, Headway Research, (15 $\mu L$, ~1 krpm, 2 min) in a $N_2$ laminar flow box followed by immediate thermal annealing under vacuum (40 ℃, 8 h). UV-vis spectra of a Coumarin 314 film in Figure 1 was deposited out of 0.4% w/w cyclopentanone (1% w/w PvPH).

Film thickness was measured by P-16+ KLA Tencor Step Profiler as an average of the step-height for two scratches/film on three replicate films of Coumarin 314/PvPh, PmAzo, and PAzo each.

Solar irradiation was simulated using a full spectrum solar filter (LS0106, LOT) coupled with a 75W Xe arc lamp (NB 075, LOT). Films or solutions (1 cm Quartz SUPRASIL cuvettes, Hellma) were placed 7.5 cm from the source. Solutions were thermally converted from cis-to-trans by heating in an oil bath for ~2 h at 110 ℃. Films were thermally converted from cis-to-trans by heating under vacuum for ~2.5 h at 90 ℃.

$^{1}$H-NMR was obtained on a Bruker Avance 250 MHz spectrometer using "Routine Spectroscopy" for PAzo (1% w/w d8-THF or d7-DMF) and PmAzo (1% w/w d6-DMSO).

UV-Vis-NIR spectra were obtained on a Perkin Elmer Lambda 900 spectrometer (1.0 nm, 196.77 nm min$^{-1}$, 0.28 s integration). Solutions were measured in double-beam mode against reference solvent. Films were measured in a single-beam against quartz reference using a homemade sample holder which limited the spectrometer slit height to 6.5 mm.

The excitation-emission spectrum for Coumarin 314 was obtained using a FL3095SL/TSpec-4 J&M TIDAS with FluoroScan 4.0 software. Excitation and emission measurements for PmAzo film was obtained on a Spex Fluorolog II (212) spectrometer.

All ab-initio calculations were performed in Gaussian09. Geometry optimization was carried out on chromophore structures initialized in the approximately trans or cis configuration using DFT with a 6-311G(d,p) basis set and B3LYP functional.

DSC was measured using a Mettler Toledo DSC-822 under $N_2$ atmosphere heating/cooling at 10℃ $min^{-1}$ using the following scan profile: 25 to -50, -50 to 150, 150 to -50, -50 to 150, 150 to -50, -50 to 25℃. The percent cis content was estimated by $^1$H-NMR in d2-DCM. Irradiation of PmAzo (530 nm, 4 mW $cm^{-2}$, 40 min) and PAzo (365 nm, 2 mW $cm^{-2}$, 20 min) yielded 6.115 mg PmAzo and 12.213 mg PAzo respectively.

A Zeiss III microscope equipped with a PixeLINK PL-A662 camera was used to capture liquid crystalline structures under crossed polarizers (90 °).

**2. Fluorescence**

Two-dimensional (emission-excitation) fluorescence plots were obtained for Coumarin 314 films (PvPh matrix). These spectra demonstrate the ability of Coumarin 314 to down-convert light absorbed across a large range of wavelengths (350-520 nm) to broad green (570 nm) emission.

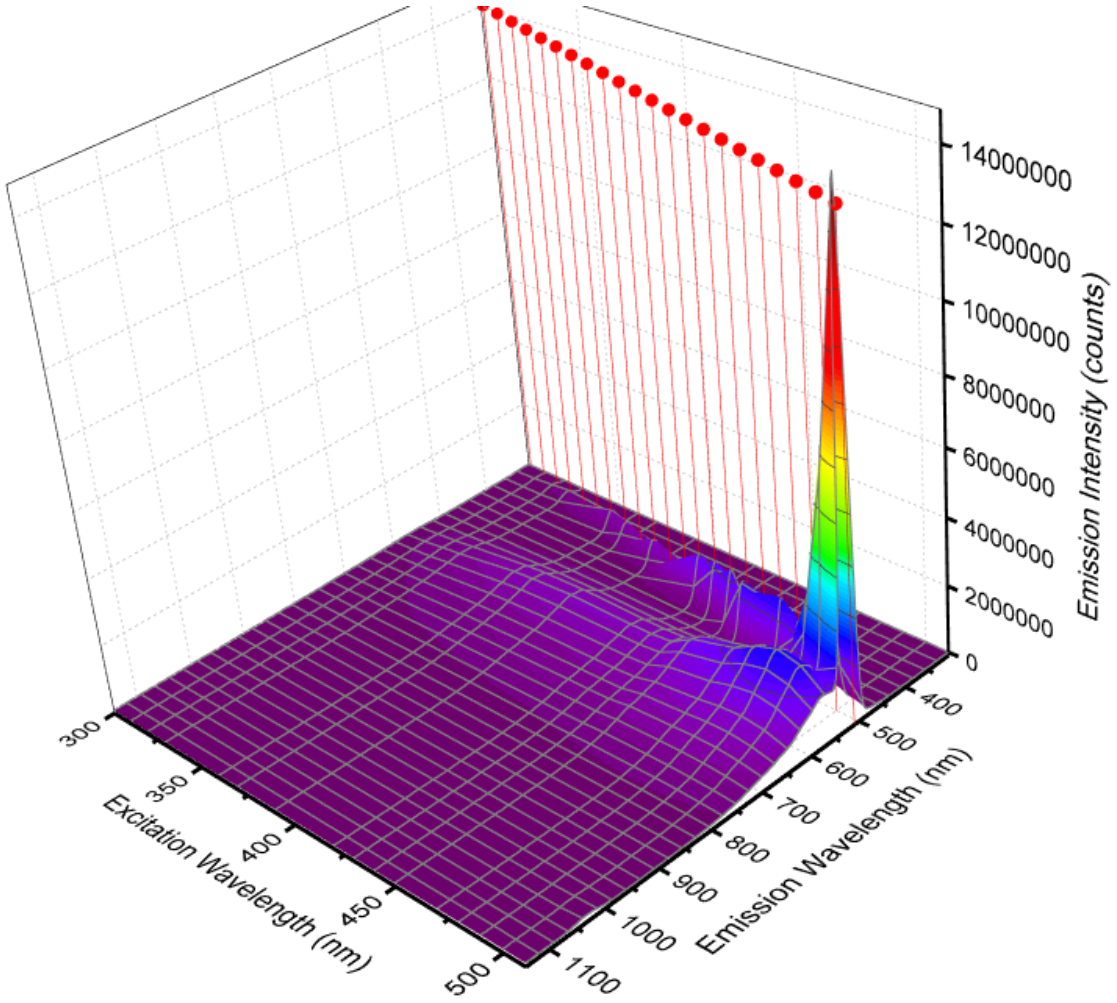


**Figure S1.** Excitation-emission spectra of Coumarin 314 film demonstrating down-conversion of blue light (470 nm) to yellow light (570 nm). Scattering from the excitation beam is identified by vertical droplines at the excitation wavelength.

**3. NMR**

Quantitation of the percent cis of PmAzo (~1% w/w) or PAzo (~1% ) was achieved taking the ratio of peaks corresponding to aromatic protons which give distinct cis and trans peaks. Only the aromatic proton peaks were assigned due to the convolution of the multitude of alkyl peaks with each other and solvent peaks.

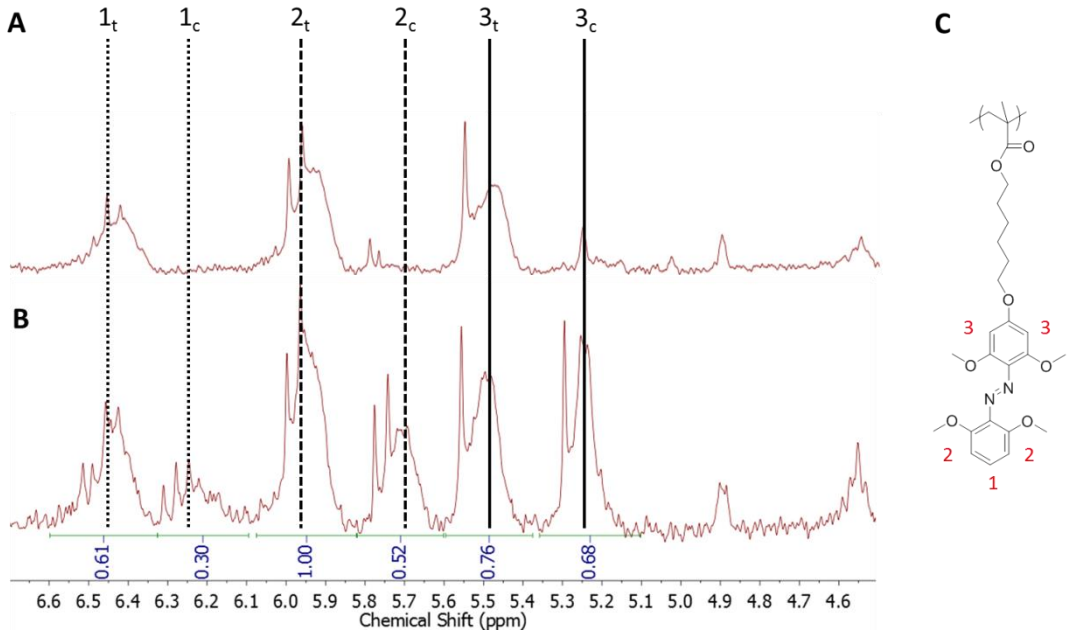


**Figure S2**. Aromatic region of $^{1}$H-NMR of PmAzo in d8-THF (A) before and (B) after 10 h solar irradiation. Peak assignments for protons used in determination of percent cis content are labeled on the figure, see (C) for structure. Subscripted t and c represent trans and cis protons respectively. This spectrum is representative of those used in quantitation of PmAzo solutions in device performance. Conversions were assessed as an average of the estimates provide by each of the three distinct proton peaks.

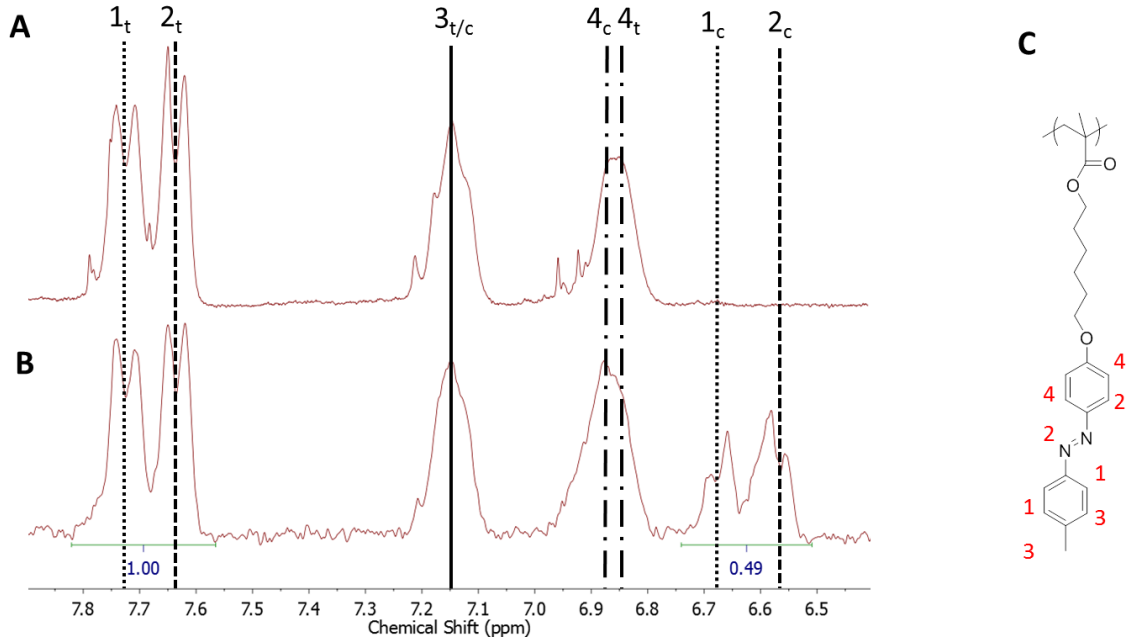


**Figure S3**. Aromatic region of $^{1}$H-NMR of PAzo in d8-THF (A) before and (B) after 10 h solar irradiation. Peak assignments for protons used in determination of percent cis content are labeled on the figure, see (C) for structure. Subscripted t and c represent trans and cis protons respectively. This spectrum is representative of those used in quantitation of PAzo solutions in device performance.

Control experiments demonstrating the role of each device component were performed by measuring the percent cis content after 2h and are summarized in Figure S4. Removing only the Coumarin 314 (Blue) filter lead to decreased conversion (50.2 compared to 61.8%) of PmAzo but increased conversion (62.8 compared to 40.8%) of PAzo. This further supports the hypothesis that the time for PAzo charging can be decreased by increasing the transmitted intensity since PAzo almost attains its solar photostationary state at 2h once the Coumarin layers are removed. Removing only the UV-pass filter does not affect PmAzo (61.3 compared to 61.8%), which was expected since the UV-pass filter is behind the PmAzo layer, However removing the UV-pass filter leads to decreased conversion of PAzo (32.0 compared to 40.8%). Removing both filter layers leads to decreased conversion for both PmAzo (50.3 compared to

61.8%) and PAzo (34.6 compared to 40.8%). Thus, in order to optimize visible light capture, the both filters were used in the device.

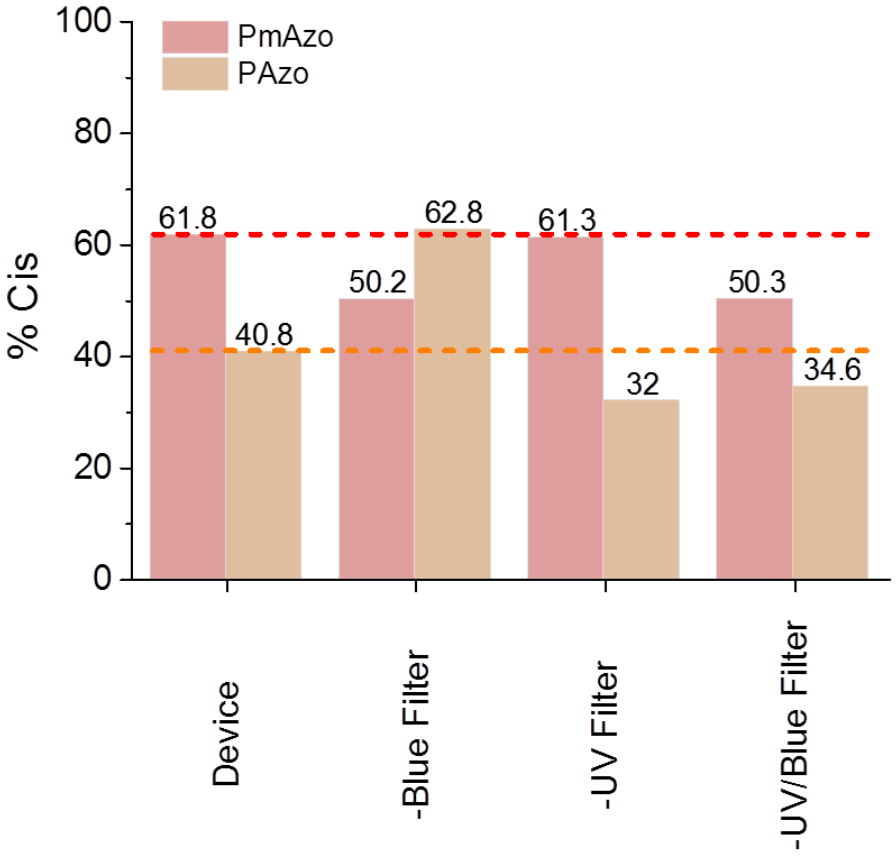


**Figure S4**. Cis-conversions (determined by $^{1}$H-NMR) after 2 h solar irradiation with the indicated filters removed, or the device as designed for reference. These solution phase control experiments demonstrate the role of each of the filters in the 4-layer device.

**4. Solid State Cis Conversion Estimate**

After solid-state charging with 10 h of solar irradiation, PmAzo and PAzo films were immediately dissolved in 2.5 mL THF. The UV-vis spectra of the dissolved azopolymers were then measured immediately, after further irradiation by 365 nm light (45 min, 2 mW $cm^{-2}$), and after thermal reversion (10 h, 110 ℃). The % cis in the solar PSS was estimated as the percentage change of absorbance at the peak $\pi^* \leftarrow \pi$ wavelength following the method of Victor et al.[S2] (Equation S1).

$$\% \, Cis \approx \frac{A - A_{trans}}{A_{cis} - A_{trans}} \qquad (\mathbf{S1})$$

Based on previous NMR data (vide supra), the PSS 365 nm was assumed to be ~100% cis and the thermal stationary state (TSS) was assumed to be ~100% trans.

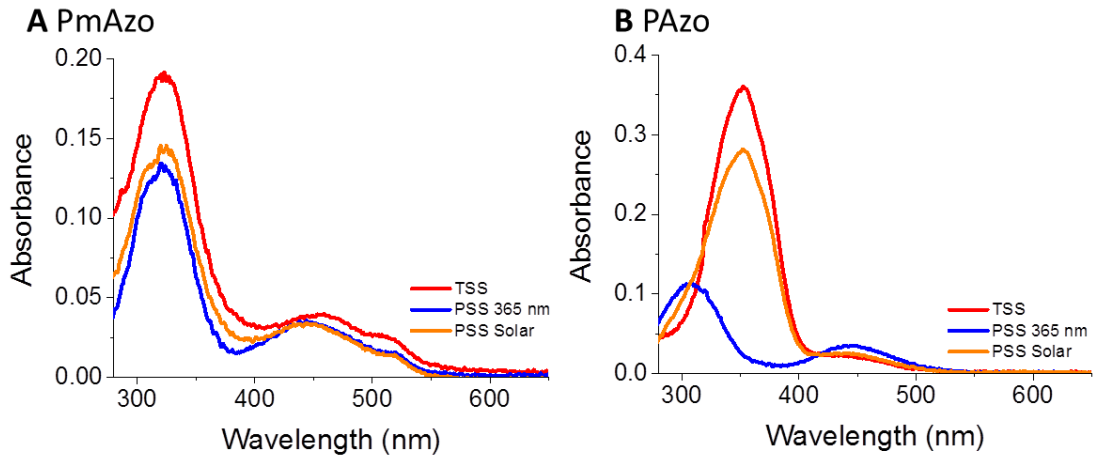


**Figure S5**. Solution UV-vis spectra for dissolved films immediately after dissolution (PSS Solar), after 365 nm irradiation at 2 mW $cm^{-2}$ for 45 min (PSS 365 nm), and after 10 h heating at 110 ℃ in an oil bath for A) PmAzo and B) PAzo. Absorbance changes at 325 nm (PmAzo) and 352 nm (PAzo) were used to estimate cis conversions (72.7% PmAzo, 23.9% PAzo) according to Equation S1.

**5. Polarized Optical Microscopy**

Both trans and cis PmAzo were isotropic (Figure S6A-C). The as-prepared trans-PAzo film showed anisotropic structures in the image from polarized optical microscopy (POM) (Figure S6D). After irradiation with UV light, the irradiated part of the film was switched from trans to cis, which was isotropic (Figure S6E). After heating the film, the azo groups switched to the thermodynamically more stable trans form and, because the film was heated above $T_g$, the chromophores can move and reform the anisotropic state after cooling to room temperature.

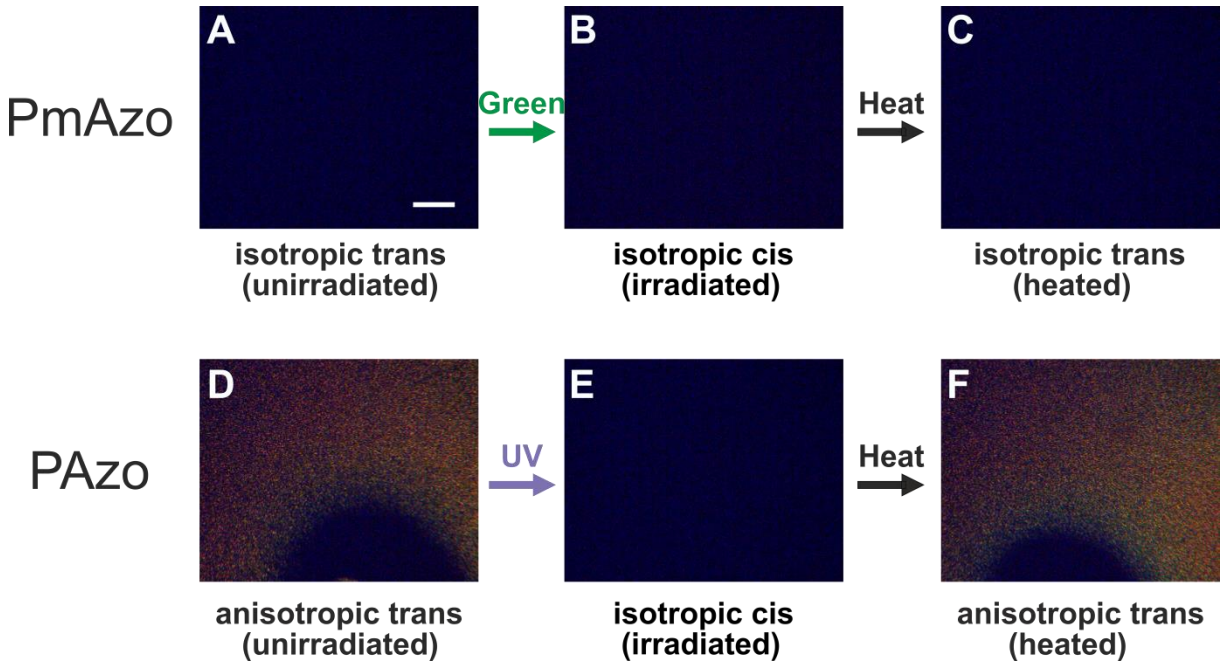


**Figure S6.** POM images of drop casted PmAzo (upper) and PAzo (lower) films A),D) before, B),E) after UV/green light irradiation (20 min, 3 mW $cm^{-2}$), and C),F) at room temperature after heating (2 h, 100 ℃). Scale bar is 250 µm.

**6. Trans-Cis Cycling Induced by Blue and Red Light**

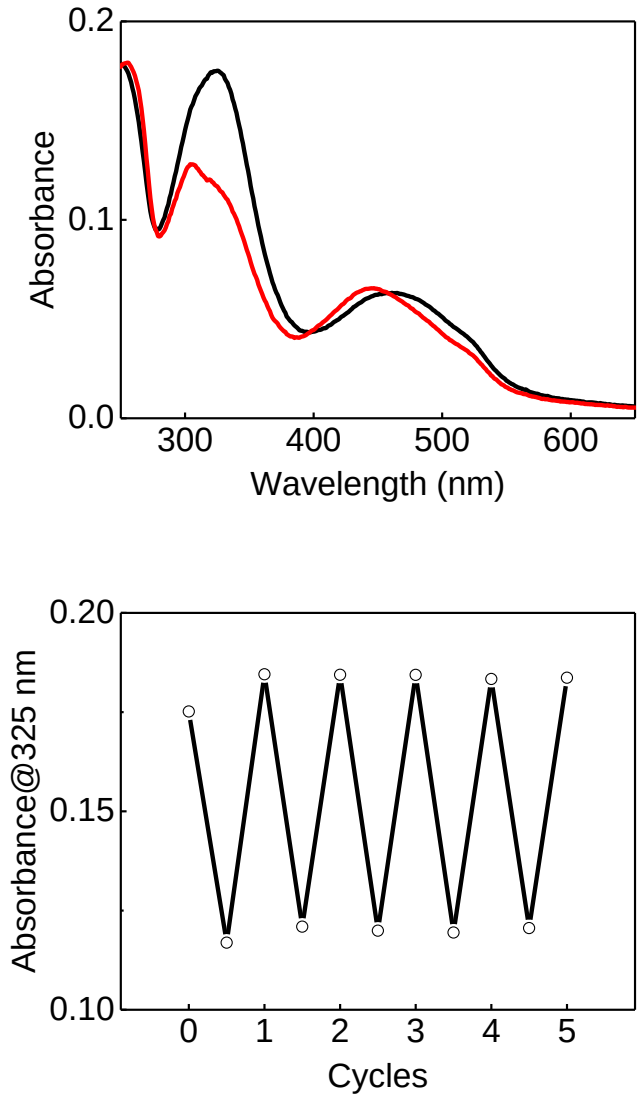


**Figure S7**. Cycling of a PmAzo film by alternating red light (625 nm, 1 mW $cm^{-2}$, 20 min) and blue light (470 nm, 1 mW $cm^{-2}$, 1 min) irradiation. Top: UV−vis absorption spectra of a trans PmAzo film (black, before irradiation) and cis PmAzo film (after red light irradiation). Bottom: Absorbance changes in the cycling process. No attenuation of the absorbance of the PmAzo film was observed, which indicates PmAzo is photostable.

**7. Ab-Initio Calculations**

As described in the experimental, the optimized geometry of model compounds for PmAzo and PAzo was obtained from a DFT calculation using a 6-311G(d,p) basis set and B3LYP functional.[S3] In order to make calculations tractable, the model compounds of PmAzo and PAzo structures were truncated, as shown in Figure S8 in the optimized geometry. Optimizations were carried out without solvent modeling (in the gas phase) on individual molecules as a first estimate. Theoretical gravimetric energy densities were derived assuming full trans-to-cis conversion with each molecule storing the difference in energy between the trans and cis optimized structures. Optimized atomic coordinates are given below. In addition to the larger mass of PmAzo relative to PAzo, the small gravimetric energy density of PmAzo partly derives from the increased steric interactions present in the trans form. This steric effect decreases the enthalpy difference upon isomerization as reflected in the theoretical calculations.

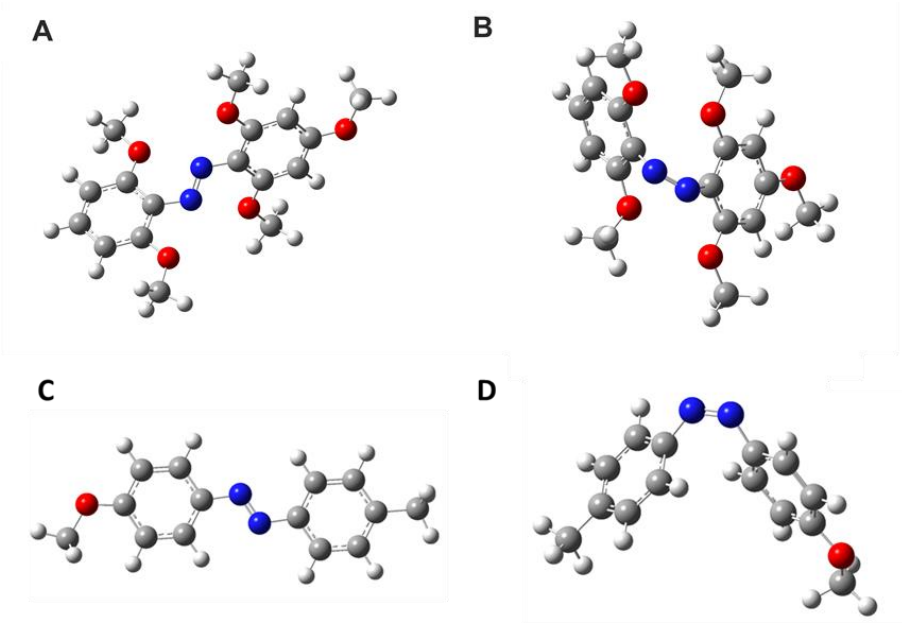


**Figure S8** A/B) Trans/cis PmAzo and C/D) trans/cis PAzo truncated chromophore geometries as calculated by DFT/6-311G(d,p)/B3LYP in Gaussian09.

Trans-PmAzo:

| | | | |
|---|---|---|---|
| C | -4.67237200 | -0.52556500 | 0.71260800 |
| C | -3.30878200 | -0.82857300 | 0.73346800 |
| C | -2.37407400 | -0.01394800 | 0.05535300 |
| C | -2.84942500 | 1.10184300 | -0.67313200 |
| C | -4.21995800 | 1.38812800 | -0.70280000 |
| C | -5.11116800 | 0.58122000 | -0.00609100 |
| H | -5.38438200 | -1.13513000 | 1.25027400 |
| H | -4.59142000 | 2.23570400 | -1.26098800 |
| N | -1.03771200 | -0.46885900 | 0.04716200 |
| N | -0.16826800 | 0.43201600 | 0.16948000 |
| C | 1.17222000 | 0.03481200 | 0.06336700 |
| C | 1.68309100 | -1.07573600 | -0.66723000 |
| C | 2.10847600 | 0.90166800 | 0.67744000 |
| C | 3.05628900 | -1.29176800 | -0.75933800 |
| C | 3.48657400 | 0.67300200 | 0.60071900 |
| C | 3.94688700 | -0.42833800 | -0.12017900 |
| H | 3.46975900 | -2.12012700 | -1.31434200 |
| H | 4.17639800 | 1.33462600 | 1.09788800 |
| O | 5.26347000 | -0.74869200 | -0.26127800 |
| C | 6.23961800 | 0.07879800 | 0.35470200 |
| H | 7.20251500 | -0.36641100 | 0.10948500 |
| H | 6.20488900 | 1.10150200 | -0.03674500 |
| H | 6.11904800 | 0.10030000 | 1.44343100 |
| O | -2.77817700 | -1.87982000 | 1.41230700 |
| O | -1.92655600 | 1.81788000 | -1.36514400 |
| O | 1.58088800 | 1.94483300 | 1.36241300 |
| O | 0.78401500 | -1.86301800 | -1.29609800 |
| C | -3.65822000 | -2.78040000 | 2.06427900 |
| H | -4.21662800 | -2.28922100 | 2.86960600 |
| H | -4.36409300 | -3.23762900 | 1.36143500 |
| H | -3.02280100 | -3.55497500 | 2.49097600 |
| C | 1.25095700 | -2.91111000 | -2.13230300 |
| H | 1.87935400 | -2.53066500 | -2.94528600 |
| H | 1.80905600 | -3.66117300 | -1.56149800 |
| H | 0.35560200 | -3.36950700 | -2.54832400 |
| C | 2.45109600 | 2.88867200 | 1.96447900 |
| H | 3.06425100 | 2.43152800 | 2.74970300 |
| H | 3.10315600 | 3.36860100 | 1.22574700 |
| H | 1.80184500 | 3.63973100 | 2.41135900 |
| C | -2.36866900 | 2.85992100 | -2.21809200 |
| H | -3.05854800 | 2.49229300 | -2.98671600 |
| H | -2.85153700 | 3.66614100 | -1.65410100 |
| H | -1.47015300 | 3.24805300 | -2.69535600 |
| H | -6.16881000 | 0.81904700 | -0.02413100 |

Cis-PmAzo:

| | | | |
|---|---|---|---|
| C | 3.11205100 | 0.00880900 | -0.06188200 |
| C | 2.06352800 | 0.66099800 | -0.71819500 |
| C | 0.81119500 | 0.04734600 | -0.88688000 |
| C | 0.64830300 | -1.27774800 | -0.43151000 |

| | | | |
|---|---|---|---|
| C | 1.69229600 | -1.94268100 | 0.20734300 |
| C | 2.91260800 | -1.29355300 | 0.39862800 |
| H | 4.05247700 | 0.51172900 | 0.09351600 |
| H | 1.59548900 | -2.95804500 | 0.56145500 |
| N | -0.13278700 | 0.71826400 | -1.72286500 |
| N | -1.32762000 | 0.88662600 | -1.41515900 |
| C | -1.84968400 | 0.62160800 | -0.11088000 |
| C | -1.38798800 | 1.29608600 | 1.02897400 |
| C | -3.02470500 | -0.15512600 | -0.01423500 |
| C | -2.04950900 | 1.16099000 | 2.25122700 |
| C | -3.67652300 | -0.29303700 | 1.21091300 |
| C | -3.17854700 | 0.36042000 | 2.33945300 |
| H | -1.65481200 | 1.68826300 | 3.11097700 |
| H | -4.56374000 | -0.90550200 | 1.29587900 |
| O | 3.86261900 | -2.02448600 | 1.04966300 |
| C | 5.13825300 | -1.44226800 | 1.27105300 |
| H | 5.06791600 | -0.54344000 | 1.89393700 |
| H | 5.72161500 | -2.19689900 | 1.79625700 |
| H | 5.63640200 | -1.19370100 | 0.32723000 |
| O | -3.42465700 | -0.75330500 | -1.16803100 |
| O | -0.28122500 | 2.10984000 | 0.96133300 |
| O | -0.54803700 | -1.85628100 | -0.70477600 |
| O | 2.15862300 | 1.92732100 | -1.20117800 |
| C | 3.41915500 | 2.57828600 | -1.17324200 |
| H | 3.26868400 | 3.53293400 | -1.67476500 |
| H | 3.75582700 | 2.76029700 | -0.14631800 |
| H | 4.18124500 | 2.00425700 | -1.71155900 |
| C | -0.74765200 | -3.21965900 | -0.36441300 |
| H | -0.68414800 | -3.37673400 | 0.71755500 |
| H | -1.75249300 | -3.45900300 | -0.70719500 |
| H | -0.02504100 | -3.86811200 | -0.87127000 |
| C | -4.68535900 | -1.40420100 | -1.18935700 |
| H | -4.83704300 | -1.72013900 | -2.22020600 |
| H | -4.69813700 | -2.28554000 | -0.53721700 |
| H | -5.49336600 | -0.72573600 | -0.89411800 |
| C | -0.53801800 | 3.42034400 | 0.44337700 |
| H | -1.24106200 | 3.96046900 | 1.08779500 |
| H | 0.42075500 | 3.93647700 | 0.43205700 |
| H | -0.93372400 | 3.37347300 | -0.57503800 |
| H | -3.68900200 | 0.24632100 | 3.28887400 |

Trans-PAzo:

| | | | |
|---|---|---|---|
| C | 4.3548360000 | -1.2927340000 | 0.0006240000 |
| C | 2.9667920000 | -1.3904040000 | 0.0004040000 |
| C | 2.1756880000 | -0.2393990000 | 0.0004820000 |
| C | 2.7984470000 | 1.0191670000 | 0.0010150000 |
| C | 4.1799870000 | 1.1044410000 | 0.0012580000 |
| C | 4.9860320000 | -0.0468700000 | 0.0007140000 |
| H | 4.9551880000 | -2.1964900000 | 0.0009280000 |
| H | 2.4706720000 | -2.3538000000 | 0.0005450000 |

| | | | |
|---|---|---|---|
| H | 2.1792870000 | 1.9063290000 | 0.0016450000 |
| H | 4.6528980000 | 2.0819100000 | 0.0021280000 |
| N | 0.7761000000 | -0.4498660000 | 0.0004330000 |
| N | 0.0789960000 | 0.5950320000 | 0.0005680000 |
| C | -1.3175510000 | 0.3922540000 | 0.0003410000 |
| C | -1.9472350000 | -0.8587120000 | 0.0006000000 |
| C | -2.1082900000 | 1.5506740000 | -0.0001000000 |
| C | -3.3315150000 | -0.9537940000 | 0.0003020000 |
| H | -1.3323430000 | -1.7489550000 | 0.0010300000 |
| C | -3.4886910000 | 1.4669250000 | -0.0004410000 |
| H | -1.6081730000 | 2.5118120000 | -0.0001970000 |
| C | -4.1129530000 | 0.2121360000 | -0.0002990000 |
| H | -3.7948780000 | -1.9312870000 | 0.0005920000 |
| H | -4.1113230000 | 2.3529560000 | -0.0007770000 |
| O | -5.4715070000 | 0.2279490000 | -0.0006880000 |
| C | -6.1720520000 | -1.0099070000 | -0.0007320000 |
| H | -5.9443880000 | -1.5992290000 | 0.8939840000 |
| H | -7.2292820000 | -0.7507810000 | -0.0015400000 |
| H | -5.9432390000 | -1.5998230000 | -0.8947690000 |
| C | 6.4895680000 | 0.0726210000 | -0.0027730000 |
| H | 6.8426850000 | 0.5860300000 | -0.9029130000 |
| H | 6.8425730000 | 0.6508850000 | 0.8567920000 |
| H | 6.9683240000 | -0.9076860000 | 0.0326890000 |

Cis-PAzo:

| | | | |
|---|---|---|---|
| C | 3.1327790000 | 0.7823090000 | 0.8703600000 |
| C | 2.1040030000 | 1.7010960000 | 0.7748430000 |
| C | 0.9981460000 | 1.4562950000 | -0.0525340000 |
| C | 0.9890020000 | 0.3056180000 | -0.8450270000 |
| C | 2.0419940000 | -0.6032460000 | -0.7877800000 |
| C | 3.1115120000 | -0.3802290000 | 0.0867060000 |
| H | 3.9805270000 | 0.9491800000 | 1.5233610000 |
| H | 2.1311030000 | 2.6246040000 | 1.3411900000 |
| H | 0.1685730000 | 0.1217880000 | -1.5261770000 |
| H | 2.0170520000 | -1.4761130000 | -1.4259790000 |
| N | 0.0466950000 | 2.5208990000 | -0.1576320000 |
| N | -1.1828540000 | 2.3601120000 | -0.2772480000 |
| C | -1.8537190000 | 1.1023530000 | -0.1197450000 |
| C | -1.6919650000 | 0.2919770000 | 1.0102390000 |
| C | -2.8554400000 | 0.7936240000 | -1.0433850000 |
| C | -2.5002670000 | -0.8246080000 | 1.1823230000 |
| H | -0.9506760000 | 0.5481040000 | 1.7570230000 |
| C | -3.6314660000 | -0.3481290000 | -0.8781770000 |
| H | -3.0143140000 | 1.4599310000 | -1.8834210000 |
| C | -3.4698700000 | -1.1787070000 | 0.2358510000 |
| H | -2.3757050000 | -1.4349300000 | 2.0712960000 |
| H | -4.3922980000 | -0.5851350000 | -1.6149440000 |
| C | -4.3110270000 | -2.4189750000 | 0.4140220000 |
| H | -4.5494020000 | -2.5920470000 | 1.4663280000 |
| H | -5.2506890000 | -2.3461120000 | -0.1378730000 |

| | | | |
|---|---|---|---|
| H | -3.7846020000 | -3.3081650000 | 0.0492300000 |
| O | 4.1778040000 | -1.2118740000 | 0.2328680000 |
| C | 4.2298440000 | -2.3974640000 | -0.5499040000 |
| H | 4.2533960000 | -2.1697790000 | -1.6212030000 |
| H | 5.1547260000 | -2.8977200000 | -0.2683820000 |
| H | 3.3818340000 | -3.0571740000 | -0.3359870000 |

## 8. Thermal Reversion Rates

One of the most salient characteristics for STCs is the storage lifetime, which is given by the half-life of the cis-isomer for azo-based systems (Table 1). The lifetims of PAzo in solution was determined by attaining the PSS 365 nm (45 min, 2 mW $cm^{-2}$) and monitoring the time-dependent change in absorbance at the peak $\pi^* \leftarrow \pi$ wavelength. The same procedure was carried out for PmAzo after charging to the PSS 365 nm (45 min, 2 mW $cm^{-2}$).

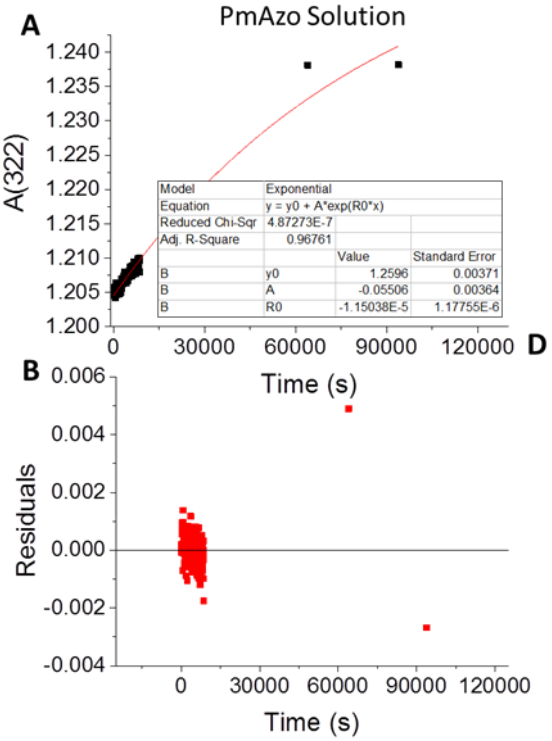


**Figure S9**. A) Absorbance at 322 nm for PmAzo solution as a function of time after achieving the PSS 365 nm (2 mW $cm^{-2}$, 45 min) along with a monoexponential fit and B) attendant residuals.

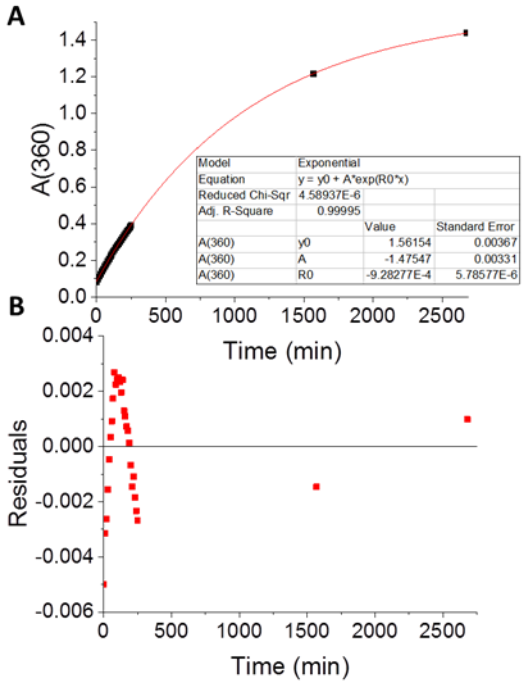


**Figure S10**. A) Absorbance at 360 nm for PAzo solution as a function of time after achieving the PSS 365 nm (2 mW $cm^{-2}$, 45 min) along with a monoexponential fit and B) attendant residuals.

Monoexponetial fits were performed in Origin9.1 using a Levenberg-Marquardt fitting routine to determine thermal half-lives. Only the PAzo solution fit displays a clear trend; however, trendless residuals for PAzo were not obtained upon a biexponential fit. This could indicate multiple relaxation pathways, or a change in the rate of isomerization due to the frequency of UV-vis measurements. In either case, the major component of the exponential decay remained unchanged upon increasing the modality of the exponential fit and hence the monoexponential approximation was reported.

**9. Solar Efficiency**

As established by Scharf et. al., the solar efficiency should account for quantum yield of isomerization $\phi$, the percentage of photonic energy stored $\eta_E$, the percentage of available (sufficient energy) photons absorbed by the low-energy isomer $\eta_{abs}$, and the fraction of energy used out of the total energy from the sun's irradiation $\eta_a$.[S4]

$$\eta = \phi \cdot \eta_E \cdot \eta_{abs} \cdot \eta_a \quad (\mathbf{S2})$$

$$\eta_E = \frac{\frac{\Delta H_{cis-trans}}{hc\,N_A}}{\frac{}{\lambda_{transition}}} \quad (\mathbf{S3})$$

$$\eta_{abs} = \frac{\int_0^{\lambda_{transition}} I_{solar}(\lambda) \cdot \lambda \cdot \frac{\varepsilon_{trans}}{\varepsilon_{total}} \left(1 - 10^{-A}\right) d\lambda}{\int_0^{\lambda_{transition}} I_{solar}(\lambda) \cdot \lambda \; d\lambda} \quad (\mathbf{S4})$$

$$\eta_a = \frac{\int_0^{\lambda_{transition}} I_{solar}(\lambda) \cdot \frac{\lambda}{\lambda_{transition}} \; d\lambda}{\int_0^{\infty} I_{solar}(\lambda) \; d\lambda} \quad (\mathbf{S5})$$

Thus, the overall equation for solar efficiency should be:

$$\eta = \phi \frac{\Delta H_{cis-trans}}{hc\,N_A} \frac{\int_0^{\lambda_{transition}} I_{solar}(\lambda) \cdot \lambda \cdot \frac{\varepsilon_{trans}}{\varepsilon_{total}} \left(1 - 10^{-A}\right) d\lambda}{\int_0^{\infty} I_{solar}(\lambda) \; d\lambda} \quad (\mathbf{S6})$$

While previous reports have used slight variations on this formula, a comparison of calculated efficiencies from both methods differed by only 0.01%.[S5] The following reasonable assumptions were made following the work of Kucharski et al.:

a) Absorbing chromophores were completely trans $\varepsilon_{trans}/\varepsilon_{total} = 1$. While cis absorption may contribute to attenuation during actual operation, this assumption at worst gives the initial efficiency

b) $\phi \approx 0.2$

c) Normalization of $\eta_{abs}$ such that the sample is defined as thick enough to absorb 100% of light at the peak wavelength of the transition.

$$\eta_{abs} = \frac{1}{0.9} \frac{\int_0^{\lambda_{transition}} I_{solar}(\lambda) \cdot \lambda \left(1 - 10^{-\frac{A}{A(\lambda_{max})}}\right) d\lambda}{\int_0^{\lambda_{transition}} I_{solar}(\lambda) \cdot \lambda \, d\lambda} \quad (\mathbf{S7})$$

However, previous estimates of solar efficiency have not addressed the problem that not all absorption bands cause trans-to-cis energy storage, but can instead promote back isomerization. An initial estimate to account for these effects is to treat the spectrum piecewise, assigning each band to either trans-to-cis or cis-to-trans isomerization. Thus, the efficiency becomes a sum over only those absorption bands causing trans-to-cis isomerization. Further, insertion of the assumed values above and the known integration of the AM 1.5 solar spectrum (1000 W $m^{-2}$) gives Eq. S8.

$$\eta = \frac{2}{9000hc\,N_A} \sum \Delta H_{cis-trans} \int_{\lambda_{lower\,bound}}^{\lambda_{upper\,bound}} I_{solar}(\lambda) \cdot \lambda \left(1 - 10^{-\frac{A}{A(\lambda_{max})}}\right) d\lambda \quad (\mathbf{S8})$$

Note that Equation S8 assumes that light at the wavelengths of bands causing cis-to-trans back-isomerization is completely blocked. However, the design presented herein does not simply block deleterious wavelengths, but also down-converts 470 nm light to broad fluorescent emission centered at 570 nm. Thus, an additional term integrated over the region absorbed by the Coumarin 314 filter using A(550 nm) for PmAzo was included. This term

also was multiplied by an additional factor of 0.5 to account for the quantum efficiency of fluorescent emission from Coumarin 314. A summary of the spectral regions included in the calculation is provided in **Table S1**.

**Table S1.** Summary of each spectral region and corresponding absorption band integral included in the summand for efficiency calculations. The enthalpy of cis-to-trans isomerization for each chromophore is also provided.

| **Spectral Region** | **Absorption Band Integrated** | $\Delta H_{cis-trans}$ **(kJ mol$^{-1}$)** |
|---|---|---|
| 280 – 400 nm | PAzo $\pi^* \leftarrow \pi$ | 56.0 |
| 280 – 400 nm | PmAzo $\pi^* \leftarrow \pi$ | 9.6 |
| 400 – 480 nm[a] | PmAzo A(550 nm) | 9.6 |
| 480 – 550 nm | PmAzo $\pi^* \leftarrow n$ | 9.6 |

[a]The resulting integral was multiplied by an additional factor of 0.5 to account for the quantum efficiency of fluorescent emission from Coumarin 314

Using this method, the efficiency was calculated to be ~0.4% (0.38% including down-conversion; 0.33% excluding down-conversion).

**10. DSC**

DSC measurements preformed as described in the experimental were used to determine the enthalpy of cis-to-trans isomerization. First, the bulk energy density was obtained by integrating the cis-to-trans isomerization peak using a linear baseline (Equatiom S9).

$$\frac{q}{m} = \frac{\left[\int_{T_1}^{T_2} P\, dT\right]}{m\, v} \qquad (\mathbf{S9})$$

Here $P$ is the power given by the DSC measurement in the temperature interval dT, $T_1$ and $T_2$ are the limits of the cis-to-trans isomerization process, m is the mass of the sample, and v is the scanning speed of the DSC measurement.

By measuring the percent cis ($\chi_{cis}$) using $^1$H-NMR, the enthalpy of cis-to-trans isomerization was obtained by Equation S10 where M is the molar mass of the repeating unit of the azopolymer in question.

$$\Delta H_{cis-trans} = \frac{qM}{m\chi_{cis}} \qquad (\mathbf{S10})$$

**11. Supplementary References**

[S1] P. Weis, D. Wang, S. Wu, *Macromolecules.* **2016**, *in press*, DOI: 10.1021/acs.macromol.6b01367.

[S2] J.G. Victor, J.M. Torkelson, *Macromolecules.* **1987**, *20*, 2241.

[S3] Gaussian 09, Revision E.01, M. J. Frisch, G. W. Trucks, H. B. Schlegel, G. E. Scuseria, M. A. Robb, J. R. Cheeseman, G. Scalmani, V. Barone, B. Mennucci, G. A. Petersson, H. Nakatsuji, M. Caricato, X. Li, H. P. Hratchian, A. F. Izmaylov, J. Bloino, G. Zheng, J. L. Sonnenberg, M. Hada, M. Ehara, K. Toyota, R. Fukuda, J. Hasegawa, M. Ishida, T. Nakajima, Y. Honda, O. Kitao, H. Nakai, T. Vreven, J. A. Montgomery, Jr., J. E. Peralta, F. Ogliaro, M. Bearpark, J. J. Heyd, E. Brothers, K. N. Kudin, V. N. Staroverov, R. Kobayashi, J. Normand, K. Raghavachari, A. Rendell, J. C. Burant, S. S. Iyengar, J. Tomasi, M. Cossi, N. Rega, J. M. Millam, M. Klene, J. E. Knox, J. B. Cross, V. Bakken, C. Adamo, J. Jaramillo, R. Gomperts, R. E. Stratmann, O. Yazyev, A. J. Austin, R. Cammi, C. Pomelli, J. W. Ochterski, R. L. Martin, K. Morokuma, V. G. Zakrzewski, G. A. Voth, P. Salvador, J. J. Dannenberg, S. Dapprich, A. D. Daniels, Ö. Farkas, J. B. Foresman, J. V. Ortiz, J. Cioslowski, and D. J. Fox, Gaussian, Inc., Wallingford CT, 2009.

[S4] H.-D. Scharf, J. Fleischauer, H. Leismann, I. Ressler, W. Schleker, R. Weitz, *Angew. Chem. Int. Ed. Engl.* **1979**, *18*, 652.

[S5] T. J. Kucharski, N. Ferralis, A. M. Kolpak, J. O. Zheng, D. G. Nocera, J. C. Grossman, *Nat. Chem.* **2014**, *6*, 441.

## 4.3 Photoswitching of Glass Transition Temperatures of Azobenzene-Containing Polymers Induces Reversible Solid-to-Liquid Transitions

nature chemistry

SUPPLEMENTARY INFORMATION

DOI: 10.1038/NCHEM.2625

**Photoswitching of Glass Transition Temperatures of Azobenzene-Containing Polymers Induces Reversible Solid-to-Liquid Transitions**

Hongwei Zhou†, Changguo Xue†, Philipp Weis†, Yasuhito Suzuki, Shilin Huang, Kaloian Koynov, Günter K. Auernhammer, Rüdiger Berger, Hans-Jürgen Butt and Si Wu*

Max Planck Institute for Polymer Research, Ackermannweg 10, 55128 Mainz, Germany

†These authors contributed equally to this work.

*e-mail: wusi@mpip-mainz.mpg.de

DOI: 10.1038/NCHEM.2625

SUPPLEMENTARY INFORMATION

## Materials

Phenol (>99%), p-toluidine (99%), 6-chloro-1-hexanol (96%), acryloyl chloride (97%), methacryloyl chloride (97%), 4-phenylazophenol (98%), and 2,2′-azobisisobutyronitrile (AIBN, 98%) were purchased from Sigma-Aldrich. 4-(4-Nitrophenylazo)phenol (97%) was purchased from TCI. AIBN was recrystallized twice from methanol before use. Cyanoisopropyl dithiobenzoate (RAFT agent, CPDB) was purchased from Sigma-Aldrich and purified by column chromatography using silica gel as the stationary phase and $CH_2Cl_2$ as the eluent before use ($^1$H NMR in DMSO-D6: δ(ppm) = 7.91 (s, 2H, Ar-*H*), 7.68 (s, 1H, Ar-*H*), 7.49 (s, 2H, Ar-*H*), 1.94 (s, 6H, C*H*$_3$)). All solvents (HPLC grade) were purchased from Sigma-Aldrich or Fisher Scientific.

## Instruments and Characterization

UV-vis absorption spectra were recorded on a Lambda 900 spectrometer (Perkin Elmer). Optical microscopy images were captured on an optical microscope (Zeiss) equipped with a CCD camera. Differential scanning calorimetry (DSC) curves were measured on a Mettler Toledo DSC 822 system. DSC measurements were conducted under a $N_2$ atmosphere from -50 °C to 150 °C with heating and cooling rates of 10 °C/min. Thermogravimetric analysis (TGA) measurements were conducted on a Mettler Toledo TGA/SDTA 851 system with a heating rate of 10 °C/min under a $N_2$ atmosphere. *Trans*-to-*cis* and *cis*-to-*trans* photoisomerization of the azopolymers were induced by LEDs at λ = 365 and 530 nm, respectively (device types LCS-0365-07-22 and LCS-0530-15-22, Mightex Systems). The output power of the LEDs was controlled by an LED controller

DOI: 10.1038/NCHEM.2625

SUPPLEMENTARY INFORMATION

(device type SLC-MA04-MU, Mightex Systems). Three-dimensional confocal microscopy images were captured by a white-light confocal microscope μsurf explorer (NanoFocus AG). The surface roughness was calculated by a method reported in literature[1]. First, the profiles of the surfaces were obtained from the three-dimensional confocal microscopy images. Then, the arithmetical mean deviation of the surface profiles ($R_a$) was used to reveal the surface roughness. $R_a$ is defined as the average value of the ordinate deviations ($Z_1$, $Z_2$,....$Z_n$) from the mean line and calculated according to the formula $R_a = \frac{1}{n}\sum_{i=1}^{n} | Z_i |$, where "n" is the number of divisions. Force-piezo position curves were measured using a VEECO digital Instruments MultiMode Scanning Probe Microscope with a tip velocity of 996 nm/s. The shear moduli of **P1** were measured using a homemade piezo-rheometer in shear mode at room temperature. *Cis* azopolymers with a thickness of 100 μm was sandwiched between two quartz plates that were used as transparent sample holders. The shear moduli of *cis* azopolymers were measured. Subsequently, *cis* azopolymers between the quartz plates were converted to *trans* azopolymers by 530 nm light. *Trans* azopolymers were measured by the piezo-rheometer under the same conditions. Dynamic mechanical analysis (DMA) was conducted on an Advanced Rheometric Expansion System (ARES, Rheometric Scientific Company). Shear deformation was applied under conditions of controlled deformation amplitude, which was kept in the range of the linear viscoelastic response of the studied samples. Plate-plate geometry was used with plate diameters of 6 mm. The experiments were conducted under dry nitrogen atmosphere at a heating rate of 3 °C/min and a constant deformation frequency of either 1 or 10 rad/s. $^{1}$H NMR and $^{13}$C NMR spectra were measured using a Bruker Spectrospin spectrometer (250 MHz) at 293 K. The molecular

DOI: 10.1038/NCHEM.2625

SUPPLEMENTARY INFORMATION

weights and polydispersity indices of the azopolymers were determined by gel permeation chromatography (GPC) (Waters Alliance 2000). THF was used as the eluent and polystyrene was used as a standard. Infrared thermometer images were captured by an infrared thermometer (testo880).

## Synthesis

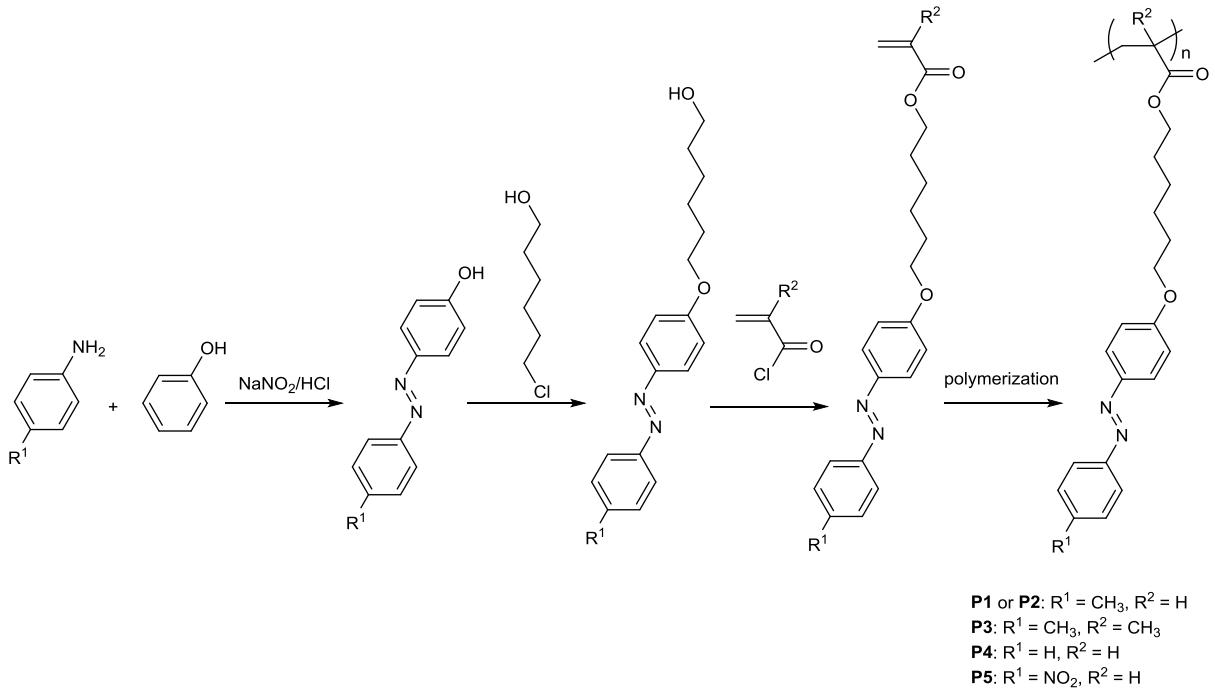


Supplementary Figure 1. Synthetic route for the azopolymers **P1**, **P2**, **P3**, **P4** and **P5**. **P1** and **P2** are two polymers with different molecular weights. The details of the syntheses were described below.

DOI: 10.1038/NCHEM.2625 SUPPLEMENTARY INFORMATION

**4-(p-tolyldiazenyl)phenol:** *p*-Toluidine (8 g, 0.075 mol) was dissolved in a mixture of hydrochloric acid (16 mL), ice (16 g), and acetone (110 mL). To the above mixture, a solution containing water (28 mL), ice (28 g), and sodium nitrite (5.020 g, 0.075 mol) was added slowly. The mixture was stirred for 30 min at -5 to 0 °C. Then, an aqueous solution of phenol (7.0 g, 0.075 mol) in 2 mol/L sodium hydroxide was added to the mixture. The reaction mixture was stirred for 2 h at pH 9 to 10. After neutralization with HCl, the resulting mixture was filtered and washed with water. The crude product was dried and purified by recrystallization from ethanol to obtain the compound as a red-brown solid. Yield: 75%. $^1$H NMR (DMSO-D6): δ (ppm) = 10.27 (s, 1H, Ar-O*H*), 7.82 (d, 2H, *J* = 8 Hz, Ar-*H*), 7.75 (d, 2H, *J* = 6 Hz, Ar-*H*), 7.37 (d, 2H, *J* = 8 Hz, Ar-*H*), 6.95 (d, 2H, *J* = 7 Hz, Ar-*H*), 2.40 (s, 3H, Ar-C$H_3$).

**6-(4-(p-tolyldiazenyl)phenoxy)hexan-1-ol:** $K_2CO_3$ (4.9 g, 0.036 mol) was added to a solution of 4-(p-tolyldiazenyl)phenol (7.5 g, 0.036 mol) in DMF (40 mL). The solution was stirred for 30 min at 30 °C. Then, KI (0.015 g, 0.090 mmol) and 6-chloro-1-hexanol (5.335 g, 0.039 mol) were added to the solution. The reaction mixture was then stirred vigorously for 24 h at 110 °C. The resulting mixture was cooled to room temperature and poured into 900 g of crushed ice, and the resulting red-brown precipitate was filtered off. The crude product was dried and purified by recrystallization from ethanol to produce Compound 2 as a red-brown solid. Yield: 86%. $^1$H NMR ($CDCl_3$): δ (ppm) = 7.92 (d, 2H, *J* = 8 Hz, Ar-*H*), 7.81 (d, 2H, *J* = 8 Hz, Ar-*H*), 7.35 (d, 2H, *J* = 6 Hz, Ar-*H*), 7.05 (d, 2H, *J* = 7 Hz, Ar-*H*), 4.08 (t, 2H, *J* = 6 Hz, Ar-O-C$H_2$), 3.71 (t, 2H, *J* = 6 Hz, HO-C$H_2$), 2.41 (s, 3H, Ar-C$H_3$), 1.86-1.58 (m, 8H, -C$H_2$-C$H_2$-C$H_2$-C$H_2$-).

DOI: 10.1038/NCHEM.2625 SUPPLEMENTARY INFORMATION

**(E)-6-(4-(p-tolyldiazenyl)phenoxy)hexyl acrylate (monomer of P1):** Under ice-water bath conditions, a solution of acryloyl chloride (1.743 g, 0.019 mol) in 10 mL dry $CH_2Cl_2$ was added drop wise into a solution containing 6-(4-(p-tolyldiazenyl)phenoxy)hexan-1-ol (4.754 g, 0.016 mol), triethylamine (1.624 g, 0.016 mol) and dry $CH_2Cl_2$ (50 mL). Afterwards, the reaction mixture was maintained at room temperature for 20 h. The reaction mixture was concentrated with a rotary evaporator, washed with diluted hydrochloric acid, a $NaHCO_3$ solution and a NaCl solution. The organic layer was collected and the solvent was removed with a rotary evaporator. The crude product was purified by elution on a silica gel column with $CH_2Cl_2$. After removing the solvent, the product was recrystallized to obtain the azobenzene-containing monomer as a yellow solid. Yield: 73%. $^1$H NMR (DMSO-d6): δ (ppm) = 7.87 (d, 2H, *J* = 8.9 Hz, Ar-*H*), 7.76 (d, 2H, *J* = 8.3 Hz, Ar-*H*), 7.39 (d, 2H, *J* = 8.3 Hz, Ar-*H*), 7.12 (d, 2H, *J* = 9.0 Hz, Ar-*H*), 6.34 (dd, 1H, *J* = 17, 2 Hz, -CH=C$H_2$), 6.18 (dd, 1H, *J* = 17, 10 Hz, -CH=C$H_2$), 5.94 (dd, 1H, *J* = 10, 2 Hz, -C*H*=CH$_2$), 4.13 (t, 2H, Ar-O-C$H_2$), 3.95 (t, 2H, -O-C$H_2$), 2.41 (s, 3H, Ar-C$H_3$), 1.45-1.77 (m, 8H, -C$H_2$-C$H_2$-C$H_2$-C$H_2$-). $^{13}$C NMR ($CDCl_3$) δ (ppm): 166.33, 161.42, 150.79, 146.88, 140.80, 130.60, 129.71, 128.59, 124.63, 122.56, 114.67, 68.10, 64.52, 29.11, 28.58, 25.78, 21.49. ESI-MS m/z: calculated 366.2 $[M]^+$, found 365.9 $[M]^+$.

**Azopolymer P1:** The azopolymer **P1** was prepared by RAFT polymerization. The azobenzene-containing monomer (1.5 g, 4.096 mmol), CPDB (5 mg, 0.023 mmol), and AIBN (1 mg, 0.006 mmol) were dissolved in anisole (4 mL). Then, the solution was treated with four freeze-pump-thaw cycles and sealed under Ar gas. The polymerization system was placed in an oil bath at 75 °C for 48 h. After polymerization, the polymer solution was added drop wise to methanol (40 mL). The precipitate was dissolved in THF

DOI: 10.1038/NCHEM.2625 SUPPLEMENTARY INFORMATION

and precipitated from methanol three times to remove the unreacted monomer. The resulting polymer (**P1**) was collected and dried in a vacuum oven at 40 °C for 24 h. *Trans* **P1** was further dried in an oven at 120 °C for 6 h and at 40 °C for two days under vacuum for the DSC measurements. Yield: 30%. $M_n$ (GPC) = 9.9 × $10^3$ g/mol and $M_w/M_n$=1.32. $^1$H NMR (DMSO-d6): δ (ppm) = 7.72-7.60, 7.12, 6.83 (protons on azobenzene group), 3.9 (Ar-O-C$H_2$, -O-C$H_2$), 2.2 (Ar-C$H_3$), 1.8-1.1 (protons on the polymer backbone and -C$H_2$-C$H_2$-C$H_2$-C$H_2$-).

**Preparation of the high-molecular-weight azopolymer P2 by cycling GPC:** To obtain **P2**, the azopolymer synthesized by RAFT polymerization was separated on a cycling GPC system using $CHCl_3$ as an eluting solvent. The pressure of the pump was 69 bar. The flow rate of the systems was 3 mL/min. The temperature of the system was 25 °C. The polymer eluted from the column during a 56-58 min run was collected, and the solvent was removed by evaporation under vacuum. The molecular weight and the polydispersity index (PDI) of the separated polymer (**P2**) measured by GPC were 2.7 × $10^4$ g/mol and 1.07, respectively.

**Azopolymer P3: P3** was synthesized using a similar method to that of **P1**. Methacryloyl chloride was used in the third step instead of acryloyl chloride (Supplementary Fig. 1). $M_n$ (GPC) = 5.8 × $10^3$ g/mol and $M_w/M_n$=1.16. $^1$H NMR ($CD_2Cl_2$): δ (ppm) = 7.97-7.71, 7.31, 6.97 (protons on azobenzene group), 3.98 (Ar-O-C$H_2$, -O-C$H_2$), 2.42 (Ar-C$H_3$), 2.1-0.9 (protons on the polymer backbone and -C$H_2$-C$H_2$-C$H_2$-C$H_2$-).

**Azopolymer P4: P4** was synthesized using a similar method to that of **P1** (Supplementary Fig. 1). 4-Phenylazophenol was used as the starting material. $M_n$ (GPC)

DOI: 10.1038/NCHEM.2625 SUPPLEMENTARY INFORMATION

= 8.5 × $10^3$ g/mol and $M_w/M_n$=1.40. $^1$H NMR ($CD_2Cl_2$): δ (ppm) = 7.86, 7.47, 6.95 (protons on azobenzene group), 4.2-3.7 (Ar-O-C$H_2$, -O-C$H_2$), 2.5-1.2 (protons on the polymer backbone and -C$H_2$-C$H_2$-C$H_2$-C$H_2$-).

**Azopolymer P5: P5** was synthesized using a similar method to that of **P1** (Supplementary Fig. 1). 4-(4-Nitrophenylazo)phenol was used as the starting material. $M_n$ (GPC) = 4.7 × $10^3$ g/mol and $M_w/M_n$=1.28. $^1$H NMR ($CD_2Cl_2$): δ (ppm) = 8.29, 7.89, 6.94 (protons on azobenzene group), 4.2-3.6 (Ar-O-C$H_2$, -O-C$H_2$), 2.3-1.1 (protons on the polymer backbone and -C$H_2$-C$H_2$-C$H_2$-C$H_2$-).

## Supplementary Figures

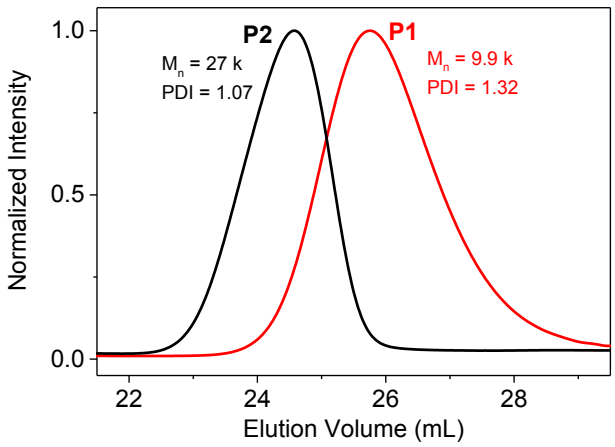


Supplementary Figure 2. GPC traces for **P1** and **P2**.

DOI: 10.1038/NCHEM.2625

SUPPLEMENTARY INFORMATION

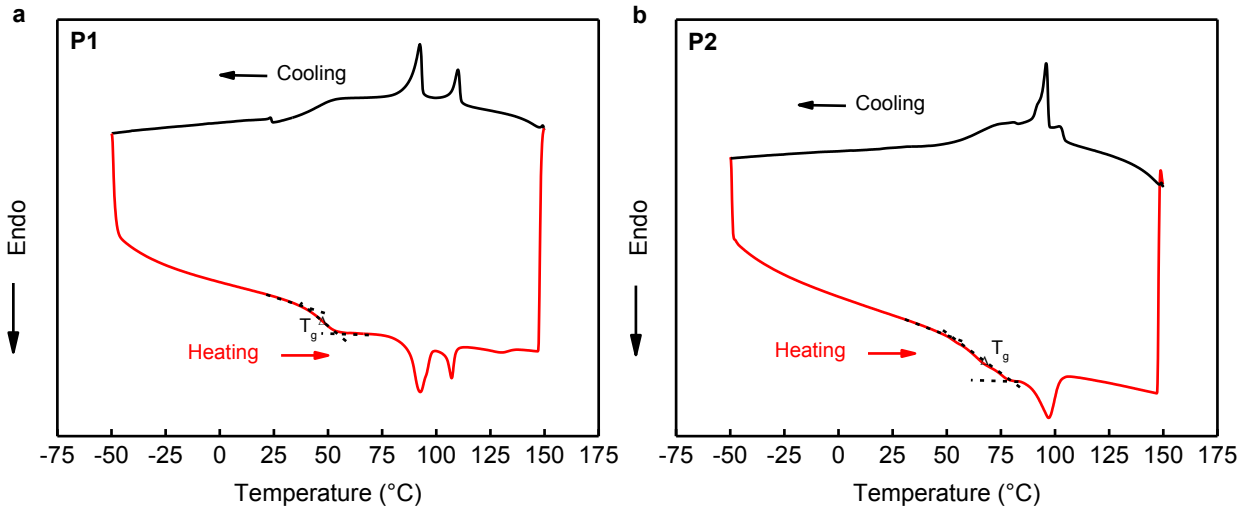


Supplementary Figure 3. Second heating and second cooling DSC curves of **P1** (**a**) and **P2** (**b**).

DOI: 10.1038/NCHEM.2625

SUPPLEMENTARY INFORMATION

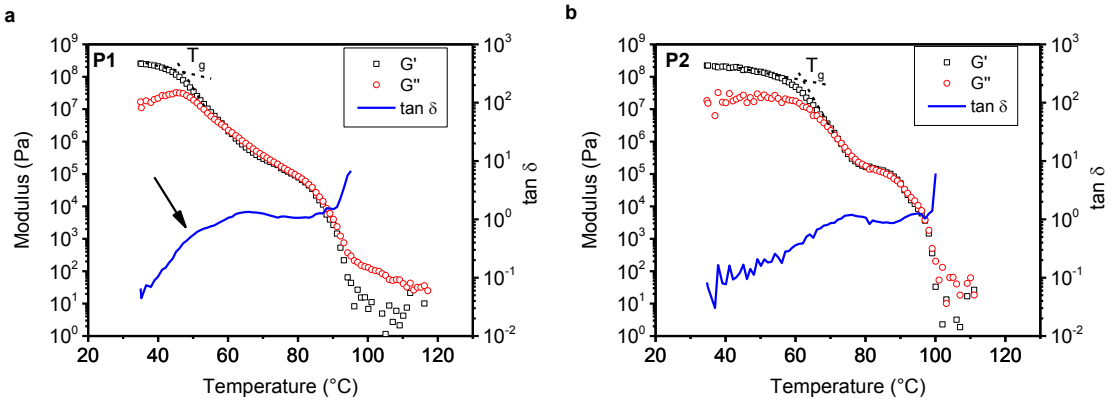


Supplementary Figure 4. Dynamic mechanical analysis of *trans* **P1** (**a**) and *trans* **P2** (**b**). $G'$: storage modulus; $G$": loss modulus; $\tan\delta = \frac{G"}{G'}$: loss tangent. The experiments were conducted under a $N_2$ atmosphere at a heating rate of 3 °C/min and a frequency of 1 rad/s.

$T_g$s of polymers can be determined from the temperature dependence of $G'$ (change in slope), $G$" (maximum) or $\tan\delta$ (maximum)[2-5]. Depending on the specific system, different methods may vary in applicability and show slightly different outcomes.

For **P1**, $G'$ decreased significantly at 47 °C and $G$" showed a maximum at 47 °C. Tan $\delta$ also showed a shoulder around 47 °C (see the arrow in **a**). These results indicated that $T_g$ of **P1** was 47 °C. Tan $\delta$ of **P1** around 47 °C was not a sharp peak but a shoulder because **P1** was a polydomain liquid crystalline polymer. Tan $\delta$ of some other polydomain liquid crystalline polymers near $T_g$ also exhibited a shoulder-like shape but not a sharp peak[6,7]. The reason is that liquid-crystalline features at higher temperatures superimpose with the expected peak in tan $\delta$.

For **P2**, $G'$ curve was used to determine $T_g$ because its signal-to-noise ratio is good. Only a small amount of **P2** was available for this measurement because **P2** was isolated by GPC. The amount of **P2** was close to the lower limit of the instrument so that noise appeared in the measurements. Moreover, the peak in tan $\delta$ was superimposed by liquid crystalline relaxations[6,7].

DOI: 10.1038/NCHEM.2625

SUPPLEMENTARY INFORMATION

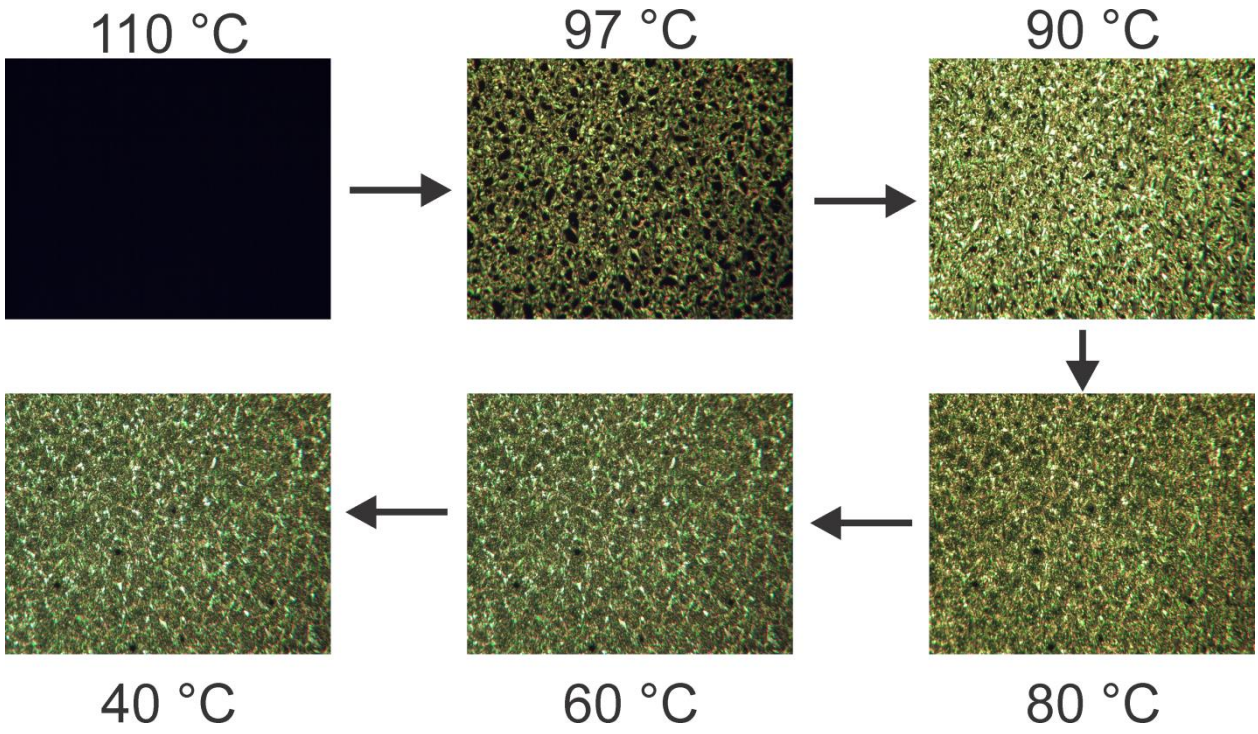


Supplementary Figure 5. Polarized optical microscopy images of **P2** at different temperatures. First, **P2** was annealed at 110 °C for 2 h. Then, it was cooled to the experimental temperature at a cooling rate of 1 °C/min.

DOI: 10.1038/NCHEM.2625

SUPPLEMENTARY INFORMATION

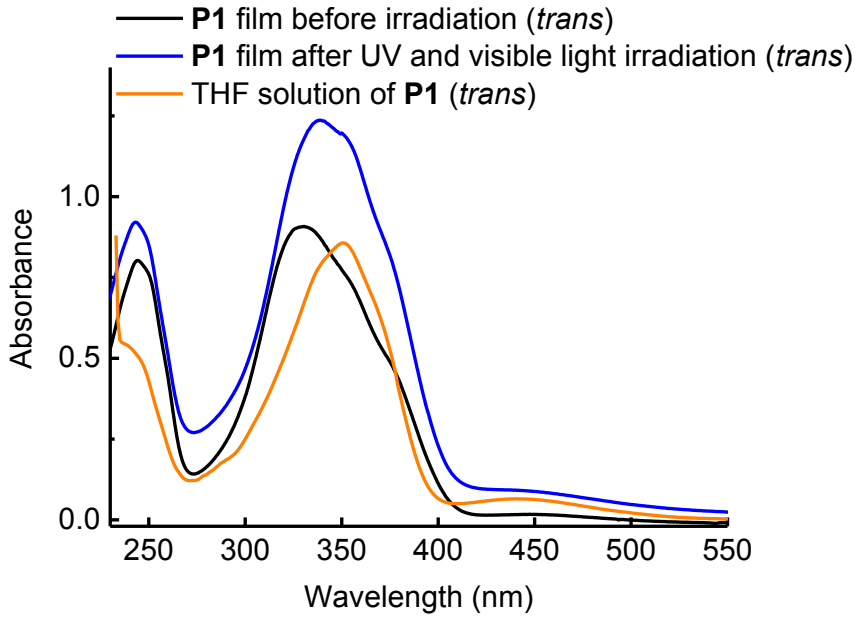


Supplementary Figure 6. UV-vis absorption spectra of **P1** film before irradiation (black) and after UV (365 nm, 67 mW/cm$^2$, 1 min) and visible light irradiation (530 nm, 0.2 mW/cm$^2$, 1 min) (blue). The absorption spectrum of **P1** in THF (orange) was also shown for comparison. The absorption spectra of **P1** film before and after irradiation were different because the orientation and stacking of azobenzene groups in the sample before and after irradiation were different (Supplementary Fig. 12). The orientation of the azobenzene groups can be roughly estimated by the ratio of absorbance of the π-π* transition of *trans* azobenzene (~340 nm) to the π-π* transition of phenyl (~243 nm, often expressed as φ-φ*)[8]. The ratios of **P1** film before and after irradiation and the THF solution of **P1** were 1.13, 1.35, and 1.56, respectively. The result indicated that the azobenzene groups before irradiation preferentially oriented perpendicular to the substrate.[8] After UV and visible light irradiation, the degree of perpendicular orientation of azobenzene groups reduced. The perpendicular orientation of azobenzene groups is common in azobenzene-containing films[8]. Additionally, the absorption maxima of **P1** film before and after irradiation, and the THF solution of **P1** are 328, 337 and 350 nm, respectively. The absorption band of **P1** film was blue-shifted, indicating azobenzene groups form H-aggregates in the film[9,10]. The shape of the spectra and the absorption maxima of **P1** film before and after irradiation are different, suggesting the degree or type of aggregation is different[9,10].

DOI: 10.1038/NCHEM.2625

SUPPLEMENTARY INFORMATION

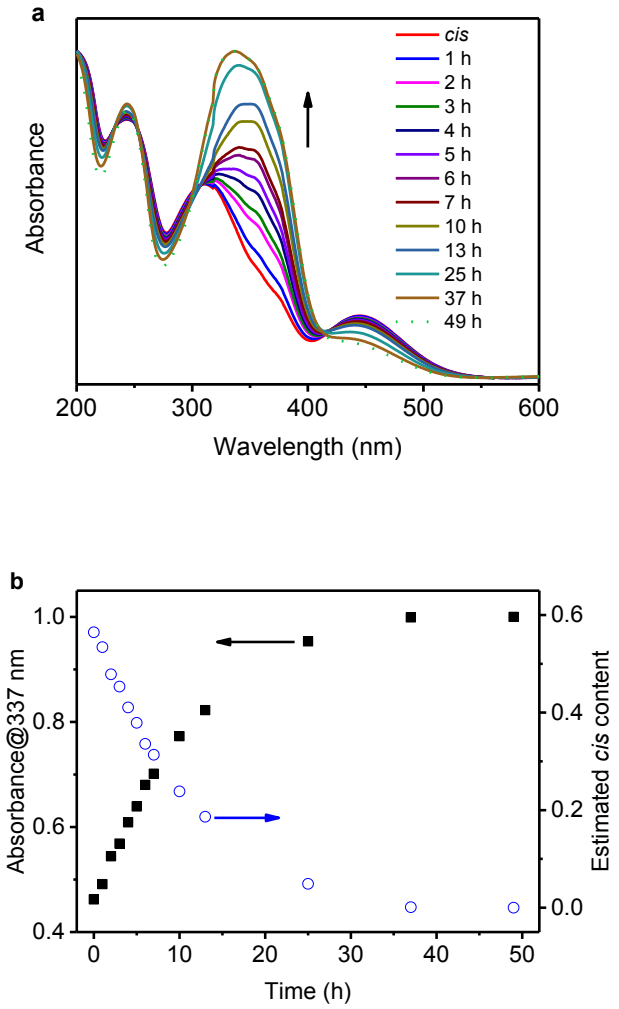


Supplementary Figure 7. **a,** UV-vis absorption spectra of thermal *cis*-to-*trans* isomerization of **P1** film at room temperature in the dark. The sample position changed a little for the measurements on the second day. **b,** Absorbance at 337 nm and the estimated *cis* content as a function of time. The *cis* content was estimated by a method in literature[11,12]:

$$Cis \text{ content} = (1\text{-}A/A_{trans})/(1\text{-}\varepsilon_{cis}/\varepsilon_{trans})$$

where A is the absorbance of **P1**, $A_{trans}$ is the absorbance of *trans* **P1**, and $\varepsilon_{cis}$ and $\varepsilon_{trans}$ are the molar absorption coefficients of *cis* and *trans* isomers, respectively, at 337 nm. $\varepsilon_{cis}/\varepsilon_{trans}$ for azobenzene is close to 0.05[11,12]. Note: the estimated *cis* content is an average number. The top layer of the film may have higher *cis* content and the bottom layer of the

DOI: 10.1038/NCHEM.2625 SUPPLEMENTARY INFORMATION

film may have lower *cis* content because UV light is strongly absorbed by the top layer (Supplementary Fig. 15).

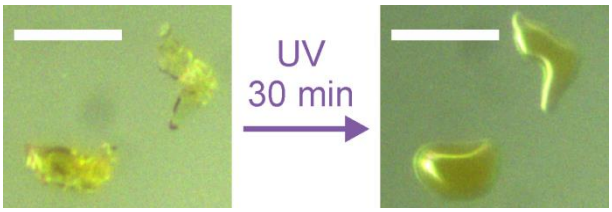


Supplementary Figure 8. Optical microscopy images of **P2** powders before and after UV (365 nm, 67 mW/cm$^2$) irradiation. Similar to **P1**, **P2** also showed photoinduced solid-to-liquid transition. The scale bars represent 20 μm.

DOI: 10.1038/NCHEM.2625

SUPPLEMENTARY INFORMATION

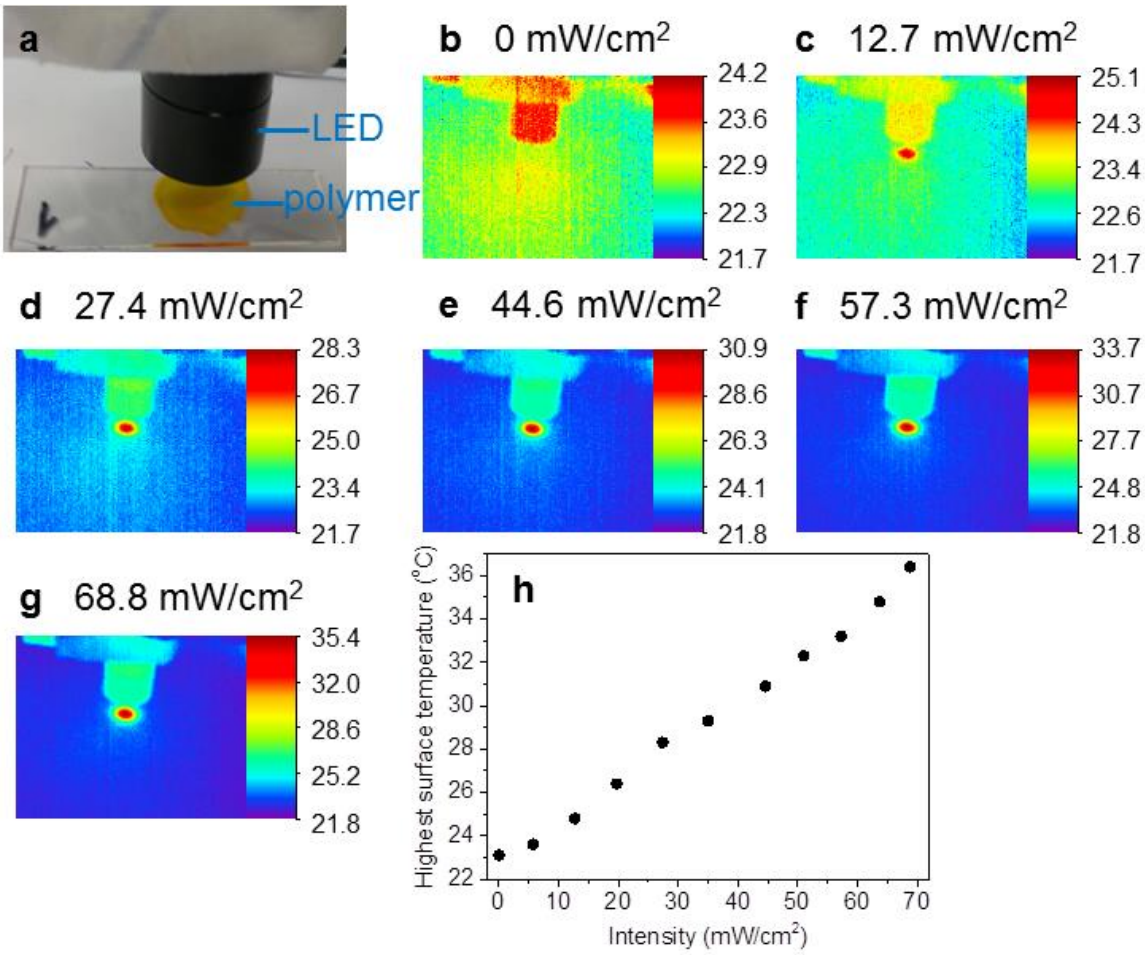


Supplementary Figure 9. **a,** Photograph of **P1** and the 365 nm LED light. **b-g,** Infrared thermometer images of **P1** under irradiation with 365 nm light at different intensities. **h,** The highest surface temperature of **P1** under different UV intensities.

DOI: 10.1038/NCHEM.2625

SUPPLEMENTARY INFORMATION

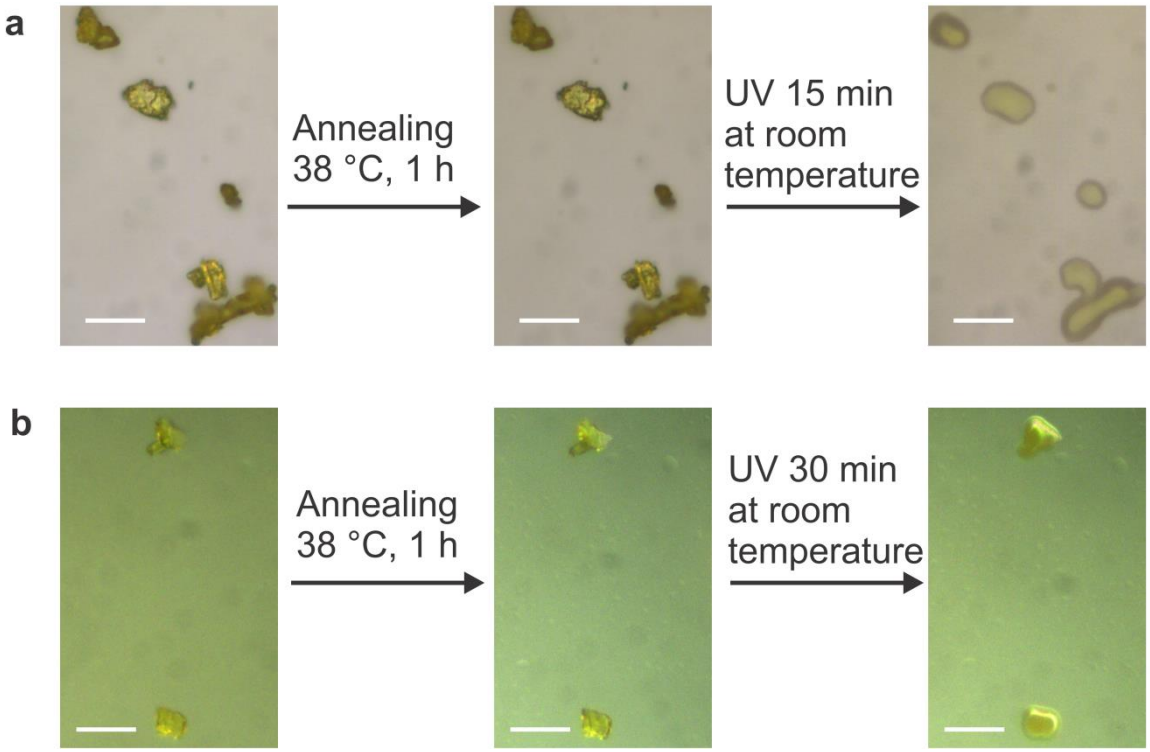


Supplementary Figure 10. Optical microscopy images of **P1** (**a**) and **P2** (**b**) at room temperature (left), after annealing at 38 °C for 1 h (middle) and after 365 nm light (67 mW/cm$^2$) irradiation at room temperature (right). The scale bars represent 20 μm. Annealing at 38 °C did not liquefy **P1** or **P2**. UV irradiation at room temperature liquefied **P1** and **P2**.

DOI: 10.1038/NCHEM.2625

SUPPLEMENTARY INFORMATION

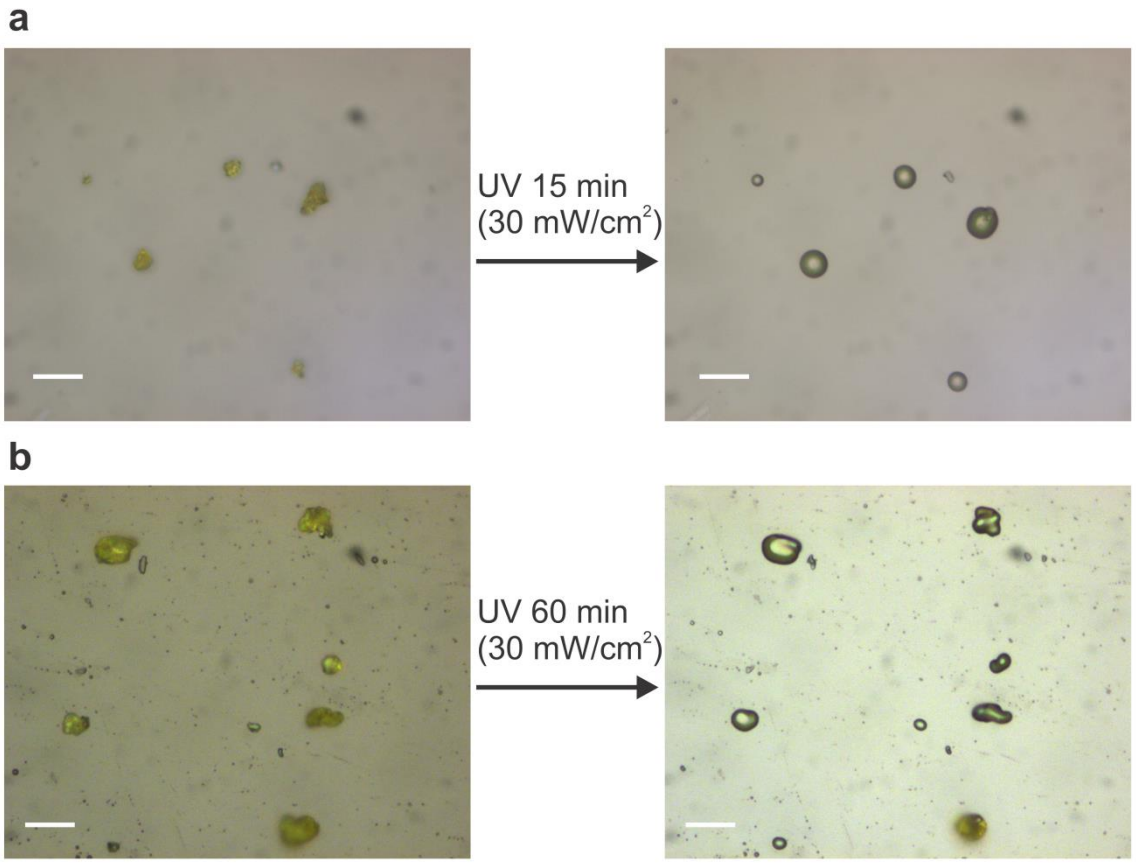


Supplementary Figure 11. Optical microscopy images of **P1** (**a**) and **P2** (**b**) before and after UV (365 nm, 30 mW/cm$^2$) irradiation. The scale bars represent 20 μm. The highest surface temperature of **P1** under 365 nm light with 30 mW/cm$^2$ was 28.5 °C (Supplementary Fig. 9).

DOI: 10.1038/NCHEM.2625

SUPPLEMENTARY INFORMATION

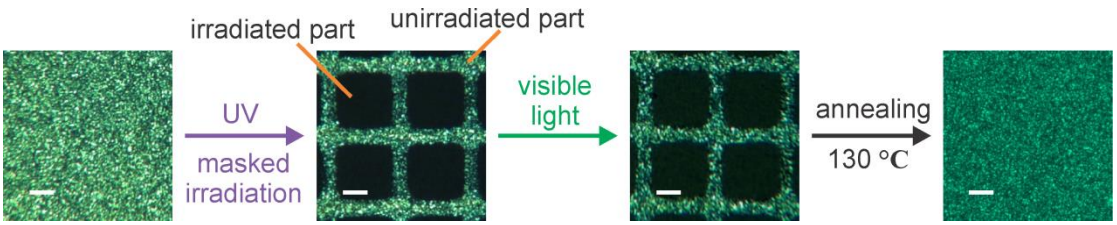


Supplementary Figure 12. Polarized optical microscopy (POM) images of **P1** film before irradiation, after patterned UV irradiation, subsequent visible light irradiation and annealing. The scale bars represent 20 μm. The UV and visible light are 365 nm at 67 mW/cm$^2$ and 530 nm at 5 mW/cm$^2$, respectively.

The *trans* azobenzene groups in **P1** film exhibited liquid crystalline order. UV irradiation changed **P1** from the anisotropic state to the isotropic *cis* state, which is known as a photochemical phase transition[13]. Subsequent visible light irradiation switched *cis* **P1** back to *trans* **P1**. The regenerated *trans* **P1** was amorphous. The liquid crystalline order was regenerated by annealing **P1** at 130 °C.

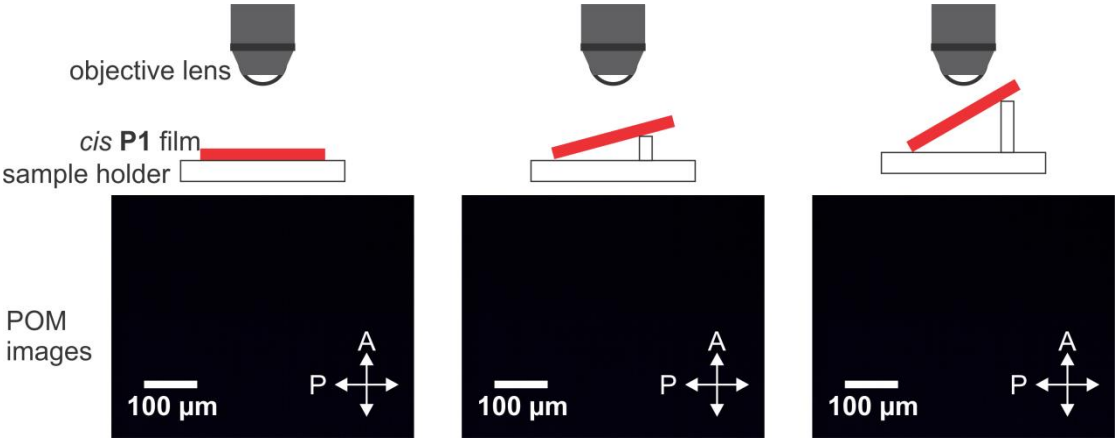


Supplementary Figure 13. Polarized optical microscopy (POM) images of *cis* **P1** film at different tilting angles. From left to right, the tilting angles are 0, 15 and 30°. P: polarizer; A: analyzer.

All POM images at different tilted angles were dark, which showed that *cis* **P1** was isotropic.

DOI: 10.1038/NCHEM.2625

SUPPLEMENTARY INFORMATION

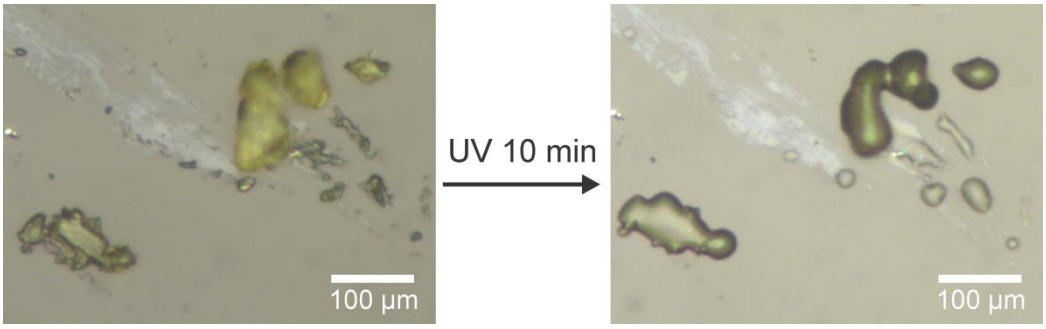


Supplementary Figure 14. Optical microscopy images of amorphous **P1** powders before and after UV (365 nm, 67 mW/cm$^2$) irradiation. To prepare amorphous **P1**, **P1** was heated to the isotropic phase at 140 °C. The sample was then quickly quenched in liquid nitrogen. The quenched **P1** was dark under POM, indicating **P1** was amorphous. The quenched **P1** was collected for this experiment. The result indicates that the photoinduced solid-to-liquid transition is not due to the liquid crystalline phase.

This experiment also further confirms the mechanism of the photoinduced solid-to-liquid transition of the azopolymer is different from that of azobenzene-containing small molecules. Azobenzene-containing small molecules usually form crystals. Hoshino and co-workers studied the photoliquefaction of an azobenzene-containing small molecule by X-ray crystal structure analysis[14]. They found the photoliquefaction of the azobenzene-containing small molecule was a crystal-melt transition.

The result in Supplementary Fig. 14 showed that the photoinduced solid-to-liquid transition of **P1** was not a crystal-melt transition. **P1** can change from an amorphous solid state to the isotropic liquid state. No change in (liquid) crystal structures was involved in the photoinduced solid-to-liquid transition of **P1**. This experiment further confirmed that the photoinduced solid-to-liquid transition of **P1** is due to the decrease of $T_g$. The photoinduced solid-to-liquid transition of **P1** is due to a collective motion of polymer chains or chain segments. The mobility of the azopolymer chains increased after UV irradiation.

DOI: 10.1038/NCHEM.2625

SUPPLEMENTARY INFORMATION

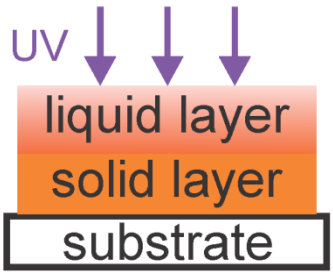


Supplementary Figure 15. Schematic illustration of the photoinduced solid-to-liquid transition in an azopolymer powder or thick film. The absorption coefficient of *trans* **P1** at 365 nm was as large as $3.3 \times 10^4$ $cm^{-1}$. The top 600 nm layer of **P1** can absorb 99% of the incident 365 nm UV light. Therefore, a photoinduced solid-to-liquid transition could only occur on the top layer of **P1**. The incident 365 nm light may penetrate deeper and liquefy the polymer underneath the top layer after the polymer on top flows away or changes into the *cis* state, which has a smaller absorption coefficient at 365 nm.

DOI: 10.1038/NCHEM.2625

SUPPLEMENTARY INFORMATION

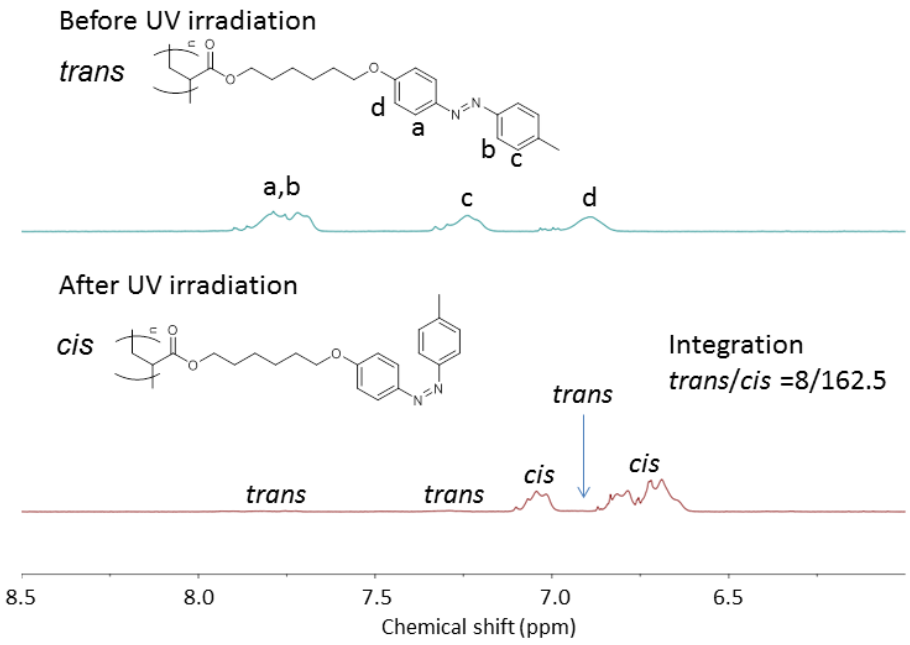


Supplementary Figure 16. $^{1}$H NMR spectra of **P1** in $CD_2Cl_2$ before (top) and after (bottom) 365 nm light irradiation (10 min, 4.5 mW/cm$^2$). The integration from the spectrum (bottom) showed that approximately 95% of the *trans* isomers was converted to *cis* isomers.

DOI: 10.1038/NCHEM.2625

SUPPLEMENTARY INFORMATION

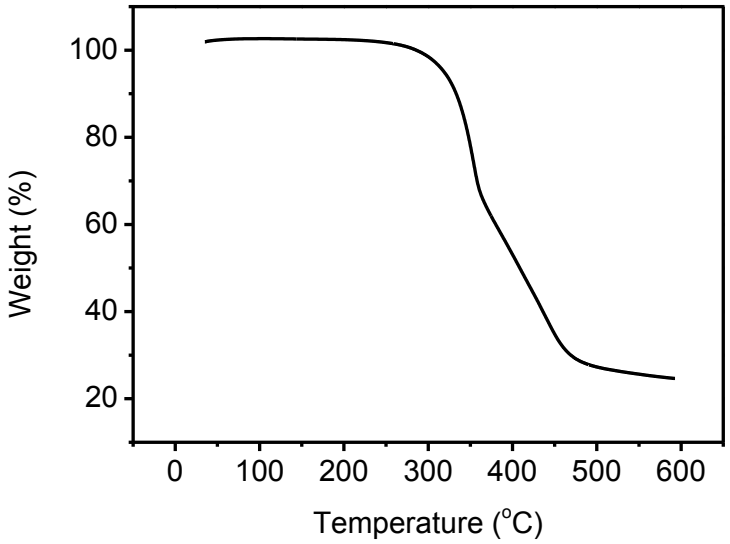


Supplementary Figure 17. TGA of *cis* **P1**. The *cis* **P1** was prepared using the process shown in Fig. 2 in the main manuscript. The sample weight did not decrease at 40 °C (boiling temperature of $CH_2Cl_2$), indicating that $CH_2Cl_2$ was removed completely.

DOI: 10.1038/NCHEM.2625

SUPPLEMENTARY INFORMATION

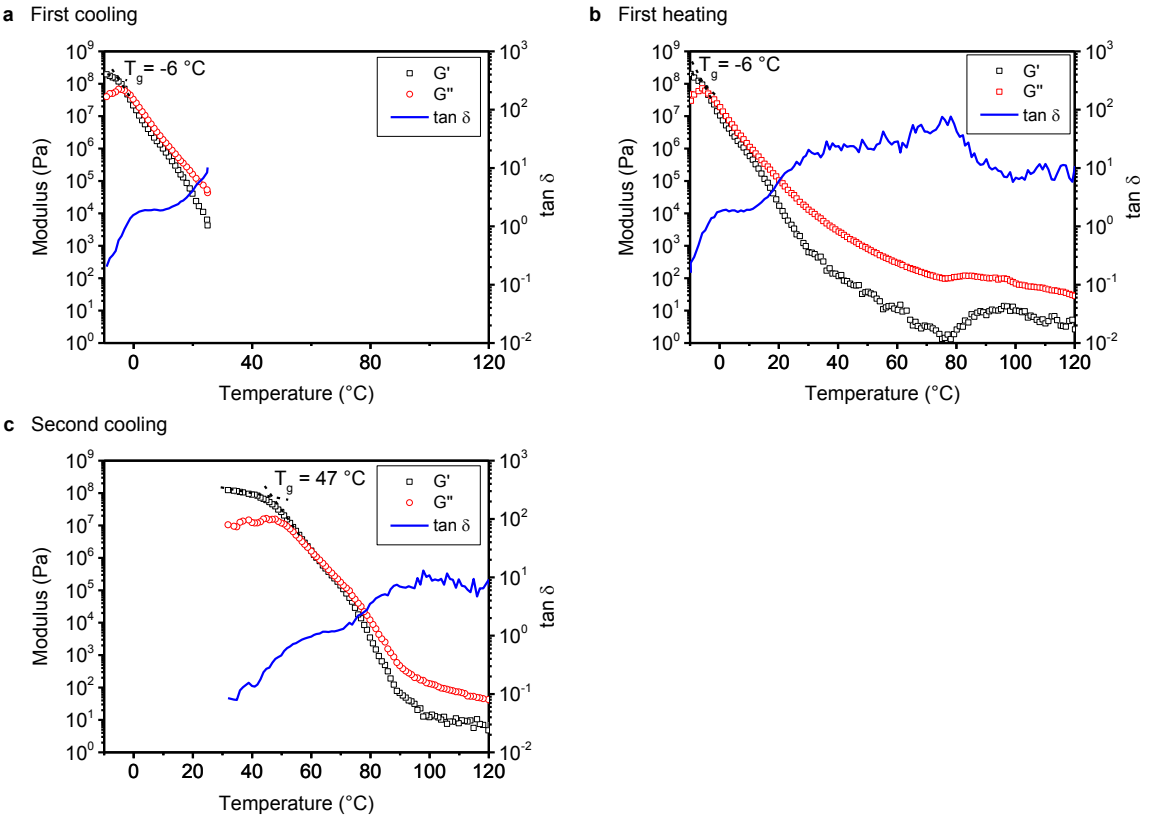


Supplementary Figure 18. Dynamic mechanical analysis of *cis* **P1**. $G'$: storage modulus; $G"$: loss modulus; $\tan\delta = \frac{G"}{G'}$: loss tangent. (**a**) *Cis* **P1** was cooled from room temperature to -10 °C. $T_g$ was -6 °C. (**b**) *Cis* **P1** was heated from -10 °C to 120 °C. $T_g$ was -6 °C. During this heating process, *cis* **P1** switched to *trans* **P1** thermally. (**c**) The sample was then cooled to room temperature. $T_g$ was 47 °C, which is in accordance with $T_g$ of *trans* **P1** measured by DSC and DMA (Supplementary Figs 3 and 4). This experiment was conducted under nitrogen atmosphere at a heating or cooling rate of 3 °C/min and a frequency of 10 rad/s. The *cis* content of azobenzene groups in *cis* **P1** was higher than 90% (Supplementary Figs 16 and 19). This experiment confirmed that *cis* **P1** was a liquid at room temperature because $G"$ was significantly larger than $G'$ at room temperature.

DOI: 10.1038/NCHEM.2625

SUPPLEMENTARY INFORMATION

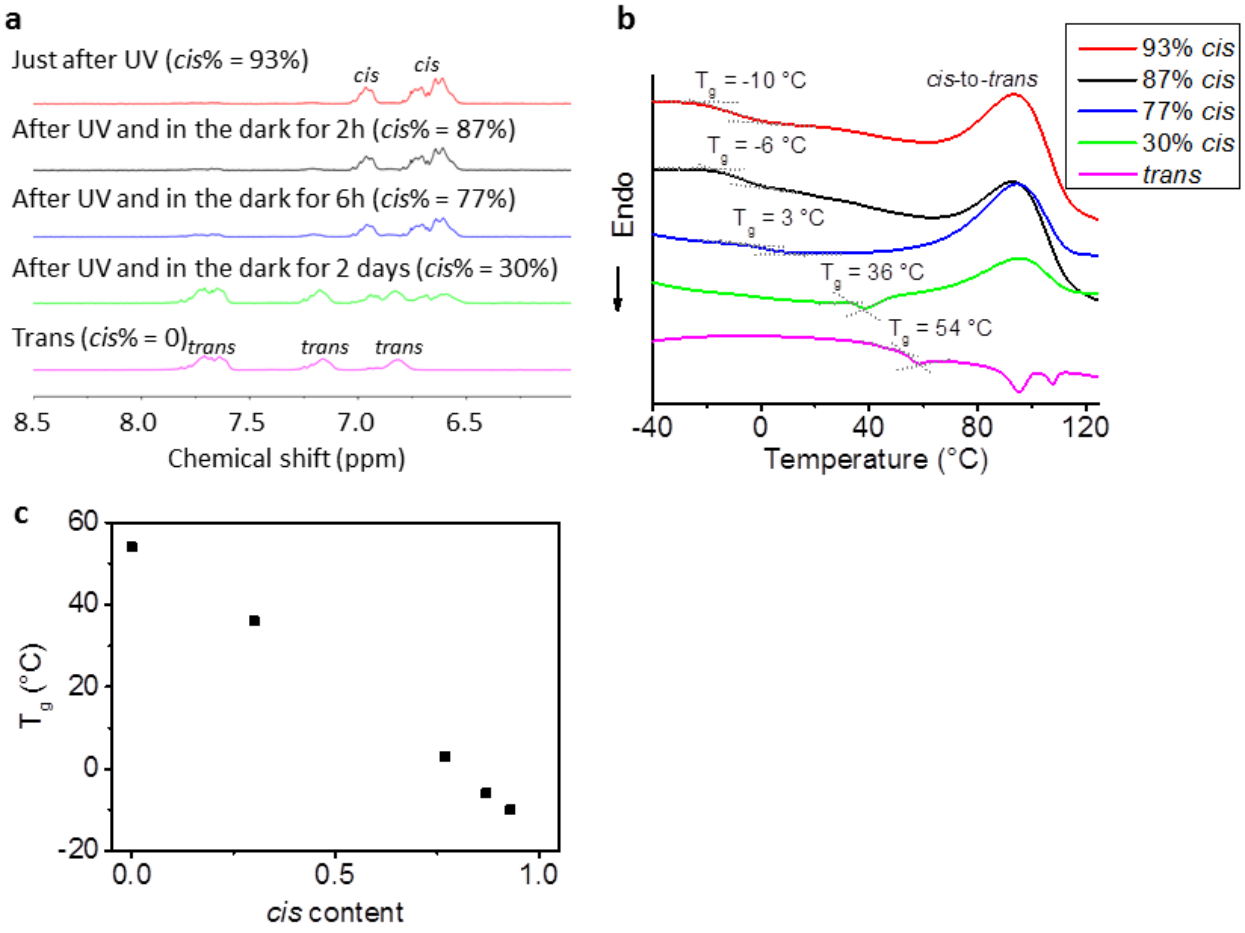


Supplementary Figure 19. **a,** $^1$H NMR spectra of **P1** with different *cis* contents. *Cis* **P1** (~30 mg) was prepared by irradiating (365 nm, 4.5 mW/cm$^2$, 10 min) a $CH_2Cl_2$ solution of **P1** and removing the solvent under vacuum (the approach in Fig. 2 of the main manuscript). After *cis* **P1** was kept in the dark for a certain time (0, 2 h, 6 h, and 2 days), *cis* **P1** (3-5 mg) was collected and dissolved in $CD_2Cl_2$. $^1$H NMR spectra were measured to determine the *cis* contents in these samples. *Trans* **P1** (*cis*% = 0) was also studied for comparison. **b,** DSC first heating curves of **P1** with different *cis* contents. The *cis* contents were measured by the approach in (**a**). **c,** $T_g$s of **P1** with different *cis* contents.

DOI: 10.1038/NCHEM.2625

SUPPLEMENTARY INFORMATION

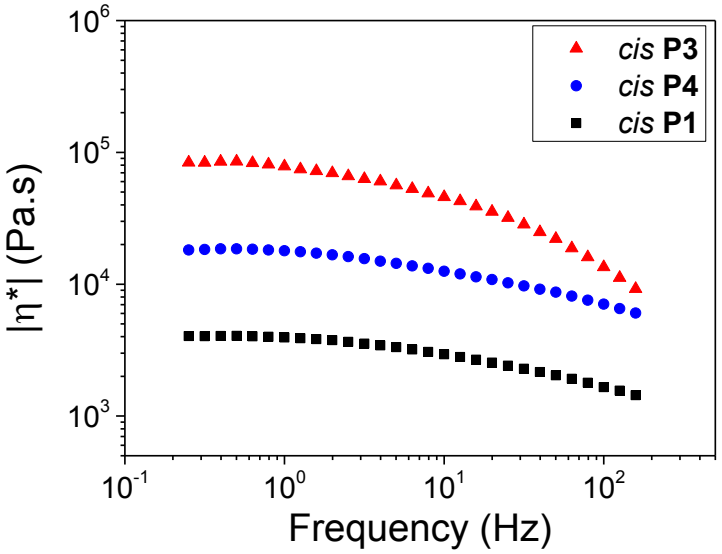


Supplementary Figure 20. The dynamic viscosity $|\eta^*|$ ($\eta^* = \frac{G^*}{2\pi f}$, where f is the frequency and $G^*$ is the complex shear modulus, $G^* = G' + iG''$) of *cis* **P1**, *cis* **P3** and *cis* **P4** measured with a piezo-rheometer. At low frequencies, the dynamic viscosities of these *cis* azopolymers were almost constants and the azopolymers behaved like a Newtonian liquid. At high frequencies, the dynamic viscosities of these azopolymers decreased as the frequency increased. Together with the behaviour of $G'$ and $G''$ (Fig. 3 and Supplementary Fig. 21), these *cis* azopolymers exhibited typical behaviour of a polymer melt. The *cis* contents in **P1**, **P3** and **P4** were more than 90% (Supplementary Figs 16 and 22).

DOI: 10.1038/NCHEM.2625

SUPPLEMENTARY INFORMATION

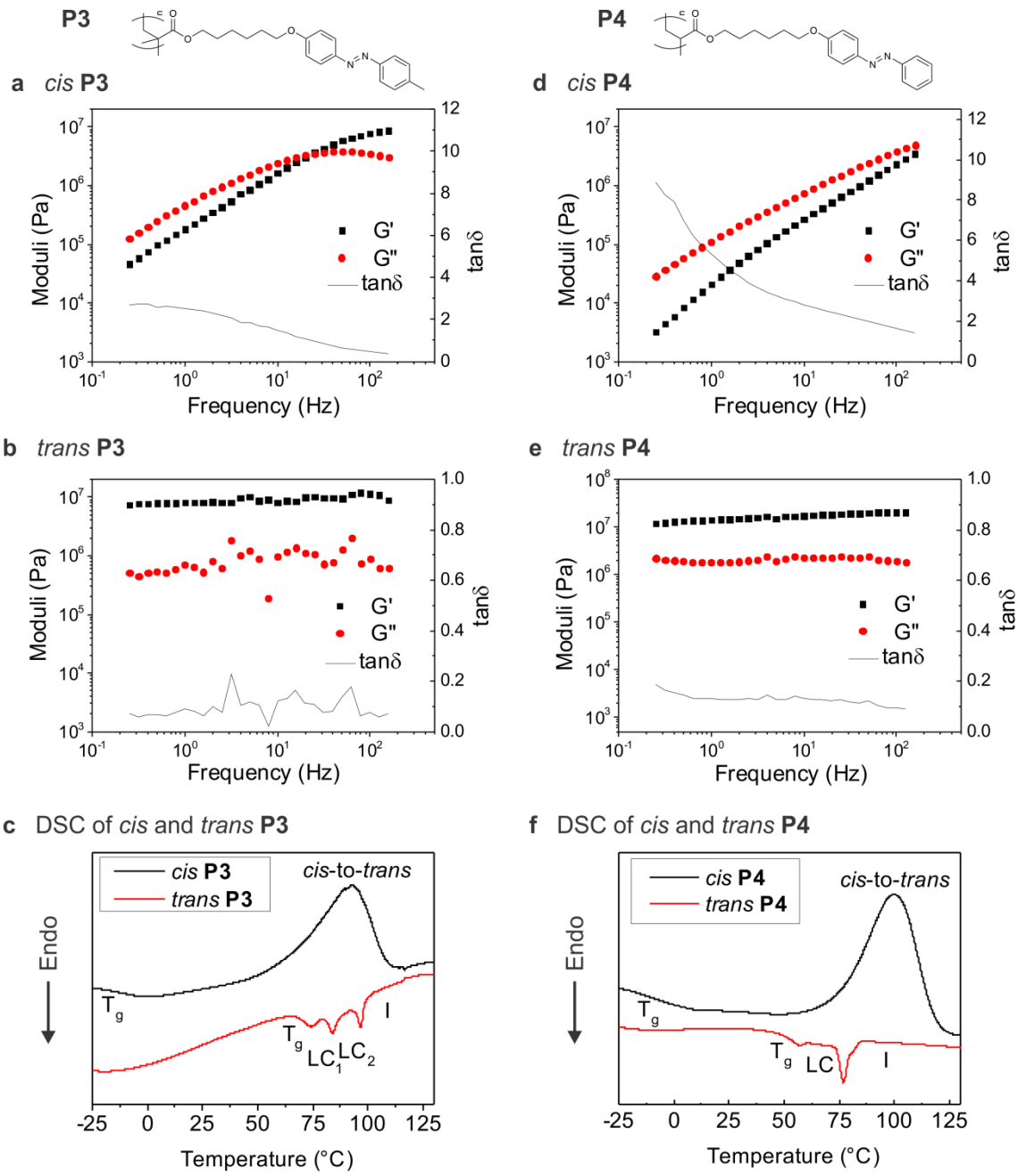


Supplementary Figure 21. Storage modulus ($G'$), loss modulus ($G''$) and loss tangent (tan $\delta$) of *cis* **P3** (**a**), *trans* **P3** (**b**), *cis* **P4** (**d**), and *trans* **P4** (**e**). DSC first heating curves of *trans* and *cis* **P3** (**c**) and *trans* and *cis* **P4** (**f**). **P3** and **P4** were measured using the same methods for **P1** (Figs 2 and 3). Note: $G'$ and $G''$ in (**b**) and (**e**) were reduced values because part of the samples lost contact with the sample holder during photoinduced liquid-to-solid transitions. The use of the relative values did not influence tan $\delta$. The low

DOI: 10.1038/NCHEM.2625

SUPPLEMENTARY INFORMATION

values of tan $\delta$ of *trans* **P3** and *trans* **P4** (tan $\delta$ < 1) indicated that visible light converted the liquid *cis* azopolymers to the solid *trans* azopolymers. $LC_1$: liquid crystalline phase 1; $LC_2$: liquid crystalline phase 2; I, isotropic phase.

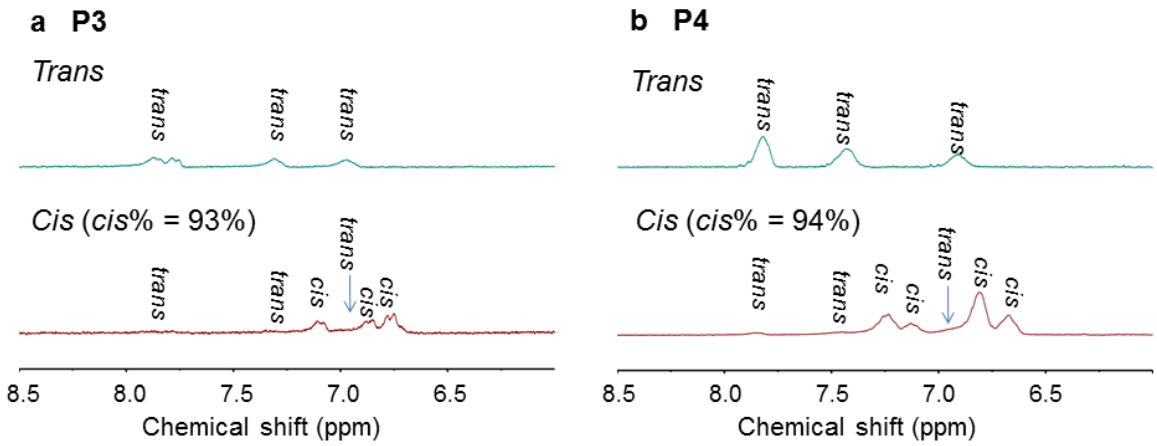


Supplementary Figure 22. **a,** $^1$H NMR spectra of *trans* and *cis* **P3** in $CD_2Cl_2$. The *cis* content calculated from the integration was ~93%. **b,** $^1$H NMR spectra of *trans* and *cis* **P4** in $CD_2Cl_2$. The *cis* content calculated from the integration was ~94%.

DOI: 10.1038/NCHEM.2625

SUPPLEMENTARY INFORMATION

**a** Model compounds for **P1**, **P2** and **P3**

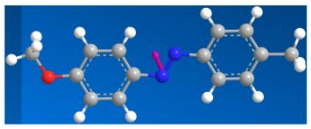

*trans* 1.6 Debye

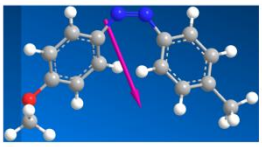

*cis* 4.5 Debye

**b** Model compounds for **P4**

*trans* 2.1 Debye

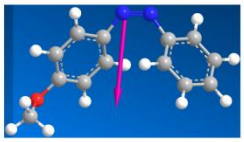

*cis* 4.7 Debye

**c** Model compounds for **P5**

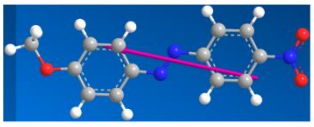

*trans* 8.2 Debye

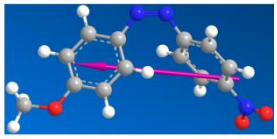

*cis* 7.6 Debye

Supplementary Figure 23. 3D structures and calculated dipole moments of *trans* and *cis* azo chromophores. White: H; grey: C; red: O; blue: N; purple: dipole moment.

The dipole moments of azo chromophores in *trans* and *cis* configurations were calculated by Chem3D 15.0 program. First, MM2 minimization was performed on the azo compounds. Then, energy/geometry minimization was performed on the azo compounds using the Density Functional Theory (DFT) (method = B3LYP and basis set = 6-311G). Finally, the dipole moments were calculated by DFT (B3LYP/6-311G).

Before the model compounds were calculated, DFT calculations were performed on *trans* and *cis* azobenzene without any substituent. Our calculated dipole moments of *trans* and *cis* azobenzene were 0 and 3.3 Debye, respectively, which are in accordance with the reported results (0 and 3.2 Debye for *trans* and *cis* azobenzene)[15].

DOI: 10.1038/NCHEM.2625

SUPPLEMENTARY INFORMATION

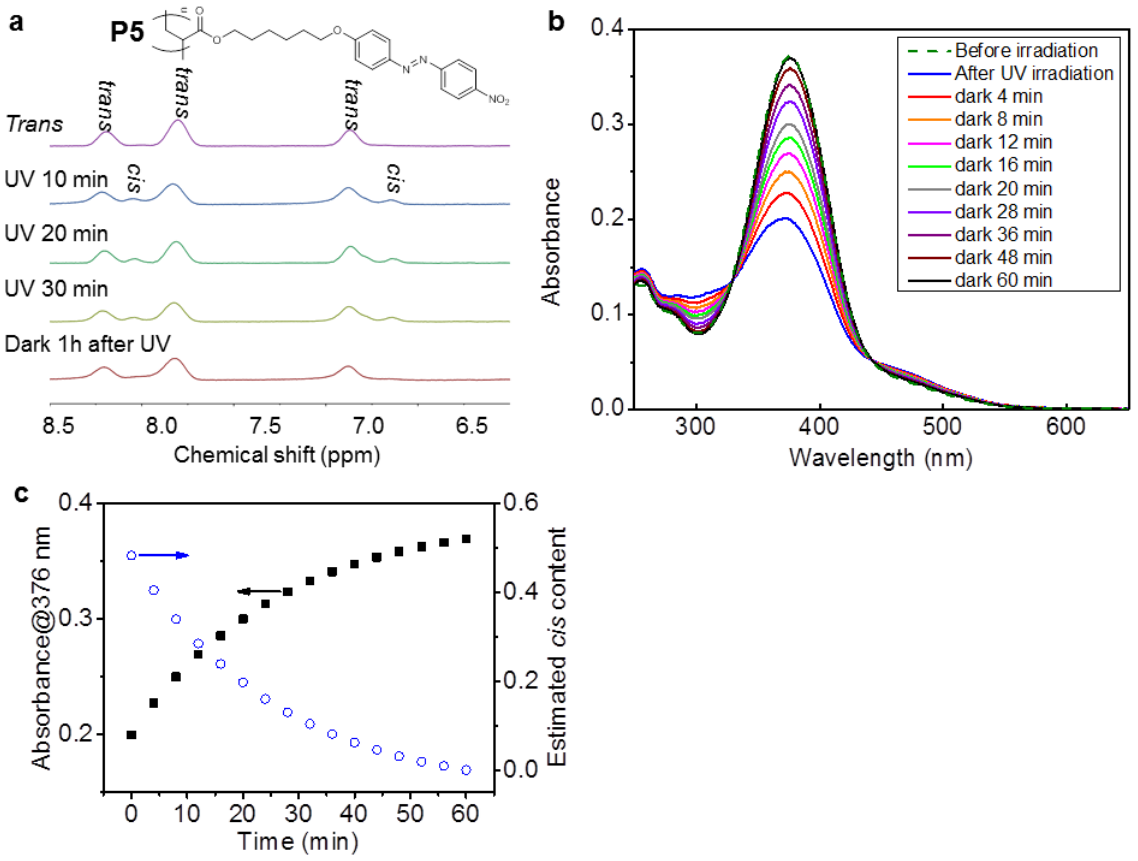


Supplementary Figure 24. **a,** $^1$H NMR spectra of **P5** in $CD_2Cl_2$. From top to down: *trans* **P5** before irradiation, after 365 nm light irradiation (4.5 mW/cm$^2$) for 10 min, 20 min and 30 min, and after the irradiated **P5** was stored in the dark for 1 h. The measurement time for a $^1$H NMR spectrum was about 10 min. Because the lifetime of *cis* **P5** was short, some *cis* isomers switched back to *trans* isomers during the measurement. **b,** UV-vis absorption spectra of **P5** in $CH_2Cl_2$ before irradiation, after 365 nm light irradiation (4.5 mW/cm$^2$) for 10 min, after stored in the dark for different time. The measurement time for an absorption spectrum was about 3 min. Because the lifetime of *cis* **P5** was short, some *cis* isomers switched back to *trans* isomers during the measurement. **c,** Absorbance at 376 nm and the estimated *cis* content as a function of time. The *cis* content estimated from the UV-vis absorption spectra was about 50%. The *cis* content was estimated by the same method shown in Supplementary Fig. 7. After the irradiated **P5** was stored in the dark for 16 min, half of the *cis* isomers switched back to *trans* isomers. The preparation of *cis* azopolymers for DSC and rheology measurements needs ~1 h. Additionally, the

DOI: 10.1038/NCHEM.2625 SUPPLEMENTARY INFORMATION

time to measure the first heating DSC curve is ~25 min. The time for a rheology test is about 1 h. The lifetime of *cis* **P5** is too short for DSC and rheology measurements.

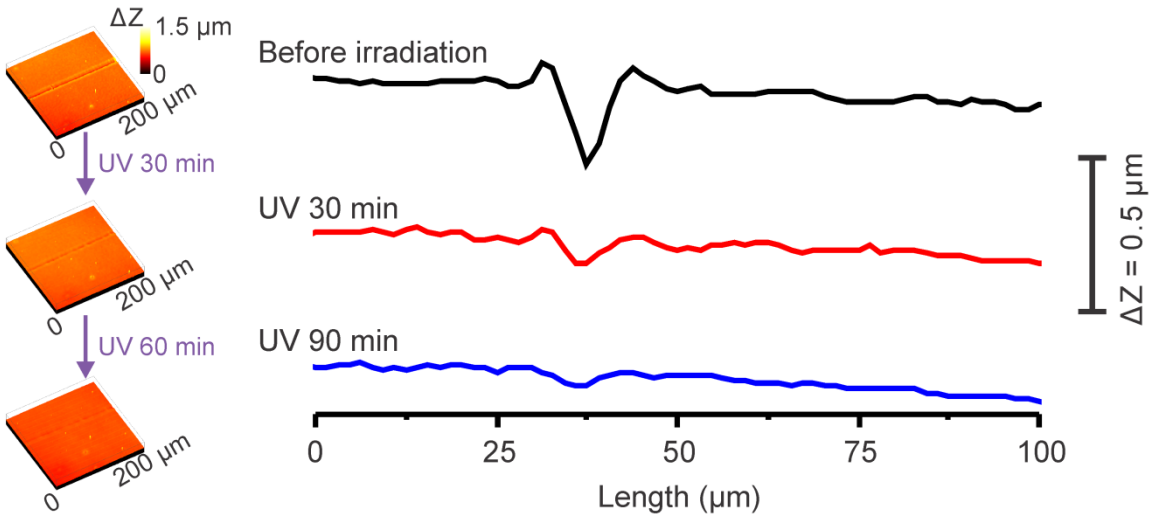


Supplementary Figure 25. Confocal microscope images and typical profiles of the damaged area on **P2** film before and after UV irradiation.

DOI: 10.1038/NCHEM.2625

SUPPLEMENTARY INFORMATION

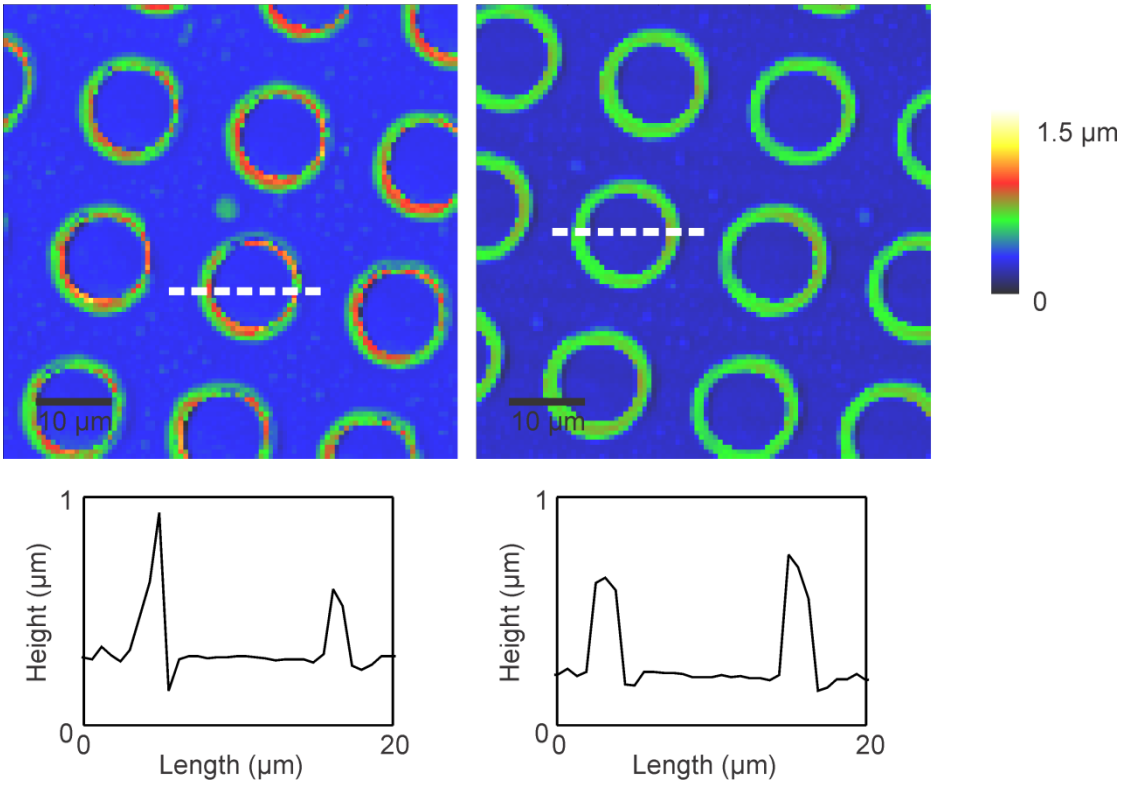


Supplementary Figure 26. Confocal microscope images and profiles of patterned **P1** before (left) and after (right) irradiation with 365 nm UV light (20 mW/cm$^2$, 30 min). The profiles were along the dashed lines on the images. Three-dimensional confocal microscope images of **P1** before and after irradiation were shown in Fig. 6b in the main manuscript.

DOI: 10.1038/NCHEM.2625 SUPPLEMENTARY INFORMATION

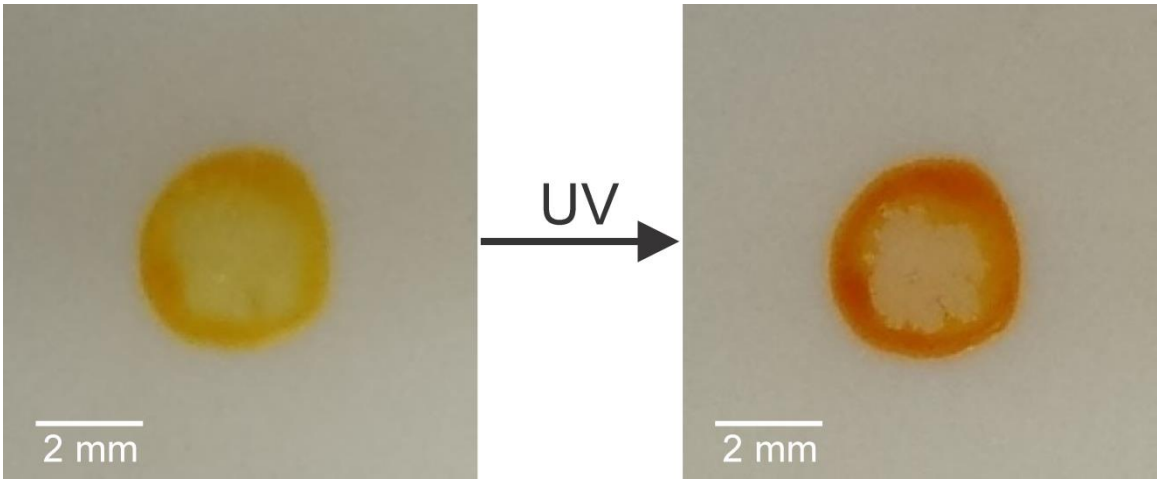


Supplementary Figure 27. Enlarged photographs of an azopolymer spot on a Teflon substrate before and after 365 nm light (67 mW/cm$^2$, 20 min) irradiation. This spot is the irradiated one in Fig. 6c in the main manuscript.

DOI: 10.1038/NCHEM.2625

SUPPLEMENTARY INFORMATION

References

1. Lee, S., Shin, J., Lee, Y. H., Fan, S. & Park, J. K. Directional Photofluidization Lithography for Nanoarchitectures with Controlled Shapes and Sizes. *Nano Lett.* **10,** 296-304 (2010).

2. Illers, K. H. Glasige Erstarrung Und Relaxationsverhalten Von Amorphen Copolymeren Im Festen Zustand. *Berich. Bunsen Gesell.* **70**, 353 (1966).

3. Peleg, M. A Note on the Tan Delta(T) Peak as a Glass-Transition Indicator in Biosolids. *Rheol. Acta* **34**, 215-220 (1995).

4. Rieger, J. The glass transition temperature $T_g$ of polymers - Comparison of the values from differential thermal analysis (DTA, DSC) and dynamic mechanical measurements (torsion pendulum). *Polym. Test* **20,** 199-204 (2001).

5. Turi, E. A. *Thermal characterization of polymeric materials*, 2nd edn. (Academic Press, San Diego, 1997).

6. Polakova, L., Sedlakova, Z., Benes, H., Valentova, H., Krakovsky, I. & Rabie, F. Dynamic mechanical and thermal behavior of novel liquid-crystalline polybutadiene-diols with azobenzene groups in side chains. *J. Rheol.* **57,** 1297-1310 (2013).

7. Weilepp, J.*, et al.* Rheology of liquid crystalline elastomers in their isotropic and smectic A state. *Macromolecules* **32**, 4566-4574 (1999).

8. Nishizawa, K., Nagano, S. & Seki, T. Novel Liquid Crystalline Organic-Inorganic Hybrid for Highly Sensitive Photoinscriptions. *Chem. Mater.* **21,** 2624-2631 (2009).

9. Menzel, H., *et al.* Small-Angle X-Ray-Scattering and Ultraviolet-Visible Spectroscopy Studies on the Structure and Structural-Changes in Langmuir-Blodgett-Films of Polyglutamates with Azobenzene Moieties Tethered by Alkyl Spacers of Different Length. *Langmuir* **10,** 1926-1933 (1994).

10. Tong, X., Cui, L. & Zhao, Y. Confinement effects on photoalignment, photochemical phase transition, and thermochromic behavior of liquid crystalline

DOI: 10.1038/NCHEM.2625 SUPPLEMENTARY INFORMATION

azobenzene-containing diblock copolymers. *Macromolecules* **37,** 3101-3112 (2004).

11. Victor, J. G. & Torkelson, J. M. On Measuring the Distribution of Local Free-Volume in Glassy-Polymers by Photochromic and Fluorescence Techniques. *Macromolecules* **20,** 2241-2250 (1987).

12. Wang, X. Azo Polymer Colloidal Spheres: Formation, Two-Dimensional Array, and Photoresponsive Properties. In *Smart Light-Responsive Materials*, (Eds. Zhao, Y. & Ikeda, T.) Chapter 5, 177-213 (John Wiley & Sons, Inc., New Jersey, 2009).

13. Ikeda, T. & Tsutsumi, O. Optical Switching and Image Storage by Means of Azobenzene Liquid-Crystal Films. *Science* **268**, 1873-1875 (1995).

14. Hoshino, M. *et al.* Crystal melting by light: X-ray crystal structure analysis of an azo crystal showing photoinduced crystal-melt transition. *J. Am. Chem. Soc.* **136**, 9158-9164 (2014).

15. Tong, X., Wang, G., Soldera, A. & Zhao, Y. How can azobenzene block copolymer vesicles be dissociated and reformed by light? *J. Phys. Chem. B* **109,** 20281-20287 (2005).

## 4.4 Photo-Healing Azopolymers Based on Photoinduced Reversible Solid-to-Liquid Transitions

### Supporting Information

**Photo-Healing Azopolymers Based on Photoinduced Reversible Solid-to-Liquid Transitions**

*Philipp Weis, Andreas Hess, Gunnar Kircher, Shilin Huang, Günter K. Auernhammer, Kaloian Koynov, Si Wu**

Philipp Weis, Andreas Hess, Gunnar Kircher, Shilin Huang, Günter K. Auernhammer, Kaloian Koynov, Si Wu
Max Planck Institute for Polymer Research, Ackermannweg 10, 55128 Mainz, Germany
E-mail: wusi@mpip-mainz.mpg.de

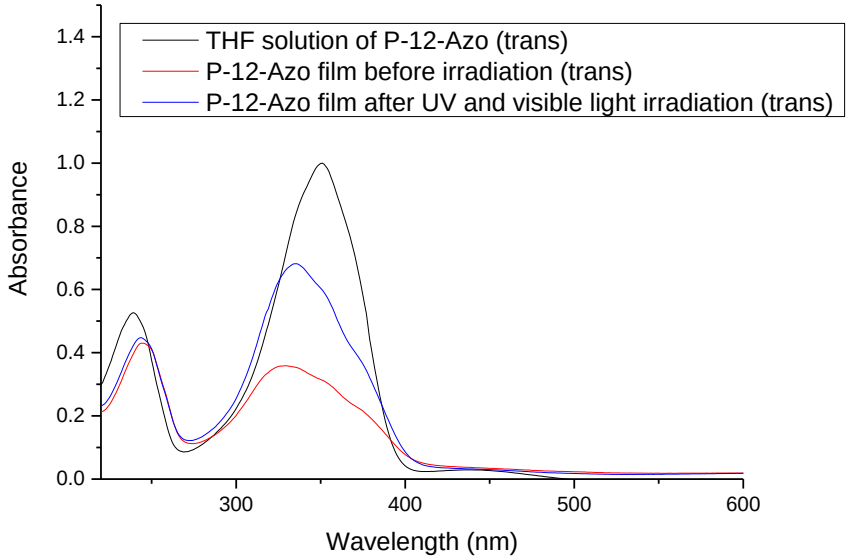


**Figure S1.** UV-vis absorption spectra of P-12-Azo in THF solution in comparison to P-12-Azo film before irradiation (red) and after UV (365 nm, 45 mW $cm^{-2}$, 10 min) and visible light irradiation (530 nm, 88 mW/cm2, 2 min) (blue). The absorption spectra of P-12-Azo film before and after irradiation are different because orientation and stacking of azo groups in the film are different before and after irradiation. Azo groups preferentially orient perpendicular to the substrate before irradiation.[1] The degree of perpendicular oriented azo groups is reduced after UV and visible light irradiation. The absorption maxima and shape of P-12-Azo in THF solution and in film are different. The absorption band of the film is blue-shifted, indicating H-aggregation of azo groups.[2-3]

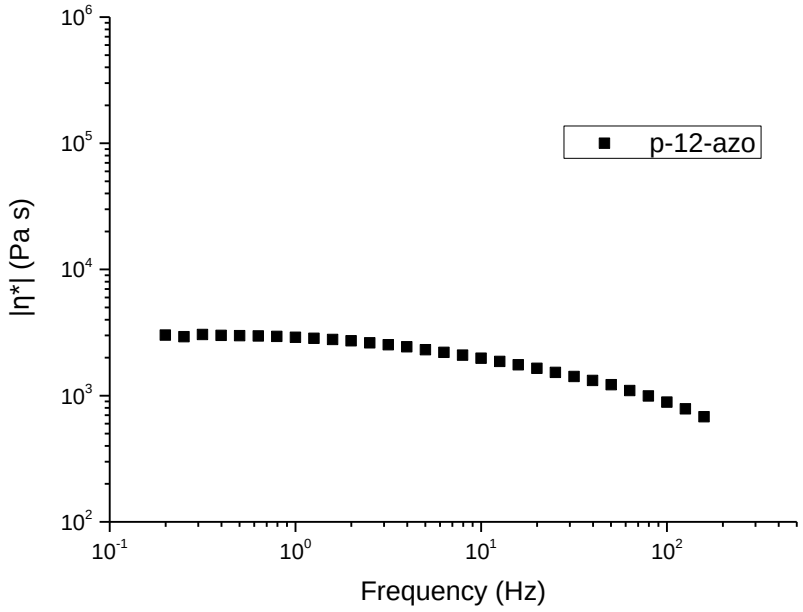


**Figure S2.** Dynamic viscosity of P-12-Azo polymer calculated from piezo rheology data of P-12-Azo.

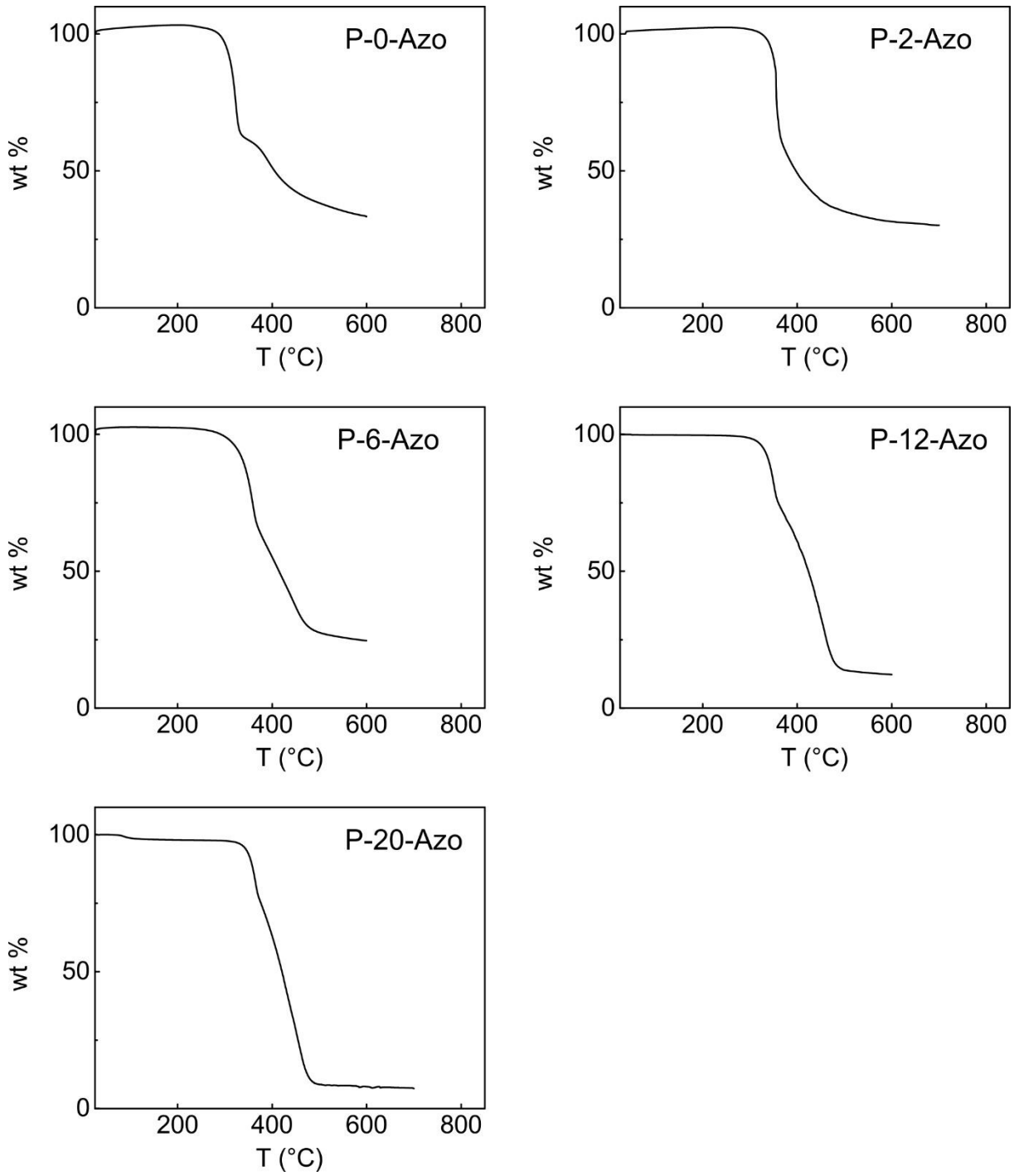


**Figure S3**. TGA of P-n-Azo. All P-n-Azo were thermally stable below 200 °C.

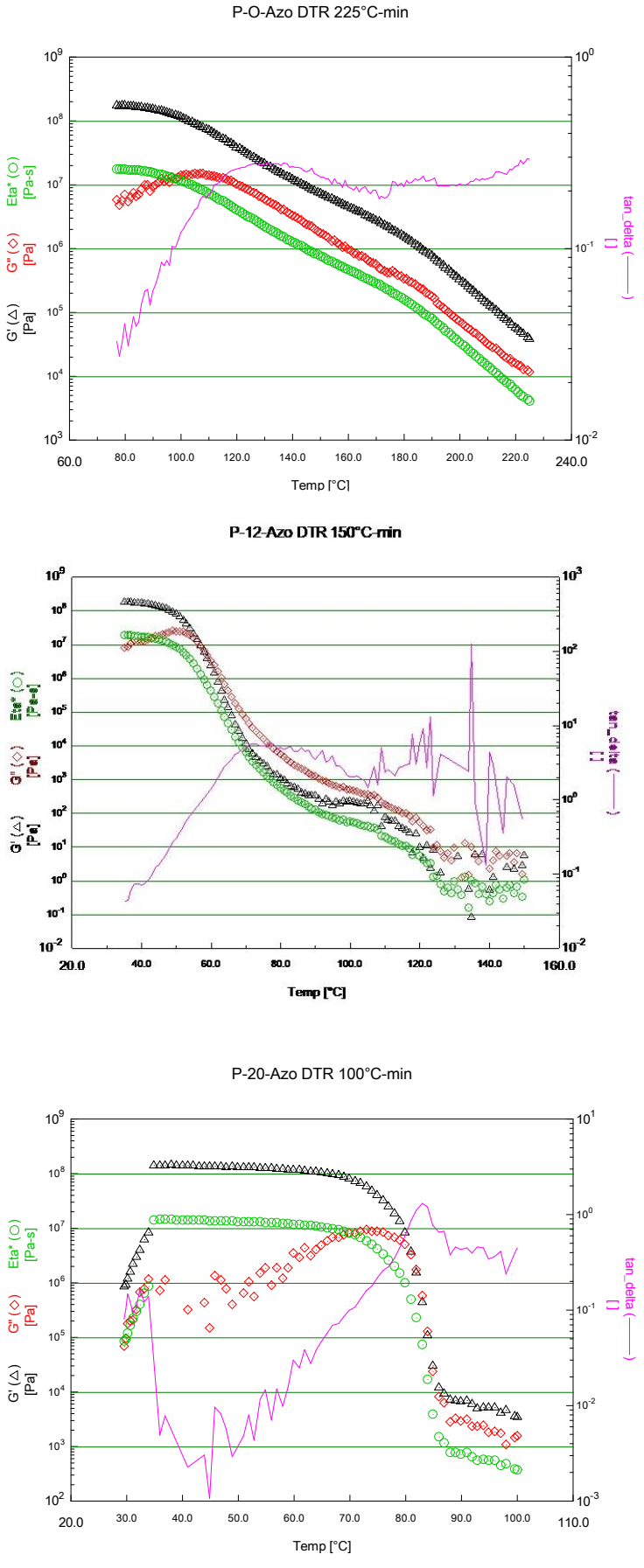


**Figure S4.** DMA cooling curves of P-n-Azo.

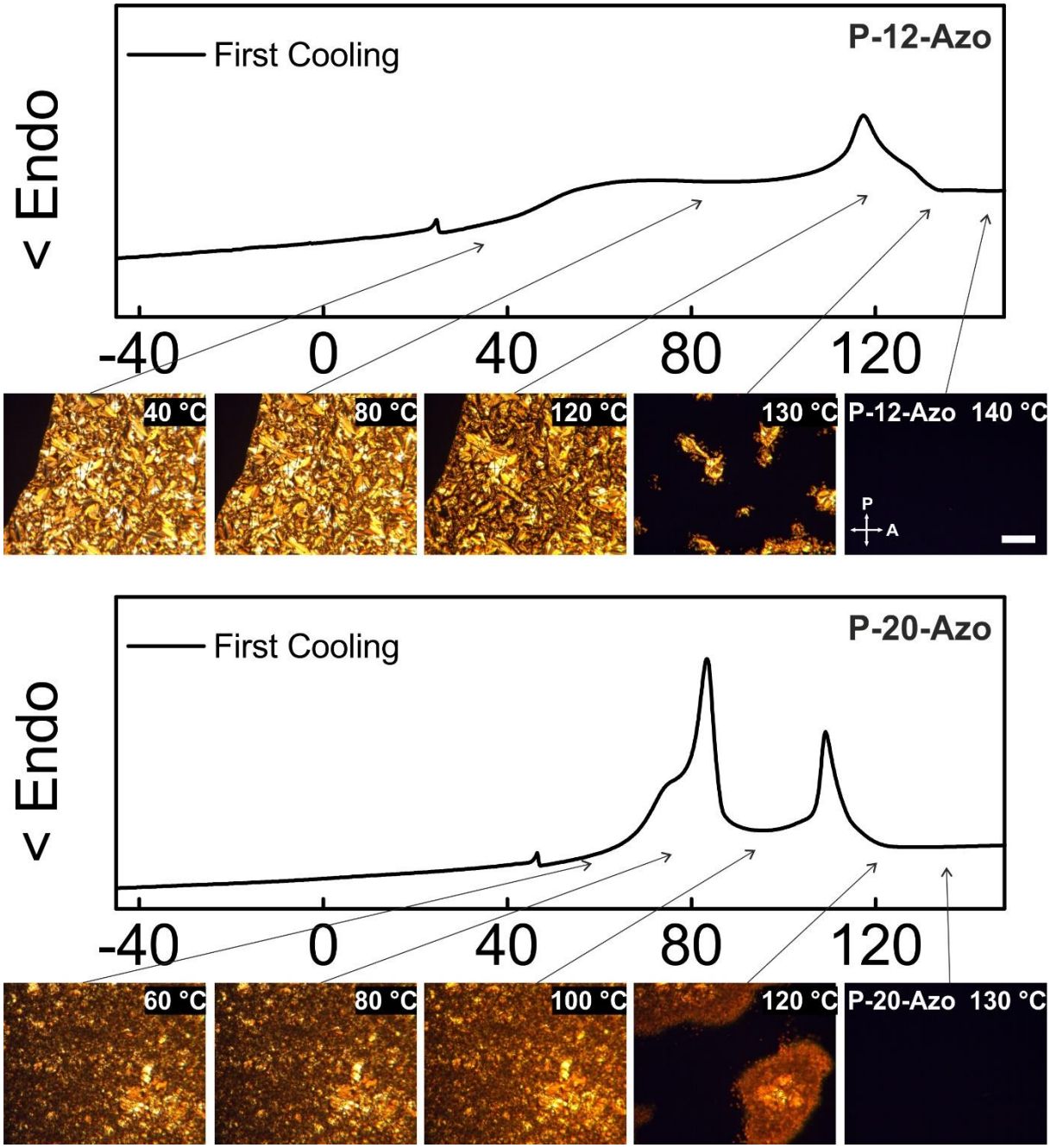


**Figure S5.** DSC curves and polarized optical microscope images of P-n-Azo during cooling from above 140 °C under crossed polarizers. Scale bar is 250 µm.

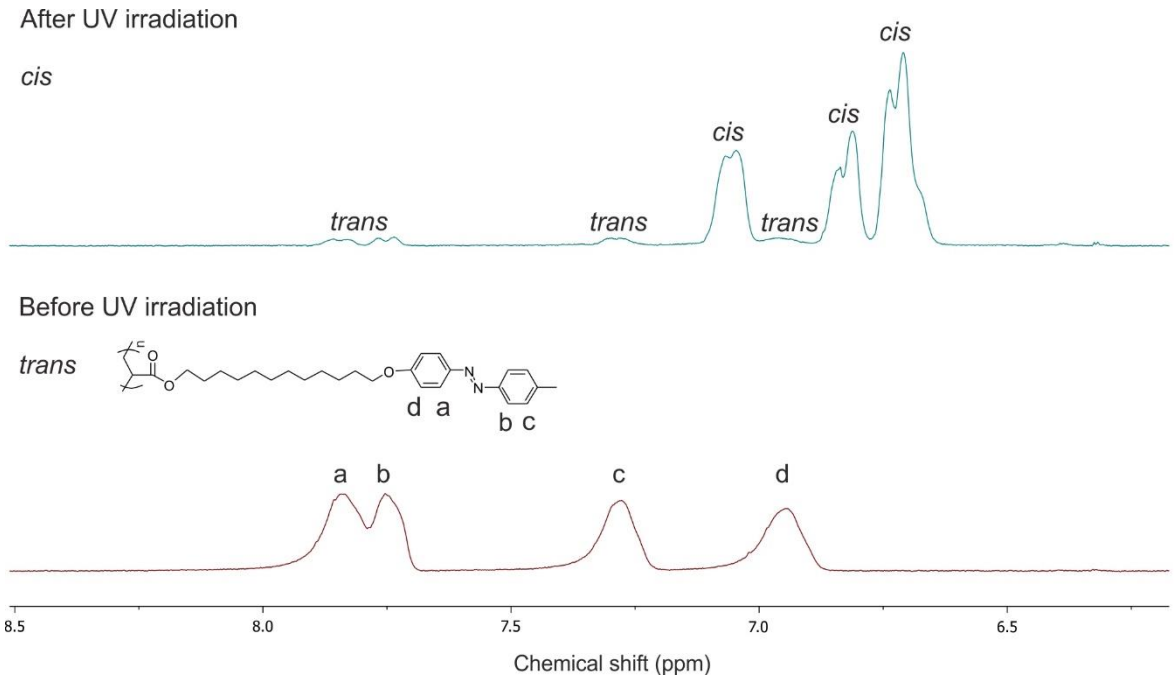


**Figure S6.** $^{1}$H-NMR spectra of of P-12-Azo in $CD_2Cl_2$ before (bottom) and after (top) 365 nm light irradiation (20 min, 29 mW cm$^{-2}$). The integration from the spectrum on top showed that approximately 93% of the *trans* form was converted into the *cis* form.

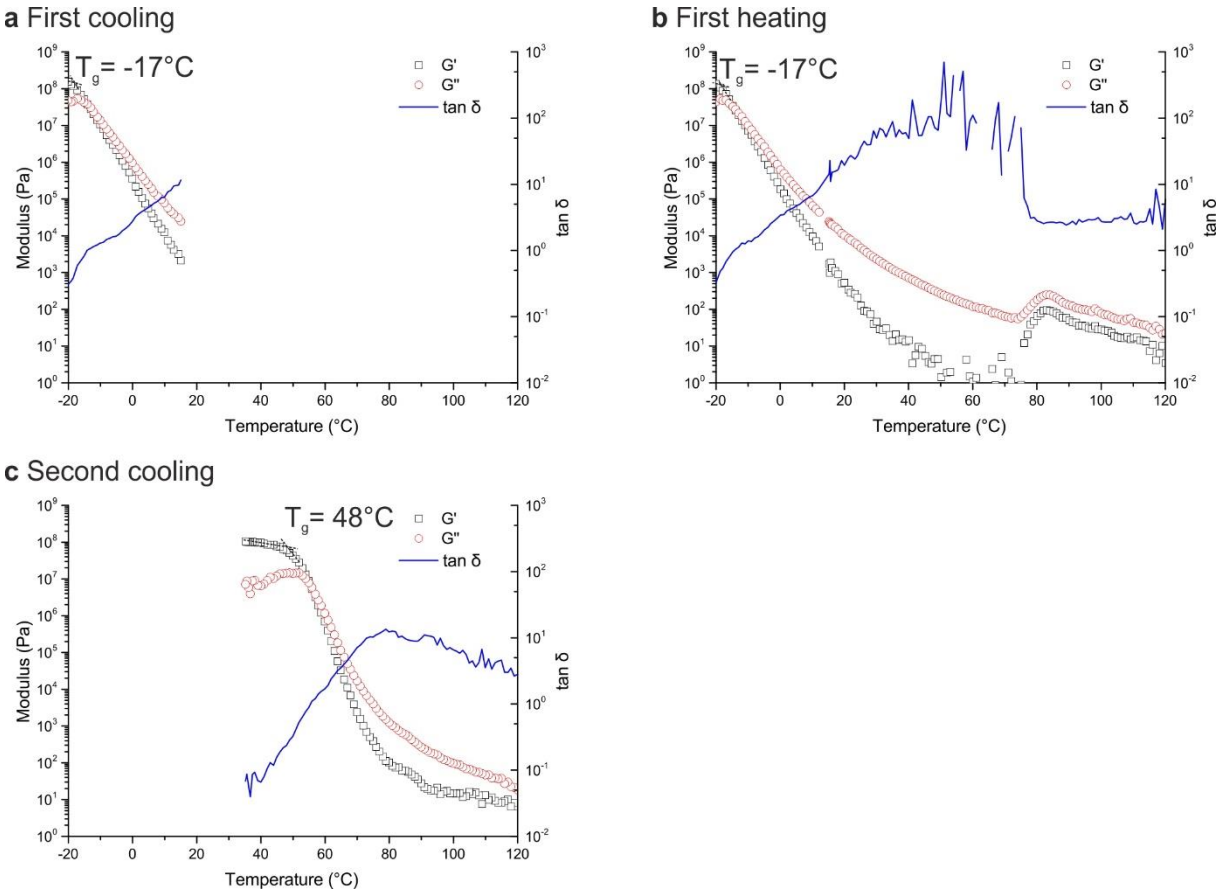


**Figure S7.** DMA data of cis P-12-Azo. $G$' = storage modulus; $G$'' = loss modulus; tan $\delta = G$''/G' = loss tangent. a) Cis P-12-Azo was cooled from room temperature to -20 °C. Tg was -17 °C. b) Cis P-12-Azo was then heated from -20 to 120 °C. Tg was -17 °C. During the heating, the cis P-12-Azo is switched to trans P-12-Azo thermally. c) Then, the sample was cooled towards room temperature. Tg was 48 °C, which is in accordance with Tg of trans P-12-Azo measured by DSC and DMA (Figure 2 in the main manuscript and Figure S21). This experiment confirmed that cis P1 was a liquid at room temperature because $G$'' was significantly larger than $G$' at room temperature.

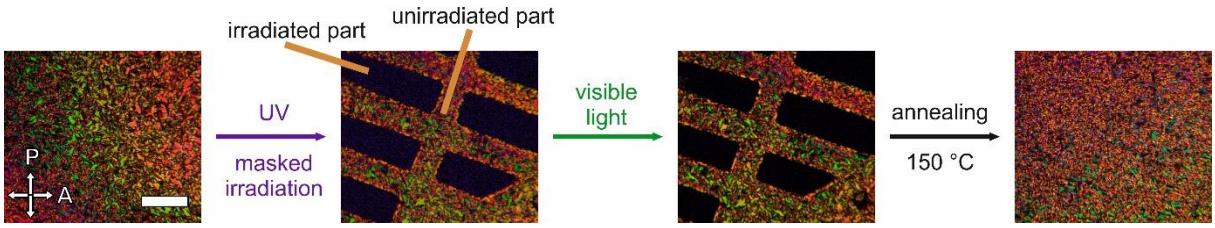


**Figure S8.** Polarized optical microscopy (POM) images of P-12-azo before irradiation, after UV irradiation (365 nm at 65 mW $cm^{-2}$) through a mask, green light irradiation (365 nm at 12 mW $cm^{-2}$) and annealing at 150°C. The scale bar is 250 μm. P: polarizer; A: analyzer. Trans azo groups exhibit liquid crystalline order. UV irradiation transforms azo groups from an anisotropic trans to an isotropic cis state. Visible light irradiation switches cis azo groups back to trans azo groups. The resulting trans state is amorphous. The anisotropic order can be regenerated by annealing at 150 °C and cooling down to room temperature.

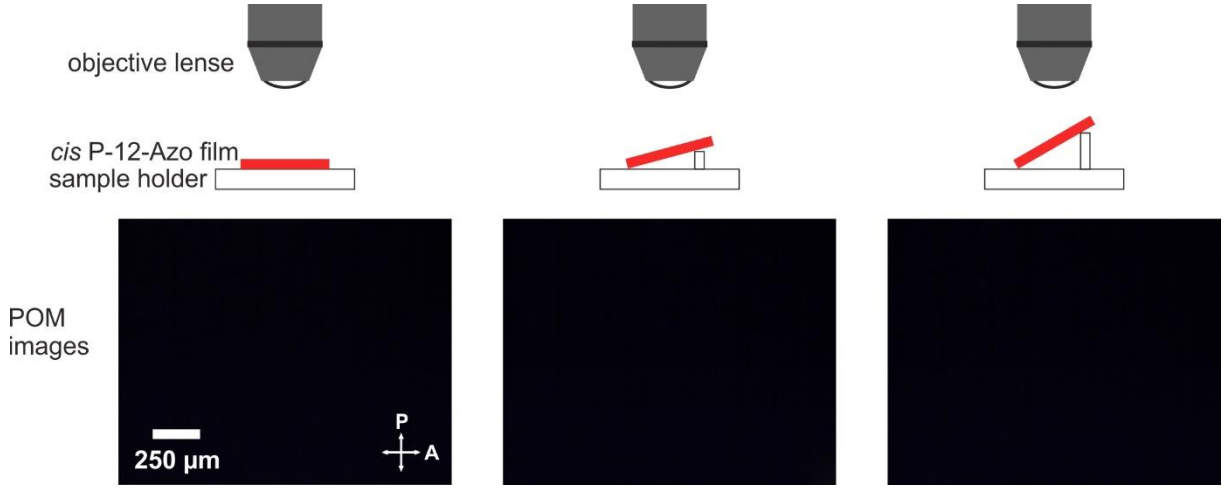


**Figure S9.** Polarized Optical microscopy (POM) images of *cis* P-12-Azo at different tilting angles. From left to right, the tilting angles are 0, 15 and 30°. P: polarizer; A: analyzer. All images at different tilted angles are dark, which shows that *cis* P-12-Azo is isotropic.

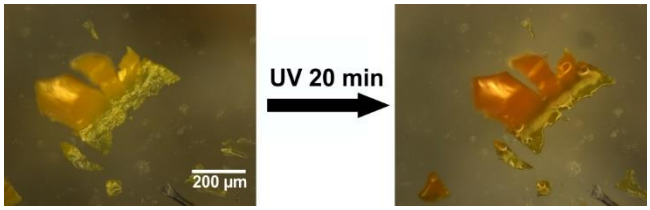


**Figure S10.** Optical microscopy images of amorphous P-12-Azo powder before and after UV (365 nm, 28 mW cm-2) irradiation. P-12-Azo was heated to 150 °C in the isotropic phase. The sample was then quenched in liquid nitrogen to get amorphous P-12-Azo. The quenched P-12-Azo was dark under polarized optical microscopy with crossed polarizers.

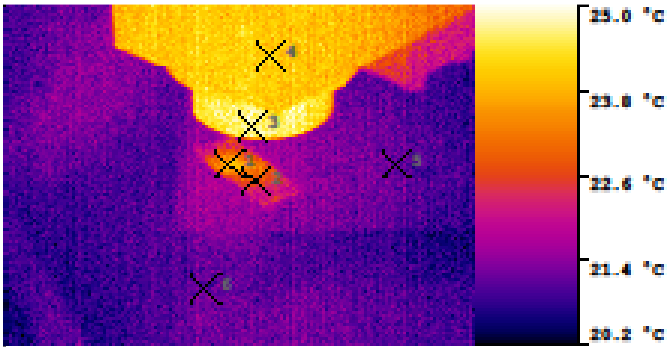


| # | Temp. |
|---|---|
| 1 | 23.8 °C |
| 2 | 22.5 °C |
| 3 | 24.8 °C |
| 4 | 24.2 °C |
| 5 | 21.2 °C |
| 6 | 21.0 °C |

**Figure S11.** Thermal image of P-12-Azo film during UV light irradiation.

**a)** After 30 seconds blue light:

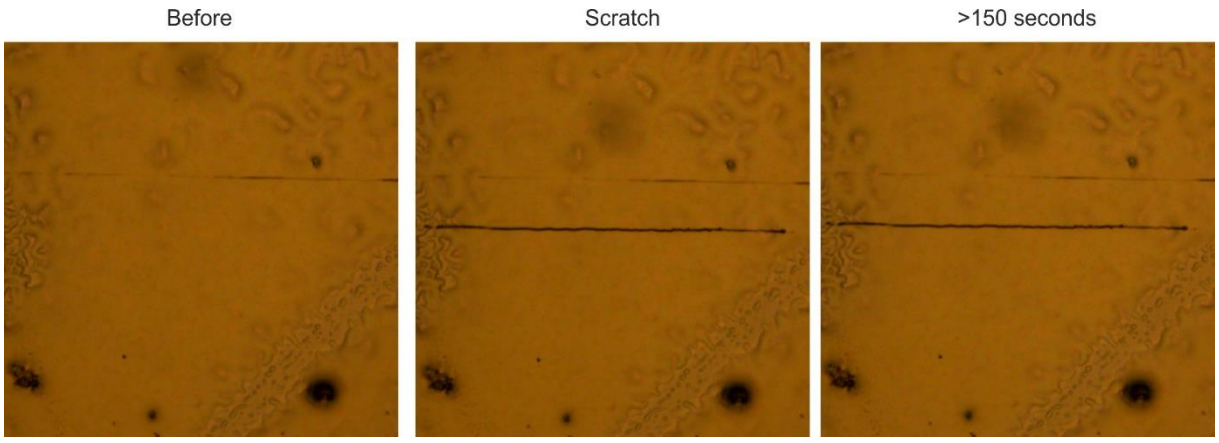


**b)** After 10 minutes at 35 °C:

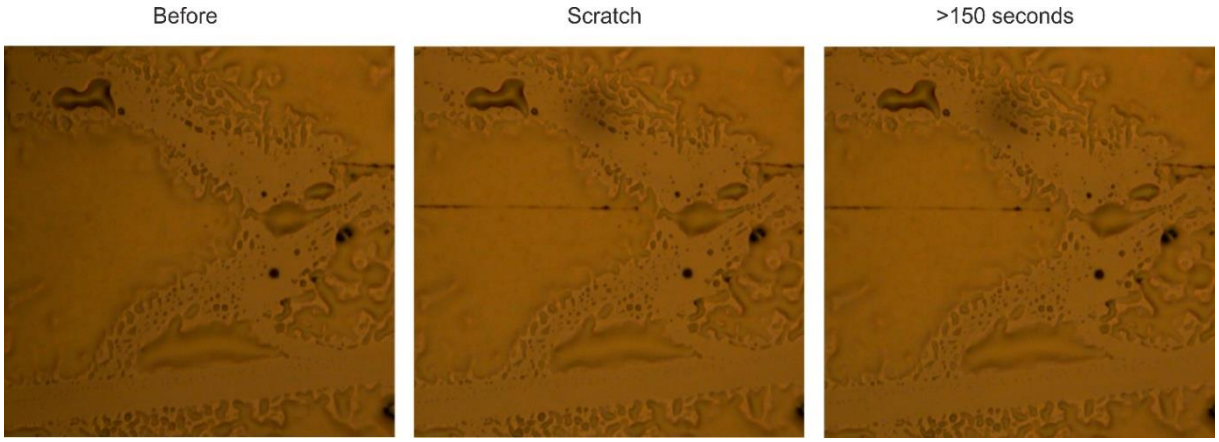


**Figure S12.** Optical microscope images of a *cis* rich P-12-Azo film a) after 30 s blue light irradiation (now *trans* rich) and b) after 10 min at 35 °C (before scratching, after scratching and after waiting for more than 150 s).

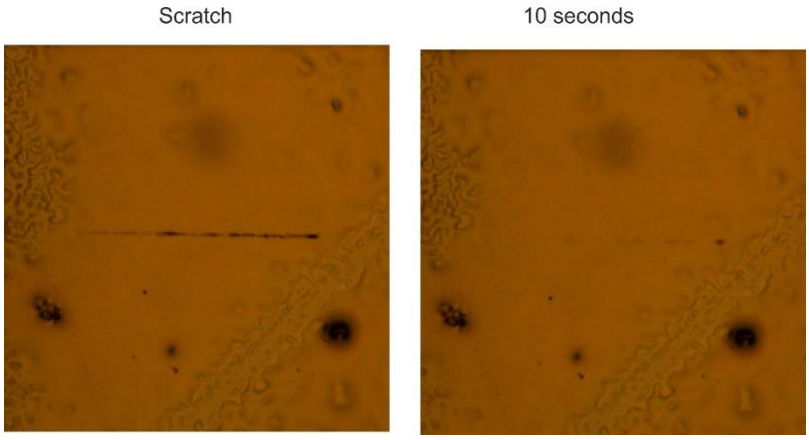


**Figure S13.** Optical microscope images of a *cis* rich P-12-Azo film (after blue light and heating and UV light again (6 min, 65 mW $cm^{-2}$)) after scratching and after waiting for 10 s.

**Synthesis:** The synthesis of the UV light-responsive azopolymers (P-0-Azo, P-2-Azo, P-12-Azo and P-20-Azo) is shown in Scheme S1, details are provided below. The synthesis of P-6-Azo is described elsewhere.[4]

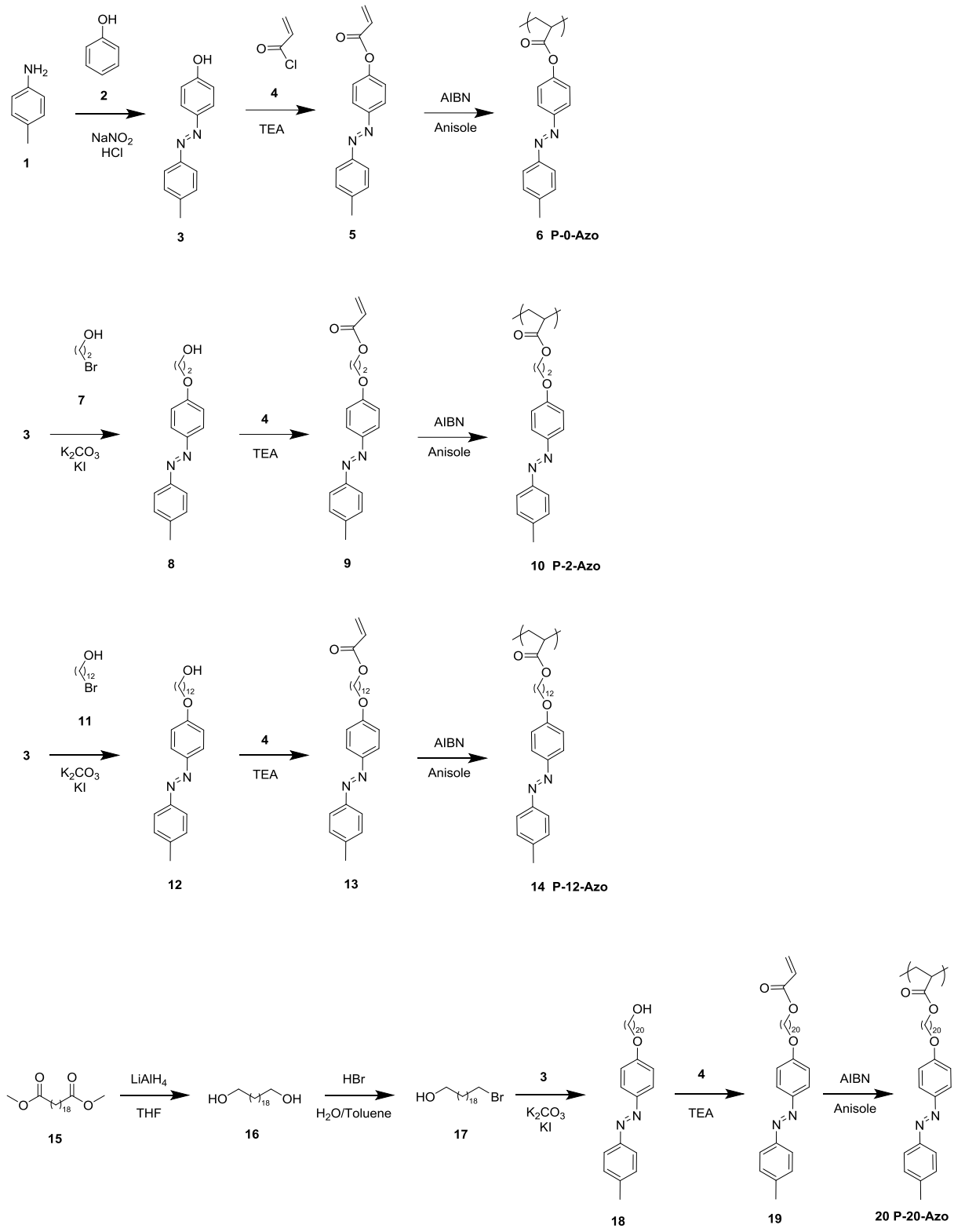


**Scheme S1.** Synthesis of the UV light responsive azobenzene-containing polymers P-n-

Azo.

Synthesis of **3**: p-toluidine **1** (8 g, 0.075 mol) was mixed with hydrochloric acid (16 mL), ice (16 g), and acetone (110 mL). To the above mixture, sodium nitrite (5.020 g, 0.075 mol) dissolved in water (28 mL) with ice (28 g) was added slowly. After 30 min an aqueous solution of phenol **2** (7.0 g, 0.075 mol) in 2 mol $L^{-1}$ sodium hydroxide was added to the mixture. The mixture was stirred for 2 h. After neutralization with HCl, the precipitate was filtered and washed with water. The crude product was dried and purified by recrystallization from ethanol to obtain the compound as a red-brown solid. Yield: 75%. $^{1}$H NMR (300.13 MHz, $CD_2Cl_2$, $\delta$): 7.84 (d, 2H, J = 9 Hz, Ar-*H*), 7.74 (d, 2H, J = 8 Hz, Ar-*H*), 7.32 (d, 2H, J = 8 Hz, Ar-*H*), 6.95 (d, 2H, J = 9 Hz, Ar-*H*), 2.43 (s, 3H, Ar-$CH_3$). $^{13}$C NMR (75.47 MHz, $CD_2Cl_2$, $\delta$): 158.82 (Ar-*C*), 151.25 (Ar-*C*), 147.64 (Ar-*C*), 141.73 (Ar-*C*), 130.26 (Ar-*C*), 125.25 (Ar-*C*), 122.99 (Ar-*C*), 116.30 (Ar-*C*), 21.72 (Ar-$CH_3$).

Synthesis of **5**: 4-(p-tolyldiazenyl)phenol **3** (5 g, 0.024 mol) was suspended in dry DCM (20 ml). TEA (5 g, 0.049 mol) was added. Then acryloyl chloride **4** (2.34 g, 0.026 mol) was added dropwise and the solution was stirred over night at room temperature. The crude product was purified by elution on a silica gel column with $CH_2Cl_2$ to obtain the azobenzene-containing monomer as a yellow solid. Yield: 73%. $^{1}$H NMR (300.13 MHz, $CDCl_3$, $\delta$): 7.91 (d, 2H, J = 9 Hz, Ar-*H*), 7.77 (d, 2H, J = 8 Hz, Ar-*H*), 7.25 (m, 4H, J = 8 Hz, Ar-*H* + Chloroform), 6.58 (d, 1H, J = 17 Hz, O=C-CH=C$H_2$), 6.30 (dd, 1H, J = 17 Hz, O=C-C*H*=$CH_2$), 6.00 (d, 1H, J = 10 Hz, O=C-CH=C$H_2$), 2.39 (s, 3H, Ar-$CH_3$). $^{13}$C NMR (75.47 MHz, $CDCl_3$, $\delta$): 164.32 (*C*=O), 152.47 (Ar-*C*-O), 150.83 (Ar-*C*-N), 150.51 (Ar-*C*-N), 141.79 (Ar-*C*-C), 133.07 (C=*C*), 129.88 (Ar-*C*), 127.90(C=*C*), 124.05 (Ar-*C*), 123.01 (Ar-*C*), 122.25 (Ar-*C*), 21.64 (Ar-$CH_3$). MS: [M-H]+ 267.3 ; found 267.1.

Synthesis of **6**: 4-(p-tolyldiazenyl)phenyl acrylate **5** (1.5 g, 0.005 mol) and 2,2'-azobisisobutyronitrile (20 mg, 0.1 mmol) were dissolved in anisole (7.5 mL). The mixture was degassed via three freeze-pump-thaw-cycles and stirred at 70 °C for 24 h. After cooling down the polymer was purified by two times precipitating in methanol to receive the product as a yellow powder. Yield: 50 %. The number averaged molecular weight of the polymer, determined by GPC was $7.6 \times 10^3$ g mol$^{-1}$ and the PDI was 1.63.

Synthesis of **8**: 4-(p-tolyldiazenyl)phenol **3** (13.5 g, 0.06 mol) was dissolved in dry DMF (70 ml), potassium carbonate (8.8 g, 0.06 mol) was added and the solution was stirred for 30 min at 30 °C. Then, KI (0.015 g, 0.09 mmol) and 2-chloroethan-1-ol **7** (5.6 g, 0.07 mol) were added to the solution. The reaction mixture was then stirred vigorously for 4 d at 105 °C. The resulting mixture was cooled to room temperature, poured into water (1 L), and the resulting precipitate was filtered off. The crude product was purified by recrystallization from ethanol/water (70:30) to obtain the compound as a red-brown solid. Yield: 72%. $^1$H NMR (250.13 MHz, $CDCl_3$, $\delta$): 7.91 (d, 2H, J = 9 Hz, Ar-*H*), 7.80 (d, 2H, J = 8 Hz, Ar-*H*), 7.30 (d, 2H, J = 8 Hz, Ar-*H*), 7.02 (d, 2H, J = 9 Hz, Ar-*H*), 4.16 (t, 2H, J = 5 Hz, Ar-O-$CH_2$), 3.99 (t, 2H, J = 5 Hz, HO-$CH_2$), 2.43 (s, 3H, Ar-$CH_3$). $^{13}$C NMR (75.47 MHz $CDCl_3$, $\delta$): 160.98 (Ar-*C*), 150.89 (Ar-*C*), 147.40 (Ar-*C*), 141.40 (Ar-*C*), 129.84 (Ar-*C*), 124.77 (Ar-*C*), 122.72 (Ar-*C*), 114.89 (Ar-*C*), 69.61 (-$H_2C$-O-Ar), 61.52 (-$H_2C$-O-H), 21.60 (Ar-$CH_3$).

Synthesis of **9**: Acryloyl chloride **4** (2.46 g, 0.03 mol) was added at room temperature drop wise into a solution containing 2-(4-(p-tolyldiazenyl)phenoxy)ethan-1-ol **8** (6.41 g, 0.03 mol), triethylamine (2.8 g, 0.03 mol) and dry $CH_2Cl_2$ (60 mL) and stirred at room temperature overnight. The crude product was purified by elution on a silica gel column with DCM to obtain the azobenzene-containing monomer as a yellow solid. Yield: 65%.

$^{1}$H NMR (250.13 MHz, $CDCl_3$, $\delta$): 7.90 (d, 2H, J = 9 Hz, Ar-*H*), 7.79 (d, 2H, J = 8 Hz, Ar-*H*), 7.30 (d, 2H, J = 9.0 Hz, Ar-*H*), 7.03 (d, 2H, J = 9.0 Hz, Ar-*H*), 6.48 (d, 1H, J = 17 Hz, C=*CH*$_2$), 6.18 (dd, 1H, J = 17 Hz, *H*C=*C*H$_2$), 5.88 (d, 1H, J = 10 Hz, C=C*H*$_2$), 4.55 (t, 2H, J = 4 Hz, Ar-O-*CH*$_2$), 4.30 (t, 2H, J = 5 Hz, -O-*CH*$_2$), 2.43 (s, 3H, Ar-*CH*$_3$). $^{13}$C NMR (75.47 MHz, $CD_2Cl_2$, $\delta$): 166.08 (*C*=O), 160.67 (Ar-*C*), 150.79 (Ar-*C*), 147.33 (Ar-*C*), 140.97 (Ar-*C*), 131.50 (-C=*C*H$_2$), 129.71 (Ar-*C*), 128.01 (-*C*=CH$_2$), 124.59 (Ar-*C*), 122.59 (Ar-*C*), 114.81 (Ar-*C*), 66.16 (-H$_2$*C*-O-Ar), 62.76 (-H$_2$*C*-O-C=O), 21.47 (Ar-*C*H$_3$). MS: [M]+ 311.4; found 311.4.

Synthesis of **10**: 2-(4-(p-tolyldiazenyl)phenoxy)ethyl acrylate **9** (1 g, 0.003 mol) and 2,2'-azobisisobutyronitrile (20 mg, 0.11 mmol) were dissolved in anisole (4 mL). The mixture was degassed via three freeze-pump-thaw-cycles and stirred at 80 °C for 8 h. After cooling down the polymer was purified by four times precipitating in methanol to receive the polymer as a yellow powder. Yield: 28 %. The number averaged molecular weight of the polymer, determined by GPC was 8.9 $\times 10^3$ g mol$^{-1}$ and the PDI was 1.60.

Synthesis of **12**: 4-(p-tolyldiazenyl)phenol **3** (7.5 g, 0.036 mol) was dissolved in dry DMF (40 ml), potassium carbonate (4.9 g, 0.036 mol) was added and the solution was stirred for 30 min at 30 °C. Then, KI (0.015 g, 0.090 mmol) and 12-bromododecan-1-ol **7** (10.34 g, 0.039 mol) were added to the solution. The reaction mixture was then stirred vigorously for 24 h at 110 °C. The resulting mixture was cooled to room temperature and poured into crushed ice (900 g), and the resulting red-brown precipitate was filtered off. The crude product was dried and purified by recrystallization from ethanol to obtain the compound as a red-brown solid. Yield: 83%. $^{1}$H NMR (250.13 MHz, $CDCl_3$, $\delta$): 7.88 (d, 2H, J = 9 Hz, Ar-*H*), 7.78 (d, 2H, J = 8 Hz, Ar-*H*), 7.29 (d, 2H, J = 8 Hz, Ar-*H*), 6.99 (d, 2H, J = 9 Hz, Ar-*H*), 4.03 (t, 2H, J = 7 Hz, Ar-O-*CH*$_2$), 3.64 (t, 2H, J = 6 Hz, HO-*CH*$_2$), 2.42 (s, 3H,

Ar-*CH*$_3$), 1.82 (q, 2H, J = 8 Hz, -O-CH$_2$-*CH*$_2$-CH$_2$), 1.54-1.18 (m, 18H, CH$_2$-*(CH$_2$)$_9$*-CH$_2$-OH). $^{13}$C NMR (75.47 MHz, $CD_2Cl_2$, $\delta$): 162.23 (Ar-*C*), 151.40 (Ar-*C*), 147.39 (Ar-*C*), 141.57 (Ar-*C*), 130.26 (Ar-*C*), 125.04 (Ar-*C*), 122.98 (Ar-*C*), 115.25 (Ar-*C*), 69.03 (-H$_2$*C*-O-Ar), 63.41 (-H$_2$*C*-O-H), 33.49-26.36 (Ar-O-H$_2$C-*(CH$_2$)$_{10}$*-CH$_2$-), 21.73 (Ar-*C*H$_3$).

Synthesis of **13**: Under ice-water bath conditions, acryloyl chloride **4** (3.22 g, 0.036 mol) was added drop wise into a solution containing 12-(4-(p-tolyldiazenyl)phenoxy)dodecan-1-ol **8** (11.91 g, 0.03 mol), triethylamine (3.04 g, 0.03 mol) and dry $CH_2Cl_2$ (100 mL) and stirred at room temperature for 17 h. The reaction mixture was concentrated with a rotary evaporator, washed with diluted hydrochloric acid, a $NaHCO_3$ solution and a NaCl solution. The organic layer was collected and the solvent was removed with a rotary evaporator. The crude product was purified by elution on a silica gel column with Acetone. After removing the solvent, the product was recrystallized from methanol to obtain the azobenzene-containing monomer as a yellow solid. Yield: 66%. $^1$H NMR (250.13 MHz, $CDCl_3$, $\delta$): 7.90 (d, 2H, J = 9 Hz, Ar-*H*), 7.78 (d, 2H, J = 8 Hz, Ar-*H*), 7.29 (d, 2H, J = 8.0 Hz, Ar-*H*), 6.99 (d, 2H, J = 9.0 Hz, Ar-*H*), 6.39 (d, 1H, J = 17 Hz, C=*CH*$_2$), 6.12 (dd, 1H, J = 17 Hz, *H*C=*C*H$_2$), 5.80 (d, 1H, J = 15 Hz, C=C*H*$_2$), 4.15 (t, 2H, J = 7 Hz, Ar-O-*CH*$_2$), 4.04 (t, 2H, J = 7 Hz, -O-*CH*$_2$), 2.43 (s, 3H, Ar-*CH*$_3$), 1.82 (q, 2H, J = 8 Hz, Ar-O-CH$_2$-*CH*$_2$-CH$_2$), 1.67 (m, 2H, O=C-O-CH$_2$-*CH*$_2$-CH$_2$), 1.53-1.23 (m, 16H, -CH$_2$-*(CH$_2$)$_8$*-CH$_2$-). $^{13}$C NMR (75.47 MHz, $CD_2Cl_2$, $\delta$): 166.65 (*C*=O), 162.23 (Ar-*C*), 151.41 (Ar-*C*), 147.34 (Ar-*C*), 141.56 (Ar-*C*), 130.55 (-C=*C*H$_2$), 130.26 (Ar-*C*), 129.32 (-*C*=CH$_2$), 125.04 (Ar-*C*), 122.99 (Ar-*C*), 115.25 (Ar-*C*), 69.03 (-H$_2$*C*-O-Ar), 65.19 (-H$_2$*C*-O-C=O), 30.14-26.52 (-H$_2$C-*(CH$_2$)$_{10}$*-CH$_2$-), 21.73 (Ar-*C*H$_3$). MS: [M]+ 450.3; found 449.5.

Synthesis of **14**: 12-(4-(p-tolyldiazenyl)phenoxy)dodecyl acrylate **9** (2 g, 0.004 mol) and 2,2'-azobisisobutyronitrile (7 mg, 0.04 mmol) were dissolved in anisole (4.4 mL). The

mixture was degassed via three freeze-pump-thaw-cycles and stirred at 85 °C for 3 d. After cooling down the polymer was purified by two times precipitating in methanol and washing with hot ethanol for two times to receive the polymer as a yellow powder. Yield: 37 %. The number averaged molecular weight of the polymer, determined by GPC was 8.6 $\times 10^3$ g mol$^{-1}$ and the PDI was 1.38.

Synthesis of **16**: $LiAlH_4$ (10 g, 0.26 mol) was suspended under argon in dry THF (500 mL). Then dimethyl icosanedioate **15** (39g, 0.11 mol) was added slowly. The mixture was stirred under reflux for 2 h. Under ice cooling water (100 mL), then half concentrated HCl (100 mL), then concentrated HCl (50 mL) was added. The precipitate was filtered and washed with diluted HCl and recrysztallized from ethanol to obtain the product as a colorless solid. Yield 95 %. $^1$H NMR (300.13 MHz, $CDCl_3$, $\delta$): 3.64 (t, 4H, J = 7 Hz, C*H*$_2$-OH), 1.56 (m, 4H, C*H*$_2$-CH$_2$-OH), 1.47 (s, 4H, C*H*$_2$-CH$_2$-CH$_2$-OH), 1.56 (m, 4H, J = 7 Hz, C*H*$_2$-CH$_2$-OH), 1.39-1.18 (s, 32 H, CH$_2$-(C*H*$_2$)$_{14}$-CH$_2$ +H2O). $^{13}$C NMR (75.47 MHz, $CDCl_3$, $\delta$): 63.26 (*C*-OH), 32.98 (*C*-CH$_2$-OH), 29.83 (CH$_2$-*(CH$_2$)$_{14}$*-CH$_2$), 25.90 (*C*-CH$_2$-CH$_2$-OH).

Synthesis of **17**: Icosane-1,20-diol **16** (15.73 g, 0.05 mol) was dissolved in toluene (150 mL) and HBr (6.8 mL, 0.06 mol) was added. The mixture was heated under reflux in a Dean-Stark apparatus for 4 d. After cooling down and filtering, ethanol was given to the solution until precipitation happened. The mixture was then cooled down and the precipitate was filtered. The crude product was purified by elution on a silica gel column with Hexan/Aceton (5:2) to obtain the product as a colorless solid. Yield: 30%. $^1$H NMR (300.13 MHz, $CDCl_3$, $\delta$): 3.64 (t, 2H, J = 7 Hz, C*H*$_2$-OH), 3.40 (t, 2H, J = 7 Hz, C*H*$_2$-Br), 1.85 (q, 2H, J = 8 Hz, C*H*$_2$-CH$_2$-Br), 1.56 (q, 2H, J = 7 Hz, C*H*$_2$-CH$_2$-OH), 1.47-1.21 (m, 34 H, CH$_2$-(C*H*$_2$)$_{16}$-CH$_2$ +H2O). $^{13}$C NMR (300 MHz, $CDCl_3$, $\delta$): $^{13}$C NMR (75.47 MHz, $CDCl_3$, $\delta$): 63.25 (*C*-OH), 34.19 (*C*-Br), 33.01 (*C*-CH$_2$-Br), 32.98 (*C*-CH$_2$-OH), 29.83-

29.59 ($CH_2$-*($CH_2$)$_{13}$*-$CH_2$), 28.93 (*C*-$CH_2$-$CH_2$-$CH_2$-Br), 28.34 (*C*-$CH_2$-$CH_2$-Br), 25.90 (*C*-$CH_2$-$CH_2$-OH).

Synthesis of **18**: 4-(p-tolyldiazenyl)phenol **3** (2.3 g, 0.01 mol), potassium carbonate (1.52 g, 0.01 mol), KI (spatula tip) and 20-bromoicosan-1-ol **17** (3.77 g, 0.01 mol) were dissolved in dry DMF (20 ml). The reaction mixture was then stirred vigorously for 4 d at 90 °C. The resulting mixture was cooled to room temperature, filtered, washed with water and dried to obtain the compound as a yellow solid. Yield: 91%. $^1$H NMR (500.13 MHz, $CDCl_3$, $\delta$): 7.88 (d, 2H, J = 9 Hz, Ar-*H*), 7.78 (d, 2H, J = 8 Hz, Ar-*H*), 7.29 (d, 2H, J = 8 Hz, Ar-*H*), 6.99 (d, 2H, J = 9 Hz, Ar-*H*), 4.03 (t, 2H, J = 6 Hz, Ar-O-*$CH_2$*), 3.64 (t, 2H, J = 6 Hz, HO-*$CH_2$*), 2.43 (s, 3H, Ar-*$CH_3$*), 1.82 (q, 2H, J = 7 Hz, -O-$CH_2$-*$CH_2$*-$CH_2$), 1.64-1.15 (m, 34H (+$H_2O$), $CH_2$-(*$CH_2$*)$_{17}$-OH). $^{13}$C NMR (125.78 MHz, $CDCl_3$, $\delta$): 161.62 (Ar-*C*), 151.01 (Ar-*C*), 147.03 (Ar-*C*), 140.87 (Ar-*C*), 129.82 (Ar-*C*), 124.70 (Ar-*C*), 122.65 (Ar-*C*), 114.82 (Ar-*C*), 68.51 (-$H_2$*C*-O-Ar), 63.27 (-$H_2$*C*-O-C=O), 32.97-25.89 (-$H_2$C-(*C*$H_2$)$_{18}$-$CH_2$-), 21.60 (Ar-*C*$H_3$).

Synthesis of **19**: 20-(4-(p-tolyldiazenyl)phenoxy)icosan-1-ol **18** (3.5 g, 0.007 mol) was dissolved in warm toluene (50 mL). TEA (1 mL, 0.007 mL) and acryloyl chloride **4** (0.59 mL, 0.007 mol) were added and the mixture was stirred at room temperature over night. The reaction mixture was concentrated with a rotary evaporator, dissolved in warm DCM and purified by elution on a silica gel column with $CH_2Cl_2$ to obtain the azobenzene-containing monomer as a yellow solid. Yield: 71%. $^1$H NMR (300.13 MHz, $CDCl_3$, $\delta$): 7.89 (d, 2H, J = 9 Hz, Ar-*H*), 7.78 (d, 2H, J = 8 Hz, Ar-*H*), 7.29 (d, 2H, J = 8 Hz, Ar-*H*), 6.99 (d, 2H, J = 9 Hz, Ar-*H*), 6.40 (d, 1H, J = 17 Hz, C=*$CH_2$*), 6.12 (dd, 1H, J = 17 Hz, *H*C=*C*$H_2$), 5.80 (d, 1H, J = 10 Hz, C=C*$H_2$*), 4.15 (t, 2H, J = 7 Hz, Ar-O-*$CH_2$*), 4.03 (t, 2H, J = 7 Hz, -O-*$CH_2$*), 2.43 (s, 3H, Ar-*$CH_3$*), 1.82 (q, 2H, J = 8 Hz, Ar-O-$CH_2$-*$CH_2$*-$CH_2$),

1.72-1.18 (m, 36H, -$CH_2$-*(*$CH_2$*)*$_{17}$-$CH_2$- + $H_2O$). $^{13}$C NMR (75.47 MHz, $CDCl_3$, $\delta$): 166.47 (*C*=O), 161.63 (Ar-*C*), 151.03 (Ar-*C*), 147.05 (Ar-*C*), 140.84 (Ar-*C*), 130.51 (-C=*C*$H_2$), 129.80 (Ar-*C*), 128.82 (-*C*=$CH_2$), 124.70 (Ar-*C*), 122.66 (Ar-*C*), 114.82 (Ar-*C*), 68.51 (-$H_2$*C*-O-Ar), 64.87 (-$H_2$*C*-O-C=O), 29.85-26.08 (-$H_2$C-*(*$CH_2$*)*$_{10}$-$CH_2$-), 21.59 (Ar-*C*$H_3$). MS: [M-H]+ 563.9 ; found 563.5.

Synthesis of **20**: 20-(4-(p-tolyldiazenyl)phenoxy)icosyl acrylate **19** (1.5 g, 0.005 mol) and 2,2'-azobisisobutyronitrile (10 mg, 0.06 mmol) were dissolved in anisole (7.5 mL). The mixture was degassed via three freeze-pump-thaw-cycles and stirred at 80 °C for 4 d. After cooling down the polymer was purified by two times precipitating in methanol. The crude product was given on silica gel and residual monomer was eluted by washing with DCM. Then the silica gel was heated in $CHCl_3$ to release the polymer which was then filtered and the solvent was removed by reduced pressure to receive the polymer as a yellow powder. Yield: 44 %. The number averaged molecular weight of the polymer, determined by GPC was $10.6 \times 10^3$ g mol$^{-1}$ and the PDI was 1.37.

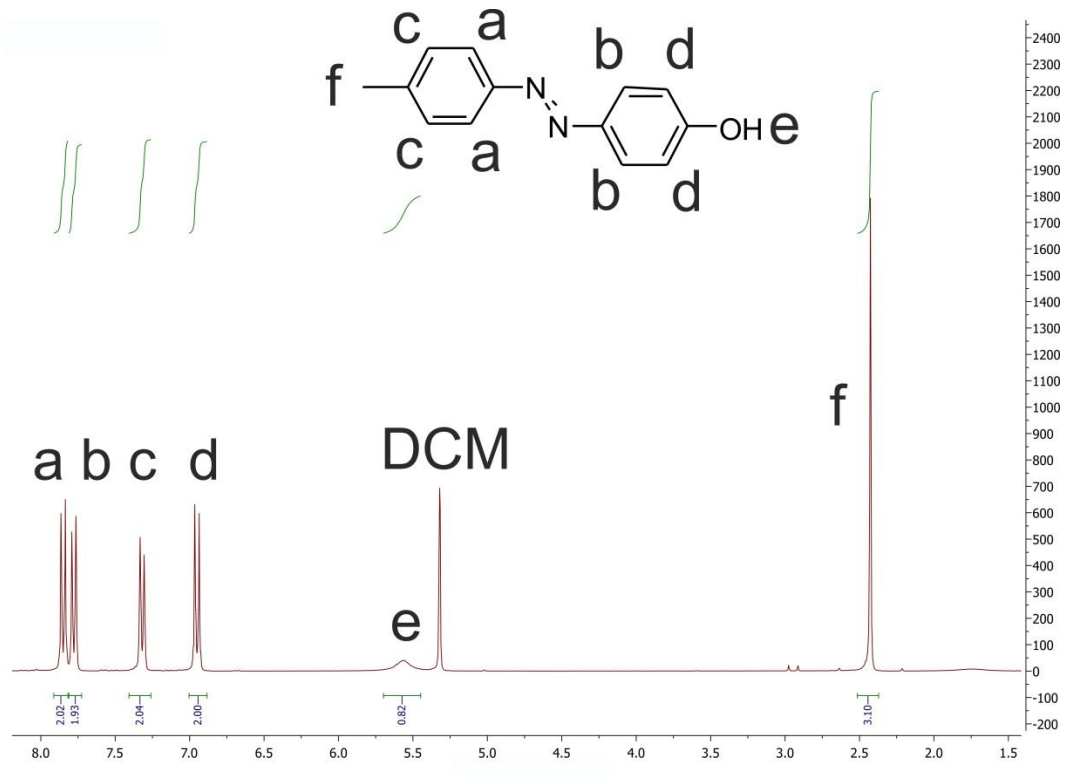


**Figure S14.** $^{1}$H-NMR spectrum (250.13 MHz, $CD_2Cl_2$) of Compound 3.

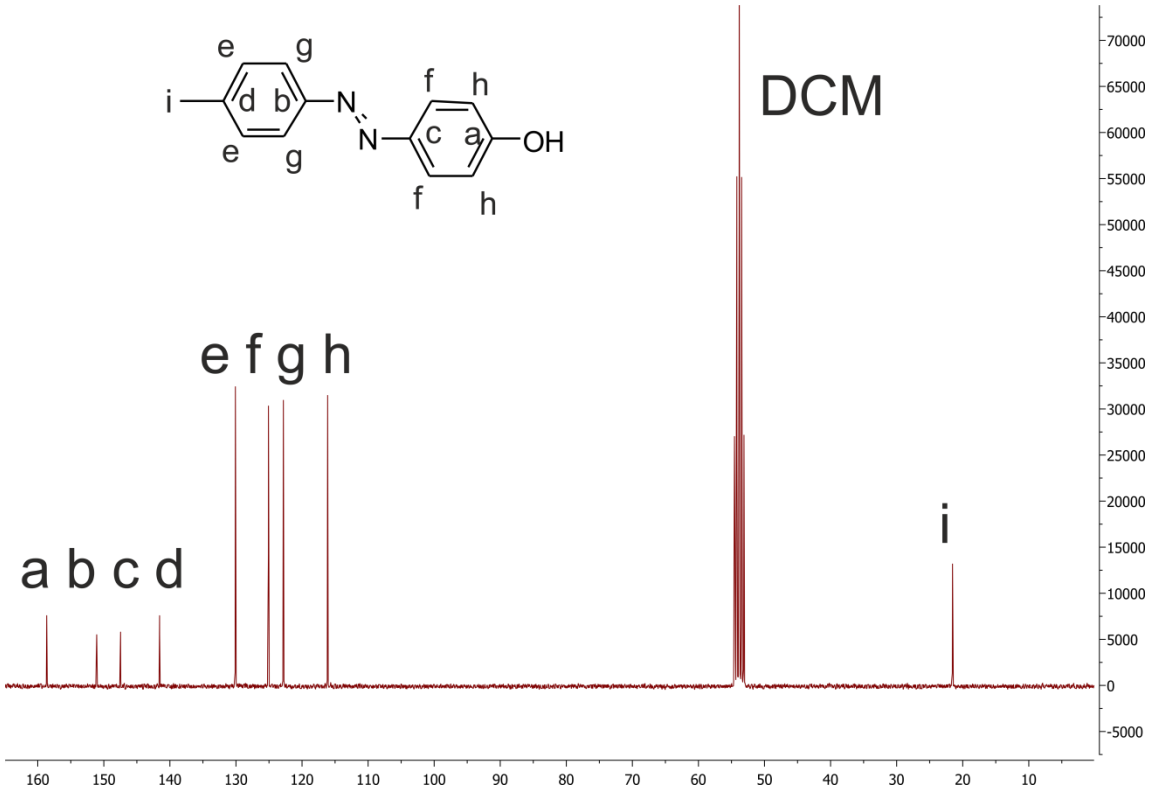


**Figure S15.** $^{13}$C-NMR spectrum (75.47 MHz, $CD_2Cl_2$) of Compound 3.

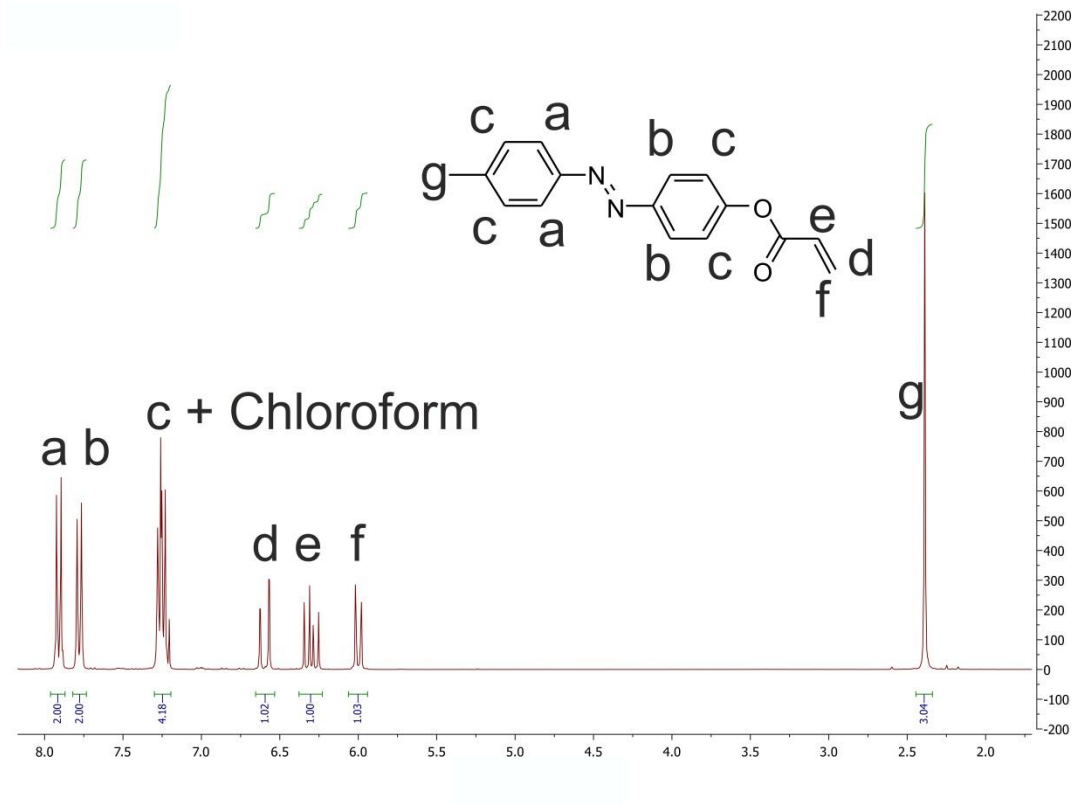


**Figure S16.** $^{1}$H-NMR spectrum (300.13 MHz, $CDCl_3$) of Compound 5.

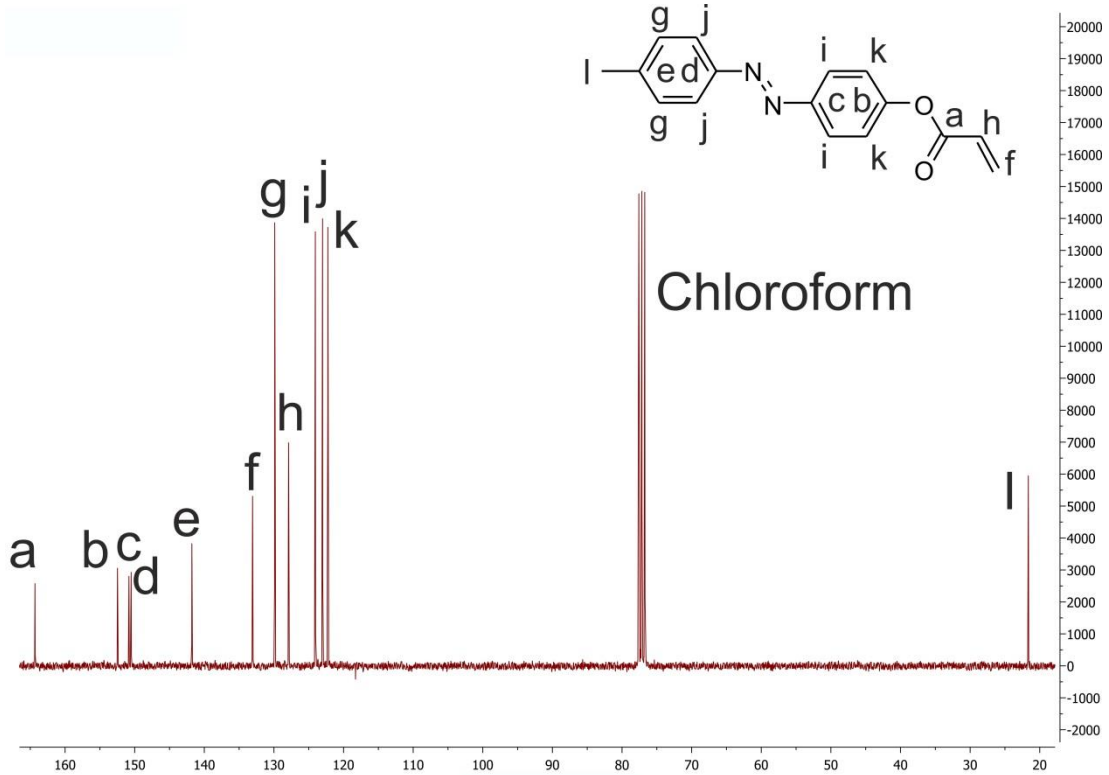


**Figure S17.** $^{13}$C-NMR spectrum (75.47 MHz, $CDCl_3$) of Compound 5.

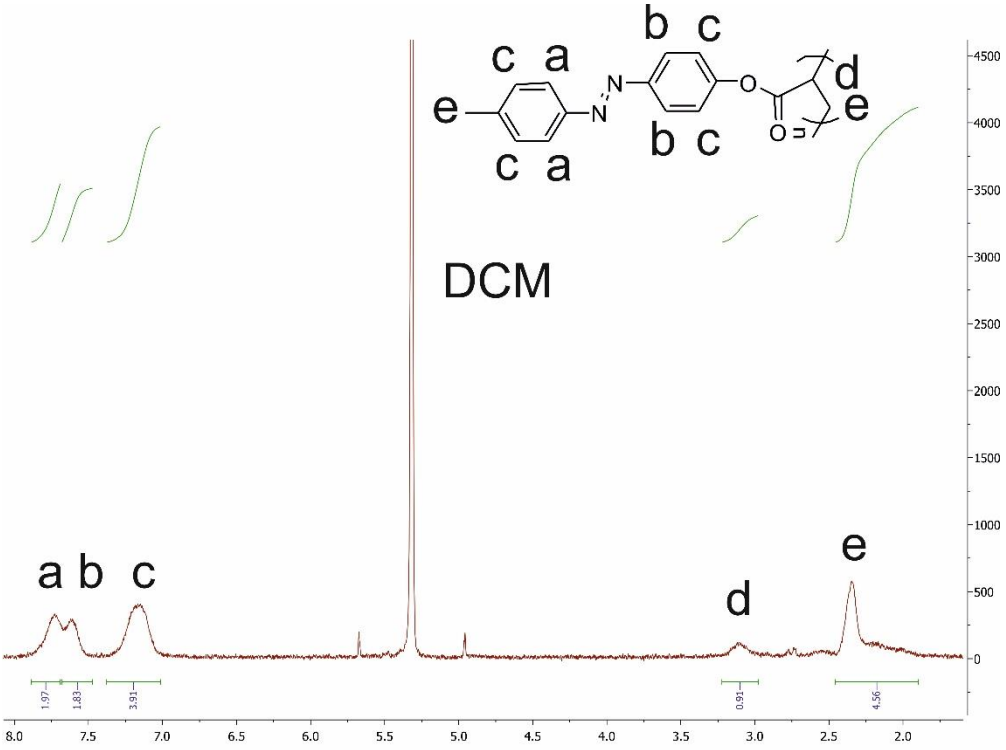


**Figure S18.** $^{1}$H-NMR spectrum (250.13 MHz, $CD_2Cl_2$) of Compound 6.

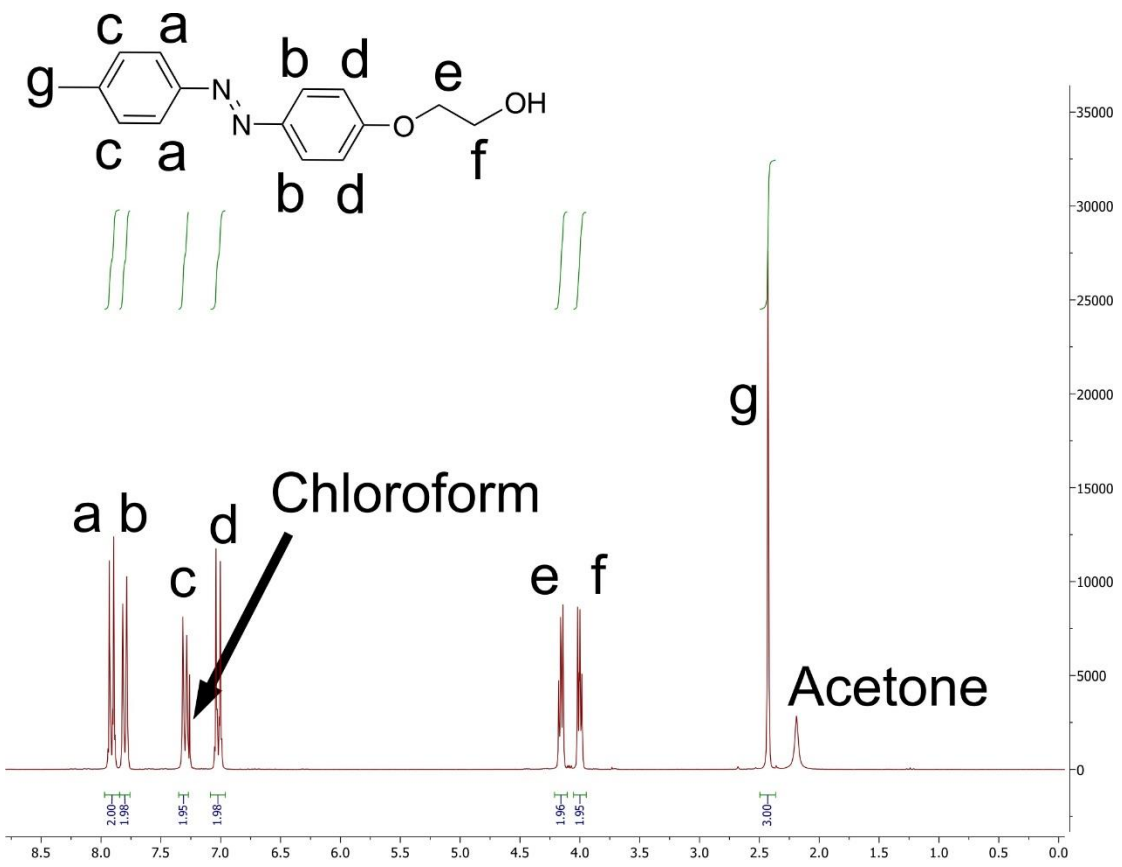


**Figure S19.** $^{1}$H-NMR spectrum (250.13 MHz, $CDCl_3$) of Compound 8.

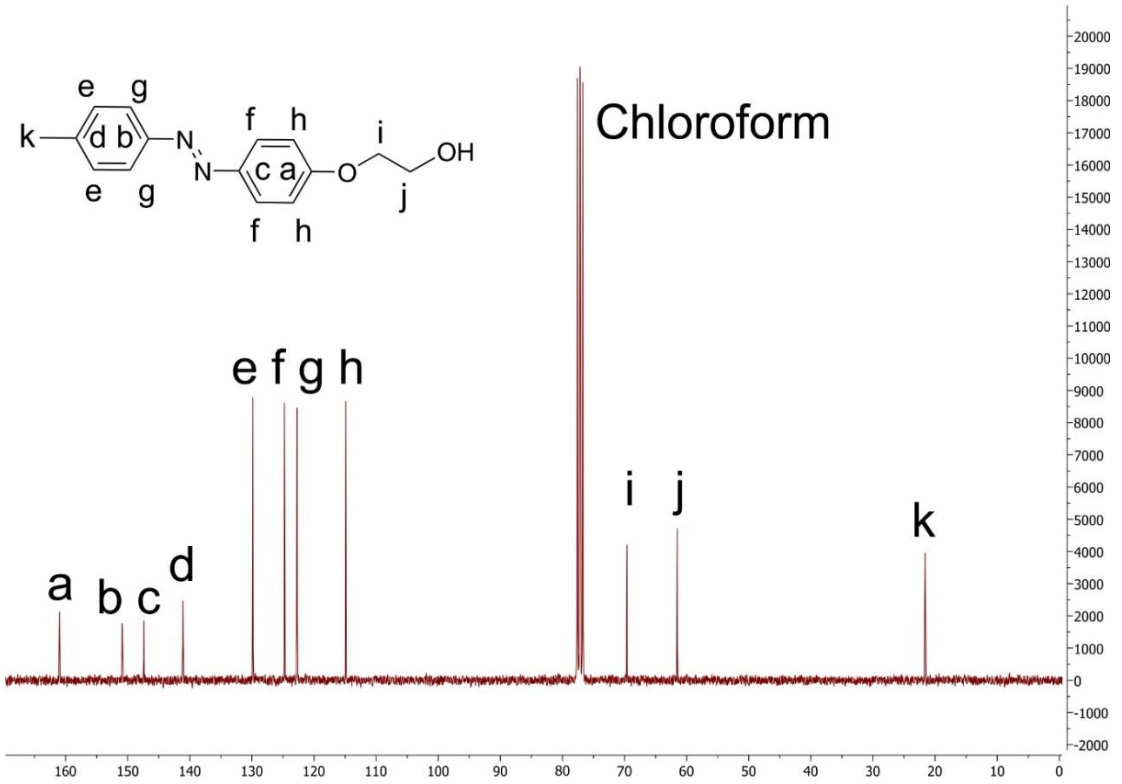


**Figure S20.** $^{13}$C-NMR spectrum (75.47 MHz, $CDCl_3$) of Compound 8.

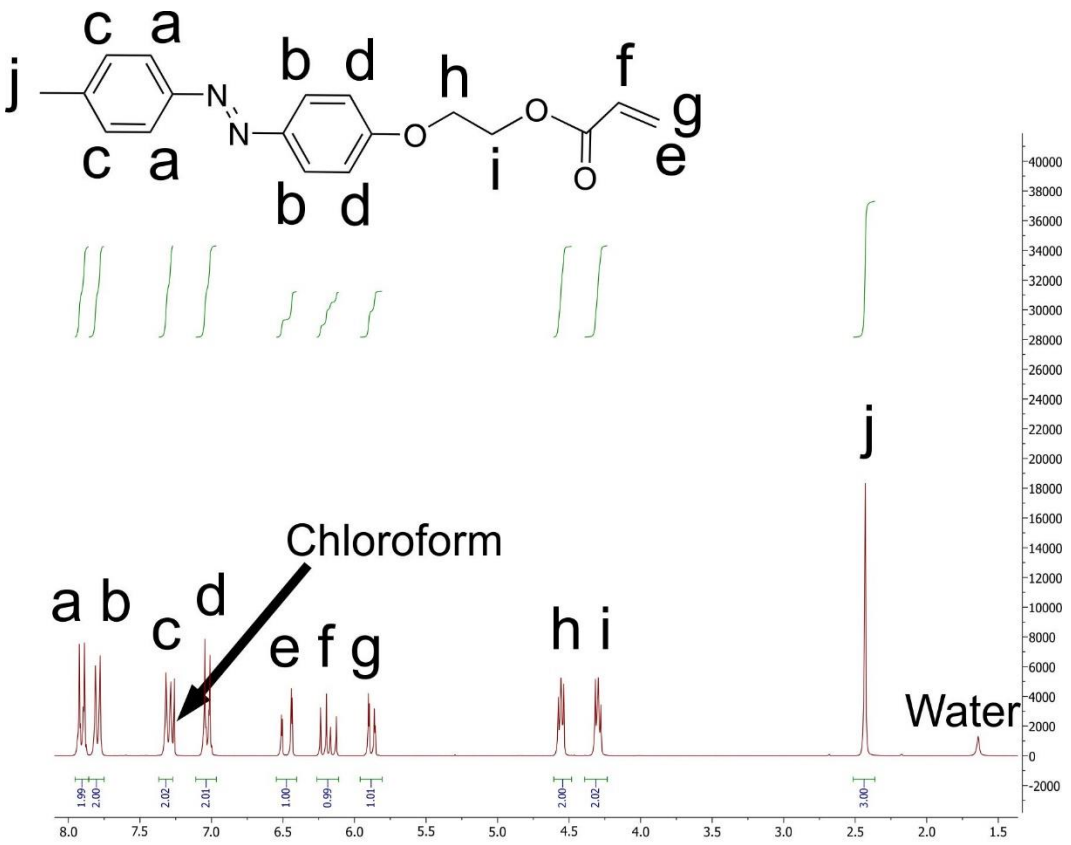


**Figure S21.** $^{1}$H-NMR spectrum (250.13 MHz, $CDCl_3$) of Compound 9.

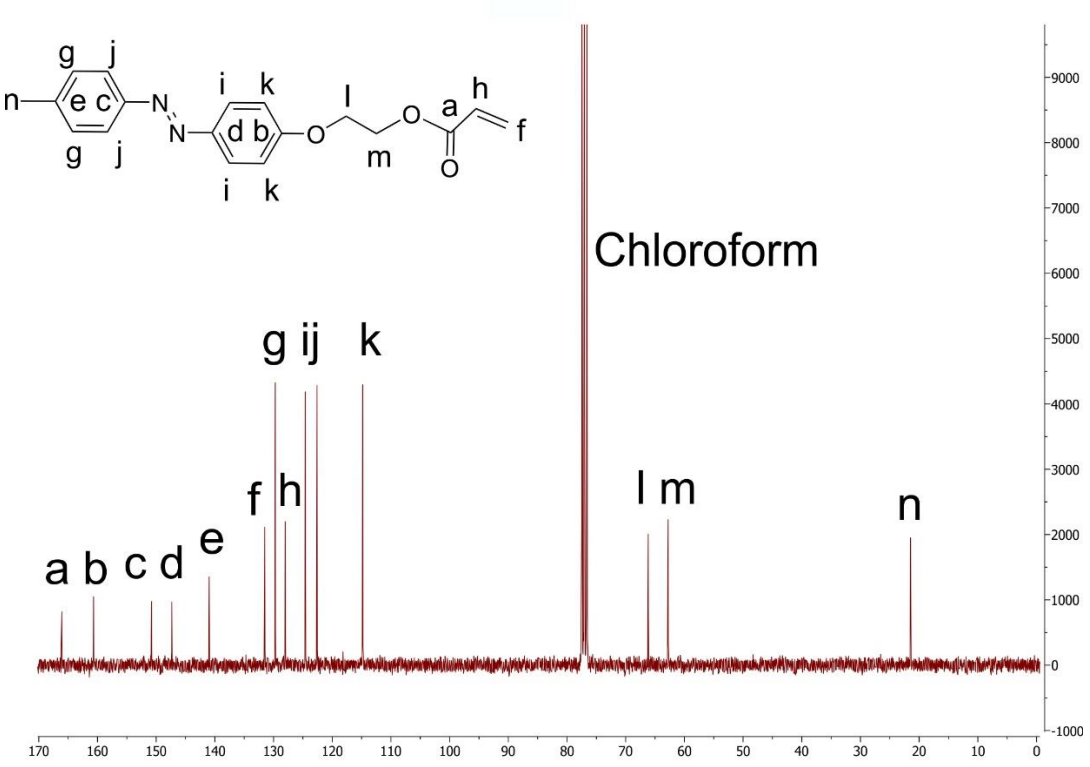


**Figure S22.** $^{13}$C-NMR spectrum (75.47 MHz, $CDCl_3$) of Compound 9.

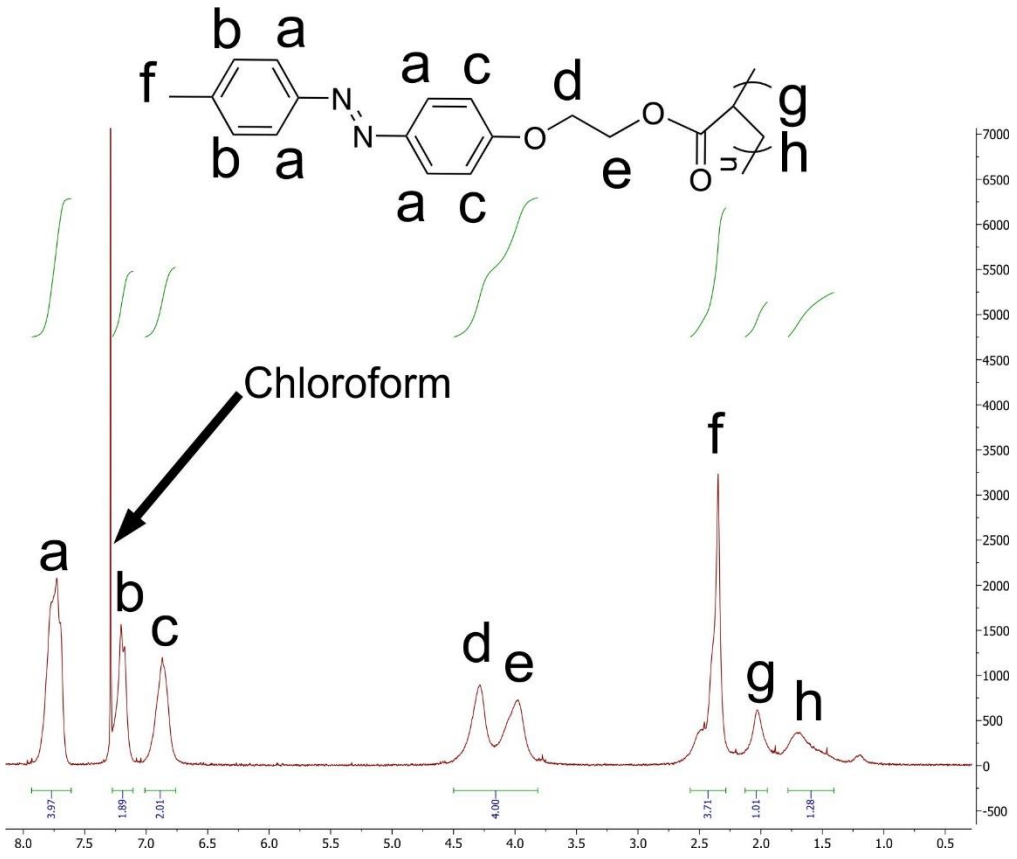


**Figure S23.** $^{1}$H-NMR spectrum (250.13 MHz, $CDCl_3$) of Compound 10.

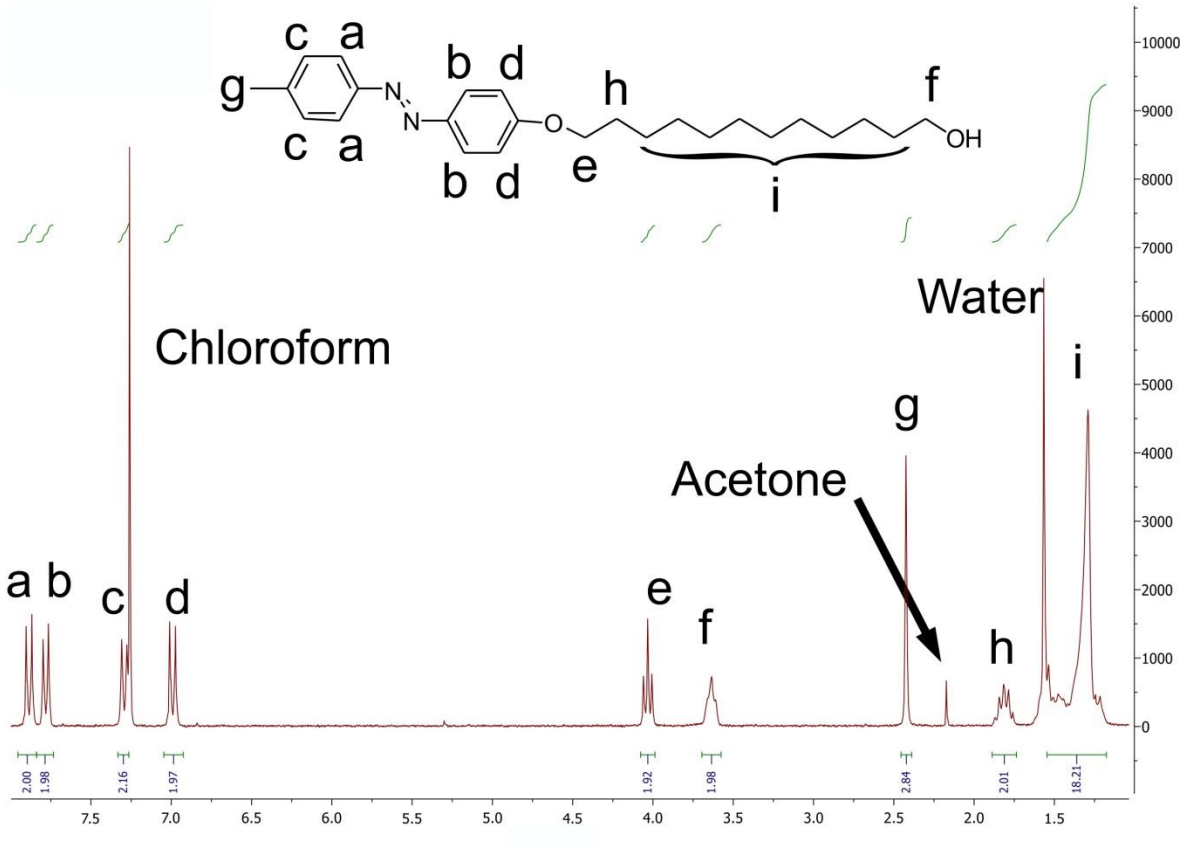


**Figure S24.** $^{1}$H-NMR spectrum (250.13 MHz, $CDCl_3$) of Compound 12.

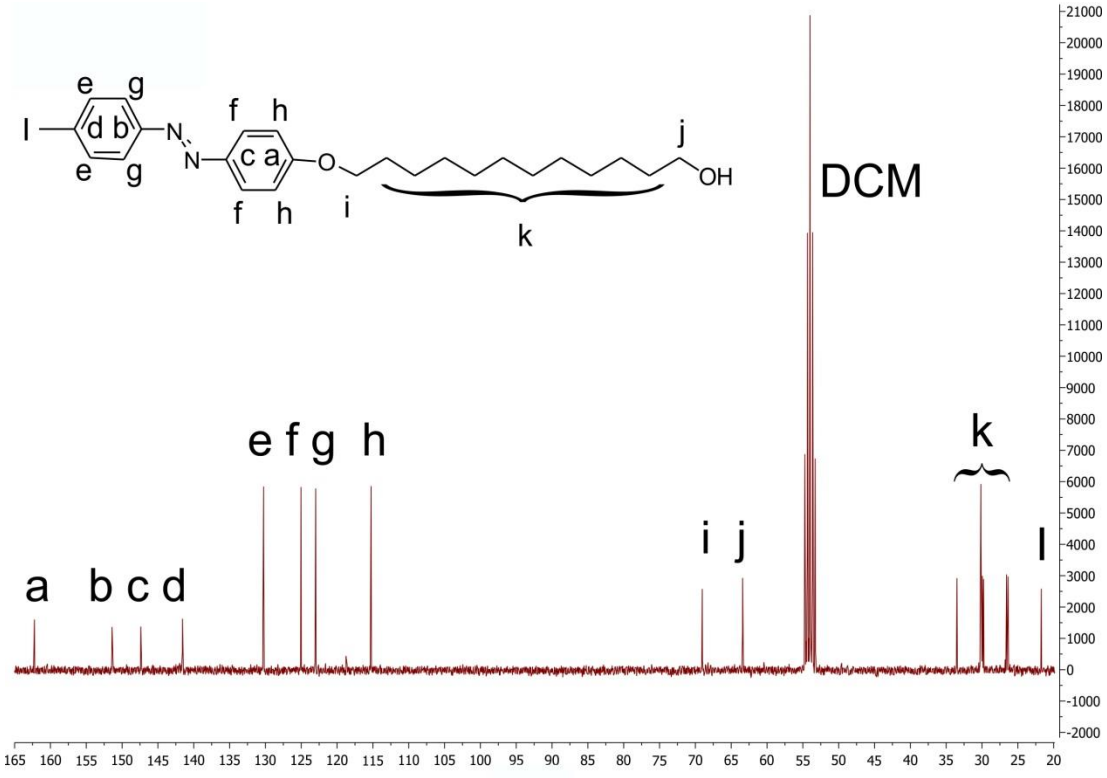


**Figure S25.** $^{13}$C-NMR spectrum (75.47 MHz, $CD_2Cl_2$) of Compound 12.

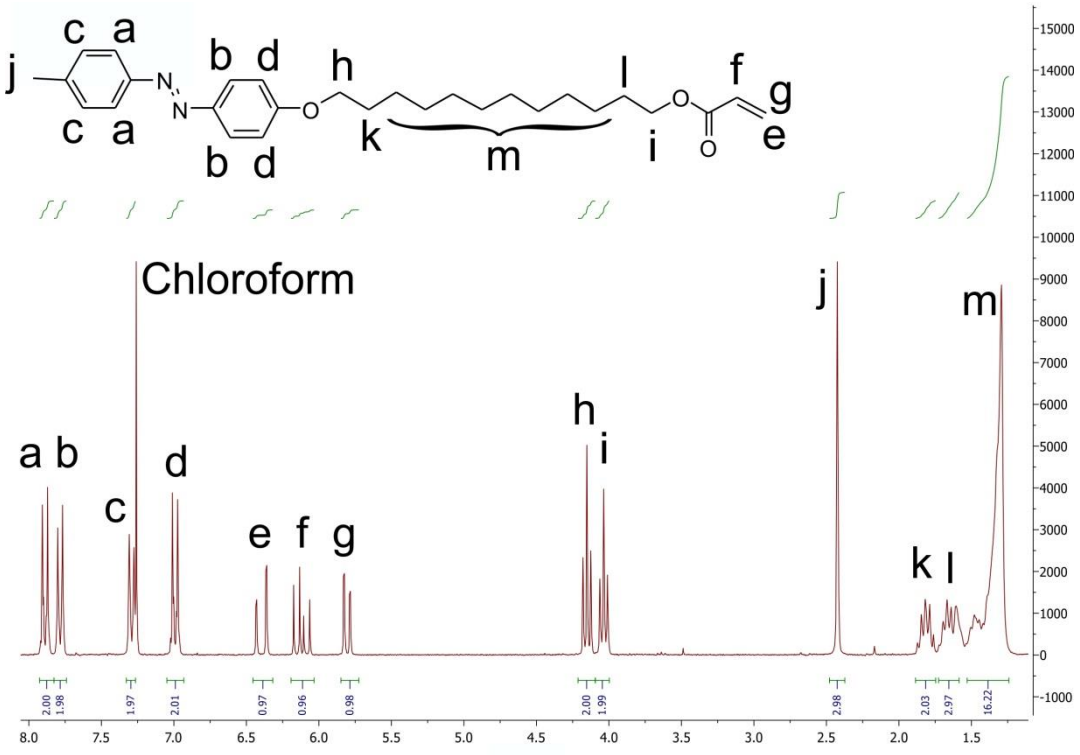


**Figure S26.** $^{1}$H-NMR spectrum (250.13 MHz, $CDCl_3$) of Compound 13.

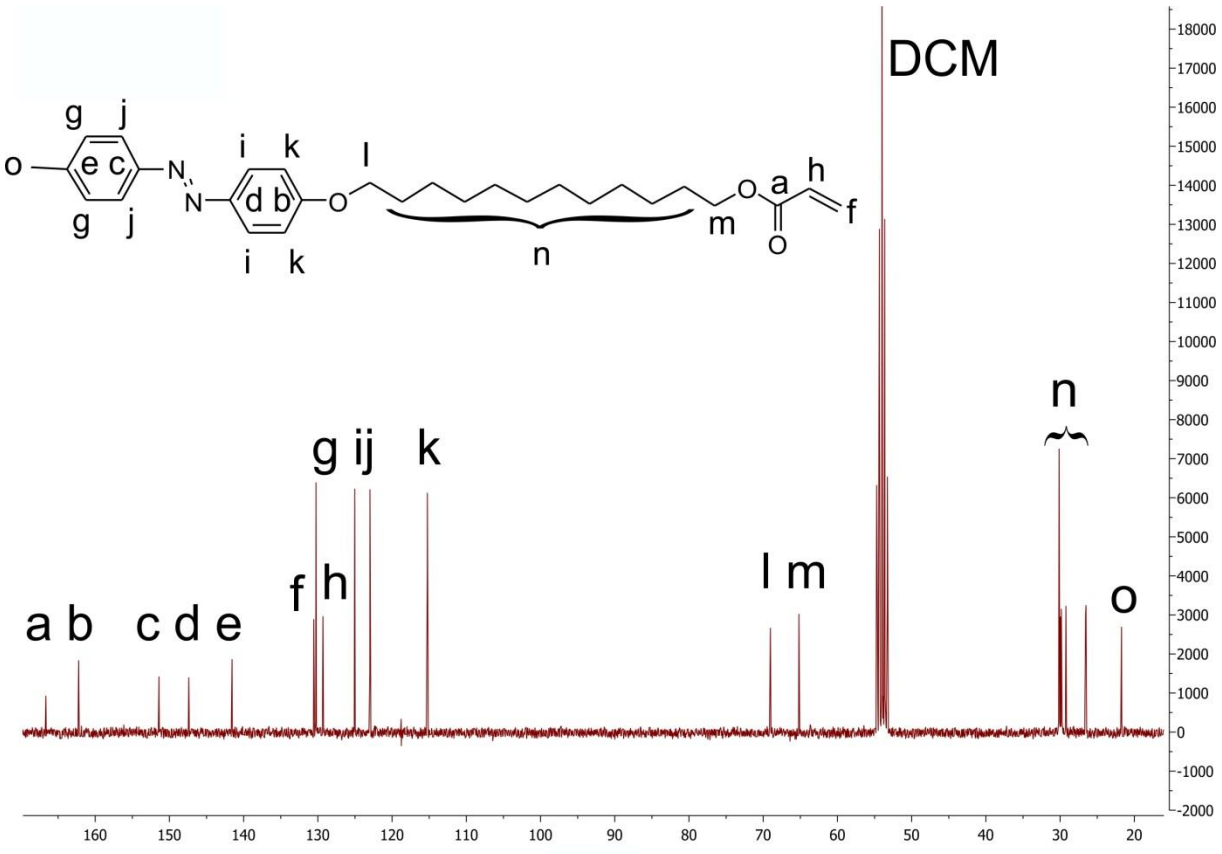


**Figure S27.** $^{13}$C-NMR spectrum (75.47 MHz, $CD_2Cl_2$) of Compound 13.

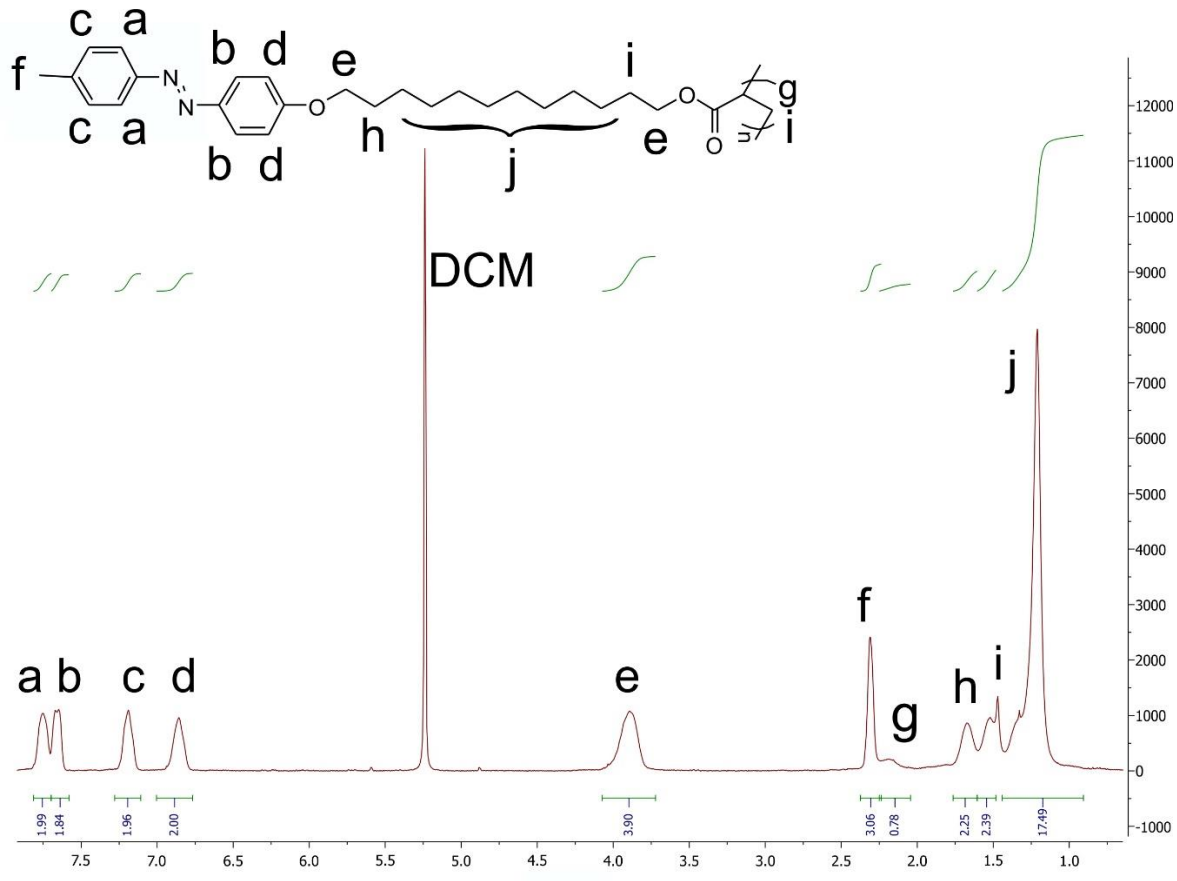


**Figure S28.** $^{1}$H-NMR spectrum (250.13 MHz, $CD_2Cl_2$) of Compound 14.

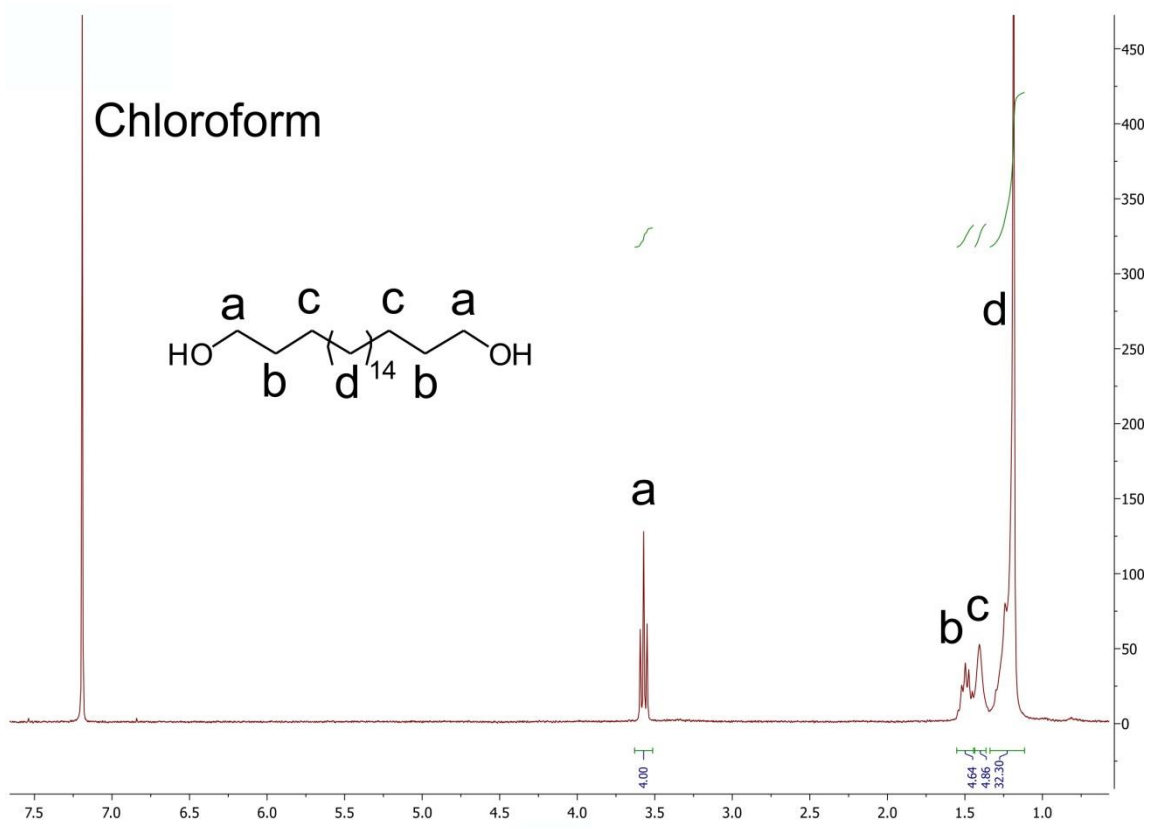


**Figure S29.** $^{1}$H-NMR spectrum (300.13 MHz, $CDCl_3$) of Compound 16.

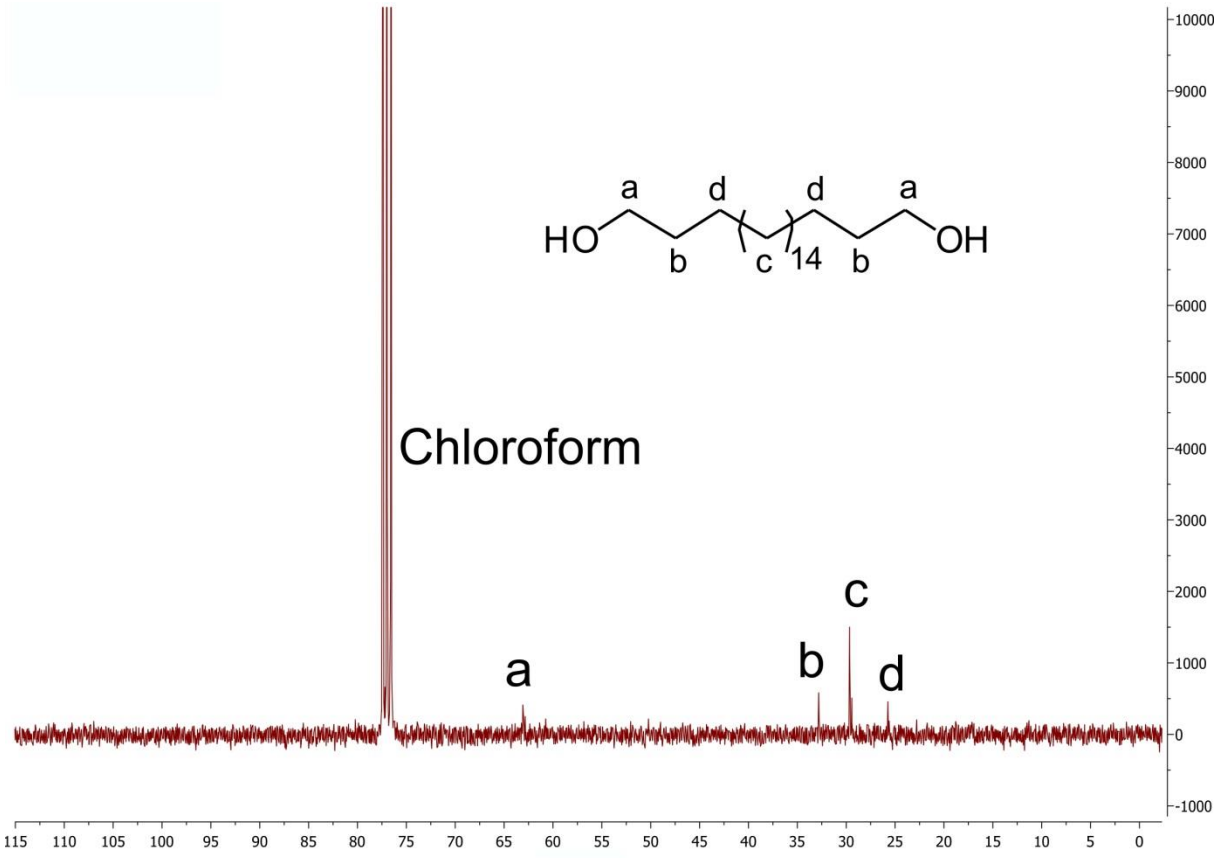


**Figure S30.** $^{13}$C-NMR spectrum (75.47 MHz, $CDCl_3$) of Compound 16.

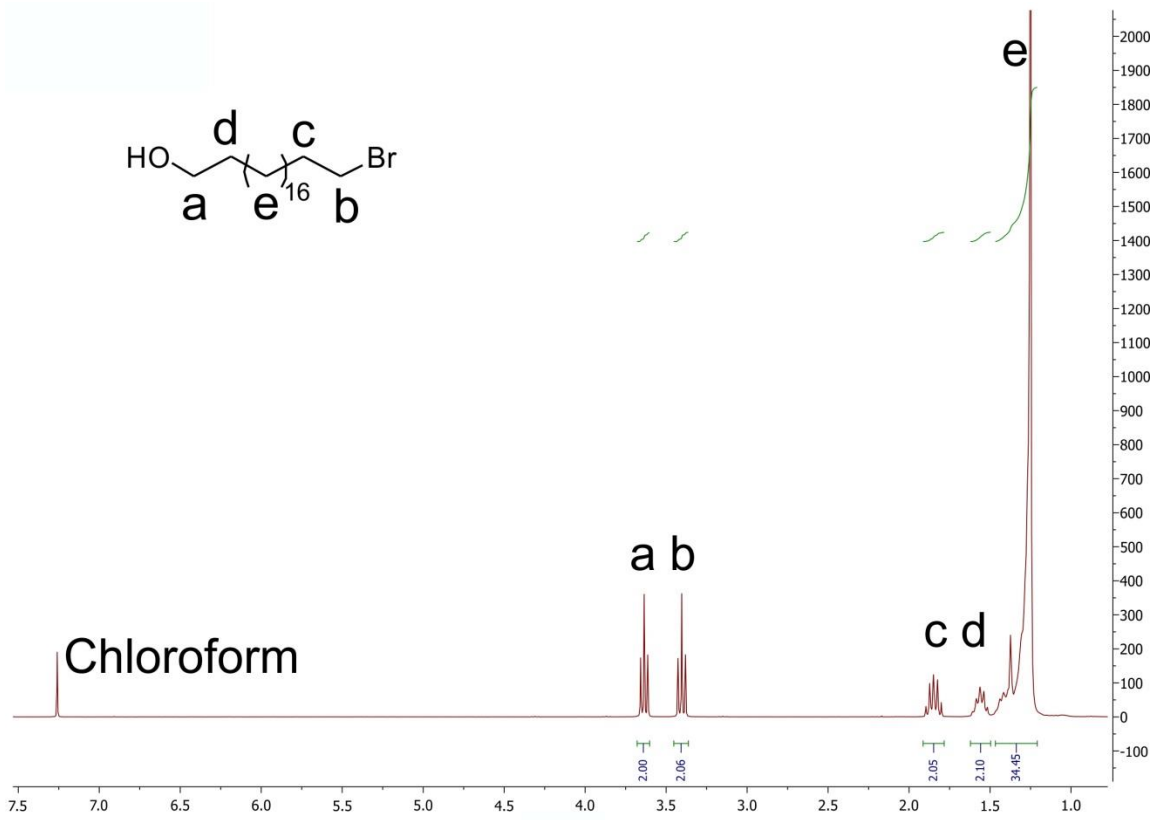


**Figure S31.** $^{1}$H-NMR spectrum (300.13 MHz, $CDCl_3$) of Compound 17.

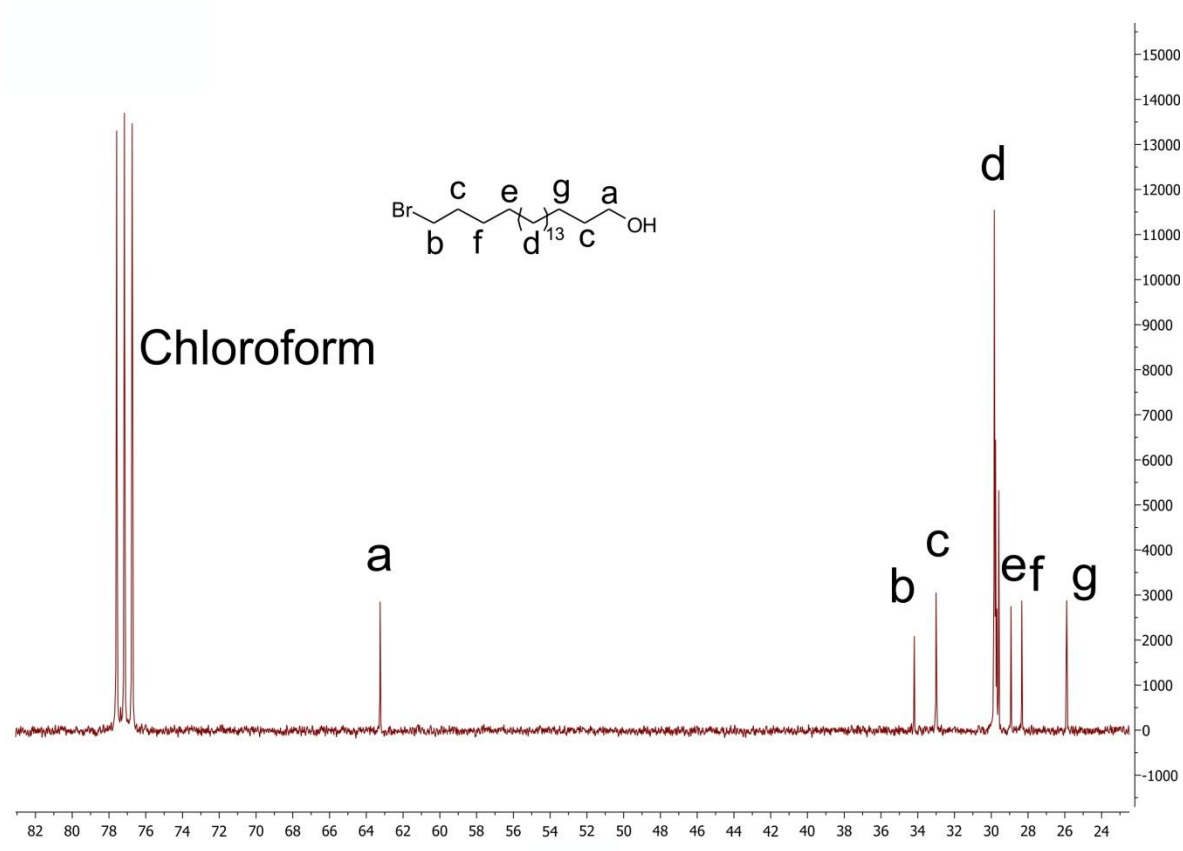


**Figure S32.** $^{13}$C-NMR spectrum (75.47 MHz, $CDCl_3$) of Compound 17.

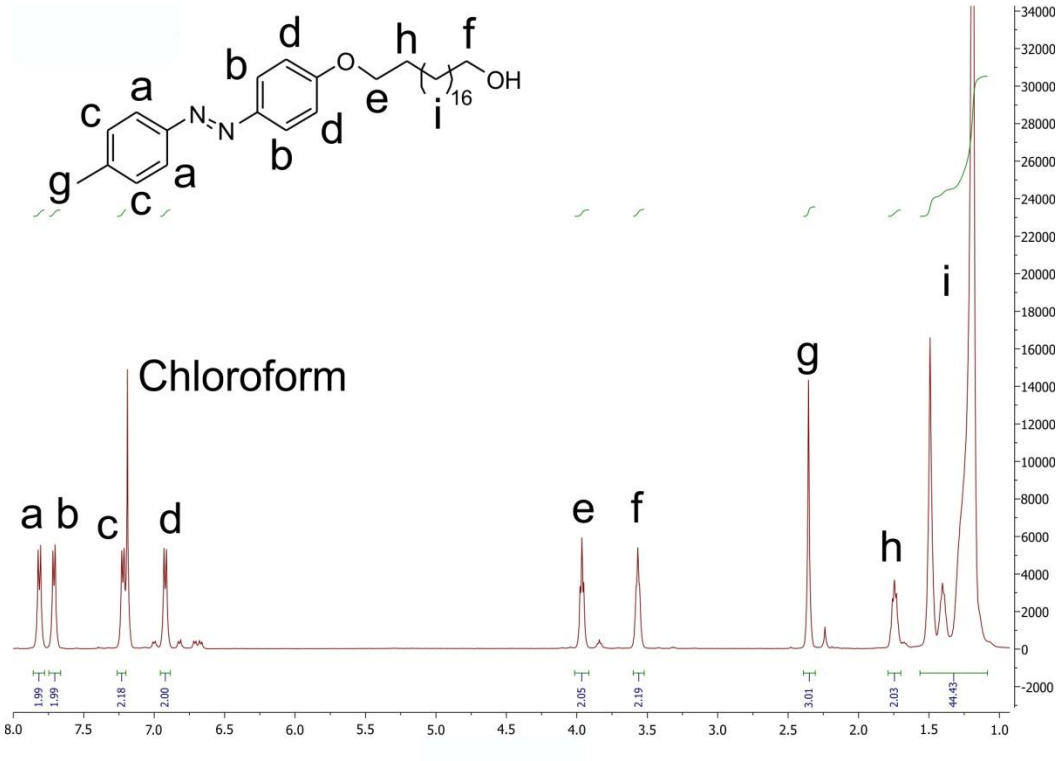


**Figure S33.** $^{1}$H-NMR spectrum (500.13 MHz, $CDCl_3$) of Compound 18.

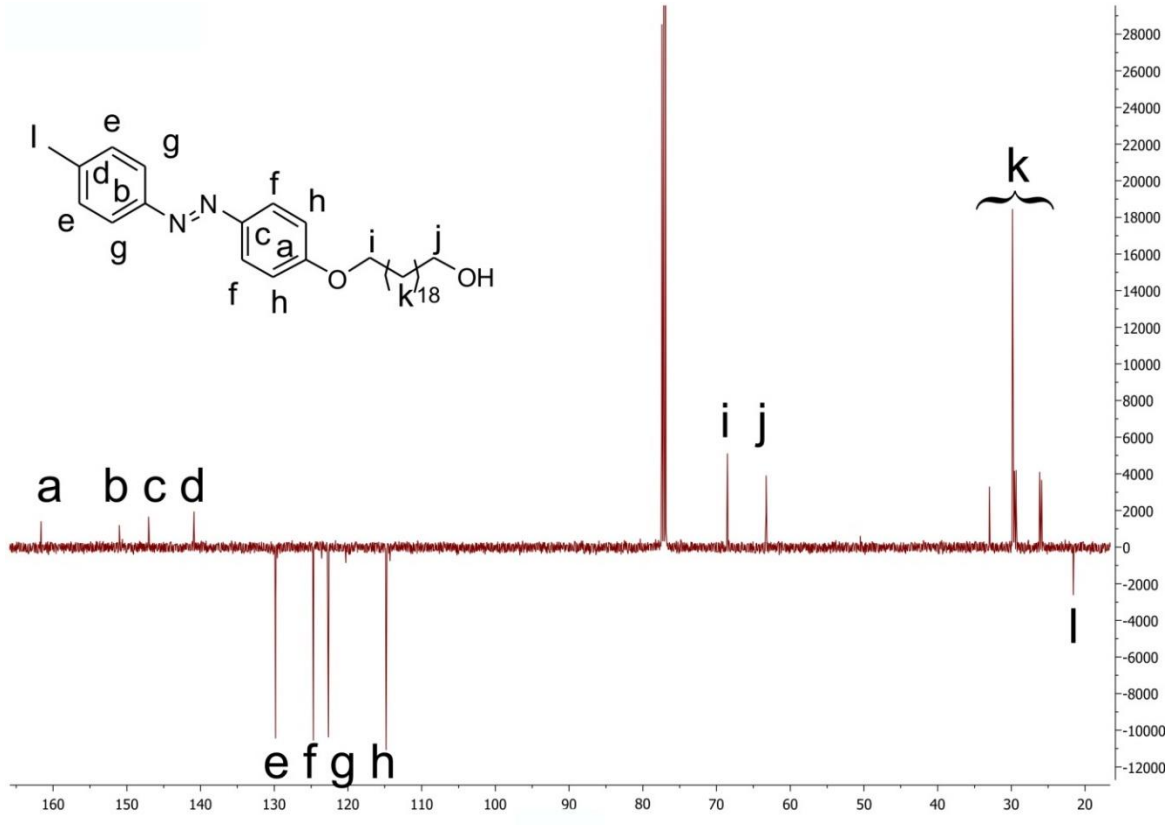


**Figure S34.** $^{13}$C-NMR spectrum (125.78 MHz, $CDCl_3$) of Compound 18.

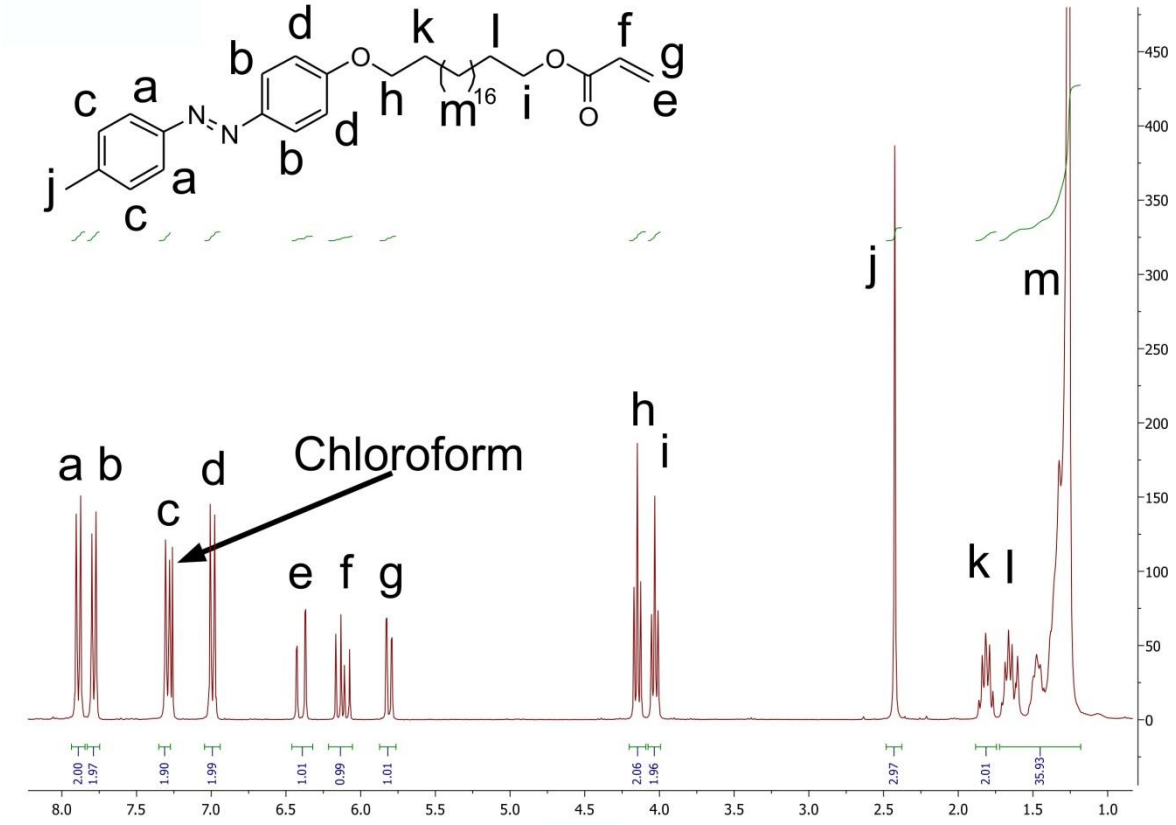


**Figure S35.** $^{1}$H-NMR spectrum (300.13 MHz, $CDCl_3$) of Compound 19.

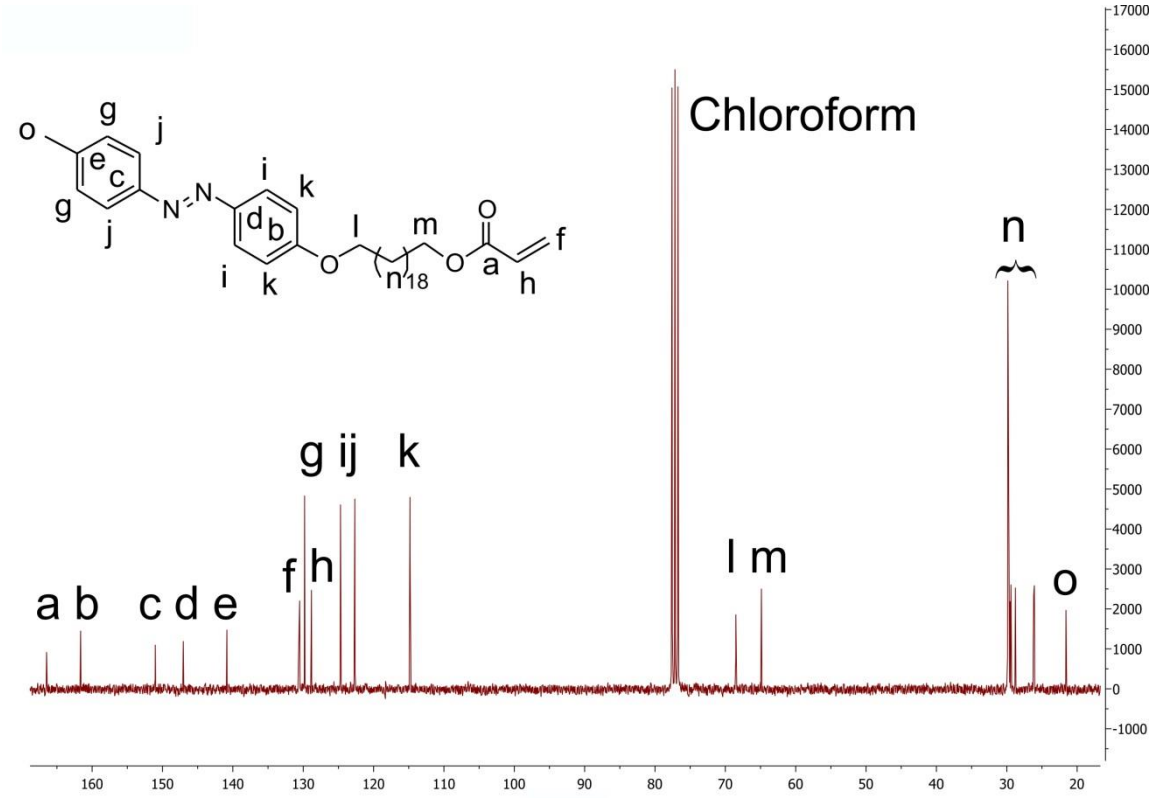


**Figure S36.** $^{13}$C-NMR spectrum (75.47 MHz, $CDCl_3$) of Compound 19.

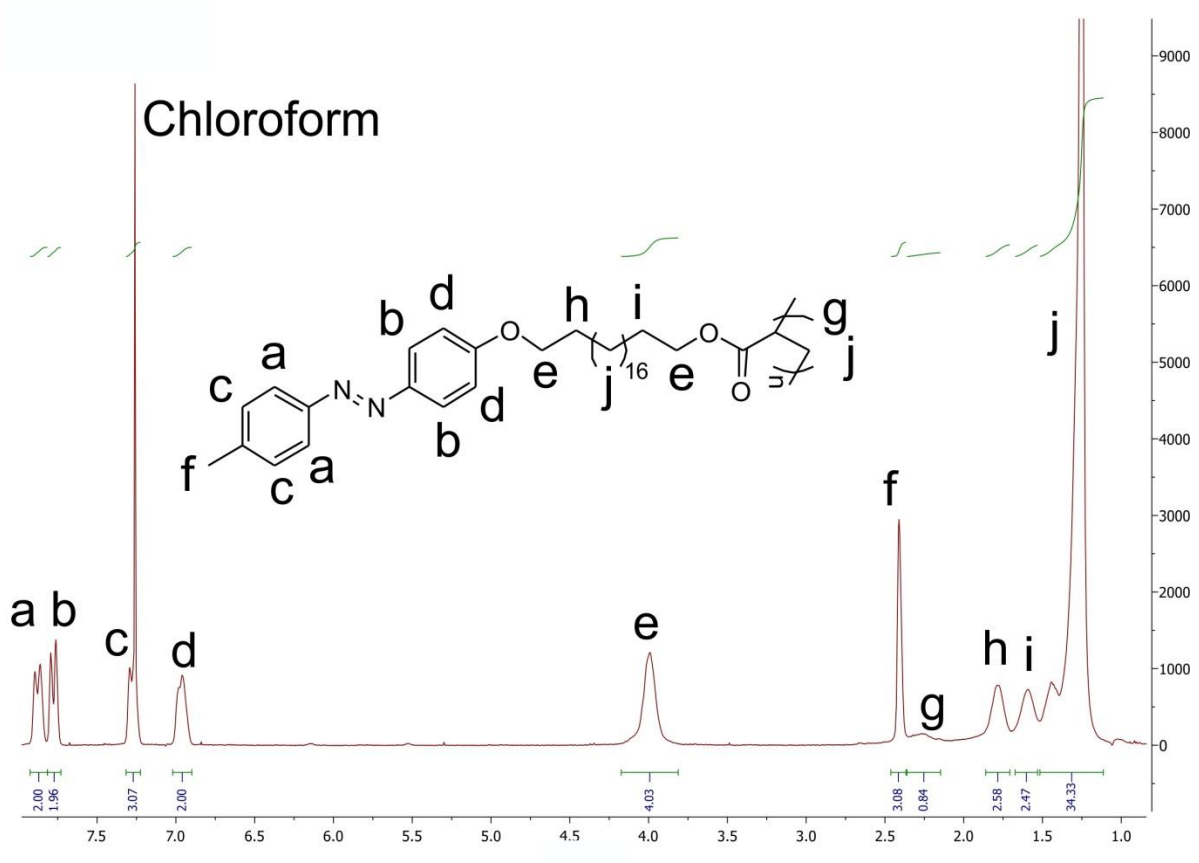


**Figure S37.** $^{1}$H-NMR spectrum (300.13 MHz, $CDCl_3$) of Compound 20.

**References:**

1. Nishizawa, K.; Nagano, S.; Seki, T., Novel Liquid Crystalline Organic−Inorganic Hybrid for Highly Sensitive Photoinscriptions. *Chemistry of Materials* **2009,** *21* (13), 2624-2631.
2. Menzel, H.; Weichart, B.; Schmidt, A.; Paul, S.; Knoll, W.; Stumpe, J.; Fischer, T., Small-Angle X-ray Scattering and Ultraviolet-Visible Spectroscopy Studies on the Structure and Structural Changes in Langmuir-Blodgett Films of Polyglutamates with Azobenzene Moieties Tethered by Alkyl Spacers of Different Length. *Langmuir* **1994,** *10* (6), 1926-1933.
3. Tong, X.; Cui, L.; Zhao, Y., Confinement Effects on Photoalignment, Photochemical Phase Transition, and Thermochromic Behavior of Liquid Crystalline Azobenzene-Containing Diblock Copolymers. *Macromolecules* **2004,** *37* (9), 3101-3112.
4. Zhou, H.; Xue, C.; Weis, P.; Suzuki, Y.; Huang, S.; Koynov, K.; Auernhammer, G. K.; Berger, R.; Butt, H.-J.; Wu, S., Photoswitching of glass transition temperatures of azobenzene-containing polymers induces reversible solid-to-liquid transitions. *Nat Chem* **2017,** *9* (2), 145-151.

# Curriculum Vitae

# Acknowledgements